Neutrino and Antineutrino Charged Current Interactions with Nuclei and Nucleons

Ignacio Ruiz Simó

Departamento de Física Teórica

Universidad de Valencia

TESIS DOCTORAL

VALENCIA 2011

D. Manuel José Vicente Vacas, Profesor Titular del Departamento de Física Teórica de la Universidad de Valencia,

> CERTIFICA: Que la presente Memoria *Neutrino and Antineutrino Charged Current Interactions with Nuclei and Nucleons* ha sido realizada bajo mi dirección en el Departamento de Física Teórica de la Universidad de Valencia por D. Ignacio Ruiz Simó como Tesis para obtener el grado de Doctor en Física.

Y para que así conste, presenta la referida Memoria, firmando el presente certificado.

Fdo: Manuel José Vicente Vacas

Contents

Agradecimientos **9**

Introduction **11**

1 Weak kaon/antikaon production **19**
1.1 Kaon production induced by neutrinos 19
1.1.1 Introduction 19
1.1.2 Formalism 20
1.1.3 Results 26
1.1.4 Summary 33
1.2 Antikaon production induced by antineutrinos 35
1.2.1 Formalism 35
1.2.2 Results 41
1.2.3 Summary 44

2 Inclusive reactions in nuclei at low and intermediate energies **47**
2.1 Introduction 47
2.2 Formalism 50
2.2.1 Selfenergy of the neutrino 50
2.2.2 Quasielastic scattering 54
2.2.3 $\Delta(1232)$ Dominance in pion production 56
2.2.4 Addition of background terms in pion production . . . 59
2.2.5 Two-particles two-holes (2p2h) absorption modes . . . 64
2.2.6 Final remarks 87
2.2.7 CC antineutrino induced reactions 93

2.3 Results . . . 93
2.4 The problem of the axial mass . . . 104
2.5 Summary . . . 111

3 Nuclear structure functions in Deep Inelastic Scattering 113
3.1 Introduction . . . 113
3.2 Deep inelastic lepton-nucleon scattering . . . 115
3.3 Nuclear effects . . . 117
3.3.1 π and ρ mesons contribution to the nuclear structure function . . . 118
3.3.2 Target mass corrections . . . 120
3.3.3 Coherent nuclear effects . . . 120
3.4 Derivative expansion of F_2 . . . 121
3.5 Results and discussion . . . 122
3.6 Summary . . . 131

4 Conclusions 133

5 Resumen de la tesis 137
5.1 Introducción . . . 137
5.2 Conclusiones . . . 144

A 149
A.1 Nucleon propagator in nuclear matter . . . 149

B 155
B.1 Low density limit . . . 155

C 157
C.1 Tensor $A_\Delta^{\mu\nu}$ . . . 157
C.2 Tensor $A_1^{\mu\nu}$ . . . 158

D 161
D.1 Selfenergy of the pion . . . 161
D.2 Selfenergy of the Δ . . . 164

E 169
E.1 Derivative expansions in DIS . . . 169

Bibliography **180**

Agradecimientos

En primer lugar, desearía agradecer al Profesor Manuel J. Vicente Vacas por todo el apoyo y ayuda prestados durante estos últimos cuatro años en que he realizado esta Tesis bajo su supervisión. También le agradezco que me pusiera en contacto con mis colaboradores indios y españoles: el Profesor Mohammad Sajjad Athar y su estudiante, Rafi Alam, por un lado; y el Profesor Juan Nieves por otro. Con cada uno de ellos he trabajado en aspectos diferentes y en lo que constituirán capítulos distintos de esta tesis. Sin ellos, este trabajo no hubiera sido posible realizarlo.

Al Profesor Sajjad le agradezco especialmente que viniera a España durante casi dos meses para intentar empezar un trabajo de dispersión profundamente inelástica de neutrinos con núcleos. Yo conocía algo el tema, porque había intentado reproducir un artículo suyo (realizado junto con los Profesores Manuel Vicente Vacas y S.K. Singh) para mi trabajo de fin de máster. Su estancia aquí sirvió para aprender bastantes cosas acerca de las funciones de estructura del nucleón y para estrechar lazos de amistad y colaboración para posteriores trabajos en común.

Supongo que, fruto del buen ambiente de trabajo que Sajjad encontró aquí en Valencia, nos envió durante una estancia de tres meses a su estudiante, Rafi Alam. Con Rafi lo pasé muy bien durante esos meses que estuvimos juntos. Trabajamos de manera independiente en realizar los mismos cálculos. Y, aunque parezca una manera un tanto extraña de trabajar (por lo que supone de duplicidad de esfuerzos), siempre nos ha servido para chequear nuestros resultados. Lo cierto es que casi siempre nos quedábamos estancados en los mismos puntos, y teníamos que acudir al despacho de Manolo para que nos resolviese las mismas dudas. Fueron unos meses que recuerdo con especial cariño.

Al profesor Juan Nieves he de agradecerle que tuviera la idea de realizar un trabajo sobre reacciones inclusivas de neutrinos con núcleos (que constituirá el centro de la tesis), trasladando de esta manera su trabajo de producción débil de piones con nucleones a núcleos.
Por último, no puedo dejar pasar la oportunidad de recordar en esta sección a todos aquellos amigos y compañeros de despacho y de grupo con los que he compartido grandes momentos: mis amigos indios, Kanchan y Alberto; mis amigos españoles, Justito (con su sonrisa taimada), el GV (con sus historias de Petrer), Francesc, Raquel, Jorge y mi amiga italiana Paola.
A todos ellos, muchísimas gracias.

Introduction

Neutrino physics has been at the heart of many major discoveries in the field of theoretical/particle physics like weak interaction, solar and supernova physics or parity violation to name a few.
When Wolfgang Pauli proposed the existence of a spin-$\frac{1}{2}$ neutral particle which would share energy and momentum with the β particles emitted by some nuclei in the process called β-decay, he doubted that such a particle would ever be observed. In 1956, many years later, the neutrino was first detected in an experiment by Reines and Cowan [1]. Enrico Fermi had proposed a theory for the β-decay with a four fermion vertex [2,3]. Soon it was found that the form of the interaction postulated by Fermi should be generalized to include spin-dependent interactions as pointed out by Gamow and Teller [4, 5]. After many attempts to find out the tensor structure of the weak interaction, Richard Feynman and Gell-Mann [6], based on previous work and conversations with Sudarshan and Marshak [7, 8], proposed the $V - A$ form for the vertex. This kind of structure for the weak current was suggested after the experimental observation of parity violation in the β-decay of ^{60}Co [9].
A few years later, Lederman, Schwartz and Steinberger [10] discovered a new kind (flavour) of neutrino related to the muon. A third flavour of neutrino (the tau neutrino) was first detected by the DONUT collaboration in 2000 at Fermilab [11].
One of the most important recent discoveries is the fact that neutrinos are massive. When neutrinos are produced, they are in an eigenstate of flavour. That can be expressed as a linear combination of mass eigenstates, which propagate with a well-defined energy. Having different energies, the phases of the different components do not evolve equally with time. Thus the initial

flavour eigenstate evolves to another state which is not simply the initial state multiplied by a global phase. Therefore, there is a probability of transition from one flavour state to another. There have been and there are enormous theoretical and experimental efforts with the aim of measuring absolute masses of the neutrinos [12–16], oscillation parameters [17–21], etc. For reviews on neutrino oscillations, see e.g., Refs. [22–26].

Nowadays, we are entering into an era of precision measurements of the parameters of the Pontecorvo-Maki-Nakagawa-Sakata (PMNS) matrix: the mixing angles and the CP-violating phase in the leptonic sector.

A good understanding of the neutrino interactions at intermediate energies (around 1 GeV) is essential for future, current and past neutrino oscillation experiments like Super-Kamiokande [27, 28], T2K [29], NOνA [30], OPERA [31], MiniBooNE [32], MicroBooNE [33]... For this purpose, dedicated neutrino scattering experiments have been planned: MINERνA [34] and others. These experiments are typically carried out at intermediate energies, i.e, around 1 GeV. This is because these energies maximize the oscillation probability (once the length for the oscillation has been set).

In this energy region, usually, the selected process to measure the oscillation parameters is the Charged Current Quasi-elastic (CCQE) scattering off nuclei $\nu_l + A \to l^- + A'$. One of the reasons is that Neutral Current Elastic (NCE) scattering is flavour-blind. Indeed, if one has to detect a $\nu_\mu \to \nu_e$ oscillation, one must be able to detect a muon or an electron in the final state. If one deals with the Neutral Current (NC) scattering, it is impossible to know if there has been any flavour oscillation because the interaction in this channel is the same for ν_μ than for ν_e and the neutrino in the final state is not detected. Other reason for the choice of Quasi-elastic (QE) scattering is because it has the largest cross section in this energy range, between the threshold and a few GeV (see for instance fig 1 in Ref [35]).

Neutrinos only interact weakly with matter and therefore their cross sections are very small. To measure them, very large detectors where neutrinos collide with nuclear targets like iron, mineral oil, water are commonly used. This fact introduces a new difficulty related to nuclear effects in neutrino scattering. Indeed, particles produced in the interaction can be rescattered or absorbed before leaving the nucleus. Therefore, these nuclear re-interactions can lead to a misidentification of the reaction channel and change the topology of the measured hadronic final state. Nuclear effects

are among the largest source of systematic uncertainties in oscillation neutrino experiments.
As mentioned before, the oscillation probability depends on the neutrino energy. However, this energy cannot be directly measured but it has to be reconstructed from the final state particles that are detected. But these particles are affected by in-medium effects. Thus, the experimental analysis has to rely on models for the neutrino-nucleus interaction. The theoretical understanding of nuclear effects is, therefore, essential for the interpretation of the data.
In addition to the interest for the properties of the neutrinos, these experiments draw the attention of nuclear and hadronic physics community due to the fact that neutrinos provide a very valuable tool to obtain more information on the structure of the nucleon and baryonic resonances, since they probe the vector but also the axial structure of the hadrons. The vector form factors are relatively well-known from electron scattering experiments. Current and future experiments will provide information on the nucleon and baryonic resonances axial form factors. As an example, the cross section of the CCQE processes depends on two vector and one axial-vector form factors. The Q^2-dependence of the axial form factor is usually assumed to have a dipole form with one free parameter (the so-called axial mass) to be fitted from the Q^2-distributions.
The aim of this thesis is to participate in the development of a reliable theoretical framework to analyze neutrino scattering on hadronic targets.
Starting from threshold we have the mentioned QE scattering and later the inelastic channels: π production, hyperon production, baryonic resonances, kaons... In nuclei we also have multi-nucleon mechanisms. And at higher energies, Deeply Inelastic Scattering (DIS) is dominant. Let us start discussing QE.
The basic ingredient for QE scattering in a model is the excitation of a nucleon by the weak probe. This is called the 1p1h (one-particle one-hole) description of QE scattering. There are many models for QE scattering in nuclei that contain several nuclear effects: SuperScaling approximation and meson exchange currents [36]; Final State Interactions (FSI) and SuperScaling [37]; FSI and Random Phase Approximation (RPA) corrections [38]; inside the framework of the GiBUU transport model [39] and many others. There is almost a theoretical consensus in the fact that all QE models in

nuclei are below the recently reported results by the MiniBooNE collaboration [40], where the analysis favored an increase of the axial mass in the axial-vector form factor in order to match the data both in the shape of the flux-averaged Q^2 distribution and in the total cross section as a function of the neutrino energy. This increase of the effective axial mass enters in contradiction with the world average value $M_A = 1.016 \pm 0.026$ GeV [41], this latter value of M_A being extracted from early CCQE measurements on deuterium targets. From π electro-production amplitudes, after applying hadronic corrections that can be calculated at low Q^2 using chiral perturbation theory [42], the resulting $M_A = 1.014 \pm 0.016$ GeV is obtained.
Several theoretical efforts have been made to go beyond this 1p1h description of the QE scattering. This means to consider 2p2h (two-particle two-hole) excitations that might contribute to the CCQE cross section defined by MiniBooNE. See for instance Refs [43] (for electron scattering) and [44–46] (for neutrino and antineutrino scattering).
In Ref. [38], CCQE was studied in the framework of a Many-Body approach keeping only the 1p1h contribution to QE scattering but including RPA corrections and FSI with the inclusion of realistic nuclear spectral functions. One of the aims of this thesis is to extend the work of Ref. [38] to higher transferred energies, where resonance degrees of freedom are important. It is also a goal of this thesis to extend the previous work of Ref. [47] for weak pion production from free nucleons to nuclei.
In addition to QE scattering, other processes like single pion production can be used to detect neutrinos. The production and decay of nucleon resonances in neutrino interactions is a significant part of the total neutrino cross section in the few GeV region. These resonances have also been explored using electron scattering experiments, but different form factors contribute in the case of neutrino scattering. Resonance production is the least certain part of the neutrino cross section picture; and experiments like NOνA and T2K expect this interactions to be a large fraction of the cross section in the energy region in which they are most interested.
Pion production in nuclei can be either coherent or incoherent. In the latter case, the final nucleus is excited. The most popular model for this process in neutrino interaction simulations was developed by Rein and Sehgal [48]. It assumes that pion production on the nucleon is dominated by baryon resonance excitation, which is described using the relativistic quark model of

Feynman, Kislinger and Ravndal [49] for resonances with invariant masses up to 2 GeV. The original model neglected final lepton masses. However, finite mass corrections in kinematics and currents have been recently investigated [50–52]. The wealth of pion photo- and electro-production data available from several experiments at MIT/Bates, MAMI/Mainz and specially JLab have been used to extract the electromagnetic transition helicity amplitudes [53, 54]. This valuable empirical information should be incorporated to the analysis of neutrino experiments.

In contrast, there is almost no information about the axial part of the weak nucleon-to-resonance transition current. Partial Conservation of the Axial Current (PCAC) and pion-pole dominance of the pseudoscalar form factor can be applied to relate the axial coupling for the dominant contribution at low Q^2 to the resonance πN decay coupling. For small values of Q^2, only the axial C_5^A form factor is relevant and some effort has been devoted to its extraction from ANL and BNL bubble chamber data.

Pion production in nuclei is coherent when the nucleus remains in its ground state. It takes place predominantly when the momentum transferred to the nucleus is small, so that the nucleus is less likely to break. Weak coherent π production has a very small cross section compared to the incoherent case, but relatively larger than equivalent reactions induced by photons or electrons. This is due to the non-vanishing contribution of the axial current at the relevant kinematics [55].

A good knowledge of pion production is very important for the interpretation of oscillation experiments. It is well known that charged current π^+ production represents the major background to the QE "signal". Indeed, if the pion, for instance, is absorbed in the nucleus or not detected, the event seems QE-like.

There are, of course, models for weak pion production off the nucleon [47, 48, 56–58] and even for two pion production induced by neutrinos [59]. These models contain the main mechanism for pion production, namely the excitation of $\Delta(1232)$ isobars but also background terms that become important at threshold and can be obtained using Chiral Perturbation Theory (χPT). We will use the model for pion production off a nucleon of Ref [47] as a base to develop a model for pion production in nuclei.

One could also mention some models for hyperon production, like the works of Refs [60–62]. The first work deals with weak QE production of hyperons

induced by antineutrinos, whereas the second and third ones deal with associated production of strange particles.
For higher neutrino energies, other channels involving strange particles could become relevant, for instance the single kaon production off the nucleon induced by neutrinos or single antikaon production off the nucleon induced by antineutrinos (in this latter case including the excitation of resonances with strangeness $S = -1$, like the Σ^*). One must mention that, although Cabibbo suppressed ($\Delta S = \pm 1$), these cross sections are larger (up to ~ 1.5 GeV) than the ones for associated production ($\Delta S = 0$ and not Cabibbo suppressed) due to the different thresholds.
Studies of exclusive strange-particle production induced by neutrinos will be possible at MINERνA. They expect to accumulate thousands of these events, depending of course on the channel. These cross section measurements will probably impact other areas of particle physics as well. For example, in estimation of atmospheric neutrino $\Delta S = 1$ backgrounds to nucleon-decay searches. Exposure to antineutrino beam will help in the study of $\Delta S = -1$ single hyperon production and would permit a novel measure of the Cabibbo-Kobayashi-Maskawa (CKM) matrix elements. In this experiment, other cross sections will be measured, as those of associated production $\Delta S = 0$, induced either by neutral or charged currents.
Existing data on neutrino resonance-production are insufficient for the task of specifying the complex overlapping between Δ and N^* resonance amplitudes and related form factors which characterize the $1 - 5$ GeV E_ν regime. Neutrino Monte Carlo programs try to simulate this kinematic region using early theoretical predictions by Rein and Sehgal [48] or results from electroproduction experiments. The theoretical and experimental picture of the resonance region is more obscure than the QE and deep inelastic scattering (DIS) regions that border it. And much of the relevant MINOS [63] event sample falls inside this resonance region.
At higher energies, the cross section is dominated by Deeply Inelastic Scattering (DIS) (see fig 1 in Ref. [35]) where the nucleon structure functions can be written in terms of Parton Distribution Functions (PDFs) for quarks, antiquarks and gluons.
Neutrino scattering also plays an essential role in extraction of fundamental PDFs. The weak charged current ability to "taste" only particular quark flavours significantly enhances the study of parton distribution functions.

It is also important the fact that weak interactions explore other structure functions (F_3), in contrast with purely electromagnetic probes.
Nuclear effects in DIS have been extensively studied using muon and electron beams, but only superficially for neutrinos. High-statistics neutrino experiments have only been possible using heavy nuclear targets such as iron-dominated target-calorimeters. For the analysis of these experiments, parameterizations of the nuclear effects obtained from $e/\mu - A$ experiments have been applied to the results. However, there are strong indications that the nuclear corrections for $e/\mu - A$ and $\nu - A$ are different.
Within the impulse approximation, the nuclear structure functions can be expressed as a convolution of the nucleon ones with the nuclear spectral function. This accounts for effects like Fermi motion and nuclear binding. Other effects like shadowing [64,65] and Target Mass Corrections (TMC) [66], and the influence of mesonic degrees of freedom are also relevant. We will develop a model based on the many body approach developed by Marco and Oset in Ref. [67]. We will compare this model with the above mentioned improvements with the recent results of JLab about the EMC effect in light nuclei [68].
The structure of this thesis will be the following: in the first chapter we will develop a model for kaon/antikaon production induced by neutrinos/antineutrinos off free nucleons [69]; in the second chapter, we will discuss several low energy processes in nuclei such as QE scattering, pion production and 2p2h excitations [46]; and finally, in the third chapter we will study DIS of leptons with nuclei [70].

Chapter 1

Weak kaon/antikaon production

1.1 Kaon production induced by neutrinos

1.1.1 Introduction

The weak kaon production off the nucleon induced by neutrinos is the first inelastic reaction creating strange quarks. In this chapter we are going to focus in single kaon production (without accompanying hyperons). This latter process where a kaon and a hyperon are produced is called associated production (with $\Delta S = 0$) and has been more studied. See, for instance, Ref. [61]. In single kaon production induced by neutrinos there is a net change in strangeness between the final and initial states ($\Delta S = 1$). This channel is particularly appealing for several reasons: firstly, because it can be the main source of background, due to atmospheric neutrino interactions, in the analysis of one of the main decay channels the proton has in many supersymmetric grand unified theories ($p \to \nu + K^+$), see Refs. [71–73]; secondly, because at low energies, it is possible to obtain model independent predictions using Chiral Perturbation Theory (χPT); and thirdly, because due to the absence of $S = 1$ baryonic resonances, the range of validity of the calculation could be extended to higher energies than for other channels (like, for instance, antikaon production induced by antineutrinos).
From the theoretical point of view, there are very few calculations which deal

with a single strange particle production at low neutrino energies. There are works on QE hyperon production induced by antineutrinos [60, 74] and also the work of Dewan, who studied in the 80's several kaon and hyperon production channels [75].
In the coming years of precision neutrino physics, the knowledge of the cross sections for these processes is important for the data analysis, apart from their own intrinsic interest related to the role played by the strange quarks in hadronic physics.
In part as a consequence of the scarcity of theoretical work, the Monte Carlo generators used in the analysis of the experiments use models that are not very well suited to describe the strangeness production at low energies. For instance, NEUT only considers associated kaon production implemented by a model based on the excitation and later decay of resonances [76] (see discussion in Ref. [77]).

1.1.2 Formalism

The basic reaction for the neutrino induced charged current kaon production is

$$\nu_l(k) + N(p) \rightarrow l^-(k') + N'(p') + K(p_k), \tag{1.1}$$

where $l = e, \mu$ and $N\&N'$=n,p. The expression for the differential cross section in the laboratory (lab) frame for the above process is given by,

$$d^9\sigma = \frac{1}{4ME(2\pi)^5}\frac{d^3\vec{k}'}{(2E_l)}\frac{d^3\vec{p}'}{(2E'_p)}\frac{d^3\vec{p}_k}{(2E_K)}\delta^4(k+p-k'-p'-p_k)\bar{\Sigma}\Sigma|\mathcal{M}|^2, \tag{1.2}$$

where $\vec{k}$ and $\vec{k'}$ are the 3-momenta of the incoming and outgoing leptons in the lab frame with energy E and E_l respectively. The kaon lab momentum is $\vec{p}_k$ having energy E_K, M is the nucleon mass, $\bar{\Sigma}\Sigma|\mathcal{M}|^2$ is the square of the transition amplitude matrix element averaged (summed) over the spins of the initial(final) state. At low energies, this amplitude can be written in the usual form as

$$\mathcal{M} = \frac{G_F}{\sqrt{2}} j_\mu^{(L)} J^\mu_{(H)} \tag{1.3}$$

where $j_\mu^{(L)}$ and $J^\mu_{(H)}$ are the leptonic and hadronic currents respectively, $G_F = 1.16639(1) \times 10^{-5}$ GeV^{-2} is the Fermi constant. The leptonic current

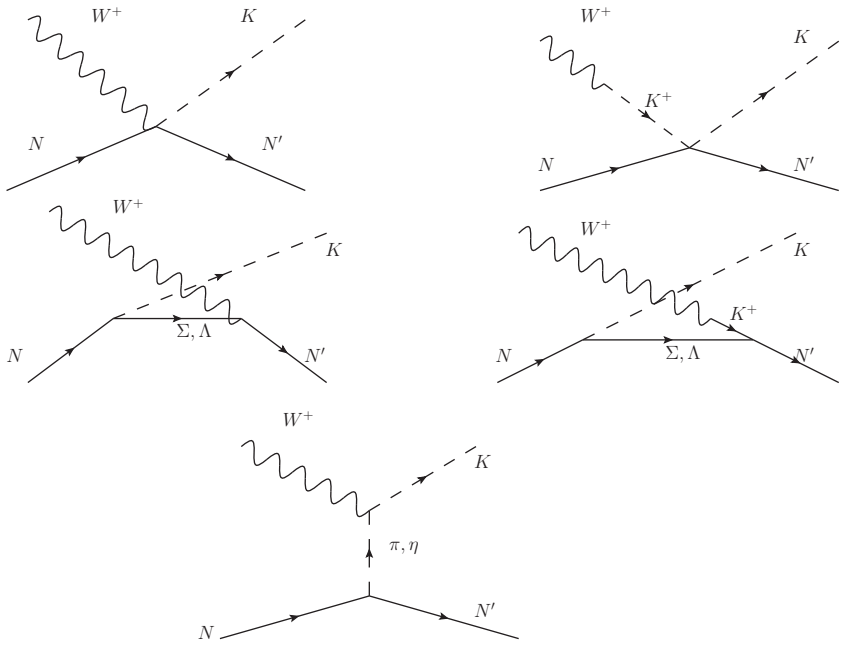

Figure 1.1: Feynman diagrams for the elementary process $W^+ + N \to N' + K$. First row, from left to right: contact term (CT) and kaon pole term (KP). Second row: u-channel diagrams with an hyperon in the intermediate state (Crossed Sigma and Crossed Lambda). Third row: pion or eta in flight (πP or ηP)

can be obtained from the Standard Model Lagrangian, and it reads:

$$j^{\mu}_{(L)} = \bar{u}_l(\vec{k}')\gamma^{\mu}(1-\gamma_5)u_{\nu}(\vec{k}) \tag{1.4}$$

We consider five different channels that contribute to the hadronic current. They are depicted in Fig. 1.1. The fourth Feynman diagram (depicted in second row of fig. 1.1) can be considered as a correction to the third one. There is a contact term (CT), a kaon pole (KP) term, a u-channel process with a Σ or Λ hyperon in the intermediate state and finally a meson (π, η) exchange term. For the specific reactions under consideration, there are not s-channel contributions given the absence of $S = 1$ baryonic resonances. The current of the KP term is proportional to q^{μ}. This implies, after contraction with the leptonic tensor, that the amplitude is proportional to the lepton mass and therefore very small.

The contribution of the different terms can be obtained in a systematic manner using χPT. This allows to identify some terms that were missing in the approach of Ref. [75], which only included the u-channel diagrams in the calculation and the diagram with a pion exchange. The lowest-order SU(3) chiral Lagrangian describing the pseudoscalar mesons in the presence of an external current is

$$\mathcal{L}^{(2)}_M = \frac{f_\pi^2}{4}\mathrm{Tr}[D_\mu U (D^\mu U)^\dagger] + \frac{f_\pi^2}{4}\mathrm{Tr}(\chi U^\dagger + U\chi^\dagger), \tag{1.5}$$

where the parameter $f_\pi = 92.4$ MeV is the pion decay constant, U is the SU(3) representation of the meson fields

$$\begin{aligned} U(x) &= \exp\left(i\frac{\phi(x)}{f_\pi}\right), \\ \phi(x) &= \begin{pmatrix} \pi^0 + \frac{1}{\sqrt{3}}\eta & \sqrt{2}\pi^+ & \sqrt{2}K^+ \\ \sqrt{2}\pi^- & -\pi^0 + \frac{1}{\sqrt{3}}\eta & \sqrt{2}K^0 \\ \sqrt{2}K^- & \sqrt{2}\bar{K}^0 & -\frac{2}{\sqrt{3}}\eta \end{pmatrix}, \end{aligned} \tag{1.6}$$

and $D_\mu U$ is its covariant derivative

$$D_\mu U \equiv \partial_\mu U - i r_\mu U + i U l_\mu \,. \tag{1.7}$$

Here, l_μ and r_μ correspond to left and right-handed currents, that for the CC case are given by

$$r_\mu = 0, \quad l_\mu = -\frac{g}{\sqrt{2}}(W^+_\mu T_+ + W^-_\mu T_-), \tag{1.8}$$

with $W^{\pm}$ the W boson fields and

$$T_+ = \begin{pmatrix} 0 & V_{ud} & V_{us} \\ 0 & 0 & 0 \\ 0 & 0 & 0 \end{pmatrix}; \quad T_- = \begin{pmatrix} 0 & 0 & 0 \\ V_{ud} & 0 & 0 \\ V_{us} & 0 & 0 \end{pmatrix}.$$

Here, V_{ij} are the elements of the Cabibbo-Kobayashi-Maskawa matrix. The second term of the Lagrangian of Eq. 1.5, that incorporates the explicit breaking of chiral symmetry coming from the quark masses [78], is not relevant for this study.
The lowest-order chiral Lagrangian for the baryon octet in the presence of an external current can be written in terms of the SU(3) matrix

$$B = \begin{pmatrix} \frac{1}{\sqrt{2}}\Sigma^0 + \frac{1}{\sqrt{6}}\Lambda & \Sigma^+ & p \\ \Sigma^- & -\frac{1}{\sqrt{2}}\Sigma^0 + \frac{1}{\sqrt{6}}\Lambda & n \\ \Xi^- & \Xi^0 & -\frac{2}{\sqrt{6}}\Lambda \end{pmatrix} \tag{1.9}$$

as

$$\mathcal{L}^{(1)}_{MB} = \mathrm{Tr}\left[\bar{B}\left(i\not{D} - M\right)B\right] - \frac{D}{2}\mathrm{Tr}\left(\bar{B}\gamma^\mu\gamma_5\{u_\mu, B\}\right) - \frac{F}{2}\mathrm{Tr}\left(\bar{B}\gamma^\mu\gamma_5[u_\mu, B]\right), \tag{1.10}$$

where M denotes the mass of the baryon octet, and the parameters $D = 0.804$ and $F = 0.463$ can be determined from the baryon semileptonic decays [79]. The covariant derivative of B is given by

$$D_\mu B = \partial_\mu B + [\Gamma_\mu, B], \tag{1.11}$$

with the connection

$$\Gamma_\mu = \frac{1}{2}\left[u^\dagger(\partial_\mu - ir_\mu)u + u(\partial_\mu - il_\mu)u^\dagger\right], \tag{1.12}$$

where we have introduced $u^2 = U$. Finally,

$$u_\mu = i\left[u^\dagger(\partial_\mu - ir_\mu)u - u(\partial_\mu - il_\mu)u^\dagger\right]. \tag{1.13}$$

The next order meson baryon Lagrangian contains many new terms (see for instance Ref. [80]). Their importance for kaon production will be small at low energies and there are some uncertainties in the coupling constants.

Nonetheless, for consistency with previous calculations (especially with that of [75]), we will include the contribution to the weak magnetism coming from the pieces

$$\mathcal{L}^{(2)}_{MB} = d_5 \mathrm{Tr}\left(\bar{B}[f^+_{\mu\nu}, \sigma^{\mu\nu}B]\right) + d_4 \mathrm{Tr}\left(\bar{B}\{f^+_{\mu\nu}, \sigma^{\mu\nu}B\}\right) + \ldots, \tag{1.14}$$

where the tensor $f^+_{\mu\nu}$ can be reduced for this study to

$$f^+_{\mu\nu} = \partial_\mu l_\nu - \partial_\nu l_\mu - i[l_\mu, l_\nu]. \tag{1.15}$$

In this case, the coupling constants are fully determined by the proton and neutron anomalous magnetic moments. This same approximation has also been used in calculations of single pion production induced by neutrinos [47]. Now, writing the amplitude for the coupling of the W boson to the hadrons for each of the terms in the form $\frac{g}{2\sqrt{2}}(J^\mu_H W^+_\mu + h.c.)$, for consistency with Eq. 1.3, we get the following contributions to the hadronic current.

$$\begin{aligned}
j^\mu\big|_{CT} &= -iA_{CT}V_{us}\frac{\sqrt{2}}{2f_\pi}\bar{N}(p')(\gamma^\mu + \gamma^\mu\gamma^5 B_{CT})N(p),\\
j^\mu\big|_{Cr\Sigma} &= iA_{Cr\Sigma}V_{us}\frac{\sqrt{2}}{2f_\pi}\bar{N}(p')\left(\gamma^\mu + i\frac{\mu_p + 2\mu_n}{2M}\sigma^{\mu\nu}q_\nu\right.\\
&\quad \left. +(D-F)(\gamma^\mu - \frac{q^\mu}{q^2 - M_k^2}\not{q})\gamma^5\right)\frac{\not{p} - \not{p}_k + M_\Sigma}{(p-p_k)^2 - M_\Sigma^2}\not{p}_k\gamma^5 N(p),\\
j^\mu\big|_{Cr\Lambda} &= iA_{Cr\Lambda}V_{us}\frac{\sqrt{2}}{4f_\pi}\bar{N}(p')\left(\gamma^\mu + i\frac{\mu_p}{2M}\sigma^{\mu\nu}q_\nu\right.\\
&\quad \left. -\frac{D+3F}{3}(\gamma^\mu - \frac{q^\mu}{q^2 - M_k^2}\not{q})\gamma^5\right)\frac{\not{p} - \not{p}_k + M_\Lambda}{(p-p_k)^2 - M_\Lambda^2}\not{p}_k\gamma^5 N(p),\\
j^\mu\big|_{KP} &= iA_{KP}V_{us}\frac{\sqrt{2}}{4f_\pi}\bar{N}(p')(\not{q} + \not{p}_k)N(p)\frac{1}{q^2 - M_k^2}q^\mu,\\
j^\mu\big|_{\pi} &= iA_{\pi P}V_{us}(D+F)\frac{\sqrt{2}}{2f_\pi}\frac{M(q^\mu - 2{p_k}^\mu)}{(q-p_k)^2 - M_\pi^2}\bar{N}(p')\gamma^5 N(p),\\
j^\mu\big|_{\eta} &= iA_{\eta P}V_{us}(D-3F)\frac{\sqrt{2}}{2f_\pi}\frac{M(q^\mu - 2{p_k}^\mu)}{(q-p_k)^2 - M_\eta^2}\bar{N}(p')\gamma^5 N(p),
\end{aligned} \tag{1.16}$$

where, $q = k - k'$ is the four momentum transfer, $V_{us} = \sin\theta_C = 0.226$ where θ_C is the Cabibbo angle, $N(\cdot)$, $\bar{N}(\cdot)$ denote the nucleon spinors, $\mu_p =$

Table 1.1: Values of the parameters appearing in the hadronic currents.

Process	A_{CT}	B_{CT}	$A_{Cr\Sigma}$	$A_{Cr\Lambda}$	A_{KP}	$A_{\pi P}$	$A_{\eta P}$
$\nu n \to lKn$	1	D-F	-(D-F)	0	1	1	1
$\nu p \to lKp$	2	-F	-(D-F)/2	(D+3F)	2	-1	1
$\nu n \to lKp$	1	-D-F	(D-F)/2	(D+3F)	1	-2	0

1.7928 and $\mu_n = -1.9130$ are the proton and neutron anomalous magnetic moments. The value of the various parameters of the formulas are shown in Table 1.1.

One can notice the induced pseudoscalar form factor in the $j^\mu\big|_{Cr\Sigma,Cr\Lambda}$ currents, which takes into account the coupling of the W boson to the baryon through a kaon. However, as for the KP term, its contribution is suppressed by a factor proportional to the final lepton mass and it is negligible. Now, we discuss in some detail the terms that appear in the coupling of the weak currents to the octet baryons in the u-channel diagrams. With very general symmetry arguments, this coupling can be described in terms of three vector and three axial form factors. Following the notation of Ref. [79] we have

$$O_V^\mu = f_1\gamma^\mu + \frac{f_2}{M_B}\sigma^{\mu\nu}q_\nu + \frac{f_3}{M_B}q^\mu, \tag{1.17}$$

$$O_A^\mu = (g_1\gamma^\mu + \frac{g_2}{M_B}\sigma^{\mu\nu}q_\nu + \frac{g_3}{M_B}q^\mu)\gamma^5\,, \tag{1.18}$$

where M_B is the baryon mass. At the order considered, the chiral Lagrangian provides finite values for f_1, the weak magnetism form factor f_2, g_1 and a pole contribution to g_3. The scalar f_3 and a non-pole part of the pseudoscalar g_3 form factors would only appear at higher orders of the chiral expansion. Furthermore, their contribution to the amplitude is suppressed by a m_l (lepton mass) factor and they are usually neglected. The value of g_2 vanishes in the limit of exact SU(3) symmetry and there is very little experimental information about it. In fact, it is also neglected in most analyses of hyperon phenomenology [81]. The values of f_1 and g_1 obtained from the lowest order chiral Lagrangians describe well the hyperon semileptonic decays [79, 81, 82].

Eventually, if the cross sections for the discussed processes were measured

with some precision, one could use them to explore these form factors at several q^2 values. The current experimental information, based on the semileptonic decays, covers only a very reduced range for this magnitude.
Finally, we consider the q^2 dependence of the weak current couplings provided by the chiral Lagrangians discussed earlier. We should remark that, even at relatively low energies and low momenta of the hadrons involved in this study, q^2 reaches moderate values. The q^2 dependence of the needed form factors (e.g. Kπ, YN) are poorly known if at all. Several prescriptions have been used in the literature. For instance, in quasielastic scattering and single pion production, the vector form factors are usually related to the well known nucleon electromagnetic ones (see e.g. [47, 83, 84] and references therein). This procedure is well suited for these two cases because of isospin symmetry. However, in the SU(3) sector we expect to have some symmetry breaking effects. Similarly, for the axial form factors, a q^2 dependence obtained from the nucleon-nucleon transition obtained in neutrino nucleon quasielastic scattering is normally used. However, the axial mass is not well established and it runs from values around 1 GeV [85, 86] up to 1.37 GeV recently obtained by the MiniBooNE [40, 87] and K2K [88] collaborations. Again here, we expect a different behavior for the hyperon-nucleon vertices. One of the possible choices (e.g. [89]) is to use a dipole form with the mass of the vector(axial) meson that could couple the baryon to the current. In this work, in view of the present uncertainties, we adopt a global dipole form factor $F(q^2) = 1/(1 - q^2/M_F^2)^2$, with a mass $M_F \simeq 1$ GeV that multiplies the hadronic currents. Its effect, that should be small at low neutrino energies will give an idea of the uncertainties of the calculation and will be explored in the next section.

1.1.3 Results

We consider the following reactions:

$$\begin{aligned} \nu_l + p &\rightarrow l^- + K^+ + p \quad (l = e,\ \mu) \\ \nu_l + n &\rightarrow l^- + K^0 + p \\ \nu_l + n &\rightarrow l^- + K^+ + n \end{aligned} \tag{1.19}$$

We show results for the total cross section σ as a function of the neutrino energy in the laboratory (LAB) frame. For each channel, the different contributions coming from every diagram are shown, except those of the Kaon

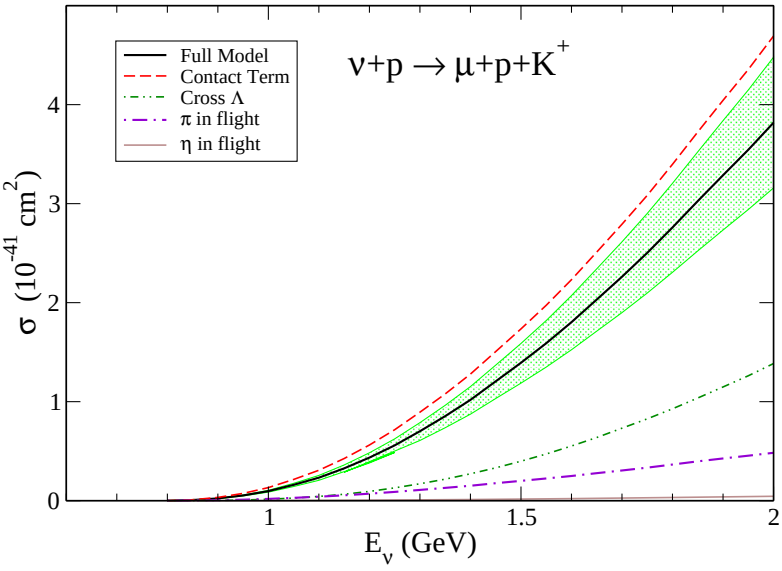

Figure 1.2: Contribution of the different terms to the total cross section for the $\nu_\mu p \to \mu K^+ p$ reaction.

Pole term alone, which are negligible at the energies considered. One can observe the importance of the contact term (CT) alone, not included in previous calculations. As observed by Dewan [75], the u-channel Σ contribution is much less important than the Λ one. This is due to the larger coupling ($NK\Lambda \gg NK\Sigma$) of the strong vertex. The band in fig 1.2 corresponds to a change of 10% in the mass M_F of the form factor. A similar effect is found in the other channels and we will only show the results for the central value of 1 GeV. These uncertainties, due to the vector/axial mass of the dipole form factor, would partially cancel in ratios of cross sections, such as $\sigma(K^0)/\sigma(K^+)$. This cancellation is not total because of the different q^2 dependence of each channel. The uncertainty bands for the ratios, when the mass M_F is changed by 10%, is less than 5%.

The process $\nu_\mu + n \to \mu^- + K^0 + p$ has a cross section of a similar size and the contact term is also the largest one, followed by the π exchange diagram and the u-channel (Λ) term. The rate of growth of the latter is somehow

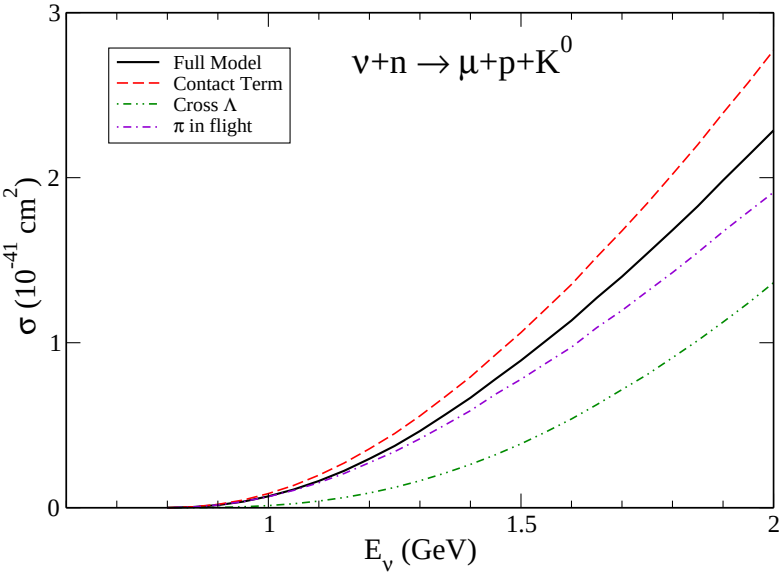

Figure 1.3: Contribution of the different terms to the total cross section for the $\nu_\mu n \to \mu K^0 p$ reaction.

larger and could become more important at higher energies.

Finally, the reaction $\nu_l + n \to l^- + K^+ + n$ has a smaller cross section. The pion exchange term is substantially bigger than the u-channel mechanisms, as already noted in Ref. [75]. The contact term is also dominant for this channel and the total cross section calculated only with this term practically coincides with the full result. Therefore, we have found that the contact terms, required by symmetry, play a major role in the description of the kaon production induced by neutrinos at low energies.

Above the energy threshold for the production of kaons accompanied by hyperons, this latter kind of processes could have larger cross sections due to the larger coupling for $\Delta S = 0$, (V_{ud} vs V_{us}). To explore this question and the range of energies where the processes we have just studied are relevant, we compare our results in Fig. 1.4, with the values for the associated production obtained by means of the GENIE Monte Carlo program [90]. We observe that, due to the difference between the energy thresholds, single

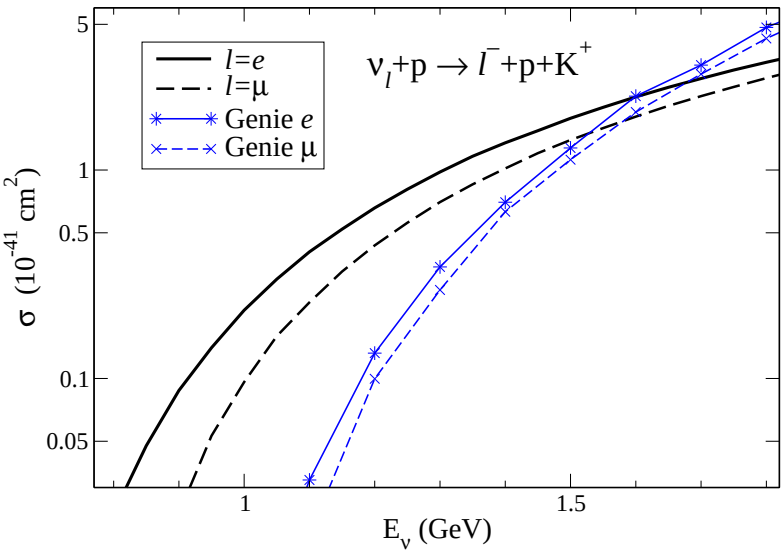

Figure 1.4: Cross sections as a function of the neutrino energy for single kaon production vs. associated production obtained with Genie [90].

Table 1.2: Cross sections averaged over the neutrino flux at different laboratories in units of 10^{-41} cm^2. Theoretical uncertainties correspond to a 10% variation of the form factor mass.

Process	ANL	MiniBooNE	T2K
$\nu_\mu n \to \mu^- K^+ n$	0.06(1)	0.07(1)	0.09(1)
$\nu_\mu p \to \mu^- K^+ p$	0.28(5)	0.32(5)	0.43(8)
$\nu_\mu n \to \mu^- K^0 p$	0.17(3)	0.20(3)	0.25(5)

kaon production for the $\nu_l + p \to l^- + K^+ + p$ is clearly dominant for neutrinos of energies below 1.5 GeV. The consideration of these $\Delta S = 1$ channels is therefore important for the description of strangeness production for all low energy neutrino spectra and should be incorporated in the experimental analysis.

At higher energies, the dominance of associated production seems to be well established experimentally. Although this model is not appropriate for those energies, we have tested that at 20 GeV, single kaon production channels would be less than 1% of the charged current total cross section.

In Table 1.2 we show the total cross section results for the three channels averaged over the ANL [91], the MiniBooNE [40] and the off-axis (2.5 degrees) T2K [92] muon neutrino fluxes, all of them peaking at around 0.6 GeV. After normalization of the neutrino flux ϕ we have

$$\bar{\sigma} = \int_{E_{\rm th}}^{E_{\rm high}} dE\, \phi(E)\sigma(E), \tag{1.20}$$

where $E_{\rm th}$ is the threshold energy for each process and $E_{\rm high}$ is the maximum neutrino energy. As discussed previously, in these three cases, the neutrino energies are low enough for single kaon production to be relevant as compared to associated kaon production. Also the invariant mass of the hadronic system and the transferred momentum only reach the relatively small values where this model is more reliable.

We can get an idea of the magnitude of these channels by comparing their cross section to some recent results. For instance, the cross section for neutral current π^0 production per nucleon has been measured by the MiniBooNE collaboration [93] obtaining $\bar{\sigma} = (4.76 \pm 0.05 \pm 0.76) \times 10^{-40}$ cm^2

Table 1.3: Number of events calculated for single kaon production in water corresponding to the SuperK analysis for atmospheric neutrinos.

Process	Events e^-	Events μ^-
$\nu_l n \to l^- n K^+$	0.16	0.27
$\nu_l n \to l^- p K^0$	0.45	0.73
$\nu_l p \to l^- p K^+$	0.95	1.55
Total	1.56	2.55

with a data set of some twenty thousand valid events. The cross sections predicted by this model with the same neutrino flux are around two orders of magnitude smaller, what means that a few hundreds of kaons should have been produced.

The atmospheric spectrum [94] also peaks at very low energies and this model should be very well suited to analyse the kaon production. In Table 1.3, we show the number of kaon events that we obtain for the 22.5 kTons of a water target and a period of 1489 days as in the SuperK analysis [72] of proton decay. As in the quoted paper, we include cuts in the electron momentum ($p_e > 100$ MeV) and muon momentum ($p_\mu > 200$ MeV). We find that single kaon production is a very small source of background. In the SuperK analysis the kaon production was modeled following Ref. [48] and only included associated kaon production. Although some of the cuts applied in their analysis, such as looking for an accompanying hyperon, are useless for this case, we find that this source of background is negligible, given the smallness of our results and the totally different energy distribution of kaons and final leptons in the production and decay reactions.

Finally, we study the values of Q^2 involved in the reaction for the typical neutrino energies we have considered. If high values of this magnitude are relevant, the results would be sensitive to higher orders of the chiral Lagrangians and/or a more precise description of the form factors. We show the Q^2 distribution in Fig. (1.5) for the three studied channels at a neutrino energy $\mathrm{E}_\nu = 1$ GeV. The reactions are always forward peaked (for the final lepton), even in the absence of any form factor ($F(q^2) = 1$), favouring relatively small values of the momentum transfer. In this figure, we also show the dependence of the cross section on the mass of the final lepton that re-

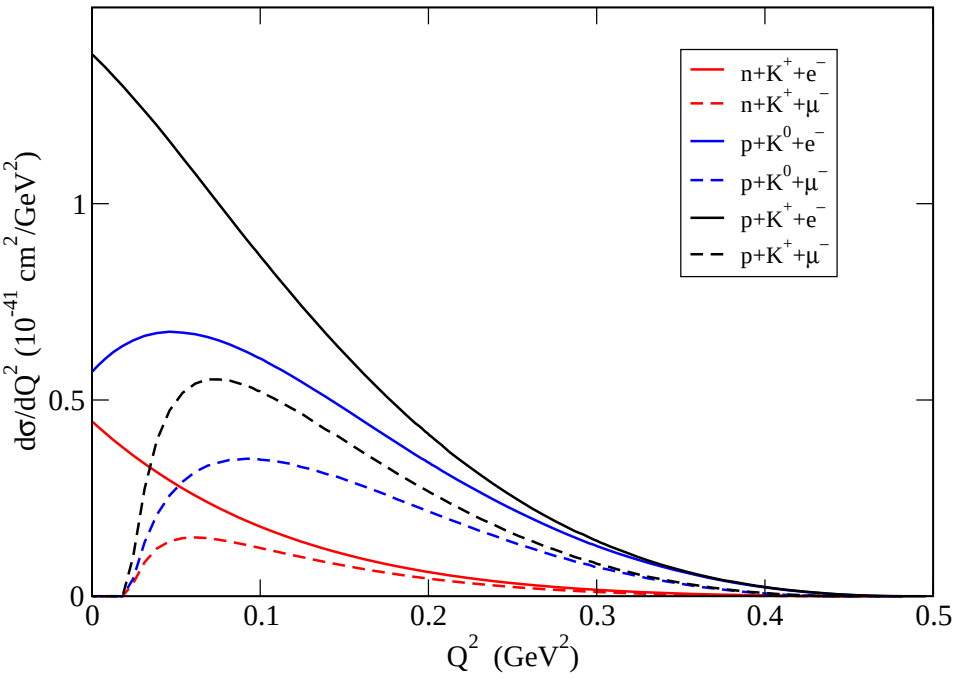

Figure 1.5: $\frac{d\sigma}{dQ^2}$ at $E_\nu = 1$ GeV for single kaon production induced by neutrinos. The curves are labeled according to the final state of the process.

duces the cross section at low Q^2 values. The process $\nu_e + n \to e^- + K^0 + p$ shows a slightly different behavior that reflects an important (and Q^2 dependent) interference between the pion exchange and the contact term.
Until now we have discussed the kaon production off free nucleons. However, most of the experiments are carried out on detectors containing complex nuclei such as iron, oxygen or carbon. On the other hand, nuclear effects are known to be quite large for pion production induced by neutrinos. Fortunately, this question is much simpler for the kaons. First, because there is no kaon absorption and the final state interaction is reduced to a repulsive potential, small when compared with the typical kaon energies. Second, because of the absence of resonant channels in the production processes. We should remember here that some of the major nuclear effects for pion production are originated by the modification of the $\Delta(1232)$ properties on nuclei. Other nuclear effects, such as Fermi motion and Pauli blocking will only produce minor changes on the cross section and can easily be implemented in the Monte Carlo codes.

1.1.4 Summary

In summary, we have developed a microscopical model for single kaon production off nucleons induced by neutrinos based on the SU(3) chiral Lagrangians. This model should be quite reliable at low and intermediate energies given the absence of $S = 1$ baryonic resonances in the s-channel. The parameters of the model are well known: f_π, the pion decay constant, Cabibbo's angle, the proton and neutron magnetic moments and the axial vector coupling constants for the baryons octet, D and F. For the latter ones, we have taken the values obtained from the analysis of the hyperon semileptonic decays. The importance of higher order terms has been estimated using a dipole form factor with a mass around 1 GeV and exploring the dependence of our results on this parameter.
We obtain cross sections that are around two orders of magnitude smaller than for pion production for neutrino spectra such as those of ANL or MiniBooNE. This can be understood because of the Cabibbo suppression and of the smaller phase space. Nonetheless, the cross sections are large enough to be measured, for instance, with the expected Minerva and T2K fluxes. We have also found, that due to the higher threshold of the associated kaon production, the reactions we have studied are the dominant source of kaons

for a wide range of energies, and thus their study is important for some low energy experiments and for the atmospheric neutrino flux.

1.2 Antikaon production induced by antineutrinos

In the previous section we have discussed single kaon production induced by neutrinos at low and intermediate energies using Chiral Perturbation Theory (χPT). We found that at $E_{\nu_\mu} < 1.2$ GeV, it is the single kaon production which dominates over the associated production of kaons along with hyperons which is mainly due to threshold effect (1.10 GeV vs. 0.79 GeV). Therefore, in the energy region of MiniBooNE or T2K neutrino spectrum, the lepton production accompanied by a single kaon production has larger contributions in comparison to the associated production processes. While the associated production has been taken into account in the Monte Carlo generators, the single kaon production is absent. This has motivated us to study the antineutrino induced single antikaon production off nucleons and to compare the results with the cross section available for the associated production in these energy regions. Its study may be useful in the analysis of antineutrino experiments at MiniBooNE or MINERνA and NOνA.
The theoretical model is necessarily more complicated than for kaons because resonant mechanisms, absent for the kaon case, could be relevant. On the other hand, the threshold for associated antikaon production corresponds to the $K - \bar{K}$ channel and it is much higher than for the kaon case (KY). This implies that the process that will be discussed in this section is the dominant source of antikaons for a wide range of energies. We shall present the results for the cross sections as well as the flux averaged cross section for the MiniBooNE experiment at Fermilab and the lepton event rates for atmospheric neutrino experiment at SuperK.

1.2.1 Formalism

The basic reaction for antineutrino induced charged-current $\Delta S = -1$ antikaon production is,

$$\bar{\nu}_l(k) + N(p) \to l(k') + N'(p') + \bar{K}(p_k), \tag{1.21}$$

where $l = e^+, \mu^+$ and $N\&N'$=n,p.
The expression for the differential cross section in the LAB frame will be the same than for kaon production, Eq. (1.2).
At low energies, again, the invariant transition matrix element can be written as the product of the leptonic current with the hadronic one, see Eq.

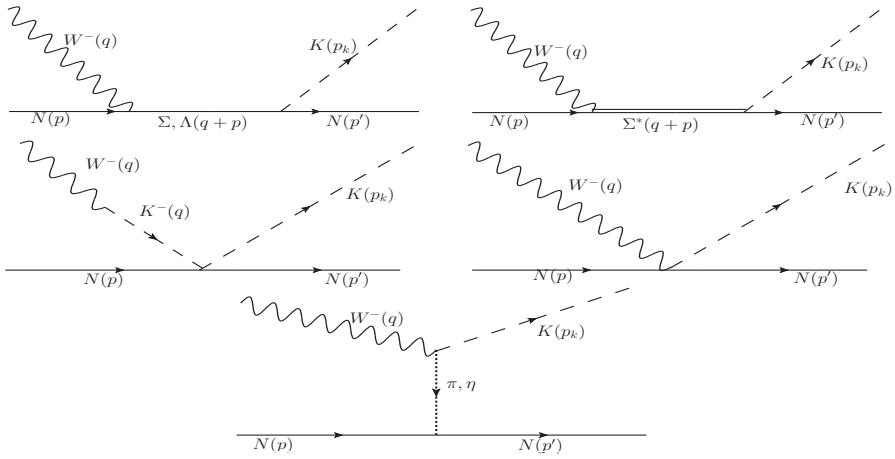

Figure 1.6: Feynman diagrams for the process $\bar{\nu}N \to lN'\bar{K}$. First row from left to right: s-channel Σ, Λ propagator (labeled SC in the text), s-channel Σ^* Resonance (SCR), second row: kaon pole term (KP); Contact term (CT) and last row: Pion(Eta) in flight πP (ηP).

(1.3). The leptonic current in this case reads:

$$j^{\mu}_{(L)} = \bar{v}_{\nu}(\vec{k})\gamma^{\mu}(1-\gamma_5)v_l(\vec{k}') \tag{1.22}$$

We consider five different channels that contribute to the hadronic current. They are depicted in Fig. 1.6. There are s-channel Σ, Λ(SC) and Σ^*(SCR) as intermediate states, a kaon pole (KP) term, a contact term (CT), and finally a meson (πP,ηP) exchange term. We take only the $\Sigma^*(1385)$ resonance. Although we know that other baryonic resonances, beyond the $\Sigma^*(1385)$ and also close to the $\bar{K}N$ threshold, could contribute to the cross section, we are not going to consider them because their weak couplings are basically unknown, and because their theoretical estimations are still quite uncertain. Nonetheless, recent advances on the radiative decays of these resonances, both experimental and theoretical (see, e.g., Refs. [95, 96]) are very promising and may help to develop a more complete model in the future.
The contribution coming from the different terms can be obtained from χPT. We are going to use the same lagrangians in the presence of an external current than in the previous section. With one additional piece, we need the

lagrangian that couples the decuplet to the baryon and meson octets.
The SU(3) Lagrangian coupling the pseudoscalar mesons with decuplet-octet baryons in presence of external weak current is given by (where a sum over repeated indices must be understood),

$$\mathcal{L}_{dec} = \mathcal{C}\left(\epsilon^{abc}\bar{T}^{\mu}_{ade}(u_\mu)^d_b B^e_c + h.c.\right) \tag{1.23}$$

where T^μ is the SU(3) representation of the decuplet fields. The physical states of the decuplet are: $T_{111} = \Delta^{++}, T_{112} = \frac{\Delta^+}{\sqrt{3}}, T_{122} = \frac{\Delta^0}{\sqrt{3}}, T_{222} = \Delta^-, T_{113} = \frac{\Sigma^{*+}}{\sqrt{3}}, T_{123} = \frac{\Sigma^{*0}}{\sqrt{6}}, T_{223} = \frac{\Sigma^{*-}}{\sqrt{3}}, T_{113} = \frac{\Xi^+}{\sqrt{3}}, T_{133} = \frac{\Xi^0}{\sqrt{3}}, T_{333} = \Omega^-$. And u_μ is a SU(3) matrix given by Eq. (1.13). To calculate $\mathcal{C}$ we fit the Δ^{++} width ($\Gamma \sim 112$ MeV) and obtained $\mathcal{C} \sim 1.0$.
As it is the case for the $\Delta(1232)$ in pion production, we expect that, at intermediate energies, the weak excitation of the $\Sigma^*(1385)$ resonance and its subsequent decay into $N\bar{K}$ is also important. To calculate amplitudes associated with Σ^* we first parameterize the $W^- N \to \Sigma^*$. For this, we can write the most general form of the vector and axial-vector transition matrix elements as,

$$\begin{aligned}
\langle \Sigma^*; P = p + q\,|V^\mu|N; p\rangle &= V_{us}\bar{u}_\alpha(\vec{P})\Gamma_V^{\alpha\mu}(p,q)\,u(\vec{p}), \\
\langle \Sigma^*; P = p + q\,|A^\mu|N; p\rangle &= V_{us}\bar{u}_\alpha(\vec{P})\Gamma_A^{\alpha\mu}(p,q)\,u(\vec{p})
\end{aligned} \tag{1.24}$$

where

$$\begin{aligned}
\Gamma_V^{\alpha\mu}(p,q) &= \left[\frac{C_3^V}{M}(g^{\alpha\mu}\not{q} - q^\alpha\gamma^\mu) + \frac{C_4^V}{M^2}(g^{\alpha\mu}q\cdot P - q^\alpha P^\mu)\right. \\
&+ \left.\frac{C_5^V}{M^2}(g^{\alpha\mu}q\cdot p - q^\alpha p^\mu) + C_6^V g^{\mu\alpha}\right]\gamma_5 \\
\Gamma_A^{\alpha\mu}(p,q) &= \left[\frac{C_3^A}{M}(g^{\alpha\mu}\not{q} - q^\alpha\gamma^\mu) + \frac{C_4^A}{M^2}(g^{\alpha\mu}q\cdot P - q^\alpha P^\mu) + C_5^A g^{\alpha\mu}\right. \\
&+ \left.\frac{C_6^A}{M^2}q^\mu q^\alpha\right]
\end{aligned} \tag{1.25}$$

In the above expression $C^V_{3,4,5,6}$ and $C^A_{3,4,5,6}$ are the q^2-dependent scalar and real vector and axial-vector form factors and u_α is the Rarita-Schwinger

spinor. Our knowledge of these form factors is quite limited. The Lagrangian of Eq. (1.23) gives us only $C_5^A(0) = -2\mathcal{C}/\sqrt{3}$ (for the Σ^{*-} case). However, using SU(3) symmetry we can relate all other form factors to those of the $\Delta(1232)$ resonance, such that $C_i^{\Sigma^{*-}}/C_i^{\Delta^+} = -1$ and $C_i^{\Sigma^{*-}}/C_i^{\Sigma^{*0}} = \sqrt{2}$. See Refs. [39, 47, 97–99] for details of the $WN\Delta$ form-factors. In the Δ case, the vector form factors are relatively well known from electromagnetic processes and there is some information on the axial ones from the study of pion production. In case of axial-vector part of the current the most dominant term is C_5^A [97]. We can obtain the kaon pole contribution to C_6^A by evaluating the Feynman diagram in which the W^- couples the nucleon to Σ^* through a kaon. But this contribution will be very small as it is proportional to $\frac{q^\mu q^\nu}{M^2}$ and can be neglected. Since there is not any other theoretical constraints on the $C_{3,4}^A$, they are fitted with the available neutrino scattering data and are found to be negligible.

Here we consider only the contribution coming from the C_5^A, C_3^V and C_4^V form factors for the $N-\Sigma^*$ weak vertex. We follow the conventions used for the $N-\Delta$ form factors (see Refs. [47, 97] for details of $N-\Delta$ form factors and for the dominance of C_5^A).

The hadronic currents are given by

$$
\begin{aligned}
j^\mu|_{CT} &= iA_{CT}V_{us}\frac{\sqrt{2}}{2f_\pi}\bar{N}(p')\,(\gamma^\mu + B_{CT}\,\gamma^\mu\gamma_5)\,N(p)\\
j^\mu|_{\Sigma} &= iA_{\Sigma}(D-F)V_{us}\frac{\sqrt{2}}{2f_\pi}\bar{N}(p')\not{p}_k\gamma_5\frac{\not{p}+\not{q}+M_\Sigma}{(p+q)^2-M_\Sigma^2}\\
&\times \left(\gamma^\mu + i\frac{(\mu_p+2\mu_n)}{2M}\sigma^{\mu\nu}q_\nu\right.\\
&+ \left.(D-F)\left\{\gamma^\mu - \frac{q^\mu}{q^2-{M_k}^2}\not{q}\right\}\gamma^5\right)N(p)\\
j^\mu|_{\Lambda} &= iA_{\Lambda}V_{us}(D+3F)\frac{1}{2\sqrt{2}f_\pi}\bar{N}(p')\not{p}_k\gamma^5\frac{\not{p}+\not{q}+M_\Lambda}{(p+q)^2-M_\Lambda^2}\\
&\times \left(\gamma^\mu + i\frac{\mu_p}{2M}\sigma^{\mu\nu}q_\nu - \frac{(D+3F)}{3}\left\{\gamma^\mu - \frac{q^\mu}{q^2-{M_k}^2}\not{q}\right\}\gamma^5\right)N(p)\\
j^\mu|_{KP} &= iA_{KP}V_{us}\frac{\sqrt{2}}{2f_\pi}\bar{N}(p')\not{q}\,N(p)\frac{q^\mu}{q^2-M_k^2}\\
j^\mu|_{\pi} &= iA_{\pi}\frac{M\sqrt{2}}{2f_\pi}V_{us}(D+F)\frac{2{p_k}^\mu - q^\mu}{(q-p_k)^2-{M_\pi}^2}\bar{N}(p')\gamma_5 N(p)\\
j^\mu|_{\eta} &= iA_{\eta}\frac{M\sqrt{2}}{2f_\pi}V_{us}(D-3F)\frac{2{p_k}^\mu - q^\mu}{(q-p_k)^2-{M_\eta}^2}\bar{N}(p')\gamma_5 N(p)\\
j^\mu|_{\Sigma^*} &= iA_{\Sigma^*}\frac{\mathcal{C}}{f_\pi}\frac{1}{\sqrt{6}}\,V_{us}\,\bar{N}(p')\frac{p_k^\alpha\,P^{RS}_{\alpha\beta}(P)}{P^2-M^2_{\Sigma^*}+i\Gamma_{\Sigma^*}M_{\Sigma^*}}\tilde{\Gamma}^{\beta\mu}(p,q)N(p);\\
&\text{where}\quad P=p+q\quad\text{and}\quad \tilde{\Gamma}^{\beta\mu}\equiv\Gamma^{\beta\mu}_{\Sigma^*-}
\end{aligned}
$$

with the constants given in the following table 1.4.

For the Σ^* resonance we have used the usual spin-3/2 propagator in the momentum space, given by

$$G^{\mu\nu}(P) = \frac{P^{\mu\nu}_{RS}(P)}{P^2 - M^2_{\Sigma^*} + iM_{\Sigma^*}\Gamma_{\Sigma^*}}, \qquad \text{where} \tag{1.26}$$

Process	B_{CT}	A_{CT}	A_Σ	A_Λ	A_{KP}	A_π	A_η	A_{Σ^*}
$\bar{\nu}n \to l^+K^-n$	D-F	1	-1	0	-1	1	1	2
$\bar{\nu}p \to l^+K^-p$	-F	2	$-\frac{1}{2}$	1	-2	-1	1	1
$\bar{\nu}p \to l^+\bar{K}^0n$	-D-F	1	$\frac{1}{2}$	1	-1	-2	0	-1

Table 1.4: Table with the values of the different constants used for the hadronic currents.

$P^{\mu\nu}_{RS}$ is the spin-3/2 Rarita-Schwinger projection operator,

$$P^{\mu\nu}_{RS}(P) = \sum_{spins} \psi^\mu \bar{\psi}^\nu = -(\not{P}+M_{\Sigma^*}) \left[g^{\mu\nu} - \frac{1}{3}\gamma^\mu\gamma^\nu - \frac{2}{3}\frac{P^\mu P^\nu}{M^2_{\Sigma^*}} + \frac{1}{3}\frac{P^\mu\gamma^\nu - P^\nu\gamma^\mu}{M_{\Sigma^*}} \right] \tag{1.27}$$

with M_{Σ^*} is the resonance mass ($\sim$ 1385 MeV) and ψ^μ is the Rarita-Schwinger spinor for spin-3/2 particles.
The Σ^* decay width Γ_{Σ^*} is around 40 MeV (see Ref. [100]), however, we have taken P-wave decay width which is given as

$$\begin{aligned} \Gamma_{\Sigma^*}(W) &= \Gamma_{\Sigma^*\to\Lambda\pi}(W) + \Gamma_{\Sigma^*\to\Sigma\pi}(W) + \Gamma_{\Sigma^*\to N\bar{K}}(W) \qquad \text{where,} \\ \Gamma_{\Sigma^*\to YM}(W) &= \frac{C_Y}{192\pi}\left(\frac{\mathcal{C}}{f_\pi}\right)^2 \frac{\left((W+M_Y)^2 - m^2_M\right)}{W^5}\lambda^{3/2}(W^2, M^2_Y, m^2_M) \\ &\times \Theta(W - M_Y - m_M) \end{aligned} \tag{1.28}$$

where M_Y is the mass of the baryon Y(Λ, Σ or N) in which the $\Sigma^*(1385)$ decays; m_M is the mass of the meson M(π or $\bar{K}$); C_Y is a SU(3) Clebsch-Gordan coefficient and it is 1 for $\Lambda\pi$ decay and $\frac{2}{3}$ for $\Sigma\pi$ and $\bar{K}N$ decays. $\lambda(x,y,z) = (x-y-z)^2 - 4yz$ is Callen lambda function and Θ is the step function. $\mathcal{C}$ is the $\bar{K}N\Sigma^*$ coupling strength taken to be 1.0 in the present calculation.
Finally, we consider the q^2 dependence of the weak current couplings provided by the chiral Lagrangians. In this section, we follow the same procedure as in the previous one and adopt a global dipole form factor $F(q^2) = 1/(1 - q^2/M_F^2)^2$, with a mass $M_F \simeq 1$ GeV that multiplies all the hadronic currents, except the resonant one, that has been previously discussed. Its effect, that should be small at low neutrino energies will give an idea of the uncertainties of the calculation and will be explored in the next subsection.

1.2.2 Results

We consider the following charged-current reactions:

$$\begin{aligned} \bar{\nu}_l + p &\rightarrow l^+ + K^- + p \quad (l = e,\ \mu) \\ \bar{\nu}_l + p &\rightarrow l^+ + \bar{K}^0 + n \\ \bar{\nu}_l + n &\rightarrow l^+ + K^- + n \end{aligned} \tag{1.29}$$

In Fig. 1.7, we show their total cross section for electronic and muonic

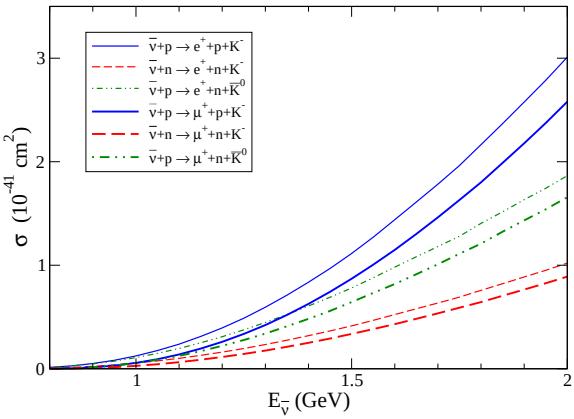

Figure 1.7: Cross-section for the processes $\bar{\nu}_\mu N \rightarrow \mu^+ N' \bar{K}$ and $\bar{\nu}_e N \rightarrow e^+ N' \bar{K}$ as a function of the antineutrino energy

antineutrinos as a function of energy. We obtain similar values for the cross sections of kaon production induced by neutrinos of the previous section, even when there are no resonant contributions. The electronic antineutrino cross sections are slightly larger, but they do not present any other distinguishing feature. For all channels, the cross sections are very small, as compared to other processes induced by antineutrinos at these energies, like pion production, due to the Cabibbo suppression and to the smallness of the available phase space.

Before discussing in more detail each of the channels, we will make some comments. First, the lowest energy antikaon associate production, ($K\bar{K}$, $\Delta S = 0$), has a quite high threshold (≈ 1.75 GeV) and thus, it leads to

Table 1.5: $< \sigma > (10^{-41} cm^2)$ for $\bar{K}$ production with MiniBooNE $\bar{\nu}_\mu$ flux and neutral current π^0 production (per nucleon) measured at MiniBooNE [93]

Process	$< \sigma >$
$\bar{\nu}_\mu + p \rightarrow \mu^+ + K^- + p$	0.11
$\bar{\nu}_\mu + p \rightarrow \mu^+ + \bar{K}^0 + n$	0.08
$\bar{\nu}_\mu + n \rightarrow \mu^+ + K^- + n$	0.04
$\bar{\nu}_\mu + N \rightarrow \bar{\nu}_\mu + N + \pi^0$	$14.8 \pm 0.5 \pm 2.3$

even smaller cross sections in the range of energies we have explored. For instance, at 2 GeV, GENIE predicts antikaon production cross sections at least two orders of magnitude smaller than our calculation.

As it was expected, our results would lead to a very minor signal in past experiments. For instance, we have evaluated the flux averaged cross section $< \sigma >$ for the MiniBooNE antineutrino flux [101] in the sub GeV energy region. The results are given in Table 1.5 and compared with the recent measurement of the neutral current π^0 production per nucleon with the same flux [93].

We find that the antikaon production cross section is around two orders of magnitude smaller than the NC π^0 one at MiniBooNE. Given the number of neutral pions observed for the antineutrino beam we expect that only a few tens of antikaons were produced in this experiment. One should notice here that the average antineutrino energy at MiniBooNE is well below the kaon threshold. Thus, we are only sensitive to the high energy tail of the flux.

One could expect a relatively larger signal for the atmospheric neutrino $\bar{\nu}_e$ and $\bar{\nu}_\mu$ induced events at SuperK, given the larger neutrino energies. But even there we find a very small background from antikaon events. Taking the antineutrino fluxes from Ref. [94] we have calculated the event rates for the 22.5kT water target and a period of 1489 days as in the SuperK analysis of Ref. [27]. We obtain 0.8 e^+ and 1.5 μ^+ events. Although the model has large uncertainties at high energies, the rapid fall of the neutrino spectrum implies that the high energy tail contributes very little to the background. Our results correspond to relatively low antineutrino energies, where our model is more reliable. However, the model could also be used to com-

pare with data obtained at much higher neutrino energies selecting events such that the invariant mass of hadronic part is close to antikaon-nucleon threshold and the transferred momentum q is small. This procedure has been used, for instance, in the analysis of two pion production induced by neutrinos [102, 103].

In Fig. 1.8, we show the size of several contributions to the $\bar{\nu}_\mu p \to \mu^+ p K^-$ reaction.

The cross section is clearly dominated by the non–resonant terms, provid-

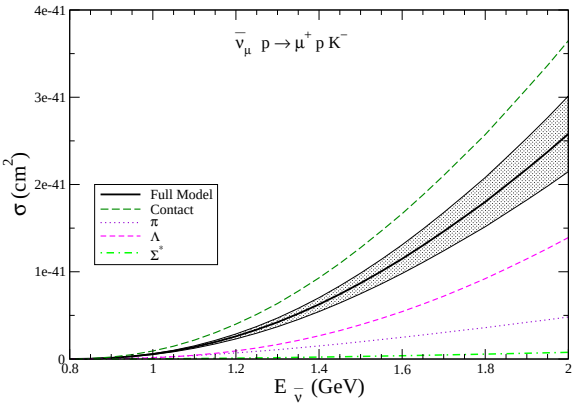

Figure 1.8: Cross-section for the process $\bar{\nu}_\mu p \to \mu^+ p K^-$.

ing the CT term the largest contribution. We see the destructive interference that leads to a total cross section smaller than that predicted by the CT term alone. We could also remark the negligible contribution of the $\Sigma^*(1385)$ channel. This fact is at variance with the strong Δ dominance for pion production and it can be easily understood because the Σ^* mass is below the antikaon production threshold.

We have also explored, the uncertainties associated with the form factor. The curve labeled as "Full Model" has been calculated with a dipole form factor with a mass of 1 GeV. The band corresponds to a 10 percent variation of this parameter. The effect is similar in the other channels and we will only show the results for the central value of 1 GeV.

In Figs. 1.9 and 1.10, we show the other two channels. As in the previous case the CT term is very important. We observe, however, that the pion-

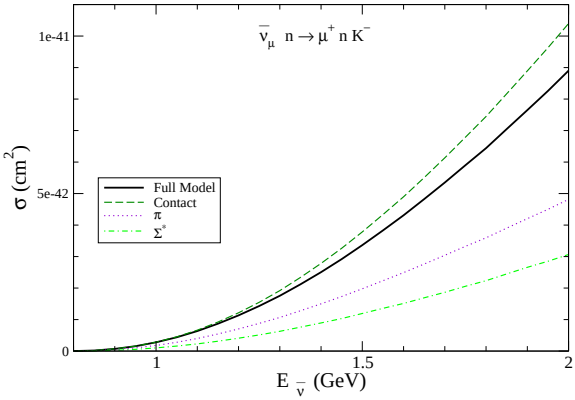

Figure 1.9: Cross-section for $\bar{\nu}_\mu n \to \mu^+ n K^-$.

pole term gives a contribution as large as the CT one for the $\bar{\nu}_\mu p \to \mu^+ n K^0$ process. For the $\bar{\nu}_\mu n \to \mu^+ n K^-$ case, we find a substantial contribution of the Σ^* resonance, due to the larger value of the couplings (see Table 1.4). As in the first case, there is some destructive interference between the different mechanisms participating in these processes.

1.2.3 Summary

In this section we have developed a model for $\bar{K}$-production off free nucleons that includes all the background terms obtained from the chiral lagrangians and also the resonant mechanism with the corresponding member of the baryon decuplet ($\Sigma^*(1385)$) in resemblance with the models for weak pion production off the nucleon.
The only parameter of the model that has been fitted is the coupling constant between the baryon decuplet, the baryon octet and the octet of pseudoscalar mesons. This coupling constant has been adjusted to reproduce the $\Delta(1232)$ width and then used to obtain the width of the $\Sigma^*(1385)$ resonance and also the coupling $C_5^A(0)$ for the $N - \Sigma^*$ weak vertex.
We have calculated cross sections as a function of the antineutrino energy that could be helpful in the analysis of strange particle production

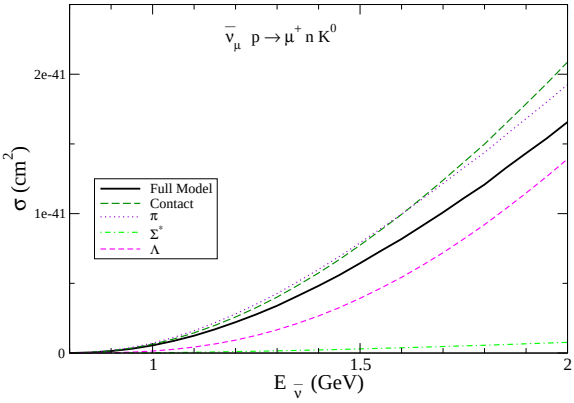

Figure 1.10: Cross-section for $\bar{\nu}_\mu p \to \mu^+ n \bar{K}^0$.

in MINERνA experiment.
We have also obtained the number of events for $\bar{K}$ production at SuperK with the atmospheric antineutrino flux.
In the case of $\bar{K}$ production event rates at MiniBooNE we have estimated that they are very small as compared to the kaon case because the average energy of the antineutrino flux in MiniBooNE is below the threshold for single $\bar{K}$ production and the size of the flux for antineutrinos is smaller than for neutrinos.

Chapter 2

Inclusive reactions in nuclei at low and intermediate energies

2.1 Introduction

The interaction of neutrinos with nuclei at intermediate energies plays an important role in the precise determination of neutrino properties such as their masses and mixing parameters. It can also provide relevant information on the axial hadronic currents. However, the data analysis needs to consider a large number of nuclear effects that distort the signals and produce new sources of background that are absent in the elementary neutrino-nucleon processes.

The aim of this chapter is the elaboration of a theoretically well founded and unified framework in which the electroweak interactions with nuclei could be systematically studied. Furthermore, the recent measurements of the cross sections for several channels [40, 104–106] provide a serious benchmark to the theoretical models. An excellent review of the current situation can be found in Ref. [107].

A suitable theoretical model should include, at least, three kinds of contributions: (i) quasielastic (QE)[1] for low energy transfers, (ii) pion production

[1] A word of caution is needed here, because the same words could refer to somehow different magnitudes in the literature. For instance, whereas in most theoretical works

and two-body processes from the QE region to that around the $\Delta(1232)$ resonance peak, and (iii) double pion production and higher nucleon resonance degrees of freedom induced processes at even higher energies.

The QE processes have been abundantly studied in the literature. Simple approaches using a global Fermi gas for the nucleons and the impulse approximation are good enough to describe qualitatively electron scattering, but more sophisticated treatments of the nuclear effects are necessary to get a detailed agreement with data. There are different kinds of models like those based on the use of proper nucleon spectral functions [83,108,109], others in which nucleons are treated in a relativistic mean field [110,111] and models based on a local Fermi gas including many body effects such as spectral functions [39] and Random-Phase Approximation (RPA)[2] [38,112–114].

Concerning the elementary process, $\nu + N \rightarrow l + N'$, the hadronic vector current is well known from electron scattering. The axial-vector current, after the use of the partial conservation of the axial current (PCAC) to relate the two form factors and assuming a dipole form, depends on two parameters: g_A, that can be fixed from neutron beta decay; and the axial mass M_A. The value of M_A established from QE data on deuterium targets is $M_A = 1.016 \pm 0.026$ GeV, see Ref. [41]. A consistent result is obtained from π electro-production after chiral corrections are incorporated [42,115]. The predicted cross sections for QE scattering are very similar for most models, see the compilation shown in Fig. 2 of Ref. [116]. On the other hand, these theoretical results are clearly below the recently published MiniBooNE data [40]. Some works try to understand these new data in terms of a larger value of M_A. For instance, in Ref. [40] a value of $M_A = 1.35 \pm 0.17$ GeV, that also fits the Q^2 shape, is extracted. Consistent values are obtained in Refs. [117–119]. This idea enters in conflict with higher energy NOMAD data [120] ($M_A = 1.06 \pm 0.02(stat) \pm 0.06(syst)$ GeV). Another idea, which

QE is used for processes where the gauge boson $W^{\pm}$ or Z^0 is absorbed by just one nucleon, which is emitted together with a lepton, in the recent MiniBooNE papers, QE is related to processes in which only a muon is detected. This latter definition could make sense because ejected nucleons are not detected in that experiment, but it also includes multinucleon processes and others like pion production followed by absorption. However, it discards pions coming off the nucleus, since they will give rise to additional leptons after their decay. In any case, their experimental results cannot be directly compared to most previous calculations.

[2] In this dissertation, for QE scattering, our work will be based on the model of Ref. [38]

has been explored in Refs. [44, 45], is to include two-nucleon mechanisms (and others related to Δ excitation). These results reproduce the MiniBooNE flux-unfolded CCQE cross section data without the need of a larger value of M_A. The calculation of these contributions will be explained with detail in this chapter.

The matter of π production is also of much interest [47,56,84,98,99,121,122]. The elementary reaction on the nucleon, at low and intermediate energies, includes both background and resonant mechanisms. The background terms can be obtained from the chiral lagrangians. The resonant terms contain some free parameters that have been adjusted to ANL and/or BNL old bubble chamber data. These experimental data have large normalization uncertainties which are certainly reflected in the theoretical models. At low energies, the $\Delta(1232)$ resonance plays a very important role in this process, and for small Q^2 values only one form factor (C_5^A) is relevant. Thus, special attention has been paid to its study with recent results ranging from $C_5^A(0) = 1.19 \pm 0.08$ [122], obtained neglecting the non-resonant background, up to $C_5^A(0) = 1.00 \pm 0.11$ [99] in a more complete model. In nuclei, several effects are expected to be important for the π production reaction. Indeed, the elementary process is modified by Fermi motion, Pauli blocking and by the changes of the spectral function of the Δ resonance in the medium. In addition, the final pion can be absorbed or scattered by one or more nucleons. This latter kind of effects does not modify the inclusive neutrino-nucleus cross section and thus it is out of the scope of this chapter.

Our aim in this chapter is to extend the model of Ref. [38], which studied QE scattering. We will include two nucleon processes and π production in a well established framework, that has been tested in electron [43] and photon scattering [123]. This will extend the range of applicability of the model to higher transferred energies (and thus higher neutrino energies) and it will allow for the comparison with inclusive data which include the QE peak, the Δ resonance peak and the dip region between them.

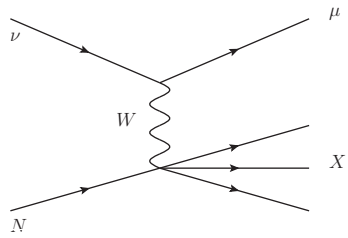

Figure 2.1: Feynman diagram for CC muon neutrino induced processes

2.2 Formalism

2.2.1 Selfenergy of the neutrino

We will focus on the inclusive nuclear reaction, corresponding to the Feynman diagram of fig. 2.1.

$$\nu_l(k) + A_Z \rightarrow l^-(k') + X \tag{2.1}$$

Neglecting the four momentum transferred with respect to the mass of the intermediate W boson, the following invariant amplitude is obtained

$$\mathcal{T} = \frac{G_F}{\sqrt{2}}\, \bar{u}_l(\vec{k'})\gamma^\mu(1-\gamma_5)u_\nu(\vec{k})\, \langle X|j_\mu^{cc+}(0)|N\rangle \tag{2.2}$$

where $G_F = 1.16639(1)\times 10^{-5}$ GeV^{-2} is the Fermi constant and $\langle X|j_\mu^{cc+}(0)|N\rangle$ stands for the weak CC transition matrix element.
After calculating $|\mathcal{T}|^2$ and summing (averaging) over the polarizations of the final (initial) states, one obtains

$$\overline{\sum}\sum |\mathcal{T}|^2 = 4\, G_F^2\; L^{\mu\nu}(k,k')\, \overline{\sum_{\mathtt{spin\,N}}} \sum_{\mathtt{spin\,X}} \langle X|j_\mu^{cc+}(0)|N\rangle \langle X|j_\nu^{cc+}(0)|N\rangle^* \tag{2.3}$$

where $L^{\mu\nu}(k,k')$ is the leptonic tensor given by[3]

$$L^{\mu\nu}(k,k') = k^\mu k'^\nu + k'^\mu k^\nu - g^{\mu\nu}(k\cdot k') \pm i\epsilon^{\mu\nu\alpha\beta}k_\alpha k'_\beta = L_s^{\mu\nu} \pm iL_a^{\mu\nu} \tag{2.4}$$

[3]We will use the convention in which $\epsilon^{0123} = 1$

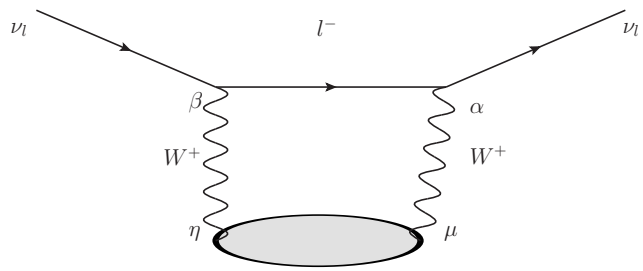

Figure 2.2: Feynman diagram for the selfenergy of a neutrino

with $L_s^{\mu\nu}(L_a^{\mu\nu})$ standing for the symmetric (antisymmetric) part of the leptonic tensor; and the plus (minus) sign in the antisymmetric piece referring to neutrino (antineutrino) scattering.
Given the Feynman diagram for the selfenergy of the neutrino, see fig. 2.2, this selfenergy can be calculated applying the Feynman rules to give

$$\begin{aligned} -i\Sigma_\nu^r(k) &= \int \frac{d^4q}{(2\pi)^4}\left(\frac{-ig}{2\sqrt{2}}\right)^2 \bar{u}_r(\vec{k})\gamma^\alpha(1-\gamma_5)\frac{i(\not{k}'+m_l)}{k'^2-m_l^2+i\epsilon}\gamma^\beta(1-\gamma_5)u_r(\vec{k}) \\ &\times \frac{(-i)g_{\beta\eta}}{q^2-M_W^2+i\epsilon}\left(-i\Pi_W^{\eta\mu}(q)\right)\frac{(-i)g_{\mu\alpha}}{q^2-M_W^2+i\epsilon} \end{aligned} \tag{2.5}$$

In the above equation, neglecting the four-momentum q carried by the W boson with respect to its mass (in fact this has been already assumed because in the numerators of the bare propagators for the W boson, we have discarded terms like $\frac{q_\beta q_\eta}{M_W^2}$) and after performing the contractions of Lorentz indices, we obtain

$$-i\Sigma_\nu^r(k) = \int \frac{d^4q}{(2\pi)^4}\frac{G_F}{\sqrt{2}M_W^2}\bar{u}_r(\vec{k})\gamma^\alpha(1-\gamma_5)\frac{(\not{k}'+m_l)}{k'^2-m_l^2+i\epsilon}\gamma^\beta(1-\gamma_5)u_r(\vec{k})\Pi_{\beta\alpha}^W(q) \tag{2.6}$$

where $\Pi_{\beta\alpha}^W(q)$ is the selfenergy of the W boson in the nuclear medium and the relation between the Fermi constant and the gauge coupling is $\frac{G_F}{\sqrt{2}} = \frac{g^2}{8M_W^2}$.
If now we perform the sum over the two polarizations of the neutrino (what is justified because the chirality projectors $(1-\gamma_5)$ filter only the physical

polarization), then a trace over the leptonic line is obtained.

$$\begin{aligned}\Sigma_\nu(k) &= \frac{iG_F}{\sqrt{2}M_W^2}\int\frac{d^4q}{(2\pi)^4}\frac{\mathtt{Tr}\left(\gamma^\alpha(1-\gamma_5)(\not{k}'+m_l)\gamma^\beta(1-\gamma_5)\not{k}\right)}{k'^2-m_l^2+i\epsilon}\Pi^W_{\beta\alpha}(q)\\ &= \frac{8iG_F}{\sqrt{2}M_W^2}\int\frac{d^4q}{(2\pi)^4}\frac{L^{\beta\alpha}(k,k')\Pi^W_{\beta\alpha}(q)}{k'^2-m_l^2+i\epsilon}\end{aligned} \tag{2.7}$$

If now we separate the tensor $\Pi^W_{\beta\alpha}(q)$ in its symmetric and antisymmetric parts, namely:

$$\Pi^W_{\beta\alpha}(q)=\frac{1}{2}\left(\Pi^W_{\beta\alpha}+\Pi^W_{\alpha\beta}\right)+\frac{1}{2}\left(\Pi^W_{\beta\alpha}-\Pi^W_{\alpha\beta}\right)\equiv\Pi^s_{\beta\alpha}+i\Pi^a_{\beta\alpha} \tag{2.8}$$

where the superscript s (a) stands for the symmetric (antisymmetric) part of $\Pi^W_{\beta\alpha}(q)$.
We can easily insert eq. (2.4) into the selfenergy of the neutrino, eq. (2.7) and perform the contractions. Thus, the following expression is obtained:

$$\Sigma_\nu(k)=\frac{8iG_F}{\sqrt{2}M_W^2}\int\frac{d^4q}{(2\pi)^4}\frac{\left(L_s^{\beta\alpha}\Pi^s_{\beta\alpha}-L_a^{\beta\alpha}\Pi^a_{\beta\alpha}\right)}{k'^2-m_l^2+i\epsilon} \tag{2.9}$$

Following the steps of Ref. [38], it can be shown that the cross section is related to the imaginary part of the selfenergy of the neutrino by means of the formula

$$\sigma=-\frac{1}{|\vec{k}|}\int d^3r\,\mathrm{Im}\Sigma_\nu(k;\rho(\vec{r})) \tag{2.10}$$

We have considered Σ_ν as a function of the nuclear density in every point. Thus, we are working in the Local Density Approximation (LDA).
To obtain the imaginary part of the selfenergy of the neutrino in the nuclear medium, we will make use of the Cutkosky rules. These rules mean that we put on-shell the intermediate states. Technically they reduce to make the following substitutions in eq. (2.9)

$$\begin{aligned}\Sigma_\nu(k) &\rightarrow 2i\,\mathrm{Im}\Sigma_\nu(k)\\ \Pi^{s(a)}_{\beta\alpha}(q) &\rightarrow 2i\theta(q^0)\,\mathrm{Im}\Pi^{s(a)}_{\beta\alpha}(q)\\ \frac{1}{k'^2-m_l^2+i\epsilon} &\rightarrow 2i\theta(k'^0)\cdot(-\pi)\cdot\delta(k'^2-m_l^2)\end{aligned} \tag{2.11}$$

where $\theta(\cdots)$ is the step function and $\delta(\cdots)$ is the Dirac delta function. With the aid of the Dirac delta function, the integral in q^0 in eq. (2.9) can be carried out and we obtain (after a change of variable) the following expression for $\mathrm{Im}\Sigma_\nu(k)$

$$\begin{aligned}\mathrm{Im}\Sigma_\nu(k) &= \frac{8G_F}{\sqrt{2}M_W^2}\int\frac{d^3k'}{(2\pi)^3}\frac{\theta(k^0-E_l')}{2E_l'(\vec{k}')}\times\Big\{L_s^{\beta\alpha}\,\mathrm{Im}\Pi^s_{\beta\alpha}(q)\\ &- L_a^{\beta\alpha}\,\mathrm{Im}\Pi^a_{\beta\alpha}(q)\Big\}_{q^0=k^0-E_l'}\end{aligned} \tag{2.12}$$

where $E_l'(\vec{k}') = \sqrt{m_l^2+\vec{k}'^2}$ is the on-shell energy for a charged lepton of mass m_l and momentum $\vec{k}'$.
Inserting eq. (2.12) in eq. (2.10) and letting the kinematic variables of the outgoing lepton without integrating, we get the following expression for the double differential cross section:

$$\begin{aligned}\frac{d\sigma}{d\Omega_{\hat{k}'}\,dE_l'} &= -\frac{|\vec{k}'|}{|\vec{k}|}\frac{G_F^2}{4\pi^2}\frac{1}{2\pi}\left(\frac{2\sqrt{2}}{g}\right)^2\int d^3r\,\theta(k^0-E_l')\times\Big(L_s^{\beta\alpha}\,\mathrm{Im}\left(\Pi^W_{\beta\alpha}+\Pi^W_{\alpha\beta}\right)\\ &+ L_a^{\beta\alpha}\,\mathrm{Re}\left(\Pi^W_{\beta\alpha}-\Pi^W_{\alpha\beta}\right)\Big)\end{aligned} \tag{2.13}$$

The hadronic tensor is given (except phase space factors) basically by:

$$W_{\mu\nu} = \overline{\sum_{\mathtt{spin\,N}}\sum_{\mathtt{spin\,X}}}\langle X|j_\mu^{cc+}(0)|N\rangle\langle X|j_\nu^{cc+}(0)|N\rangle^* \tag{2.14}$$

and it accomplishes

$$W^{\mu\nu} = W_s^{\mu\nu} + iW_a^{\mu\nu} \tag{2.15}$$

with $W_s^{\mu\nu}$ ($W_a^{\mu\nu}$) real symmetric (antisymmetric) tensors.
Thus, the double differential cross section can be cast as (see eq. 3 in Ref. [38]):

$$\frac{d\sigma}{d\Omega_{\hat{k}'}\,dE_l'} = \frac{|\vec{k}'|}{|\vec{k}|}\frac{G_F^2}{4\pi^2}L^{\alpha\beta}W_{\alpha\beta} = \frac{|\vec{k}'|}{|\vec{k}|}\frac{G_F^2}{4\pi^2}\left(L_s^{\beta\alpha}\,W^s_{\beta\alpha} - L_a^{\beta\alpha}\,W^a_{\beta\alpha}\right) \tag{2.16}$$

Comparing the above equation with eq. (2.13), we can obtain the following assignments:

$$W^s_{\beta\alpha} = -\theta(q^0)\left(\frac{2\sqrt{2}}{g}\right)^2 \int \frac{d^3r}{2\pi}\,\mathrm{Im}\left(\Pi^W_{\beta\alpha}+\Pi^W_{\alpha\beta}\right) \tag{2.17}$$

$$W^a_{\beta\alpha} = \theta(q^0)\left(\frac{2\sqrt{2}}{g}\right)^2 \int \frac{d^3r}{2\pi}\,\mathrm{Re}\left(\Pi^W_{\beta\alpha}-\Pi^W_{\alpha\beta}\right) \tag{2.18}$$

The in medium gauge boson ($W^{\pm}$) selfenergy now depends on the nuclear density $\rho(r)$. We propose a many body expansion for $\Pi^{\mu\nu}_W$, where the relevant gauge boson absorption modes would be systematically incorporated: absorption by one nucleon, or a pair of nucleons or even three nucleon mechanisms, real and virtual meson (π, ρ,...) production, excitation of Δ isobars or higher resonance degrees of freedom, etc. In addition, nuclear effects such as Random Phase Approximation (RPA) or Short Range Correlations (SRC) will be also taken into account. Some of the basic W-absorption modes are depicted in Fig 2.3.

2.2.2 Quasielastic scattering

It is not the purpose of this thesis to discusse in detail the QE scattering, this was done in Ref. [38]. But as we are going to use their results, we must devote some words to it.
The virtual W^+ can be absorbed by one nucleon leading to the QE contribution of the nuclear response function. Such a process corresponds to a one particle-one hole (1p1h) nuclear excitation (first of the diagrams depicted in fig 2.3). We are going to briefly discuss the main features of the model of Ref. [38]. Starting from a Local Fermi Gas (LFG) picture of the nucleus, which automatically accounts for Pauli blocking and Fermi motion, several nuclear corrections were incorporated, among others:

1. A correct energy balance, using the experimental Q-values, was enforced.

2. Coulomb distortion of the charged leptons, important at low energies, was implemented by using the so called "modified effective momentum approximation".

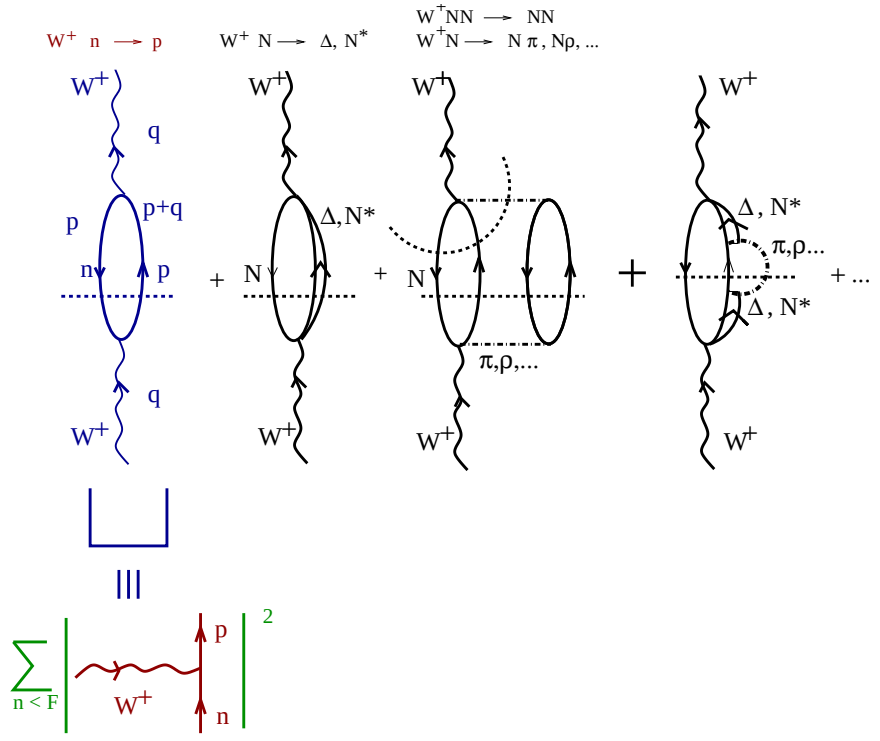

Figure 2.3: Diagrammatic representation of some mechanisms contributing to the W^+-selfenergy

3. Medium polarization (RPA), including Δ-hole degrees of freedom and explicit pion and rho exchanges in the vector-isovector channel of the effective nucleon-nucleon force, and SRC effects were computed.

4. The nucleon propagators were dressed in the nuclear medium, which means to work with nucleon spectral functions (a LFG of interacting nucleons) and it also accounts for some reaction mechanisms where the gauge boson is absorbed by two nucleons.

This model is a natural extension of previous studies on electron [43], photon [123] and pion [124–128] dynamics in nuclei.
The theoretical errors which affect the predictions of Ref. [38] were discussed in Ref. [129]. There, it was concluded that it is sound to assume errors of about 10-15% on the QE neutrino-nucleus (differential and integrated) cross section results of Ref. [38].
The LFG description of the nucleus has been shown to be well suited for inclusive processes and nuclear excitation energies of around 100 MeV or higher. The reason is because in these circumstances one should sum up over several nuclear configurations, both in the discrete and in the continuum. This inclusive sum is almost insensitive to the details of the nuclear wave function. This is in sharp contrast to what happens in the case of exclusive processes, when the final nucleus is left in a determined nuclear level. On the other hand, the LFG description of the nucleus allows for an accurate treatment of the dynamics of the elementary processes (interaction of gauge bosons with nucleons, nucleon resonances and mesons, interaction between nucleons or between mesons and nucleons, etc.) which occur inside the nuclear medium. Within a finite nuclei scenario, such a treatment becomes hard to implement, and often the dynamics is simplified in order to deal with more elaborated nuclear wave functions.

2.2.3 $\Delta(1232)$ Dominance in pion production

The first diagram that we are going to consider is the second one depicted in Fig 2.3. This corresponds to a Nucleon-Δ transition. The transition matrix element is given by:

$$\left\langle \Delta^+; p_\Delta = p + q | j^\mu_{cc+}(0) | n; p \right\rangle = \bar{u}_\alpha(\vec{p}_\Delta) \Gamma^{\alpha\mu}(p,q) u(\vec{p}) \cos\theta_c \qquad (2.19)$$

where $\bar{u}_\alpha(\vec{p}_\Delta)$ is the Rarita-Schwinger spinor for the Δ; θ_c is the Cabibbo angle for the transition of a down quark into an up quark; and the weak vertex function is given by:

$$\begin{aligned}\Gamma^{\alpha\mu}(p,q) &= \Big[\frac{C_3^V}{M}(g^{\alpha\mu}\not{q} - q^\alpha\gamma^\mu) + \frac{C_4^V}{M^2}(g^{\alpha\mu}(q\cdot p_\Delta) - q^\alpha p_\Delta^\mu) \\ &+ \frac{C_5^V}{M^2}(g^{\alpha\mu}(q\cdot p) - q^\alpha p^\mu) + C_6^V g^{\alpha\mu}\Big]\gamma_5 \\ &+ \Big[\frac{C_3^A}{M}(g^{\alpha\mu}\not{q} - q^\alpha\gamma^\mu) + \frac{C_4^A}{M^2}(g^{\alpha\mu}(q\cdot p_\Delta) - q^\alpha p_\Delta^\mu) + C_5^A g^{\alpha\mu} \\ &+ \frac{C_6^A}{M^2}q^\alpha q^\mu\Big] \qquad (2.20)\end{aligned}$$

where $p_\Delta = p + q$ and the $C_i^{V,A}$ are scalar and real vector (V) and axial (A) form factors depending on q^2. The determination of the form factors follows from general principles and also from experimental results. We will use the set of form factors from Ref. [47] with only one exception, namely the value for C_5^A at $q^2 = 0$. For $C_5^A(0)$ we will take advantage from a recent analysis of the pion production process induced by neutrinos, done in Ref. [99], to set it to 1.0 and for $M_{A\Delta}$ (the axial mass that governs the q^2 dependence) we will take 0.93 GeV. In summary, that we are going to use the set IV given in table I of Ref. [99].

Let us begin with the following Feynman diagram for the Δ-hole contribution, depicted in fig 2.4. Its contribution to the W^+ selfenergy can be written as:

$$-i\Pi_{\Delta h}^{\mu\nu} = -\cos^2\theta_c\left(\frac{g}{2\sqrt{2}}\right)^2\int\frac{d^4p}{(2\pi)^4}G(p;\rho_n)\frac{1}{p_\Delta^2 - M_\Delta^2 + iM_\Delta\Gamma_\Delta}A_\Delta^{\mu\nu}(p,q) \qquad (2.21)$$

with $p_\Delta = p + q$, M_Δ the resonance mass and Γ_Δ its width, which can be found for instance in Eq. (45) of Ref. [47]. $G(p;\rho_n)$ is the neutron propagator given by[4]:

$$G(p;\rho) = \frac{1}{p^0 + E(\vec{p}) + i\epsilon}\left(\frac{n(\vec{p})}{p^0 - E(\vec{p}) - i\epsilon} + \frac{1 - n(\vec{p})}{p^0 - E(\vec{p}) + i\epsilon}\right) \qquad (2.22)$$

In the above equation, $n(\vec{p})$ stands for the hole occupation number, i.e, $n(\vec{p}) = \theta(k_F - |\vec{p}|)$. And finally, the tensor $A_\Delta^{\mu\nu}(p,q)$ is given by the following

[4]In appendix A it will be shown a derivation of Eq. (2.22)

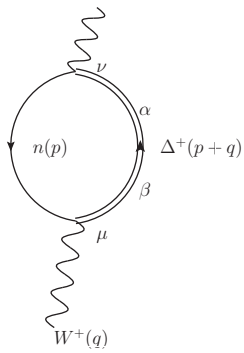

Figure 2.4: Diagrammatic representation of the Δh weak nuclear excitation term

trace:

$$A^{\mu\nu}_{\Delta}(p,q) = \mathrm{Tr}\left[(\not{p} + M)\gamma^0\Gamma^{\alpha\nu\dagger}\gamma^0 P_{\alpha\beta}(p_\Delta)\Gamma^{\beta\mu}\right] \tag{2.23}$$

$P_{\alpha\beta}(p_\Delta)$ is the spin-3/2 on-shell projection operator:

$$P_{\alpha\beta}(p_\Delta) = (\not{p}_\Delta + M_\Delta)\left[-g_{\alpha\beta} + \frac{1}{3}\gamma_\alpha\gamma_\beta + \frac{2}{3}\frac{p_{\Delta\alpha}p_{\Delta\beta}}{M^2_\Delta} - \frac{1}{3}\frac{p_{\Delta\alpha}\gamma_\beta - p_{\Delta\beta}\gamma_\alpha}{M_\Delta}\right] \tag{2.24}$$

The tensor $A^{\mu\nu}_{\Delta}(p,q)$ accomplishes the following fundamental relation:

$$A^{\mu\nu *} = A^{\nu\mu} \tag{2.25}$$

This relation means that the symmetric part of such a tensor is real and that its antisymmetric part is purely imaginary. And furthermore, the statement is also valid in the opposite direction, i.e, the real part of such a tensor is symmetric and the imaginary one is antisymmetric.
Therefore, the tensor $A^{\mu\nu}_{\Delta}(p,q)$ can be written like the hadronic one, eq. (2.15). These properties of symmetry are very useful to obtain the contributions of this absorption mode to the hadronic tensor, eqs. (2.17) and (2.18). Coming back to eq. (2.21), we can take the symmetric or antisymmetric parts of the W^+ selfenergy, just replacing the tensor $A^{\mu\nu}_{\Delta}(p,q)$ by its symmetric or antisymmetric parts. Thus, it is trivial to obtain the following expression:

$$\Pi^{\mu\nu}_{s(a)}(q) = -i\cos^2\theta_c\left(\frac{g}{2\sqrt{2}}\right)^2\int\frac{d^4p}{(2\pi)^4}G(p;\rho_n)G_\Delta(p_\Delta)A^{\mu\nu}_{s(a)}(p,q) \tag{2.26}$$

where $A^{\mu\nu}_{s(a)}(p,q)$ stands for the symmetric (antisymmetric) part of $A^{\mu\nu}_{\Delta}(p,q)$. Now, we can perform the integration in p^0 and we would pick up the pole for the hole state in the nucleon propagator, eq. (2.22). After that integration, we easily obtain the following expression for a neutron hole:

$$\begin{aligned} W^{\mu\nu}_n &= -\theta(q^0)\int\frac{d^3r}{2\pi}\cos^2\theta_c\int\frac{d^3p}{(2\pi)^3}\frac{\theta(k^n_F(r)-|\vec{p}|)}{E(\vec{p})}\mathrm{Im}G_\Delta(p+q)\mid_{p^0=E(\vec{p})} \\ &\times A^{\mu\nu}_{\Delta}(p,q)\mid_{p^0=E(\vec{p})} \end{aligned} \tag{2.27}$$

What would happen if the W^+ is absorbed by a proton? Well, invoking isospin symmetry, the weak transition vertex for proton to Δ^{++} is a factor $\sqrt{3}$ bigger than the one in eq. (2.19). As this weak vertex appears twice when folding it with its complex conjugate, we would have a factor 3 with respect to the previous equation:

$$\begin{aligned} W^{\mu\nu}_p &= -3\,\theta(q^0)\int\frac{d^3r}{2\pi}\cos^2\theta_c\int\frac{d^3p}{(2\pi)^3}\frac{\theta(k^p_F(r)-|\vec{p}|)}{E(\vec{p})}\mathrm{Im}G_\Delta(p+q)\mid_{p^0=E(\vec{p})} \\ &\times A^{\mu\nu}_{\Delta}(p,q)\mid_{p^0=E(\vec{p})} \end{aligned} \tag{2.28}$$

The sum of both hadronic tensors, eqs. (2.27) and (2.28), can be written in a compact way:

$$\begin{aligned} W^{\mu\nu}_{\Delta h}(q) &= -\theta(q^0)\cos^2\theta_c\int\frac{d^3r}{2\pi}\int\frac{d^3p}{(2\pi)^3}\sum_N C^2_N\,\frac{\theta(k^N_F(r)-|\vec{p}|)}{E(\vec{p})} \\ &\times \mathrm{Im}G_\Delta(p+q)\mid_{p^0=E(\vec{p})}\,A^{\mu\nu}_{\Delta}(p,q)\mid_{p^0=E(\vec{p})} \end{aligned} \tag{2.29}$$

where the isospin factor C_N takes the values 1 and $\sqrt{3}$ for neutron and proton hole contributions, respectively. And we have defined $G_\Delta(p_\Delta)$ as the Δ-propagator, namely:

$$G_\Delta(p_\Delta) = \frac{1}{p^2_\Delta - M^2_\Delta + iM_\Delta\Gamma_\Delta} \tag{2.30}$$

2.2.4 Addition of background terms in pion production

In this subsection we are going to calculate the contribution to the cross section from W^+ gauge boson selfenergy diagrams which contain pion production in the intermediate states. We will use the model for the CC pion

production reaction off the nucleon induced by neutrinos,

$$\nu_l(k) + N(p) \to l^-(k') + N(p') + \pi(k_\pi) \tag{2.31}$$

derived in Refs. [47, 99]. This process, at intermediate energies, is traditionally described in the literature by means of the weak excitation of the $\Delta(1232)$ resonance and its subsequent decay into $N\pi$. In Ref. [47], some background terms required by the pattern of spontaneous chiral symmetry breaking of QCD were also included. Their contributions are sizable and lead to significant effects in total and partially integrated pion production cross sections even at the $\Delta(1232)$-resonance peak, and they are dominant near pion thresold. The model consists of seven Feynman diagrams for the $W^+N \to N'\pi$ reaction (see right panel of Fig. 2.5). The contributions of the different diagrams are calculated by using the effective Lagrangian of the SU(2) nonlinear σ-model, supplemented with some form factors (see Ref. [47] for details). As we have mentioned in the previous subsection, in this work, we will use the set IV of form factors compiled in Table I of Ref. [99]. The available data set on neutrino and antineutrino pion production on nucleons is described reasonably well. Nonetheless, we must mention that the experimental data still have large uncertainties and there exist conflicting data for some channels.

The discussed model can be considered an extension of that developed in Ref. [43] for the $eN \to e'N\pi$ reaction. For the latter case, the model, which contains a theoretically well founded description of the background amplitudes, provides the same level of accuracy [56] as the MAID model [53], which ensures its applicability to the leptoproduction processes at least up to $W < 1.4$ GeV, being W the outgoing πN invariant mass.

We move now to the computation of the W^+-selfenergy diagrams which contain pion production in the intermediate states. This can be accomplished by taking the $W^+N \to N'\pi$ amplitudes of Fig. 2.5 and folding them with themselves. One thus obtains the diagram of Fig. 2.6 where the circle stands for the total amplitude (sum of the seven terms of the elementary model for $W^+N \to N'\pi$) that connects the states $N \to N'\pi^\lambda$.

Let us do the calculation only for one channel, for instance for the $p \to p\pi^+$ channel. The generalization to all the channels is simply the sum of the W^+-selfenergies for every channel. Just applying the Feynman rules, we

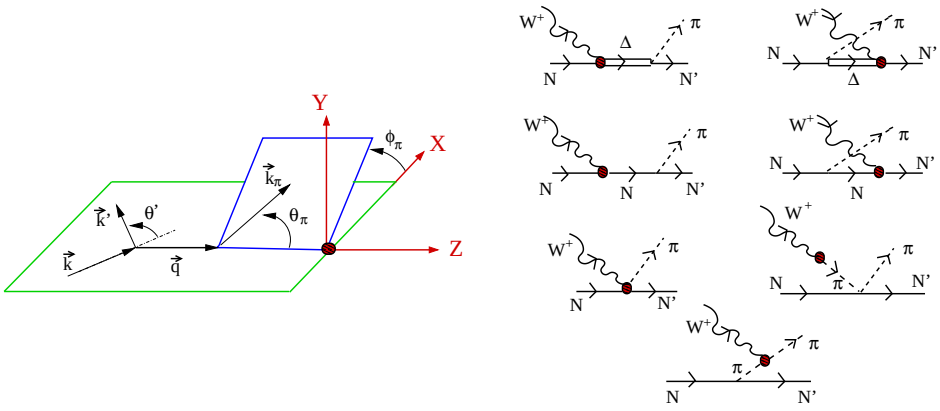

Figure 2.5: Left: Definition of the kinematical variables. Right: Model for the $W^+N \to N'\pi$ reaction. It consists of seven diagrams: Direct and crossed $\Delta(1232)$-pole (first row) and nucleon-pole (second row) terms; contact term and pion pole contribution (third row); and finally the pion-in-flight term. Throughout this work, we will label these contributions by: ΔP, $C\Delta P$,NP,CNP,CT,PP and PF, respectively. The circle in the diagrams stands for the weak transition vertex.

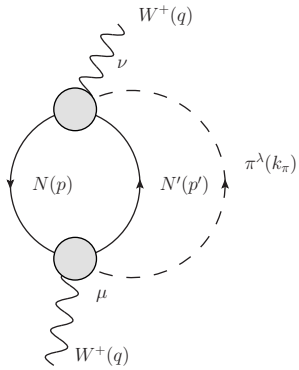

Figure 2.6: W-selfenergy obtained by folding the $WN \to N'\pi$ amplitude with itself (λ is the charge of the pion).

obtain for the selfenergy:

$$-i\Pi^{\mu\nu}_{p\to p\pi^+}(q) = -i\left(\frac{g}{2\sqrt{2}}\right)^2 \int \frac{d^4k_\pi}{(2\pi)^4} D_0(k_\pi) \int \frac{d^4p}{(2\pi)^4} G(p;\rho_p) G(p+q-k_\pi;\rho_p) \times A^{\mu\nu}_{p\to p\pi^+}(p,q,k_\pi) \tag{2.32}$$

where $D_0(k_\pi)$ is the pion propagator:

$$D_0(k_\pi) = \frac{1}{k_\pi^2 - m_\pi^2 + i\epsilon} \tag{2.33}$$

and $A^{\mu\nu}_{p\to p\pi^+}(p,q,k_\pi)$ is given by the trace of the fermionic loop:

$$A^{\mu\nu}_{p\to p\pi^+}(p,q,k_\pi) = \mathrm{Tr}\left[J^{\mu}_{p\to p\pi^+}(\not{p}+M)\gamma^0 J^{\nu\dagger}_{p\to p\pi^+}\gamma^0(\not{p}+\not{q}-\not{k}_\pi+M)\right] \tag{2.34}$$

where $J^{\mu}_{p\to p\pi^+}$ is the total amputated amplitude (without nucleon spinors) for the $W^+p \to p\pi^+$ process, i.e, the sum of the seven amputated amplitudes of the right panel of Fig. 2.5 for this channel. The contribution to $J^{\mu}_{p\to p\pi^+}$ from every diagram is given by their relation with the full amplitudes given in Eq. (51) of Ref. [47],

$$j^{\mu}_{cc+}|_i = \bar{u}(\vec{p}\,')\, j^{\mu}_{A_i}(p,q,p'=p+q-k_\pi,k_\pi)\, u(\vec{p}), \qquad i = \Delta P, C\Delta P, NP, CNP, CT, PP, PF \tag{2.35}$$

and

$$J^{\mu} = \sum_i j^{\mu}_{A_i} \qquad i = \Delta P, C\Delta P, NP, CNP, CT, PP, PF \tag{2.36}$$

Performing the integration in p^0 in eq. (2.32) and neglecting the contribution coming from the antiparticle pole ($p^0 = -E(\vec{p}) - i\epsilon$), i.e, we must replace the propagator of eq. (2.22) by the following one:

$$G(p) = \frac{1}{2E(\vec{p})}\left\{\frac{n(\vec{p})}{p^0 - E(\vec{p}) - i\epsilon} + \frac{1-n(\vec{p})}{p^0 - E(\vec{p}) + i\epsilon}\right\} \tag{2.37}$$

then, we obtain

$$\Pi^{\mu\nu}_{p\to p\pi^+}(q) = i\left(\frac{g}{2\sqrt{2}}\right)^2 \int \frac{d^4k_\pi}{(2\pi)^4} D_0(k_\pi) \int \frac{d^3p}{(2\pi)^3} \frac{1}{2E(\vec{p})} \frac{1}{2E(\vec{p}\,')} A^{\mu\nu}_{p\to p\pi^+}|_{p^0=E(\vec{p})} \times \left\{\frac{n(\vec{p})(1-n(\vec{p}\,'))}{q^0 - k^0_\pi + E(\vec{p}) - E(\vec{p}\,') + i\epsilon} + \frac{(1-n(\vec{p}))n(\vec{p}\,')}{-q^0 + k^0_\pi - E(\vec{p}) + E(\vec{p}\,') + i\epsilon}\right\} \tag{2.38}$$

where $\vec{p}' = \vec{p} + \vec{q} - \vec{k}_\pi$.
A simplification can be done by evaluating the $J^\mu_{p\to p\pi^+}$ amplitudes at an average momentum, which allows us to take out the spin trace (tensor $A^{\mu\nu}$) from the d^3p integration. This latter integration can now be done, and it gives, up to some constants, the Lindhard function $\bar{U}_R(q-k_\pi; k_F^p, k_F^p)$ defined in appendix B of Ref. [38]. We take $\langle|\vec{p}|\rangle = \sqrt{\frac{3}{5}}k_F^p$ (where $k_F^p = (3\pi^2\rho_p(r))^{1/3}$, being $\rho_p(r)$ the density of protons normalized to the number of protons) and a direction orthogonal to the plane defined by the pion and the virtual gauge boson. Within this approximation, we find

$$\Pi^{\mu\nu}_{p\to p\pi^+}(q) = \frac{i}{8M^2}\left(\frac{g}{2\sqrt{2}}\right)^2 \int \frac{d^4k_\pi}{(2\pi)^4} D_0(k_\pi)\bar{U}_R(q-k_\pi; k_F^p, k_F^p) A^{\mu\nu}_{p\to p\pi^+}|^{<\vec{p}>}_{p^0=E(\vec{p})} \tag{2.39}$$

where $A^{\mu\nu}_{p\to p\pi^+}|^{<\vec{p}>}_{p^0=E(\vec{p})}$ stands for the following expression

$$A^{\mu\nu}_{p\to p\pi^+}|^{<\vec{p}>}_{p^0=E(\vec{p})} = \mathrm{Tr}\left[\left\langle J^\mu_{p\to p\pi^+}\right\rangle (\langle\not{p}\rangle + M)\gamma^0 \left\langle J^{\nu\dagger}_{p\to p\pi^+}\right\rangle \gamma^0(\langle\not{p}\rangle + \not{q} - \not{k}_\pi + M)\right] \tag{2.40}$$

and the amputated amplitudes $\left\langle J^\mu_{p\to p\pi^+}\right\rangle$ have been calculated with the average hole momentum $\langle\vec{p}\rangle$. We remind that, by construction, the tensor $A^{\mu\nu}_{p\to p\pi^+}$ accomplishes eq. (2.25) and thus, it can be decomposed in the following form

$$A^{\mu\nu} = A^{\mu\nu}_s + iA^{\mu\nu}_a \tag{2.41}$$

with $A^{\mu\nu}_s$ ($A^{\mu\nu}_a$) real symmetric (antisymmetric) tensors. And furthermore, given the decomposition in eq. (2.8), we readily obtain

$$\mathrm{Im}\left(\Pi^{\mu\nu} + \Pi^{\nu\mu}\right) = 2\,\mathrm{Im}\Pi^{\mu\nu}_s \tag{2.42}$$

$$\mathrm{Re}\left(\Pi^{\mu\nu} - \Pi^{\nu\mu}\right) = -2\,\mathrm{Im}\Pi^{\mu\nu}_a \tag{2.43}$$

Here, $\Pi^{\mu\nu}_{s(a)}$ is defined as in Eq. (2.39) but replacing the full tensor $A^{\mu\nu}$ by its symmetric (antisymmetric) $A^{\mu\nu}_{s(a)}$ parts. The imaginary part of $\Pi^{\mu\nu}_{s(a)}$ can be obtained by following the prescription of the Cutkosky's rules. In this case we cut with a straight horizontal line the intermediate particle and hole states and the pion. These states are then placed on-shell by taking the imaginary part of the propagator. Considering that the Lindhard function

plays the role of a particle-hole propagator, then the Cutkosky's rules reduce to make the following substitutions:

$$\begin{aligned} \Pi^{\mu\nu}_{s(a)} &\rightarrow 2i\,\mathrm{Im}\Pi^{\mu\nu}_{s(a)} \\ D_0(k_\pi) &\rightarrow 2i\,\theta(k^0_\pi)\mathrm{Im}D_0(k_\pi) = -2\pi i\delta(k^2_\pi - m^2_\pi)\theta(k^0_\pi) \\ \bar{U}_R(q-k_\pi;k^p_F,k^p_F) &\rightarrow 2i\,\theta(q^0-k^0_\pi)\mathrm{Im}\bar{U}_R(q-k_\pi;k^p_F,k^p_F) \end{aligned} \tag{2.44}$$

With the aid of the imaginary part of the bare pion propagator, we can perform the integration in the variable k^0_π and then we are left with the integration in the 3-momentum of the pion. Until now, we have focused on the channel $p \rightarrow p + \pi^+$. The kind of calculation is similar for the channels $n \rightarrow n + \pi^+$ and $n \rightarrow p + \pi^0$. There are some different isospin factors in the amputated amplitudes (currents) in each vertex, because these currents depend on the particular channel that one is considering. And there will be changes in the Lindhard's functions as well because of the dependence of these functions on the local Fermi momenta for hole and particle states. The final contribution to the hadronic tensor will be the sum of the contributions for every channel. This can be written in a compact way like this [5]

$$\begin{aligned} W^{\mu\nu}_{1\mathrm{ph}1\pi}(q) &= -\frac{1}{8M^2}\theta(q^0)\int\frac{d^3r}{2\pi}\int\frac{d^3k_\pi}{(2\pi)^3}\frac{\theta(q^0-E_\pi)}{E_\pi(\vec{k}_\pi)} \\ &\times \sum_{N,N',\lambda}\mathrm{Im}\bar{U}_R(q-k_\pi;k^N_F,k^{N'}_F)A^{\mu\nu}_{N\rightarrow N'\pi^\lambda} \end{aligned} \tag{2.45}$$

2.2.5 Two-particles two-holes (2p2h) absorption modes

2p2h mechanisms driven by the longitudinal part of the effective spin-isospin ph-ph interaction

In this section we are going to deal with diagrams in which the pion is allowed to excite a particle-hole. This leads us to the diagram of Fig. 2.7. This is still a generic diagram which actually contains 49 diagrams when in the shaded circle we put each one of the terms of the $W^+p \rightarrow \pi^+p$ amplitude of the right pannel of Fig. 2.5.

[5] In appendix B it will be shown that this hadronic tensor fulfills the Impulse Approximation in the Low Density Limit

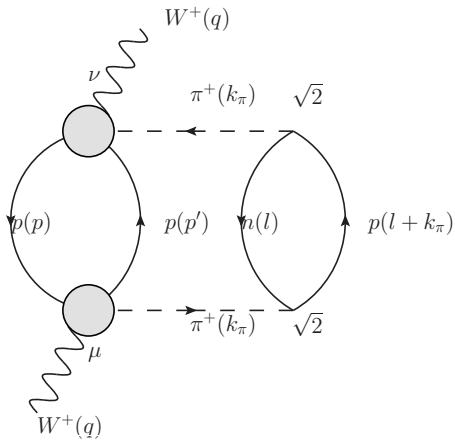

Figure 2.7: W-selfenergy obtained from the one in Fig. 2.6 when the pion line is allowed to excite a particle-hole. This is one of the four channels that we have.

For the πNN vertex that couples the pion to a particle-hole pair in the right bubble of Fig 2.7, we are going to take the following lagrangian:

$$\mathcal{L} = \frac{g_A}{2f_\pi}\bar{\psi}(x)\gamma^\mu\gamma_5\vec{\tau}\cdot\partial_\mu\vec{\phi}(x)\psi(x) \tag{2.46}$$

where $g_A = 1.26$, f_π is the pion decay constant, $\psi(x)$ is the isospin doublet which contains the Dirac fields of the nucleons, $\vec{\phi}(x)$ are the pionic fields and $\vec{\tau}$ are the three Pauli matrices acting in isospin space. If we expand the scalar product $\vec{\tau}\cdot\partial_\mu\vec{\phi}$ in the spherical basis, then we finally get the following couplings

$$\begin{aligned}\mathcal{L} &= \frac{g_A}{2f_\pi}\Big(\bar{p}(x)\gamma^\mu\gamma_5 p(x)\partial_\mu\phi_0(x) - \bar{n}(x)\gamma^\mu\gamma_5 n(x)\partial_\mu\phi_0(x) \\ &+ \sqrt{2}\,\bar{p}(x)\gamma^\mu\gamma_5 n(x)\partial_\mu\phi_-(x) + \sqrt{2}\,\bar{n}(x)\gamma^\mu\gamma_5 p(x)\partial_\mu\phi_-^\dagger(x)\Big)\end{aligned} \tag{2.47}$$

where $\phi_0(x)$ is the field that creates or annihilates a π^0 and $\phi_-(x)$ is the field that creates a π^- or annihilates a π^+.
Just applying the Feynman rules, we can obtain the selfenergy associated

to the diagram of Fig. 2.7. It reads

$$\begin{aligned} -i\Pi^{\mu\nu}(q) &= -\int \frac{d^4p}{(2\pi)^4}\frac{d^4k_\pi}{(2\pi)^4}\frac{d^4l}{(2\pi)^4}\left(\frac{g}{2\sqrt{2}}\right)^2 A^{\mu\nu}_{p\to p\pi^+} G(p;\rho_p)G(p';\rho_p) \\ &\times D_0^2(k_\pi)\left(\frac{g_A}{2f_\pi}\right)^2\left(\sqrt{2}\right)^2 \mathrm{Tr}\left[\not{k}_\pi\gamma_5(\not{l}+M)\not{k}_\pi\gamma_5(\not{l}+\not{k}_\pi+M)\right] \\ &\times G(l;\rho_n)G(l+k_\pi;\rho_p) \end{aligned} \tag{2.48}$$

where $A^{\mu\nu}_{p\to p\pi^+}$ is the same than in Eq. (2.34); and $p' = p+q-k_\pi$.
The trace of the second fermionic loop (the one that does not involve the amputated amplitudes) is a scalar function of k_π and l and simplifies to $-8M^2k_\pi^2$ when one assumes that the pair particle-hole is on-shell, i.e, that the following relations hold:

$$l^2 = M^2 \qquad (l+k_\pi)^2 = M^2 \Rightarrow l\cdot k_\pi = -\frac{k_\pi^2}{2} \tag{2.49}$$

Then, with these assumptions, the trace gives:

$$\begin{aligned} B(k_\pi,l) &= \mathrm{Tr}\left[\not{k}_\pi\gamma_5(\not{l}+M)\not{k}_\pi\gamma_5(\not{l}+\not{k}_\pi+M)\right] \\ &= 8\left(l\cdot k_\pi\right)^2 - 4M^2k_\pi^2 + 4k_\pi^2\left(l\cdot k_\pi\right) - 4k_\pi^2 l^2 \\ &= -8M^2k_\pi^2 \end{aligned} \tag{2.50}$$

This allows us to take out this trace from the integral in d^4l and we easily obtain (when performing the integral in d^4l) the Lindhard function of k_π. Let us remind the relation between the relativistic Lindhard function and the following integral

$$\int \frac{d^4l}{(2\pi)^4} G(l;\rho_N)G(l+k_\pi;\rho_{N'}) = \frac{i}{8M^2}\bar{U}_R(k_\pi;k_F^N,k_F^{N'}) \equiv \frac{i}{8M^2}\bar{U}_R^{N,N'}(k_\pi) \tag{2.51}$$

where N and N' stand for n (neutron) or p (proton). In the case of Fig. 2.7, the Lindhard function is $\bar{U}_R^{n,p}(k_\pi)$.
With this, Eq. (2.48) gets simplified to

$$\begin{aligned} -i\Pi^{\mu\nu}(q) &= i\left(\frac{g}{2\sqrt{2}}\right)^2\left(\frac{g_A}{2f_\pi}\right)^2\left(\sqrt{2}\right)^2\int\frac{d^4k_\pi}{(2\pi)^4}k_\pi^2 D_0^2(k_\pi)\bar{U}_R^{n,p}(k_\pi) \\ &\times \int\frac{d^4p}{(2\pi)^4}A^{\mu\nu}_{p\to p\pi^+}(p,q,k_\pi)\; G(p;\rho_p)G(p+q-k_\pi;\rho_p) \end{aligned} \tag{2.52}$$

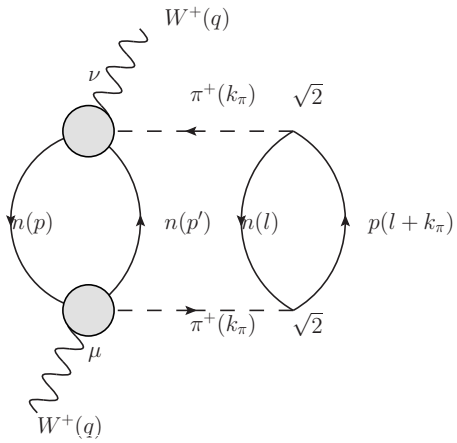

Figure 2.8: The only differences between this Feynman diagram and the one of Fig. 2.7 are the couplings (amputated amplitudes) in the first bubble. One must substitute the currents $J^\mu_{p\to p\pi^+}$ by the currents $J^\mu_{n\to n\pi^+}$

The integral in d^4p has been already done in the previous section. See discussion to obtain eq. (2.39) starting from eq. (2.32). With the assumption of taking an average momentum and a direction orthogonal to the plane defined by $\vec{q}$ and $\vec{k}_\pi$, we can again take the tensor $A^{\mu\nu}$ out of the integral in d^4p and the Lindhard function with argument $q-k_\pi$ appears again. It is straightforward to obtain

$$\begin{aligned}\Pi_1^{\mu\nu}(q) &= -\frac{i}{8M^2}\left(\frac{g}{2\sqrt{2}}\right)^2\left(\frac{g_A}{2f_\pi}\right)^2\left(\sqrt{2}\right)^2\int\frac{d^4k_\pi}{(2\pi)^4}k_\pi^2 D_0^2(k_\pi)\bar{U}_R^{n,p}(k_\pi)\\ &\times\ \bar{U}_R^{p,p}(q-k_\pi)A^{\mu\nu}_{p\to p\pi^+}|^{<\vec{p}>}_{p^0=E(\vec{p})}\end{aligned}\tag{2.53}$$

Until now, we have been discussing the calculation for one isospin channel, but there are more channels. For instance, we could have the following Feynman diagram (Fig. 2.8) where the amputated amplitudes now are for the process $W^+n\to n\pi^+$. The result for this channel is

$$\begin{aligned}\Pi_2^{\mu\nu}(q) &= -\frac{i}{8M^2}\left(\frac{g}{2\sqrt{2}}\right)^2\left(\frac{g_A}{2f_\pi}\right)^2\left(\sqrt{2}\right)^2\int\frac{d^4k_\pi}{(2\pi)^4}k_\pi^2 D_0^2(k_\pi)\bar{U}_R^{n,p}(k_\pi)\\ &\times\ \bar{U}_R^{n,n}(q-k_\pi)A^{\mu\nu}_{n\to n\pi^+}|^{<\vec{p}>}_{p^0=E(\vec{p})}\end{aligned}\tag{2.54}$$

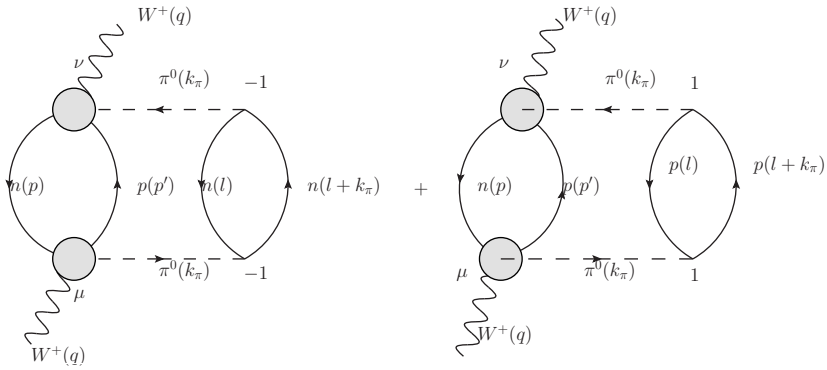

Figure 2.9: W-selfenergy diagram in which the exchanged meson is a π^0

where now $A^{\mu\nu}_{n\to n\pi^+}$ is given by the same trace as in Eq. (2.34) but replacing $J^\mu_{p\to p\pi^+}$ and $J^\nu_{p\to p\pi^+}$ by $J^\mu_{n\to n\pi^+}$ and $J^\nu_{n\to n\pi^+}$, respectively.
There are two more isospin channels and in both the exchanged meson is a π^0. Furthermore, these two channels involve the charge-exchange current ($J^\mu_{n\to p\pi^0}$) for the process $W^+ n \to p\pi^0$ (see Fig. 2.9). With few changes, we can write the contribution to the selfenergy coming from the diagrams in Fig. 2.9. It reads

$$\begin{aligned}\Pi^{\mu\nu}_{3+4}(q) &= -\frac{i}{8M^2}\left(\frac{g}{2\sqrt{2}}\right)^2\left(\frac{g_A}{2f_\pi}\right)^2\int\frac{d^4k_\pi}{(2\pi)^4}k_\pi^2 D_0^2(k_\pi)\left(\bar{U}_R^{n,n}(k_\pi)+\bar{U}_R^{p,p}(k_\pi)\right)\\ &\times\ \bar{U}_R^{n,p}(q-k_\pi)A^{\mu\nu}_{n\to p\pi^0}|^{<\vec{p}>}_{p^0=E(\vec{p})}\end{aligned} \tag{2.55}$$

Now again, the selfenergy will be the sum of the four channels that we have explicitly written ($\Pi^{\mu\nu}_W(q)=\sum_{i=1}^4\Pi^{\mu\nu}_i(q)$). Separating the symmetric and antisymmetric parts of the W-selfenergy with the aid of the symmetry properties of the tensors $A^{\mu\nu}$, and applying the Cutkosky's rules putting

on-shell the 2p2h states, the result is

$$\begin{aligned} W^{\mu\nu}_{2p2h}(q) &= -\theta(q^0)\frac{1}{M^2}\left(\frac{g_A}{2f_\pi}\right)^2 \int \frac{d^3r}{2\pi}\int \frac{d^4k_\pi}{(2\pi)^4} k_\pi^2 D_0^2(k_\pi) F_\pi^4(k_\pi) \\ &\times \theta(k_\pi^0)\theta(q^0-k_\pi^0)\Big\{ \mathrm{Im}\bar{U}_R^{n,p}(k_\pi)\Big[\mathrm{Im}\bar{U}_R^{p,p}(q-k_\pi)A^{\mu\nu}_{p\to p\pi^+} \\ &+ \mathrm{Im}\bar{U}_R^{n,n}(q-k_\pi)A^{\mu\nu}_{n\to n\pi^+}\Big] + \frac{1}{2}\mathrm{Im}\bar{U}_R^{n,p}(q-k_\pi) \\ &\times \left[\mathrm{Im}\bar{U}_R^{n,n}(k_\pi)+\mathrm{Im}\bar{U}_R^{p,p}(k_\pi)\right] A^{\mu\nu}_{n\to p\pi^0}\Big\} \end{aligned} \tag{2.56}$$

where now, the pion form factor $F_\pi^4(k_\pi)$ appears because the pions are off-shell. We will use

$$F_\pi(k_\pi) = \frac{\Lambda_\pi^2 - m_\pi^2}{\Lambda_\pi^2 - k_\pi^2} \tag{2.57}$$

with $\Lambda_\pi = 1.2$ GeV.

Several improvements for 2p2h mechanisms

We could have considered as well the Feynman diagram of Fig. 2.6, but instead of taking the bare pion propagator, we could have taken the dressed pion propagator and after that, we would have applied the Cutkosky's rules to obtain the imaginary part of the W-selfenergy. The dressed pion propagator reads

$$D_\pi(k_\pi) = \frac{1}{k_\pi^2 - m_\pi^2 - \Pi(k_\pi)} \tag{2.58}$$

where for the selfenergy of a pion[6] of charge λ, we take [127]

$$\Pi(k_\pi) = F_\pi^2(k_\pi)\left(\frac{g_A}{2f_\pi}\right)^2 \vec{k}_\pi^2 \frac{U(k_\pi)}{1-\left(\frac{g_A}{2f_\pi}\right)^2 g' U(k_\pi)} \tag{2.59}$$

[6]Quite often in the literature it is written $\frac{f_{\pi NN}}{m_\pi}$ instead of $\frac{g_A}{2f_\pi}$. This equality (known as the Goldberger-Treiman relation) is satisfied phenomenologically better than a 5% [47].

In Eq. (2.59), $U(k_\pi) = U_N(k_\pi) + U_\Delta(k_\pi)$ is the non-relativistic Lindhard function for ph + Δh excitations[7] including direct and crossed bubbles [130, 131], in contrast to $\bar{U}_R$, which only contains the direct bubble of a particle-hole excitation (the only one which contributes to $\mathrm{Im}U_N$ for $q^0 > 0$). When we apply the Cutkosky's rules with the dressed pion propagator, we obtain

$$\begin{aligned} \mathrm{Im}\Pi^{\mu\nu}_{s(a)} &= -\left(\frac{g}{2\sqrt{2}}\right)^2 \frac{1}{4M^2} \int \frac{d^4k_\pi}{(2\pi)^4} \theta(k_\pi^0)\theta(q^0 - k_\pi^0) \mathrm{Im}D_\pi(k_\pi) \\ &\times \sum_{N,N',\lambda} \mathrm{Im}\bar{U}_R^{N,N'}(q - k_\pi) A^{\mu\nu}_{s(a),N\to N'\pi^\lambda} \end{aligned} \tag{2.60}$$

Using Eqs. (2.42) and (2.43), and putting their results into Eqs. (2.17) and (2.18), we easily obtain for the hadronic tensor

$$\begin{aligned} W^{\mu\nu} &= \frac{1}{2M^2}\theta(q^0) \int \frac{d^3r}{2\pi} \int \frac{d^4k_\pi}{(2\pi)^4} \theta(k_\pi^0)\theta(q^0 - k_\pi^0) \mathrm{Im}D_\pi(k_\pi) F_\pi^2(k_\pi) \\ &\times \sum_{N,N',\lambda} \mathrm{Im}\bar{U}_R^{N,N'}(q - k_\pi) A^{\mu\nu}_{N\to N'\pi^\lambda} \end{aligned} \tag{2.61}$$

It seems that Eq. (2.61) is lacking a factor $F_\pi^2(k_\pi)$ with respect to Eq. (2.56), but that factor is hidden in $\mathrm{Im}D_\pi(k_\pi)$. Indeed, we have

$$\mathrm{Im}D_\pi(k_\pi) = \frac{\mathrm{Im}\Pi(k_\pi)}{\left|k_\pi^2 - m_\pi^2 - \Pi(k_\pi)\right|^2} \tag{2.62}$$

And for $\mathrm{Im}\Pi(k_\pi)$ I have

$$\mathrm{Im}\Pi(k_\pi) = F_\pi^2(k_\pi) \left(\frac{g_A}{2f_\pi}\right)^2 \vec{k}_\pi^2 \frac{\mathrm{Im}U(k_\pi)}{\left|1 - \left(\frac{g_A}{2f_\pi}\right)^2 g' U(k_\pi)\right|^2} \tag{2.63}$$

Therefore, for $\mathrm{Im}D_\pi(k_\pi)$ we will have

$$\mathrm{Im}D_\pi(k_\pi) = \frac{F_\pi^2(k_\pi) \left(\frac{g_A}{2f_\pi}\right)^2 \vec{k}_\pi^2 \, \mathrm{Im}U(k_\pi) D_0^2(k_\pi)}{\left|1 - V_l(k_\pi)U(k_\pi)\right|^2} \tag{2.64}$$

[7] The functions U_N and U_Δ are defined, for instance, in Eqs. (2.9) and (3.4) of Ref. [130]. U_N incorporates a factor two of isospin with respect to $\bar{U}_R$, such that $\mathrm{Im}U_N = 2\,\mathrm{Im}\bar{U}_R$ for symmetric nuclear matter, up to relativistic corrections.

where $V_l(k_\pi)$ is an effective longitudinal interaction which, besides pion exchange, includes Short Range Correlations (SRC) driven by the Landau-Migdal parameter g'. We will assume that this parameter has no k-dependence (actually it has a smooth k-dependence, see Refs. [124, 131]) and that it is equal for the effective transverse interaction $V_t(k)$, which will be discussed later. For the longitudinal and transverse channel interactions we will take

$$V_l(k_\pi) = \left(\frac{g_A}{2f_\pi}\right)^2 \left(F_\pi^2(k_\pi)\frac{\vec{k}_\pi^2}{k_\pi^2 - m_\pi^2} + g'_l(k_\pi)\right) \tag{2.65}$$

$$V_t(k) = \frac{f_{\pi NN}^2}{m_\pi^2}\left(C_\rho F_\rho^2(k)\frac{\vec{k}^2}{k^2 - m_\rho^2} + g'_t(k)\right) \tag{2.66}$$

We will take $g'_l(k) = g'_t(k) = g' = 0.63$, as it was done in the study of inclusive nuclear electron scattering carried out in Ref. [43], and also in the previous work on the QE region of Ref. [38]. Furthermore, $C_\rho = 2$ and

$$F_\rho(k) = \frac{\Lambda_\rho^2 - m_\rho^2}{\Lambda_\rho^2 - k^2} \tag{2.67}$$

is the ρ-meson form factor with $\Lambda_\rho = 2.5$ GeV and $m_\rho = 0.77$ GeV.
When we evaluate $\mathrm{Im}D_\pi(k_\pi)$ in Eq. (2.64), in the numerator we have not considered the part that arises from putting the Δh excitation on-shell that would correspond to a 2p2h+1π mechanism. In other words, in the numerator of Eq. (2.64) we have only considered the imaginary part of the non-relativistic nucleon Lindhard function $U_N(k_\pi)$. We expect that the contribution coming from taking into account the imaginary part of $U_\Delta(k_\pi)$ is small at the considered energies. Note also, that by using U to compute the pion selfenergy, we have neglected small relativistic and $\rho_p \neq \rho_n$ corrections which could be important for non-symmetric nuclei. By means of Eq. (2.62), we have implemented the Dyson re-summation of the pion selfenergy, and we have improved on this latter one by incorporating the Lorentz-Lorenz effect, driven by the short range Landau-Migdal parameter g' [126], going in this way beyond 1p1h excitation[8] in the evaluation of $\Pi(k_\pi)$.

When in one (or both) of the weak vertices of Fig. 2.7 the NP term is

[8]This corresponds to replace the ph excitation of the right-hand side in Fig. 2.7 by a series of RPA excitations through ph and Δh excitations, driven by the longitudinal part of the effective spin-isospin interaction. We will do something similar for the case of 2p2h mechanisms driven by ρ-meson exchange.

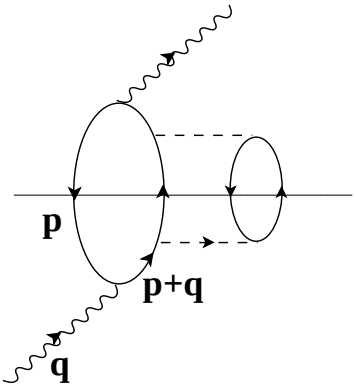

Figure 2.10: W-selfenergy diagram obtained from the QE 1p1h excitation term (first of the diagrams depicted in Fig. 2.3) by dressing up the nucleon propagator of the particle state in the ph excitation. It can be also considered as coming from the generic diagram of Fig. 2.7 when in both shaded circles the NP amputated amplitudes are selected.

considered, the prescription of taking an average nucleon momentum of the Fermi sea that led us to Eqs. (2.56) or (2.61) turns out to be not adequate. The reason is because when placing the 2p2h excitation on-shell, through Cutkosky's rules, we still have the nucleon propagator with momentum $p+q$ (this is part of the amputated amplitude $j^{\mu}_{A_{NP}}$), see Fig. 2.10. This propagator can be still placed on-shell for a virtual W and thus, there exists a single pole in the d^3p integration[9]. In this situation, we cannot take an average for $\vec{p}$, as we have implicitly assumed in Eqs. (2.56) or (2.61). We have improved such prescription as follows. In these latter equations, the tensor $A^{\mu\nu}$ appeared, which in turn is defined in Eq. (2.40) by using an average for the hole 3-momentum $\vec{p}$ to calculate both, the amputated $W^+N \to N'\pi$ amplitudes $J^{\mu}_{N\to N'\pi^{\lambda}}$ and $\not{p}$, that also appears in the trace that defines $A^{\mu\nu}$. Instead of this, we have computed an average of the whole trace. To this end, we have numerically performed the integral over the angle formed by $\vec{p}$ and $\vec{q}$, using still an average for the modulus of $\vec{p}$. All pathologies arise from

[9]This cut will also contribute to the nuclear response to the weak probe. But, while it will affect to the QE region, it is expected to be small and considerably difficult to calculate from the computational point of view (see Eq. (80) in Ref. [43]). Thus, for the sake of simplicity we have not considered such contribution.

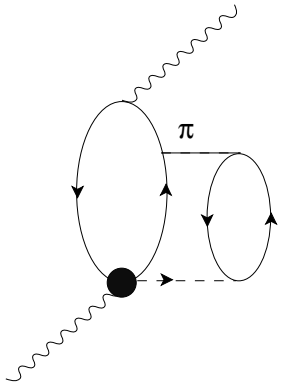

Figure 2.11: W-selfenergy diagram in which one of the vertices contains the NP term of the $WN \to N'\pi^{\lambda}$ amplitude, while the other one (filled circle) contains all terms except that one.

the $p+q$ nucleon propagator hidden in the amputated amplitudes, which can be put on the mass shell and thus the contribution of these diagrams depends critically on the angle formed by $\vec{p}$ and $\vec{q}$, while it shows a very smooth dependence on the rest of kinematical variables of the hole momentum $\vec{p}$. Thanks to the approximations of using an average for the modulus of $\vec{p}$ and fixing the ($\vec{p}$,$\vec{q}$)-plane, we avoid to perform two nested integrals, with the obvious benefit in computation time. We have checked that the results are accurate at the level of 5-10%. To speed up the numerical integration, we have also given a small width ($\sim$ 10 MeV) to the $p+q$ nucleon. The results do not depend significantly on this choice. For consistency, we have also performed this angular average for all contributions implicit in Fig. 2.7, although the prescription of using an average for $\vec{p}$ leads to accurate results in all cases except those involving the NP amputated amplitude discussed above.

In the terms involving the NP amputated amplitude (interferences with the rest of amplitudes of Fig. 2.5) there always appears a pion emitted after the WN vertex that couples to the second ph excitation (see for instance the line labeled as π in Fig. 2.11). There, we are assuming a pion exchange interaction among the two ph excitations. We have improved on that, and we have replaced it by the effective longitudinal interaction V_l, eq. (2.65),

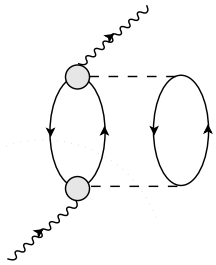

Figure 2.12: Same as Fig. 2.7, but showing the cut that places one particle-hole and the pion on-shell

which besides pion exchange includes SRC driven by the Landau-Migdal parameter g_l' (see Refs. [126, 127, 131]). To achieve this, we have multiplied the amputated amplitude $j^\mu_{A_{NP}}$ by a suitable factor

$$j^\mu_{A_{NP}} \Longrightarrow j^\mu_{A_{NP}} \times \left(1 + \frac{g_l'}{F_\pi^2 D_0 \vec{k}_\pi^2}\right) \tag{2.68}$$

We have taken the same prescription also for those terms that include the CNP, ΔP and CΔP amputated amplitudes.
The cut which places the two ph on-shell in the diagrams of Figs. 2.7, 2.8 and 2.9 is not the only possible one. In Fig. 2.12, we show a different cut (dotted line) which places one ph and the pion on-shell. As done for real [123] and virtual [43] photons, we neglect this contribution in the non-resonant terms. This is because at low energies, where these pieces are important, the (W, π) channel is small; and at high energies, where the (W, π) contribution is important, this channel is dominated by the Δ excitation and there this correction will be properly incorporated.

Another 2p2h absorption mode

We have also considered two-body diagrams where each W boson couples to different pairs particle-hole, see Fig. 2.13. Let us take the first diagram of Fig. 2.13. Applying the Feynman rules, we easily obtain the following

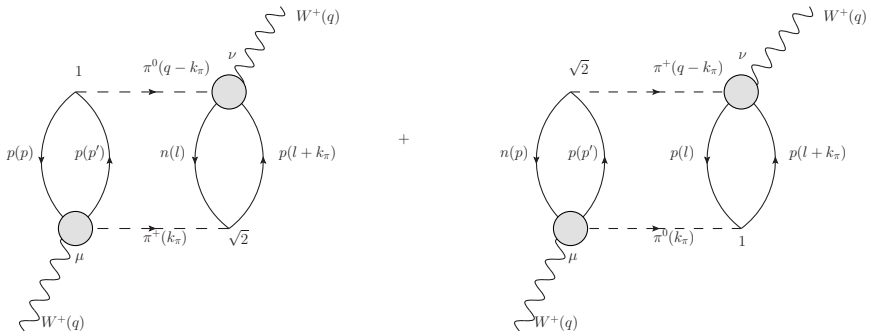

Figure 2.13: Two particle-two hole (2p2h) W-selfenergy Feynman diagram where the outgoing gauge boson couples to the second pair particle-hole

contribution for the selfenergy of the W boson

$$\begin{aligned}
-i\Pi_1^{\mu\nu}(q) &= -\left(\frac{g}{2\sqrt{2}}\right)^2\left(\frac{g_A}{2f_\pi}\right)^2\sqrt{2}\int\frac{d^4k_\pi}{(2\pi)^4}\int\frac{d^4l}{(2\pi)^4}\int\frac{d^4p}{(2\pi)^4} \\
&\times \mathrm{Tr}\left[J^\mu_{p\to p\pi^+}(\not{p}+M)(\not{q}-\not{k}_\pi)\gamma_5(\not{p}+\not{q}-\not{k}_\pi+M)\right] \\
&\times \mathrm{Tr}\left[\not{k}_\pi\gamma_5(\not{l}+M)\gamma^0 J^{\nu\dagger}_{n\to p\pi^0}\gamma^0(\not{l}+\not{k}_\pi+M)\right]G(p;\rho_p) \\
&\times G(p+q-k_\pi;\rho_p)D_0(k_\pi)D_0(q-k_\pi)G(l;\rho_n)G(l+k_\pi;\rho_p)
\end{aligned} \tag{2.69}$$

where $J^\mu_{p\to p\pi^+}$ is function of (p,q,k_π), and $J^{\nu\dagger}_{n\to p\pi^0}$ is function of $(l,q,q-k_\pi)$. And now, let us do the following changes of variables in the integrals of the four-momenta

$$\begin{aligned}
k_\pi &= q-k'_\pi \\
l &= p' \\
p &= l'
\end{aligned} \tag{2.70}$$

As k'_π, p' and l' are dummy arguments, we can redefine them without the symbol ($\prime$) and the result for the W-selfenergy of Eq. (2.69) is

$$\begin{aligned}
-i\Pi_1^{\mu\nu}(q) &= -\left(\frac{g}{2\sqrt{2}}\right)^2\left(\frac{g_A}{2f_\pi}\right)^2\sqrt{2}\int\frac{d^4k_\pi}{(2\pi)^4}\int\frac{d^4l}{(2\pi)^4}\int\frac{d^4p}{(2\pi)^4} \\
&\times \mathrm{Tr}\left[J^\mu_{p\to p\pi^+}(l,q,q-k_\pi)(\not{l}+M)\not{k}_\pi\gamma_5(\not{l}+\not{k}_\pi+M)\right]G(l;\rho_p) \\
&\times \mathrm{Tr}\left[(\not{q}-\not{k}_\pi)\gamma_5(\not{p}+M)\gamma^0 J^{\nu\dagger}_{n\to p\pi^0}(p,q,k_\pi)\gamma^0(\not{p}+\not{q}-\not{k}_\pi+M)\right] \\
&\times G(l+k_\pi;\rho_p)D_0(q-k_\pi)D_0(k_\pi)G(p;\rho_n)G(p+q-k_\pi;\rho_p)
\end{aligned} \tag{2.71}$$

Again, just applying the Feynman rules, we easily can obtain the contribution to the W-selfenergy from the diagram on the right-hand side of Fig. 2.13

$$\begin{aligned}
-i\Pi_2^{\mu\nu}(q) &= -\left(\frac{g}{2\sqrt{2}}\right)^2\left(\frac{g_A}{2f_\pi}\right)^2\sqrt{2}\int\frac{d^4k_\pi}{(2\pi)^4}\int\frac{d^4l}{(2\pi)^4}\int\frac{d^4p}{(2\pi)^4} \\
&\times \mathrm{Tr}\left[J^\mu_{n\to p\pi^0}(p,q,k_\pi)(\not{p}+M)(\not{q}-\not{k}_\pi)\gamma_5(\not{p}+\not{q}-\not{k}_\pi+M)\right]G(p;\rho_n) \\
&\times \mathrm{Tr}\left[\not{k}_\pi\gamma_5(\not{l}+M)\gamma^0 J^{\nu\dagger}_{p\to p\pi^+}(l,q,q-k_\pi)\gamma^0(\not{l}+\not{k}_\pi+M)\right] \\
&\times G(l+k_\pi;\rho_p)D_0(q-k_\pi)D_0(k_\pi)G(l;\rho_p)G(p+q-k_\pi;\rho_p)
\end{aligned} \tag{2.72}$$

And then, summing both contributions, we get

$$\begin{aligned}
-i\Pi_{1+2}^{\mu\nu}(q) &= -\left(\frac{g}{2\sqrt{2}}\right)^2\left(\frac{g_A}{2f_\pi}\right)^2\sqrt{2}\int\frac{d^4k_\pi}{(2\pi)^4}\int\frac{d^4l}{(2\pi)^4}\int\frac{d^4p}{(2\pi)^4} \\
&\times G(l;\rho_p)G(l+k_\pi;\rho_p)D_0(q-k_\pi)D_0(k_\pi)G(p;\rho_n)G(p+q-k_\pi;\rho_p) \\
&\times A_1^{\mu\nu}(p,l,q,k_\pi)
\end{aligned} \tag{2.73}$$

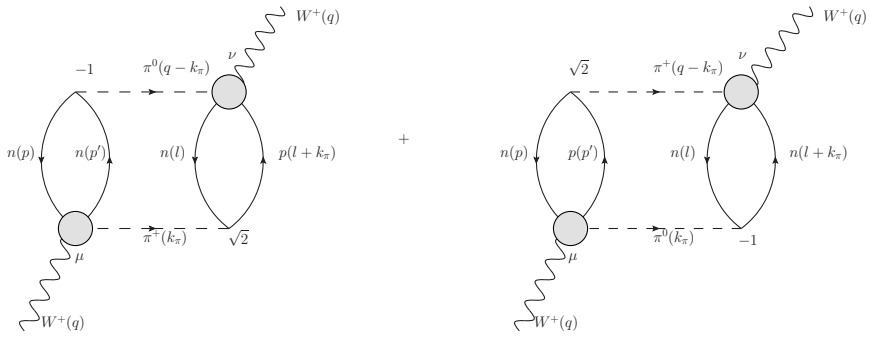

Figure 2.14: Two particle-two hole (2p2h) W-selfenergy Feynman diagram where the outgoing gauge boson couples to the second pair particle-hole. This figure contains the two Feynman diagram not displayed in Fig. 2.13

where now, the tensor $A_1^{\mu\nu}(p,l,q,k_\pi)$ is

$$\begin{aligned} A_1^{\mu\nu}(p,l,q,k_\pi) &= \mathrm{Tr}\left[J^{\mu}_{n\to p\pi^0}(p,q,k_\pi)(\not{p}+M)(\not{q}-\not{k}_\pi)\gamma_5(\not{p}+\not{q}-\not{k}_\pi+M)\right] \\ &\times \mathrm{Tr}\left[\not{k}_\pi\gamma_5(\not{l}+M)\gamma^0 J^{\nu\dagger}_{p\to p\pi^+}(l,q,q-k_\pi)\gamma^0(\not{l}+\not{k}_\pi+M)\right] \\ &+ \mathrm{Tr}\left[J^{\mu}_{p\to p\pi^+}(l,q,q-k_\pi)(\not{l}+M)\not{k}_\pi\gamma_5(\not{l}+\not{k}_\pi+M)\right] \\ &\times \mathrm{Tr}\left[(\not{q}-\not{k}_\pi)\gamma_5(\not{p}+M)\gamma^0 J^{\nu\dagger}_{n\to p\pi^0}(p,q,k_\pi)\gamma^0(\not{p}+\not{q}-\not{k}_\pi+M)\right] \end{aligned} \tag{2.74}$$

And this last tensor can be decomposed in a symmetric part which is real plus an antisymmetric part which is pure imaginary. In other words, this tensor fulfills the condition expressed by Eq. (2.25)[10].
Analogously, we can do the same trick done in eq. (2.70) for one of the Feynman diagrams of Fig. 2.14. When we sum the two contributions to the W-selfenergy coming from the diagrams in Fig 2.14, we obtain

$$\begin{aligned} -i\Pi^{\mu\nu}_{3+4}(q) &= \left(\frac{g}{2\sqrt{2}}\right)^2\left(\frac{g_A}{2f_\pi}\right)^2\sqrt{2}\int\frac{d^4k_\pi}{(2\pi)^4}\int\frac{d^4l}{(2\pi)^4}\int\frac{d^4p}{(2\pi)^4} \\ &\times G(l;\rho_n)G(l+k_\pi;\rho_n)D_0(q-k_\pi)D_0(k_\pi)G(p;\rho_n)G(p+q-k_\pi;\rho_p) \\ &\times A_2^{\mu\nu}(p,l,q,k_\pi) \end{aligned} \tag{2.75}$$

[10]This will be shown in Appendix C.

Where now, the tensor $A_2^{\mu\nu}(p,l,q,k_\pi)$ is given by the following expression

$$\begin{aligned} A_2^{\mu\nu}(p,l,q,k_\pi) &= \mathrm{Tr}\left[J^{\mu}_{n\to p\pi^0}(p,q,k_\pi)(\not{p}+M)(\not{q}-\not{k}_\pi)\gamma_5(\not{p}+\not{q}-\not{k}_\pi+M)\right] \\ &\times \mathrm{Tr}\left[\not{k}_\pi\gamma_5(\not{l}+M)\gamma^0 J^{\nu\dagger}_{n\to n\pi^+}(l,q,q-k_\pi)\gamma^0(\not{l}+\not{k}_\pi+M)\right] \\ &+ \mathrm{Tr}\left[J^{\mu}_{n\to n\pi^+}(l,q,q-k_\pi)(\not{l}+M)\not{k}_\pi\gamma_5(\not{l}+\not{k}_\pi+M)\right] \\ &\times \mathrm{Tr}\left[(\not{q}-\not{k}_\pi)\gamma_5(\not{p}+M)\gamma^0 J^{\nu\dagger}_{n\to p\pi^0}(p,q,k_\pi)\gamma^0(\not{p}+\not{q}-\not{k}_\pi+M)\right] \end{aligned} \tag{2.76}$$

And again, this last tensor fulfills the requirement expressed by Eq. (2.25). If we sum the four contributions to the W-selfenergy, then we get the general expression

$$\begin{aligned} \sum_{j=1}^{4} -i\Pi_j^{\mu\nu}(q) &= \left(\frac{g}{2\sqrt{2}}\right)^2\left(\frac{g_A}{2f_\pi}\right)^2\sqrt{2}\int\frac{d^4k_\pi}{(2\pi)^4}\int\frac{d^4l}{(2\pi)^4}\int\frac{d^4p}{(2\pi)^4} \\ &\times G(p;\rho_n)G(p+q-k_\pi;\rho_p)D_0(k_\pi)D_0(q-k_\pi) \\ &\times \Big(G(l;\rho_n)G(l+k_\pi;\rho_n)A_2^{\mu\nu}(p,l,q,k_\pi) \\ &- G(l;\rho_p)G(l+k_\pi;\rho_p)A_1^{\mu\nu}(p,l,q,k_\pi)\Big) \end{aligned} \tag{2.77}$$

If we take average momenta for both hole nucleon momenta $\langle\vec{p}\rangle$ and $\left\langle\vec{l}\right\rangle$, then we can take the tensors $A^{\mu\nu}$ out of the integrals in d^4p and d^4l and we obtain two relativistic Lindhard functions in this approximation. The final result for the W-selfenergy is

$$\begin{aligned} \Pi^{\mu\nu}(q) &= -i\left(\frac{g}{2\sqrt{2}}\right)^2\left(\frac{g_A}{2f_\pi}\right)^2\sqrt{2}\,\frac{1}{64M^4}\int\frac{d^4k_\pi}{(2\pi)^4}D_0(k_\pi)D_0(q-k_\pi) \\ &\times \bar{U}_R^{n,p}(q-k_\pi)\left(\bar{U}_R^{n,n}(k_\pi)\left\langle A_2^{\mu\nu}\right\rangle - \bar{U}_R^{p,p}(k_\pi)\left\langle A_1^{\mu\nu}\right\rangle\right) \end{aligned} \tag{2.78}$$

where in the tensors $\langle A_i^{\mu\nu}\rangle$ we have performed an average of the whole trace, i.e, we have numerically performed the integral over the angle formed by the hole momenta $(\vec{p},\vec{l})$ and $\vec{q}$, to avoid all the pathologies related to the NP amputated amplitude and the $p+q$ or $l+q$ nucleon propagator hidden in the amputated amplitudes. We have also considered the improvement of multiplying the amputated amplitudes (ΔP, CΔP, NP and CNP) by the

suitable correction factor of Eq. (2.68) that takes into account, besides pion exchange, the Short Range Correlations driven by the Landau-Migdal parameter g'_l. As in Ref. [43] for the inclusive electron-nucleus case, we have only considered the contributions stemming from the longitudinal part of the effective spin-isospin ph-ph interaction and we have neglected those induced by the transverse one.
Now, from eq. (2.78), we can separate the W-selfenergy into its symmetric part and its antisymmetric one and then apply the Cutkosky's rules to obtain the imaginary part of the selfenergy. The final result for the hadronic tensor is

$$\begin{aligned} W^{\mu\nu}_{2p2h-2b} &= -\theta(q^0)\left(\frac{g_A}{2f_\pi}\right)^2 \frac{4\sqrt{2}}{64M^4}\int\frac{d^3r}{2\pi}\int\frac{d^4k_\pi}{(2\pi)^4}D_0(k_\pi)D_0(q-k_\pi) \\ &\times \theta(q^0-k^0_\pi)\theta(k^0_\pi)\mathrm{Im}\bar{U}^{n,p}_R(q-k_\pi)\Big(\mathrm{Im}\bar{U}^{n,n}_R(k_\pi)\,\langle A^{\mu\nu}_2\rangle \\ &- \mathrm{Im}\bar{U}^{p,p}_R(k_\pi)\,\langle A^{\mu\nu}_1\rangle\Big)F^2_\pi(k_\pi)F^2_\pi(q-k_\pi) \end{aligned} \tag{2.79}$$

where now the pion form factors $F^2_\pi(k_\pi)$ and $F^2_\pi(q-k_\pi)$ appear because the pions are off-shell.

2p2h mechanisms driven by the transverse part of the effective spin-isospin ph-ph interaction

In this subsection we evaluate the contribution to the weak nuclear response of the 2p2h absorption terms driven by the transverse part of the effective spin-isospin ph-ph potential used in previous studies of electron [43], photon [123] and pion [124–128] interactions with nuclei. In the model of Ref. [124], this transverse interaction arises from ρ-exchange modulated by SRC. The major difficulty here, as compared with the previous works mentioned above, arises from the fact that we are using a relativistic description of the weak transition process. Thus, the first step is to model $NN\rho$ and $N\Delta\rho$ relativistic Lagrangians, which give rise, in the non-relativistic limit, to the transverse potential of Eq. (2.66). A convenient set of interaction

Lagrangians is,

$$\mathcal{L}_{NN\rho} = \frac{f_{\pi NN}}{m_\pi}\sqrt{C_\rho}\bar{\Psi}(x)\sigma_{\mu\nu}\left(\partial^\mu\vec{\rho}^{\,\nu}(x)\cdot\vec{\tau}\right)\Psi(x) \tag{2.80}$$

$$\mathcal{L}_{N\Delta\rho} = -i\frac{f^*_{\pi N\Delta}}{m_\pi}\sqrt{C_\rho}\bar{\Psi}_\nu(x)\gamma_5\gamma_\mu\left(\vec{T}^\dagger\cdot\left(\partial^\mu\vec{\rho}^{\,\nu}(x)-\partial^\nu\vec{\rho}^{\,\mu}(x)\right)\right)\Psi(x)+h.c. \tag{2.81}$$

where $\Psi = \begin{pmatrix} p \\ n \end{pmatrix}$ is the isospin doublet that contains the nucleon fields, $\vec{\rho}^{\,\nu}$ is the ρ-meson Proca field[11], $\Psi_\nu = \begin{pmatrix} \Delta^{++} \\ \Delta^{+} \\ \Delta^{0} \\ \Delta^{-} \end{pmatrix}_\nu$ is the isospin 4-plet that contains the Rarita-Schwinger $J^\pi = 3/2^+$ fields for the Δ, $\vec{T}^\dagger$ is the isospin transition operator[12], $\vec{\tau}$ are the isospin Pauli matrices and $f^*_{\pi N\Delta} = 2.14$. Next, we consider the $W^+N \to N'\rho$ process and we find the NP, CNP, ΔP and CΔP amputated amplitudes obtained from the above Lagrangians. The Feynman diagrams for these four amplitudes are depicted in Fig. 2.15. We will denote the amputated amplitudes by $t^{\mu\alpha}_{A_i}$. They are defined by their relation to the full amplitudes

$$t^{\mu\alpha}_{cc+}|_i = \bar{u}(\vec{p}\,')t^{\mu\alpha}_{A_i}(p,q,p'=p+q-k,k)u(\vec{p}), \qquad i=\Delta P, C\Delta P, NP, CNP \tag{2.82}$$

where, if one wants to calculate the full amplitude, the Lorentz index μ must be contracted with the polarization vector of the W ($\epsilon_\mu(\vec{q})$) and the Lorentz index α must be contracted with the ρ-meson polarization vector

[11] Here $\rho^\nu_- = (\rho^\nu_x - i\rho^\nu_y)/\sqrt{2}$ is the field that creates a ρ^- from the vacuum or annihilates a ρ^+. And $\rho^\nu_0 = \rho^\nu_z$ is the field that creates or annihilates a ρ^0.

[12] It is a vector under isospin rotations and its Wigner-Eckart irreducible matrix element is taken to be one.

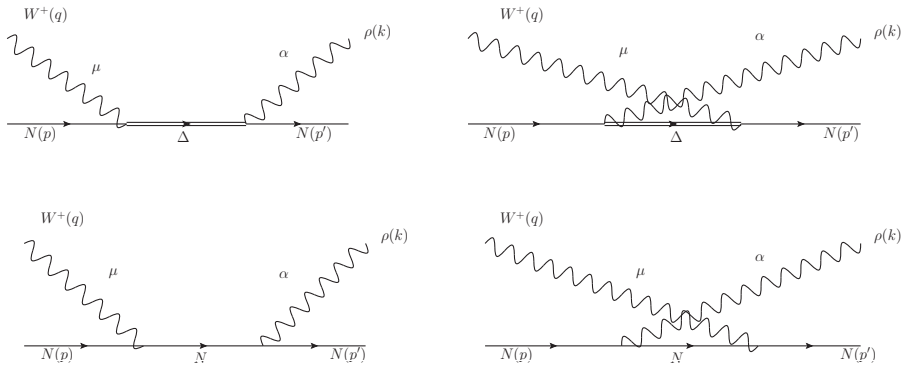

Figure 2.15: Feynman diagrams for the process $W^+N \to N'\rho$. First row, from left to right, ΔP and CΔP diagrams. Second row, also from left to right, NP and CNP diagrams

$(\epsilon^*_\alpha(\vec{k}))$. We find the following amplitudes

$$
\begin{aligned}
t^{\mu\alpha}_{\Delta P} &= -\sqrt{C_\rho}\,\frac{f^*_{\pi N\Delta}}{m_\pi}\sqrt{3}\,C^{\Delta P}\frac{\cos\theta_c}{p^2_\Delta - M^2_\Delta + iM_\Delta\Gamma_\Delta} \\
&\times\ \bar{u}(\vec{p}\,')\gamma_5\Big(\not{k}g^{\nu\alpha} - k^\nu\gamma^\alpha\Big)P_{\nu\beta}(p_\Delta)\Gamma^{\beta\mu}(p,q)u(\vec{p}), \qquad p_\Delta = p+q \\
t^{\mu\alpha}_{C\Delta P} &= \sqrt{C_\rho}\,\frac{f^*_{\pi N\Delta}}{m_\pi}\frac{1}{\sqrt{3}}\,C^{C\Delta P}\frac{\cos\theta_c}{p^2_\Delta - M^2_\Delta + iM_\Delta\Gamma_\Delta} \\
&\times\ \bar{u}(\vec{p}\,')\gamma^0\Gamma^{\nu\mu\dagger}(p',-q)\gamma^0 P_{\nu\beta}(p_\Delta)\gamma_5\Big(\not{k}g^{\beta\alpha} - k^\beta\gamma^\alpha\Big)u(\vec{p}), \qquad p_\Delta = p'-q \\
t^{\mu\alpha}_{NP} &= -i\sqrt{C_\rho}\,\frac{g_A}{\sqrt{2}f_\pi}\,C^{NP}\frac{\cos\theta_c}{(p+q)^2 - M^2 + i\epsilon} \\
&\times\ \bar{u}(\vec{p}\,')\sigma^{\nu\alpha}k_\nu\Big(\not{p}+\not{q}+M\Big)\Big(V^\mu_N(q) - A^\mu_N(q)\Big)u(\vec{p}) \\
t^{\mu\alpha}_{CNP} &= -i\sqrt{C_\rho}\,\frac{g_A}{\sqrt{2}f_\pi}\,C^{CNP}\frac{\cos\theta_c}{(p-k)^2 - M^2 + i\epsilon} \\
&\times\ \bar{u}(\vec{p}\,')\Big(V^\mu_N(q) - A^\mu_N(q)\Big)\Big(\not{p}-\not{k}+M\Big)\sigma^{\nu\alpha}k_\nu u(\vec{p})
\end{aligned}
\tag{2.83}
$$

The isospin coefficients are:

$$
C^{\Delta P} = \begin{pmatrix} 1 & \text{for} & p\,\rho^+ \\ \frac{1}{3} & \text{for} & n\,\rho^+ \end{pmatrix}
\tag{2.84}
$$

$$C^{C\Delta P} = \begin{pmatrix} 1 & \text{for} & p\,\rho^+ \\ 3 & \text{for} & n\,\rho^+ \end{pmatrix} \tag{2.85}$$

$$C^{NP} = \begin{pmatrix} 0 & \text{for} & p\,\rho^+ \\ 1 & \text{for} & n\,\rho^+ \end{pmatrix} \tag{2.86}$$

$$C^{CNP} = \begin{pmatrix} 1 & \text{for} & p\,\rho^+ \\ 0 & \text{for} & n\,\rho^+ \end{pmatrix} \tag{2.87}$$

In Eqs. (2.83), Γ_Δ is the width of the Δ resonance; $P_{\nu\beta}(p_\Delta)$ is the spin-$\frac{3}{2}$ projection operator defined in eq. (2.24); $\Gamma^{\beta\mu}$ is the weak $N-\Delta$ transition vertex already defined in eq. (2.20). And finally, $V_N^\mu(q)$ and $A_N^\mu(q)$ are the weak vector and axial-vector nucleon currents, respectively; and they can be found in Eq. (34) of Ref. [47]. We are going to use the vector and axial form factors given in this last reference.
The weak currents are related among themselves. Only two of them are independent. We are going to take as the independent currents those that connect the states $p \to p\rho^+$ and $n \to n\rho^+$. We will also need the current that connects the states $n \to p\rho^0$. This last current is related to the two previous ones by the relation [47]:

$$\langle p\,\rho^0|j^\mu_{cc+}(0)|n\rangle = -\frac{1}{\sqrt{2}}\left[\langle p\,\rho^+|j^\mu_{cc+}(0)|p\rangle - \langle n\,\rho^+|j^\mu_{cc+}(0)|n\rangle\right] \tag{2.88}$$

where the currents $j^\mu_{cc+}|_i$ are related to the amplitudes $t_i^{\mu\alpha}$ by

$$j^\mu_{cc+}|_i = t_i^{\mu\alpha}\epsilon^*_\alpha(\vec{k}), \qquad i = \Delta P, C\Delta P, NP, CNP \tag{2.89}$$

An important property of the amplitudes given in Eq. (2.83) is the fact that they are orthogonal to k (four-momentum of the ρ-meson). Indeed, we have

$$t_i^{\mu\alpha}(p,q,k)k_\alpha = 0, \qquad i = \Delta P, C\Delta P, NP, CNP \tag{2.90}$$

With all these properties for the amputated amplitudes of Eq. (2.83), we can calculate the contribution to the W-selfenergy coming from the Feynman diagram depicted in fig. 2.16. Let us assume that it is a ρ^+ which excites a ph and let us assume that in the fermion loop in the left of fig. 2.16 we have a proton hole. With this, applying the Feynman rules, we obtain for

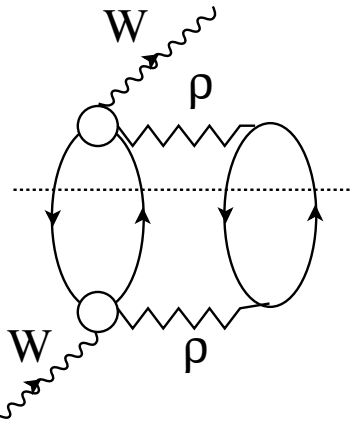

Figure 2.16: Two particle-two hole W-selfenergy Feynman diagram driven by ρ-exchange. The cut (dotted line) that places the 2p2h on-shell is also displayed. The empty circle contains the direct and crossed nucleon and Δ-pole terms of the $W^+N \to N'\rho$ amplitude.

the W-selfenergy

$$\begin{aligned} -i\Pi^{\mu\nu}(q) &= -\left(\frac{g}{2\sqrt{2}}\right)^2 \left(\sqrt{2}\right)^2 \frac{f^2_{\pi NN}}{m^2_\pi} C_\rho \int \frac{d^4p}{(2\pi)^4} \int \frac{d^4k}{(2\pi)^4} \int \frac{d^4l}{(2\pi)^4} \\ &\times \mathrm{Tr}\left[T^{\mu\alpha}_{p\to p\rho^+}\left(\not{p}+M\right)\gamma^0 T^{\nu\eta\dagger}_{p\to p\rho^+}\gamma^0\left(\not{p}+\not{q}-\not{k}+M\right)\right] \\ &\times \mathrm{Tr}\left[\sigma^{\beta'\beta}k_{\beta'}\left(\not{l}+M\right)\sigma^{\delta'\delta}k_{\delta'}\left(\not{l}+\not{k}+M\right)\right] g_{\alpha\beta}g_{\eta\delta} \\ &\times D^2_{0\rho}(k)G(p;\rho_p)G(p+q-k;\rho_p)G(l;\rho_n)G(l+k;\rho_p) \quad (2.91) \end{aligned}$$

where

$$T^{\mu\alpha}_{p\to p\rho^+} = \sum_i t^{\mu\alpha}_{A_i} \qquad i = \Delta P, C\Delta P, NP, CNP \quad \text{for} \quad p \to p\rho^+ \qquad (2.92)$$

$$D_{0\rho}(k) = \frac{1}{k^2 - m^2_\rho} \qquad (2.93)$$

Some remarks must be here: Firstly, the factor $\left(\sqrt{2}\right)^2$ appears because it is a ρ^+ which excites the second ph. It comes from isospin counting. Secondly,

the second trace in Eq. (2.91) comes from the trace of the second fermion loop in the right-hand side of fig. 2.16. And thirdly, the factor $g_{\alpha\beta}g_{\eta\delta}$ is the only one which survives from the product of the tensorial components of the ρ-meson propagators $\left(-g_{\alpha\beta}+\frac{k_\alpha k_\beta}{m_\rho^2}\right)\left(-g_{\eta\delta}+\frac{k_\eta k_\delta}{m_\rho^2}\right)$[13].
The second trace in Eq. (2.91) is a symmetric Lorentz tensor given by

$$\begin{aligned} B^{\beta\delta}(k,l) &= -4k^\beta k^\delta M^2 + 4g^{\beta\delta}k^2M^2 - 8g^{\beta\delta}(k\cdot l)^2 - 8l^\beta l^\delta k^2 \\ &+ 4k^\beta k^\delta(k\cdot l) + 8l^\beta k^\delta(k\cdot l) + 8k^\beta l^\delta(k\cdot l) - 4g^{\beta\delta}k^2(k\cdot l) - 4k^\beta k^\delta l^2 \\ &+ 4g^{\beta\delta}k^2l^2 \end{aligned} \tag{2.94}$$

It accomplishes that is orthogonal to k. Indeed, we have the following relations:

$$B^{\beta\delta}(k,l)\cdot k_\beta = 0 \tag{2.95}$$
$$B^{\beta\delta}(k,l)\cdot k_\delta = 0 \tag{2.96}$$

If now we assume that the second pair ph is on-shell, i.e

$$l^2 = M^2, \qquad (l+k)^2 = M^2 \Longrightarrow k\cdot l = -\frac{k^2}{2} \tag{2.97}$$

Then the tensor reduces to

$$\begin{aligned} g_{\alpha\beta}g_{\eta\delta}B^{\beta\delta}(k,l) &\equiv B_{\alpha\eta}(k,l) = -8k_\alpha k_\eta M^2 + 8g_{\alpha\eta}k^2M^2 - 2k_\alpha k_\eta k^2 \\ &- 4l_\alpha k_\eta k^2 - 4k_\alpha l_\eta k^2 - 8l_\alpha l_\eta k^2 \end{aligned} \tag{2.98}$$

It can be demonstrated that the tensor

$$A^{\mu\nu}(p,q,k,l) \equiv \mathrm{Tr}\left[T^{\mu\alpha}\left(\not{p}+M\right)\gamma^0 T^{\nu\eta\dagger}\gamma^0\left(\not{p}+\not{q}-\not{k}+M\right)\right]B_{\alpha\eta} \tag{2.99}$$

accomplishes the fundamental relation expressed by Eq. (2.25).
In the contraction of Eq. (2.99), only the terms that do not contain either a k_α or a k_η survive, so we are left with the following reduced expression

$$\begin{aligned} A^{\mu\nu}(p,q,k,l) &= \mathrm{Tr}\left[T^{\mu\alpha}\left(\not{p}+M\right)\gamma^0 T^{\nu\eta\dagger}\gamma^0\left(\not{p}+\not{q}-\not{k}+M\right)\right]8k^2M^2 \\ &\times \left(g_{\alpha\eta}-\frac{l_\alpha l_\eta}{M^2}\right) \end{aligned} \tag{2.100}$$

[13] One should remember that $T^{\mu\alpha}k_\alpha = 0$, and the same for $T^{\nu\eta\dagger}k_\eta$.

And neglecting the contribution coming from the contraction with $\frac{l_\alpha l_\eta}{M^2}$, Eq. (2.91) reads

$$\begin{aligned} -i\Pi^{\mu\nu}(q) &= -\left(\frac{g}{2\sqrt{2}}\right)^2\left(\sqrt{2}\right)^2\frac{f^2_{\pi NN}}{m^2_\pi}C_\rho\int\frac{d^4p}{(2\pi)^4}\int\frac{d^4k}{(2\pi)^4}G(p;\rho_p) \\ &\times G(p+q-k;\rho_p)D^2_{0\rho}(k)8k^2M^2A^{\mu\nu}_{p\to p\rho^+}(p,q,k) \\ &\times \underbrace{\int\frac{d^4l}{(2\pi)^4}G(l;\rho_n)G(l+k;\rho_p)} \end{aligned} \tag{2.101}$$

where the expression over the symbol $\underbrace{\quad}$ is $\frac{i}{8M^2}\bar{U}^{n,p}_R(k)$. And now

$$A^{\mu\nu}_{p\to p\rho^+}(p,q,k) = g_{\alpha\eta}\mathrm{Tr}\left[T^{\mu\alpha}_{p\to p\rho^+}\left(\not{p}+M\right)\gamma^0T^{\nu\eta\dagger}_{p\to p\rho^+}\gamma^0\left(\not{p}+\not{q}-\not{k}+M\right)\right] \tag{2.102}$$

Therefore, the final result is

$$\begin{aligned} -i\Pi^{\mu\nu}(q) &= (-i)\left(\frac{g}{2\sqrt{2}}\right)^2\left(\sqrt{2}\right)^2\frac{f^2_{\pi NN}}{m^2_\pi}C_\rho\int\frac{d^4k}{(2\pi)^4}D^2_{0\rho}(k)k^2\bar{U}^{n,p}_R(k) \\ &\times \int\frac{d^4p}{(2\pi)^4}G(p;\rho_p)G(p+q-k;\rho_p)A^{\mu\nu}_{p\to p\rho^+}(p,q,k) \end{aligned} \tag{2.103}$$

If one compares the above equation with Eq. (2.52) one sees the following replacements

1. A minus global sign with respect to the 2p2h selfenergy diagram with pions.
2. $\frac{g_A}{2f_\pi}$ is replaced by $\frac{f_{\pi NN}}{m_\pi}\sqrt{C_\rho}$.
3. $k_\pi \longrightarrow k$,
4. $D_0(k_\pi)$ is replaced by $D_{0\rho}(k)$.
5. And finally $A^{\mu\nu}_{p\to p\pi^+}$ is replaced by $A^{\mu\nu}_{p\to p\rho^+}$

Therefore, summing all the isospin channels, the result will be the same than in Eq. (2.56) with the above replacements and a minus global sign

with respect to Eq. (2.56).

$$\begin{aligned} W^{\mu\nu}_{2p2h-t}(q) &= \theta(q^0)\frac{1}{M^2}\frac{f^2_{\pi NN}}{m^2_\pi}C_\rho\int\frac{d^3r}{2\pi}\int\frac{d^4k}{(2\pi)^4}k^2D^2_{0\rho}(k)F^4_\rho(k) \\ &\times \theta(k^0)\theta(q^0-k^0)\Bigg\{\mathrm{Im}\bar{U}^{n,p}_R(k)\Big[\mathrm{Im}\bar{U}^{p,p}_R(q-k)A^{\mu\nu}_{p\to p\rho^+} \\ &+ \mathrm{Im}\bar{U}^{n,n}_R(q-k)A^{\mu\nu}_{n\to n\rho^+}\Big]+\frac{1}{2}\mathrm{Im}\bar{U}^{n,p}_R(q-k) \\ &\times \left[\mathrm{Im}\bar{U}^{n,n}_R(k)+\mathrm{Im}\bar{U}^{p,p}_R(k)\right]A^{\mu\nu}_{n\to p\rho^0}\Bigg\} \end{aligned} \tag{2.104}$$

The form factor $F^4_\rho(k)$ appears because the ρ-mesons are off-shell. Also here, when placing the 2p2h excitations on-shell, we have that the nucleon propagator with momentum $p+q$ (this is part of the amputated amplitude $t^{\mu\alpha}_{A_{NP}}$) can be placed on-shell for a virtual W. Thus, we perform an angular average of the traces that appear in the evaluation of the diagram, namely

$$A^{\mu\nu}_{N\to N'\rho^\lambda}=\frac{1}{2}\int_{-1}^{1}d\mu\; g_{\alpha\eta}\mathrm{Tr}\left[T^{\mu\alpha}_{N\to N'\rho^\lambda}\left(\not{p}+M\right)\gamma^0T^{\nu\eta\dagger}_{N\to N'\rho^\lambda}\gamma^0\left(\not{p}+\not{q}-\not{k}+M\right)\right] \tag{2.105}$$

with $\mu=\cos(\widehat{\vec{p},\vec{q}})$. To simplify the numerical integration, we have given a small width (~ 10 MeV) to the $p+q$ nucleon propagator and we have used an average for the modulus of $\vec{p}$ and fixed the $(\vec{p},\vec{q})$-plane, avoiding thus to perform two nested integrals.

We could have deduced Eq. (2.104) by approximating the ph ρ-selfenergy (right-hand part of the diagram depicted in Fig. 2.16) by

$$\Pi_{\alpha\beta}(k)=\left(-g_{\alpha\beta}+\frac{k_\alpha k_\beta}{k^2}\right)\hat{\Pi}^\lambda(k),\qquad \hat{\Pi}^\lambda(k)=F^2_\rho(k)C_\rho\frac{f^2_{\pi NN}}{m^2_\pi}\vec{k}^2U_\lambda(k) \tag{2.106}$$

with λ the charge of the ρ-meson, and $U_\lambda(k)$ the Lindhard function for a particle-hole excitation by an object of charge λ: this is, twice $\bar{U}^{p,n}_R$ or $\bar{U}^{n,p}_R$ for the excitation by a charged ρ-meson or $\bar{U}^{p,p}_R+\bar{U}^{n,n}_R$ for the excitation by a neutral ρ-meson.

Eq. (2.106) is obtained by neglecting higher order terms, $\mathcal{O}(\vec{l}^2/M^2)$, being $\vec{l}=\vec{p},\vec{q}$ or $\vec{k}$. This is consistent with the non-relativistic reduction that leads

to the effective potentials given in Eqs. (2.65) and (2.66).
As previously done in the case of the 2p2h mechanisms driven by the longitudinal spin-isospin ph-ph interaction, we replace in Eq. (2.104),

$$\mathrm{Im}\bar{U}_R^{N,N'}(k) \Rightarrow \frac{\mathrm{Im}\bar{U}_R^{N,N'}(k)}{|1 - V_t\, U(k)|^2} \tag{2.107}$$

By including the non-relativistic Lindhard function for ph + Δh excitations in the denominator, we replace the ph excitation of the right-hand in Fig. 2.16 by a series of RPA excitations through ph and Δh excitations, driven by V_t.
We also multiply every amputated amplitude $t_{A_i}^{\mu\alpha}$ by a suitable factor which allows us to replace the ρ-exchange interaction in Fig. 2.16 by the transverse part (V_t) of the effective ph-ph potential.

$$t_{A_i}^{\mu\alpha} \Rightarrow t_{A_i}^{\mu\alpha} \times \left(1 + \frac{g'_t}{F_\rho^2(k) D_{0\rho}(k) C_\rho \vec{k}^2}\right) \tag{2.108}$$

2.2.6 Final remarks

Some remarks are here in order. We must be careful to avoid double counting. Indeed, for instance, the contribution to the hadron tensor of the Δh excitation term arises from the imaginary part of the Δ propagator and in particular from the Δ-width, see Eq. (2.29). One of the terms implicit in Fig. 2.6 (depicted diagrammatically in Fig. 2.17(a)) is the one that picks up the ΔP term both in J^μ and in $J^{\nu\dagger}$. This term gives precisely the same contribution than the bare Δh diagram (Fig. 2.4) plus some medium corrections that take into account the Pauli blocking effects. Thus, if we would naively add it to the hadronic tensor, the contribution of Eq. (2.29) would be counted twice. Indeed, the term of Fig. 2.17(a) can be cast in the form of the diagram of Fig. 2.4, but with a Δ-selfenergy insertion constructed from a pion loop. When the pion is put on the mass shell to build the hadron tensor, we obtain the Δ-width and thus qualitatively the equivalence is shown[14]. In a similar way, the diagram of Fig. 2.17(b) is one of the terms implicit in the diagram of Fig. 2.7 that produces a 2p2h excitation.
However, given the importance of the Δ-pole contribution and since the Δ

[14] In Appendix D, this equivalence will be shown quantitatively.

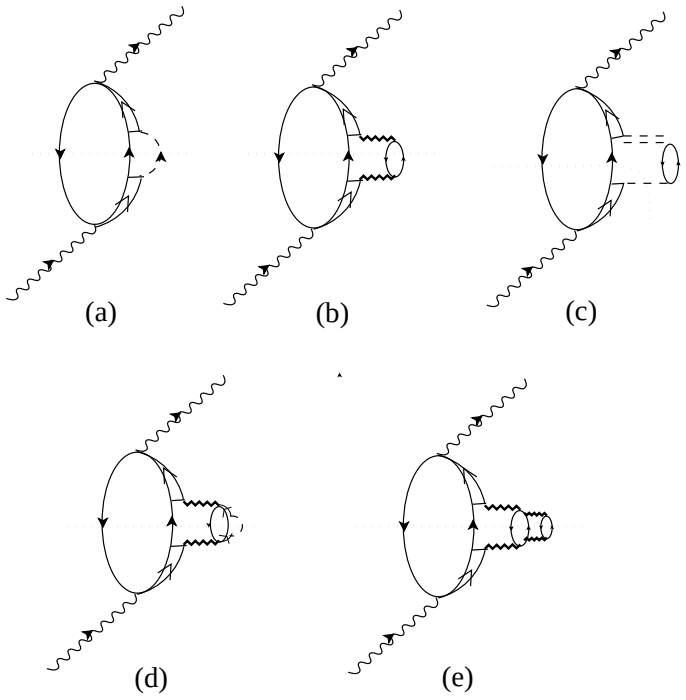

Figure 2.17: Diagrammatic representation of the different contributions of the Δh weak-nuclear excitation term.

properties are strongly modified inside the nuclear medium [43, 55, 124, 126, 132–134], a more careful treatment of the Δ mechanisms is advisable. This implies some additional nuclear corrections to eq. (2.29) to include the full effect of the selfenergy of the Δ in the medium $\Sigma_\Delta(\rho(\vec{r}))$ in a systematic manner. In addition, these correction provide genuinely new contributions to the hadronic tensor (e.g. 3p3h mechanisms). Here, we follow the same approach as in Ref. [43], which is based on Refs. [126, 127, 131]. In the nuclear medium, the resonance selfenergy is modified because of several effects such as Pauli blocking of the final nucleon and absorption processes: $\Delta N \to NN$, $\Delta N \to NN\pi$, or $\Delta NN \to NNN$. This is done using a ph-ph interaction that includes, besides pion exchange, short range correlations, a transverse channel driven by ρ-exchange and a RPA re-summation.
Following this approach, in the Δ-propagator, we approximate

$$\frac{1}{p_\Delta^2 - M_\Delta^2 + iM_\Delta\Gamma_\Delta} \sim \frac{1}{(W + M_\Delta)(W - M_\Delta + i\Gamma_\Delta/2)} \tag{2.109}$$

with $W^2 = p_\Delta^2$. In the propagator of the right-hand side of the above equation, we make the substitution: $\Gamma_\Delta/2 \to \Gamma_\Delta^{\rm Pauli}/2 - {\rm Im}\Sigma_\Delta$ and we take ${\rm Im}\Sigma_\Delta(\rho(\vec{r}))$ and $\Gamma_\Delta^{\rm Pauli}/2$ as follows. Firstly, the Pauli blocking of the πN decay reduces the Γ_Δ free width to $\Gamma_\Delta^{\rm Pauli}$, which can be found in Eq. (15) of Ref. [127]. Next, the imaginary part of the selfenergy accounts for the diagrams depicted in Fig. 2.17, where the double dashed line stands for the effective spin-isospin interaction, while the wavy line accounts for the induced interaction. The effective spin-isospin interaction is originated by π and ρ exchange in the presence of short range correlations. It is obtained by substituting [126, 127, 131]

$$\left(\frac{f_{\pi NN}}{m_\pi}\right)^2 \hat{q}_i\hat{q}_j\vec{q}^{\,2}D_0(q) \to \hat{q}_i\hat{q}_j V_l(q) + (\delta_{ij} - \hat{q}_i\hat{q}_j)V_t(q) \tag{2.110}$$

with $\hat{q}_i = q_i/|\vec{q}|$. The induced interaction accounts for the series of diagrams depicted in Fig. 2.18. There is an RPA sum through particle-hole and Δh excitations and it is readily obtained as

$$V_{\rm ind} = \hat{q}_i\hat{q}_j\frac{V_l(q)}{1 - U(q)V_l(q)} + (\delta_{ij} - \hat{q}_i\hat{q}_j)\frac{V_t(q)}{1 - U(q)V_t(q)} \tag{2.111}$$

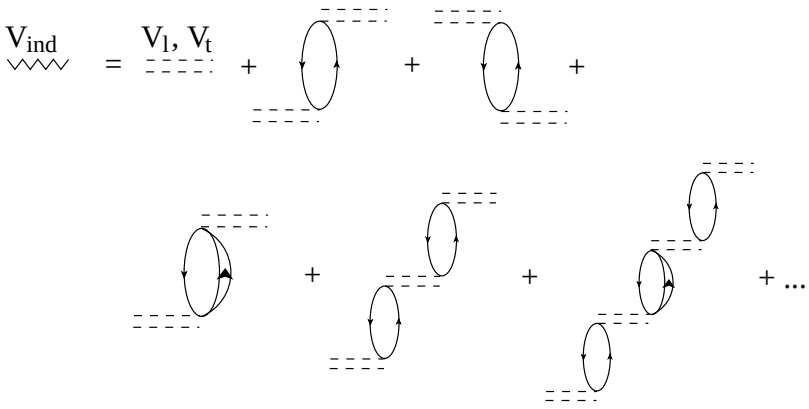

Figure 2.18: Diagrammatic representation of the induced interaction

where $U(q)$ is the non-relativistic Lindhard function por ph + Δh excitations[15]. The evaluation of Σ_Δ was done in Ref. [131]. The imaginary part of Σ_Δ can be parameterized as

$$-\mathrm{Im}\Sigma_\Delta(\rho(\vec{r})) = C_Q \left(\frac{\rho}{\rho_0}\right)^\alpha + C_{A_2} \left(\frac{\rho}{\rho_0}\right)^\beta + C_{A_3} \left(\frac{\rho}{\rho_0}\right)^\gamma \qquad (2.112)$$

where the different coefficients are given[16] in Eq. (4.5) and Table 2 of Ref. [131]. The separation of terms in Eq. (2.112) is very useful because the term C_Q comes from the $\Delta N \to NN\pi$ process (diagrams (c) and (d) of Fig. 2.17 when the lines cut by the dotted line are placed on-shell, and hence this term is related to the (W^*, π) channel). While, C_{A_2} and C_{A_3} come from diagrams (b) and (e) respectively and are related to two $(W^*NN \to NN)$

[15]The different couplings for N and Δ are incorporated in U_N and U_Δ and then the same interaction strenghts V_l and V_t are used for ph and Δh excitations [124].

[16]The parameterizations are given as a function of the kinetic energy in the laboratory system of a pion that would excite a Δ with the corresponding invariant mass and are valid in the range 85 MeV $< T_\pi <$ 315 MeV. Below 85 MeV the contributions from C_Q and C_{A_3} are rather small and are taken from Ref. [127], where the model was extended to low energies. The term with C_{A_2} shows a very mild energy dependence and we still use the parameterization from Ref. [131] even at low energies. For T_π above 315 MeV we have kept these selfenergy terms constant and equal to their values at the bound. The uncertainties in these pieces are not very relevant there because the $\Delta \to N\pi$ decay becomes very large and absolutely dominant.

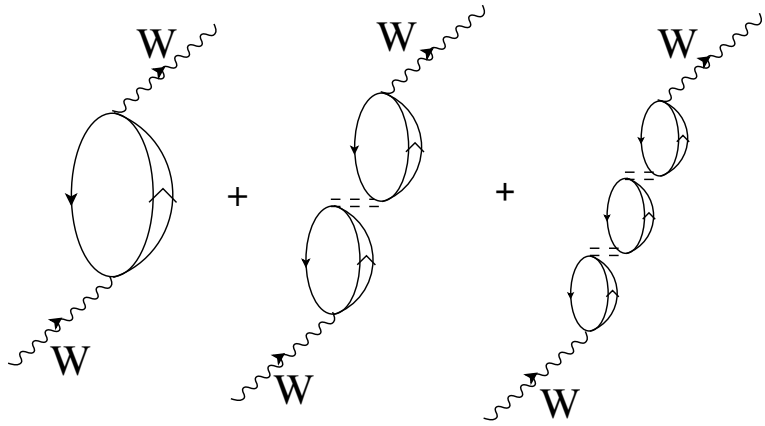

Figure 2.19: Irreducible pieces in the Δh channel from the Δh interaction

and three ($W^*NNN \to NNN$) body absorption. Therefore, the separation in this formula allows us to separate the final cross section into different channels.

To avoid double counting, we must substract the contribution of the $\Delta P - \Delta P$ diagram of Fig. 2.17(a) from Eq. (2.45), because this has been taken into account through the $\Gamma_\Delta^{\rm Pauli}$ piece of the Δ selfenergy. We must also substract the contribution of the $\Delta P - \Delta P$ diagram of Fig. 2.17(b) from Eqs. (2.61) and (2.104), because these terms were already taken into account in the evaluation of the C_{A_2} contribution of the Δ-selfenergy [131].

To end this subsection, we would like to devote a few words to the real part of the Δ-selfenergy and the RPA sum of Δh excitations shown in Fig. 2.19. Both of them produce effects on the nuclear response to the weak probe that partially cancel out. In Ref. [131], the dispersive contributions to ${\rm Re}\Sigma_\Delta$ associated to the diagrams that gave rise to ${\rm Im}\Sigma_\Delta$ were also computed. There, it was found ${\rm Re}\Sigma_\Delta^{(0)} \sim -50\rho/\rho_0$ [MeV] at $T_\pi = 50$ MeV and a smooth dependence on the pion energy. In principle, ${\rm Re}\Sigma_\Delta^{(0)}$ could have been taken into account by replacing $M_\Delta \to M_\Delta + {\rm Re}\Sigma_\Delta^{(0)}$ in the particle propagator of the right-hand side of Eq. (2.109). On the other hand, it is easy to realize that the RPA sum of Δh excitations, shown in Fig. 2.19 can be cast as a contribution to the real part of the Δ-selfenergy [43]. Actually, the latter depends on the particular component of the hadron tensor which is being

evaluated. Thus, for instance, the RPA series depicted in Fig. 2.19 can be taken into account, when computing $W^{xx}_{\Delta h}$ or $W^{yy}_{\Delta h}$ (transverse components to the direction of the W-boson) by replacing $\mathrm{Re}\Sigma^{(0)}_{\Delta}$ by $\mathrm{Re}\Sigma^{(0)}_{\Delta} + 4\rho V_t/9$. This latter sum, in good approximation, is positive for the whole range of energies studied here. This was the situation for the inclusive (e, e') nuclear reaction studied in Ref. [43], since there, the excitation of the Δ resonance by the virtual photon selected the transverse mode of the RPA series (see discussion of Eq. (44) in Ref. [43]). However, when the longitudinal component $W^{zz}_{\Delta h}$ is evaluated, the longitudinal part of the effective spin-isospin interaction is selected and now, this RPA sum is taken into account by substituting $\mathrm{Re}\Sigma^{(0)}_{\Delta}$ by $\mathrm{Re}\Sigma^{(0)}_{\Delta} + 4\rho V_l/9$, which shows a more pronounced q^2-dependence than the combination that appeared in the RPA renormalization of the transverse components of the hadronic tensor. Indeed, it turns out that the $\mathrm{Re}\Sigma^{(0)}_{\Delta} + 4\rho V_l/9$ combination does not have a well defined sign for the whole kinematical range of energies studied in this work. Setting to M_Δ the position of the pole of the Δ-propagator, or changing it by adding or substracting to M_Δ about 30 MeV, as it could be inferred from the typical values that $\mathrm{Re}\Sigma^{(0)}_{\Delta} + 4\rho V_{l(t)}/9$ takes for the relevant kinematics to this work, leads to trivial shifts in the position of the Δ-peak, moderately changes in the strength (around 20 %) at the maximum and very tiny changes in the q^0-differential shape. Of course, all these effects induced by the RPA resummation might be properly taken into account, as it was done for the case of the QE-region[17] in Ref. [38], but they, in conjunction with $\mathrm{Re}\Sigma^{(0)}_{\Delta}$, would induce changes smaller than both, the precision in the current experimental determination of cross sections, and the uncertainties due to our lack of a precise knowledge of the axial $N - \Delta$ transition form factor C_5^A [99]. For simplicity, in this work we will not renormalize the real part of the position of the Δ-peak, which eventually could be studied in the future when more accurate measurements will become available.

[17] For QE kinematics, taking into account properly the RPA effects is much more important [38] than in the Δ-region, since the cancellation of their effects with the difference between particle and hole selfenergies is much less effective.

2.2.7 CC antineutrino induced reactions

If we now focus in the antineutrino induced nuclear reaction

$$\bar{\nu}_l(k) + A_Z \rightarrow l^+(k') + X \tag{2.113}$$

and we calculate the selfenergy of the antineutrino, we will obtain the same equations than in the previous sections with the following changes:

1. A change of the sign for the antisymmetric part of the leptonic tensor ($L_a^{\mu\nu}$).

2. To relate the $W^- N \rightarrow N'\pi^\lambda$ amplitudes to the W^+ ones by means of the equations (11), (12) and (13) of Ref. [47].

3. In the asymmetrical Lindhard functions, make the replacement $p \leftrightarrow n$, $\pi^+ \rightarrow \pi^-$ and $\pi^0 \rightarrow \pi^0$.

4. We take the $\bar{\nu}$-QE cross sections from Ref. [38].

2.3 Results

We will mainly focus here in the dip and $\Delta-$peak regions, since the QE contribution was discussed at length in Ref. [38]. In Fig. 2.20, we show results for both muon neutrino (top) and antineutrino (bottom) induced CC differential cross sections at 30 degrees as a function of the energy transferred to the nucleus (^{16}O). The incoming neutrino (anti neutrino) energy is 750 MeV. We clearly observe both the $\Delta(1232)$ and the QE peaks; for this scattering angle, the QE contribution turns out to be significantly larger than that of the Δ resonance. We split the full contribution into the QE and non QE (Δ+1p1h1π+ 2p2h) parts. General features are the same for both neutrino and antineutrino induced cross sections, and the main difference is an homogeneous reduction in the size of the differential cross section. For comparison, in the upper panel (blue dashed-dotted line) we also display some results from Ref. [39], obtained within the Giessen Boltzmann-Uehling-Uhlenbeck (GiBUU) framework, which takes into account various nuclear effects: the local density approximation for the nuclear ground state, mean-field potentials, and in-medium spectral functions, but does not those due

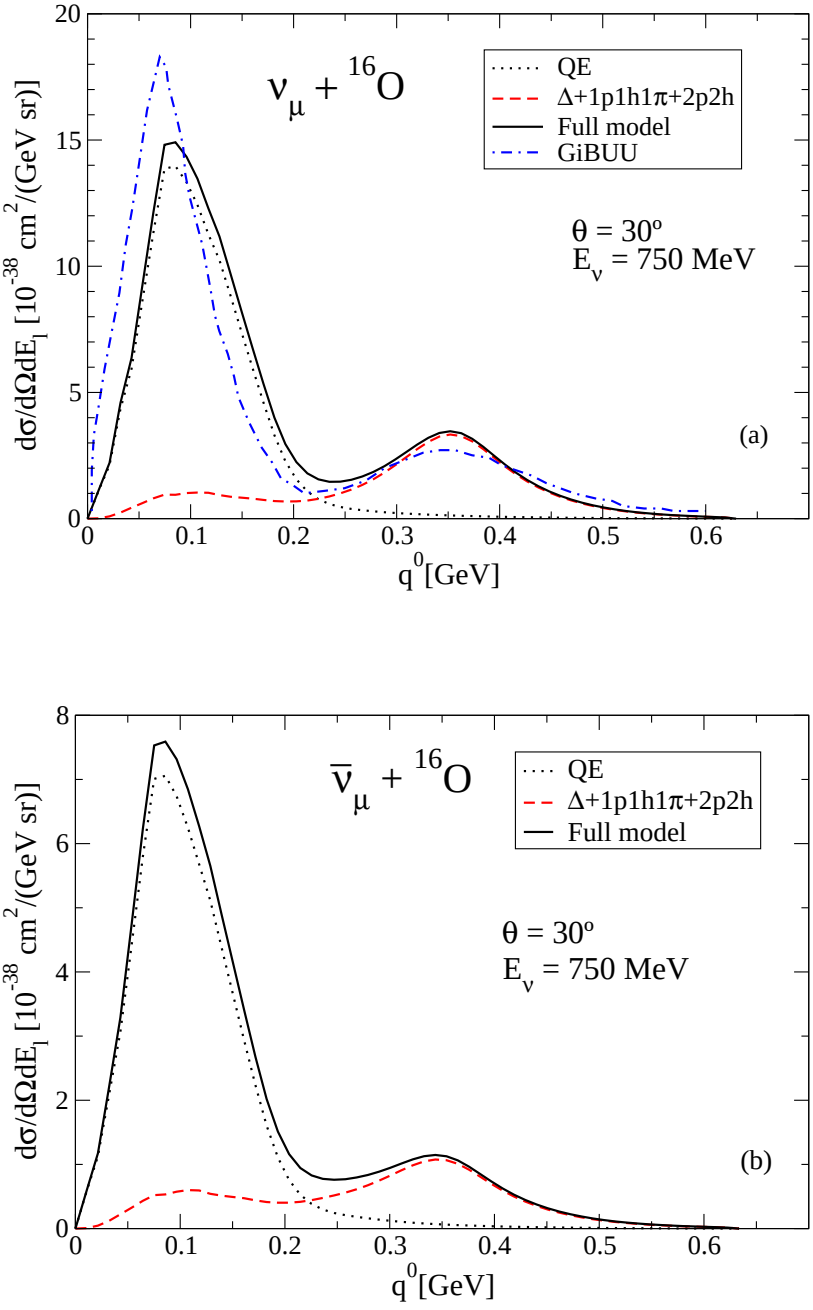

Figure 2.20: Muon neutrino (up) and antineutrino (down) CC differential cross section $\frac{d\sigma}{d\Omega dE_\mu}$ in oxygen, at 30 degrees of scattering angle in ^{16}O and with an incident neutrino energy of 750 MeV, plotted against the transferred energy to the nucleus. Different contributions are displayed, standing the solid lines for our full model results. Besides in the upper panel, we also show results (blue dash-dotted line) from Ref. [39] and obtained within the GiBUU framework.

to RPA correlations. We note first, some discrepancies between these results and ours in the QE region, which origin can be traced back to the implementation of RPA corrections in our scheme [38]. Indeed, the found differences (small shift in the position and reduction in size (about 25%) of the QE peak) are qualitatively identical to those existing between data and GiBUU predictions for the case of inclusive electron cross section at a similar kinematics (incident electron energy of 700 MeV and scattering angle of 32 degrees), and showed in the upper panel of Fig. 9 of Ref. [39]. On the other hand, in this latter figure can be also appreciated the limitations of the GiBUU model to describe the dip region. Indeed, we see in Fig. 2.20 that in the dip region, our model predicts also larger cross sections than those obtained within the GiBUU scheme. This is due to the 2p2h mechanisms of Figs. 2.7 and 2.16 included in our model. Actually, these contributions make also our cross section at the $\Delta-$peak larger than the one predicted by the GiBUU model, despite we use a value of $C_5^A(0)$ smaller than that used in Ref. [39] (1 vs 1.2). For larger scattering angles, the dip-region cross section becomes relatively much more important, and thus the inclusion of the 2p2h contributions would turn out to be of larger relevance. This is clearly appreciated in Fig. 2.21, where we show now results at 60 degrees. In this figure, and besides the separation between QE and non QE contributions to the differential cross section, the 2p2h part[18] of this latter contribution is shown (orange double dashed-dotted curves). The blue dash-dotted lines stand in this figure for the results obtained from only the Δh weak–nuclear excitation term of Fig. 2.17(a), neglecting also there, Pauli blocking effects affecting to the in medium resonance width. We note, that the the systematic many body $W-$absorption modes and the in medium effects considered here change drastically the nuclear response function in the $\Delta-$peak as well, and it was also the case in the QE region [38].

The 2p2h cross section accounts for events were the gauge boson is absorbed by a pair of nucleons, in contrast to QE events for which it is absorbed by one nucleon, and furthermore no pions are being produced in this first step. Up to re-scattering processes which could eventually produce secondary pions, those events will give rise to only one muon to be detected. Thus, they could be experimentally misidentified as QE events. Yet, 1p1h1π events, in

[18] A small three body absorption (3p3h) contribution, induced by C_{A_3} in the $\Delta-$selfenergy of Eq. (2.112) is also included under the label 2p2h in Fig. 2.21.

which the resulting pion from the W absorption is subsequently absorbed and does not come off the nucleus, could be also misinterpreted as QE events, if only leptons are being detected. A correct identification of CCQE events, which is the signal channel in oscillation experiments, is relevant for neutrino energy reconstruction and thus for the oscillation result. By looking at the 2p2h contribution in Fig. 2.20, We see that at least about 10% of the quasielastic cross section might be misidentified in present-day experiments and need to be corrected for by means of event generators. As mentioned above, 1p1h1π mechanisms followed by the absorption of the resulting pion, will even make worse the situation [135].

In Fig. 2.22, we show CC q^2 differential cross sections in carbon and for an incident energy of 1 GeV. We observe that the 2p2h contribution is sizeable for both, neutrino and antineutrino induced reactions, and that it shows a less pronounced q^2 dependence than the QE or the Δ+1p1h1π components of the total result. On the other hand, the antineutrino distribution is much more narrower than the neutrino one. Neglecting lepton masses, both distributions should be equal at $q^2 = 0$, and since antineutrino cross sections are smaller than neutrino ones, is reasonable to expect ν distributions to be wider than $\bar{\nu}$ ones.

The MiniBooNE collaboration has measured [40] the muon neutrino CCQE cross section on ^{12}C. The flux-unfolded results as a function of the neutrino energy are depicted in the upper panel of Fig. 2.23, together with different predictions from the scheme presented here. The first observation is that our QE curve misses the data-points, being our predicted cross section significantly smaller than those reported by the MiniBooNE collaboration. Actually in [40], and to achieve a reasonable description of the data, an unexpectedly high effective axial mass $M_A^{\rm eff}$ (entering in the axial-vector WNN form-factor) of 1.35 GeV had to be used in the relativistic FG model implemented in the NUANCE event generator employed by the MiniBooNE collaboration. This value of M_A is significantly larger than the world average value $M_A = 1.03$ GeV. It is interesting to note, however, that in Ref. [40] is also pointed out the NOMAD [120] and LSND [136] high energy ($E_\nu > 4$ GeV) CCQE cross sections are better described with the world average value for M_A. The situation become even more worrying, after the work of O. Benhar et al. [118]. The authors of that work find that their theoretical approach based on the impulse approximation and realistic spectral

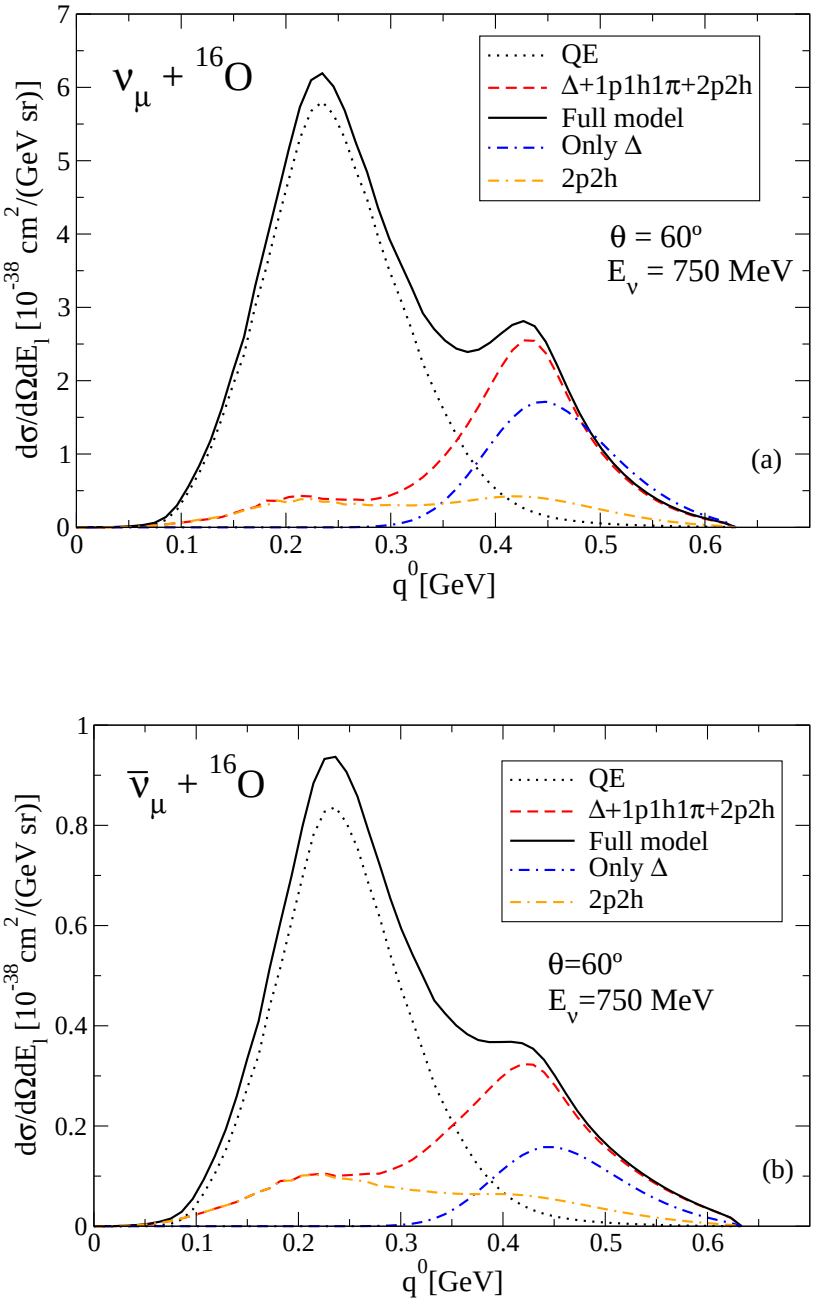

Figure 2.21: Muon neutrino (up) and antineutrino (down) CC differential cross section $\frac{d\sigma}{d\Omega dE_\mu}$ in oxygen, at 60 degrees of scattering angle in ^{16}O and with an incident neutrino energy of 750 MeV, plotted against the transferred energy to the nucleus. Different contributions are displayed, standing the solid lines for our full model results.

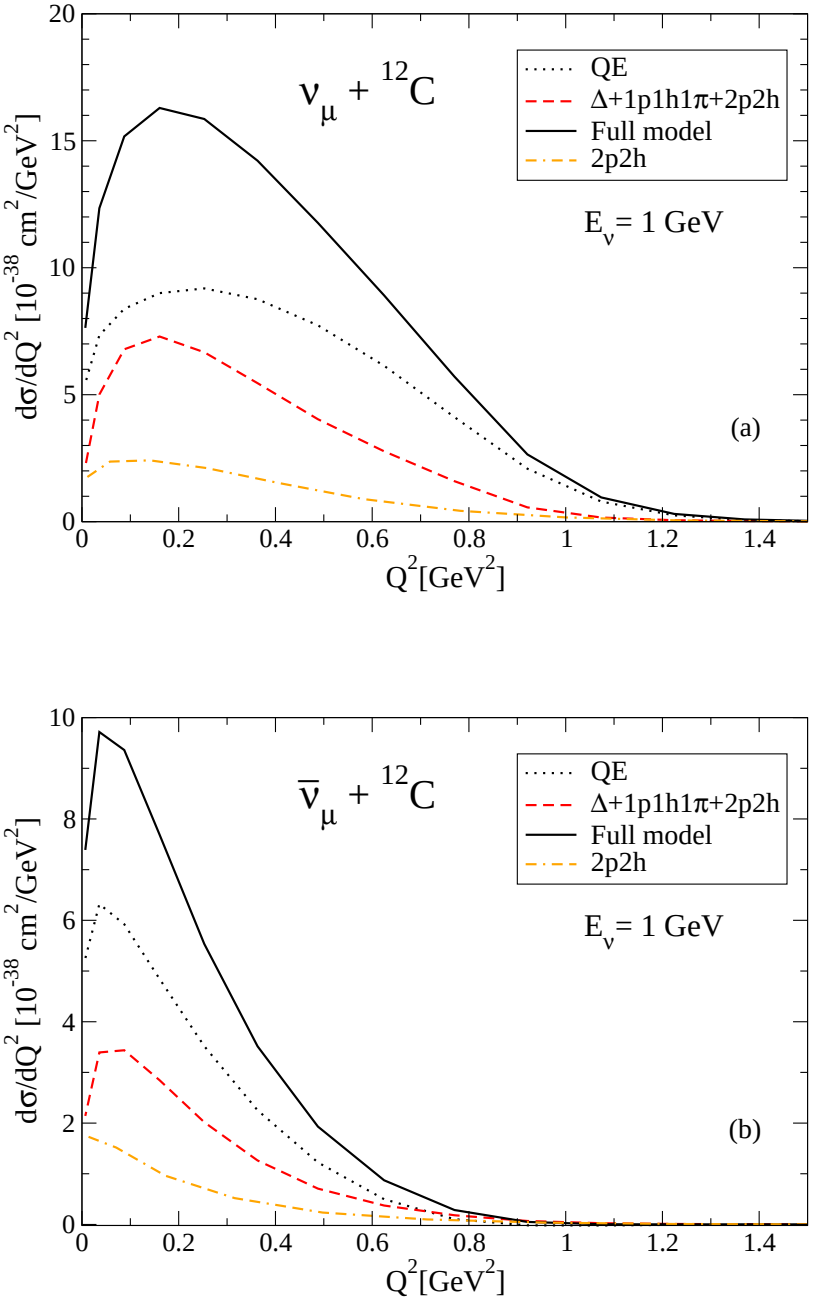

Figure 2.22: Muon neutrino (up) and antineutrino (down) CC differential cross section $\frac{d\sigma}{dQ^2}$ in carbon for an incident neutrino energy of 1 GeV ($Q^2 = -q^2$). Different contributions are displayed, standing the solid lines for our full model results.

functions, successfully applied to QE electron scattering, fails to reproduce the CCQE neutrino-nucleus cross section, unless the value of the nucleon axial mass resulting from deuteron measurements is significantly increased. In addition, they also rule out the possibility, advocated in Ref. [40], of interpreting the large M_A resulting from the MiniBooNE analysis as an effective axial mass, modified by nuclear effects beyond the FG model [137]. Actually, in [118], it is suggested that the same many body techniques successfully applied in QE electron-nucleus scattering are not able to explain neutrino induced cross sections and it is even argued that the development of a new *paradigm*, suitable for application to processes in which the lepton kinematics is not fully determined, will be required.

Our results do not support this last statement/interpretation at all, and rather support the picture that emerges from the works of M. Martini et al. [44,45]. These latter works, in our opinion, constituted a significant step forward to clarify the situation. As mentioned above, in the MiniBooNE analysis, ejected nucleons are not detected and the QE cross section is defined as the one for processes in which only a muon is detected in the final state. The MiniBooNE analysis of the data corrects (through a Monte Carlo estimate) for events, where in the neutrino interaction a pion is produced, but it escapes detection because it is reabsorbed in the nucleus, leading to multinucleon emission. However, in [44, 45] it is pointed out that 2p2h or 3p3h mechanisms are susceptible to produce an apparent increase in the "QE" cross section, since those events will give rise to only one muon to be detected, and the MiniBooNE analysis does not correct for them. Within the scheme followed by Benhar and collaborators in Ref. [118], the occurrence of 2p2h final states is described by the continuum part of the spectral function, arising from nucleon-nucleon correlations, and there, this contribution is found to be quite small (less than 10% of the integrated spectrum). This is not surprising, since our QE results (dashed line) in the upper panel of Fig.2.23 contain also this contribution[19], and as we mentioned above we underestimate the data. However, the 2p2h contribution considered in [118] is far from being complete and it corresponds only to the many body diagram depicted in Fig. 2.10. Here, we compute all the contributions contained in

[19] The CCQE cross sections calculated in Ref. [38], were obtained using both particle and hole dressed propagators, determined from a realistic in medium nucleon selfenergy [138], and thus account for the spectral function effects considered in [118].

the generic diagrams of Figs. 2.7, 2.13 and 2.16, as it was previously done in Ref. [43] for electron scattering, obtained from a realistic model for the weak pion production off the nucleon. When these latter contributions are added to the QE prediction of Ref. [38], we obtain the solid green line in the upper plot of Fig. 2.23 in a better agreement with the MiniBooNE data.
Note that the spectral function model of Ref. [118], though successful to account for the QE electron–nucleus scattering, at intermediate energies, badly fails to describe both the dip and the $\Delta-$regions, as can be appreciated for instance in Figs. 5-8 of Ref. [83] or in the Fig. 1 of Ref. [118]. This is because the lack of a proper model to account for the absorption of the virtual photon for two or three nucleons in this model. As commented before, these multinucleon knockout events are likely part of the CC"QE" cross section measured by MiniBooNE, and that naturally explains the failure of the scheme of Ref. [83].
Coming back to the upper panel of Fig. 2.23, there we also display the band of theoretical uncertainties affecting to our results. To estimate this band, we have summed in quadratures a 15% relative error of our QE results, as discussed in Ref. [129], with the error induced by the uncertainties on the parametrization of the $C_5^A(q^2)$ form factor used here (set IV in Table I of Ref. [99]). Once our theoretical uncertainties are taken into account, we find a reasonable agreement with the MiniBooNE data. We would like to stress that we have not fitted here any parameter, and that we have just extended our previous work on electron-scattering of Ref. [43] to the study of CCQE cross sections.
In Fig. 2.23, we also show the results of Martini and collaborators (blue dashed-dotted line), taken from the *QE+np-nh RPA* curves of Fig. 5 of Ref. [44], which nicely fall within our band of theoretical predictions. Details of the model used by M. Martini and collaborators can be found in Ref. [45]. The evaluation of the nuclear response induced by this 2p2h mechanisms carried out in Ref. [45] is approximated, as the same authors recognize. The contributions in [45] that can be cast as a $\Delta-$selfenergy diagram should be quite similar to those obtained here in Subsect. 2.2.6, since in both cases the results of Salcedo and Oset of Ref. [131] for the $\Delta-$selfenergy are being used. However, some other contributions included here are, either not considered or not properly taken into account in [45]. For example, we believe that none of diagrams of Fig. 2.13 or those in Fig. 2.7 involving the *CT*,

PP and PF vertices of Fig. 2.5 have been considered in the work of Martini and collaborators. Moreover, the $NP-NP$, $CNP-CNP$, $NP-CNP$, $NP-\Delta P$, $NP-C\Delta P$, $CNP-\Delta P$, $CNP-C\Delta P$ and $\Delta P-C\Delta P$ diagrams implicit in Fig. 2.7, are not directly evaluated in [45], but instead there, a rough indirect estimate is given for them by relating their contribution to some absorptive part of the $p-$wave pion-nucleus optical potential. Given, all this, we find remarkable the agreement exhibited in Fig. 2.23 between our results and those previously published in Refs. [44, 45].

On the other hand, we see that in our calculation the relative contribution of the 2p2h mechanisms with respect to the QE cross section, is quite similar for both neutrino and antineutrino induced processes. Thus, our results do not support the claims of Ref. [44] of a minor role of the 2p2h mechanisms in the antineutrino mode.

We should mention that the MiniBooNE collaboration has also published the flux-integrated CC"QE" double differential cross section $d^2\sigma/dE_\mu d\cos\theta_\mu$ in bins of muon energy E_μ and cosine of the muon scattering angle with respect to the incoming neutrino direction. We must be careful before comparing with these valuable data. The reason is that the MiniBooNE flux remains sizeable up to neutrino energies too high to make meaningful the predictions of the model presented here. Indeed, neutrino energies of 1 or 1.2 GeV at most, is a clear upper limit of validity of our predictions.

To end this section in Fig. 2.24, we show total and QE inclusive cross sections for both neutrino and antineutrino modes. In the neutrino case, we compare our results with the recent data published by the SciBooNE collaboration. We display SciBooNE data-sets based on NEUT and NUANCE Monte Carlo event generators. We find a reasonable description, taking into account experimental and theoretical uncertainties, until neutrino energies around 1 GeV. At larger energies, we underestimate the cross section, as anticipated above. For instance, we see how some 2p2h1π contributions neglected in our model, become relatively important at $E_\nu = 1$ GeV. More specifically, the blue empty circle is obtained when the $\Delta-$resonance contribution to the imaginary part of U is kept in the evaluation of the imaginary part of the $\pi-$ and $\rho-$selfenergies in Eqs. (2.64) and (2.107). There are some other $W^+NN \to NN\pi$ mechanisms which should be taken into account, as well as the contribution of higher resonances or two pion production channels to end up with a robust and theoretical model above 1 GeV.

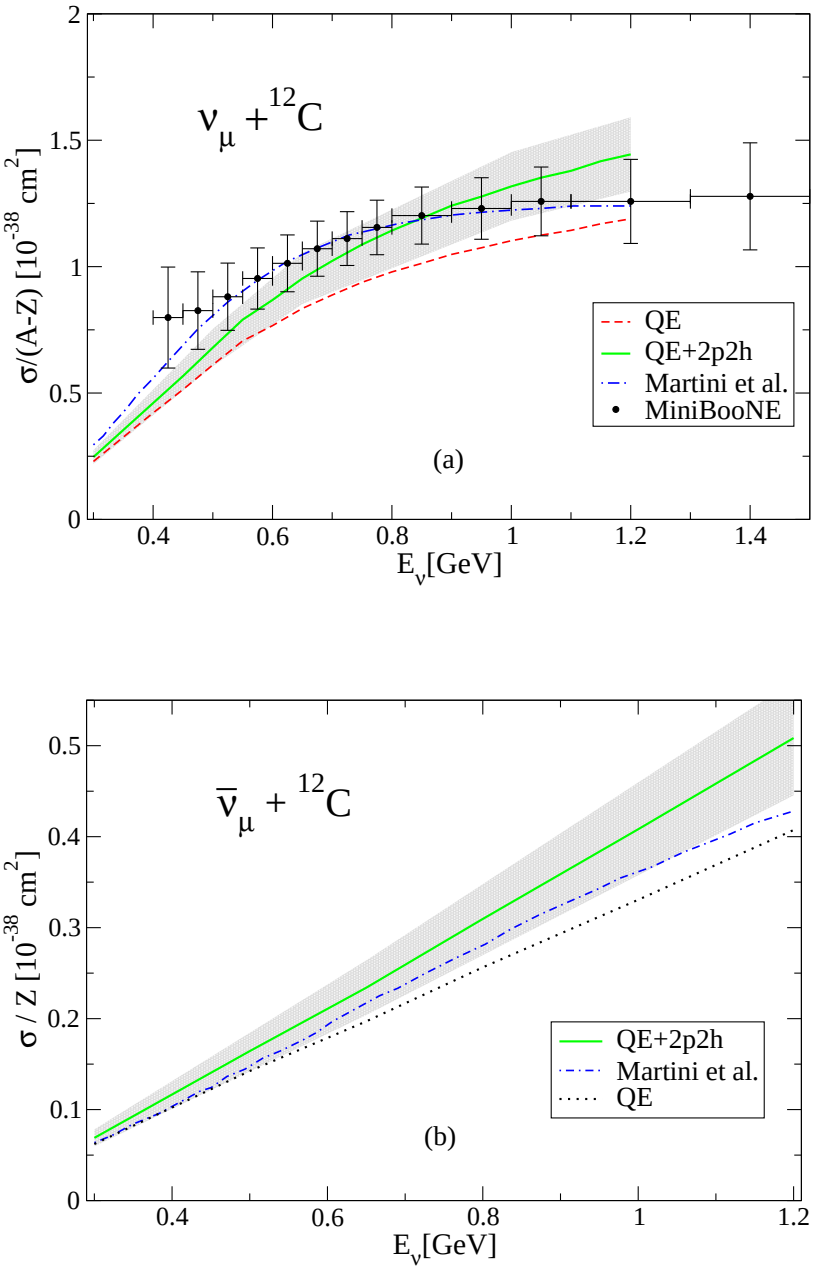

Figure 2.23: Up: Flux-unfolded MiniBooNE ν_μ CCQE cross section per neutron as a function of neutrino energy (data-points) from Ref. [40], together with different theoretical predictions from this work. Down: Different theoretical calculations for antineutrino cross sections per proton off ^{12}C as a function of the antineutrino energy. For comparison, in both plots, we also show the results (blue dashed-dotted line) of Martini and collaborators taken from Ref. [44].

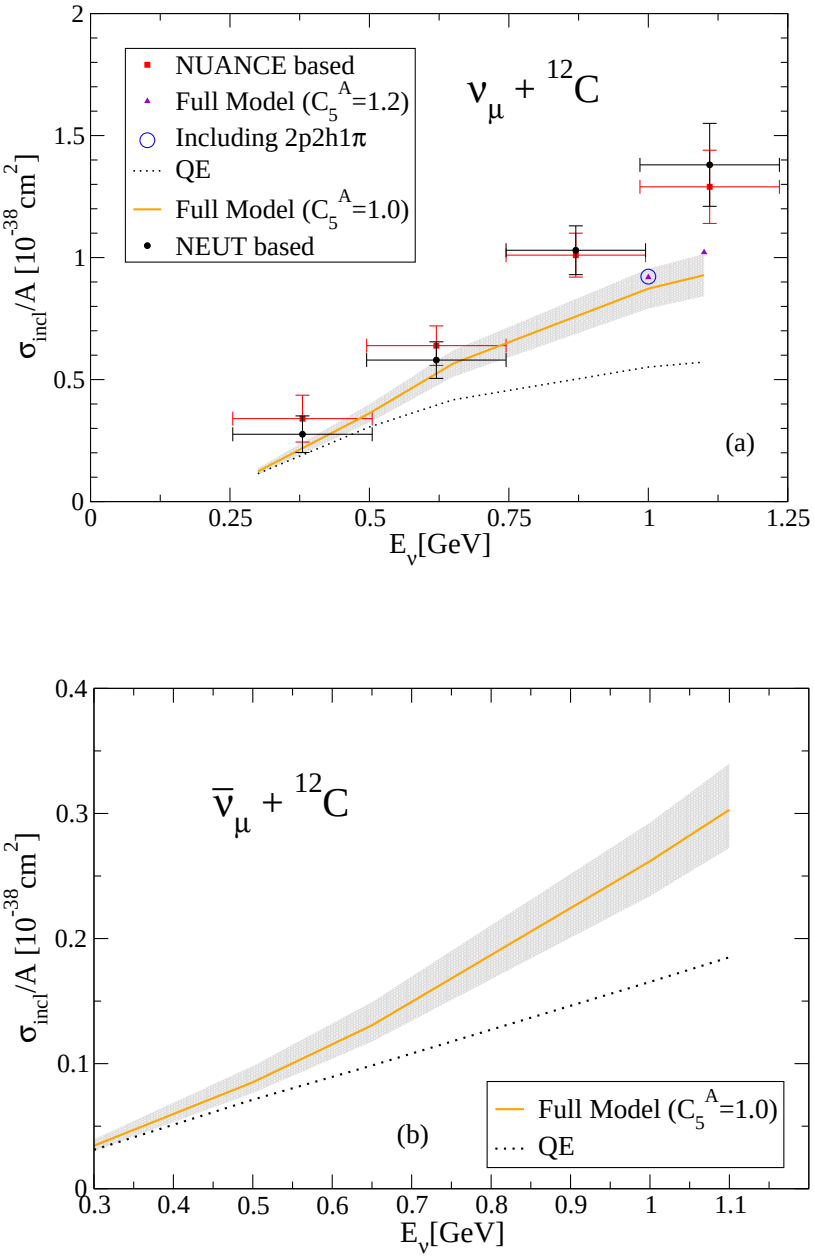

Figure 2.24: Up: Data points stand for the SciBooNE neutrino CC inclusive interaction cross section per nucleon [106]. We also show our QE and full model results, and in this latter case the theoretical uncertainty band is also displayed. At 1 GeV, we depict the full model cross sections obtained when the GTR value of 1.2 for $C_5^A(0)$ is used instead of 1 (violet triangle), and when some 2p2h1π contributions (blue empty circle), neglected in the present work, are taken into account (see text for some more details). Down: QE and full model predicted antineutrino CC inclusive cross section per nucleon, as a function of the antineutrino energy.

2.4 The problem of the axial mass

Elastic neutrino nucleon scattering can be described by three dominant form factors. The two vector form factors $F_{1,2}(Q^2)$ are well known from electron scattering (see, e.g. [139], for a review). The axial-vector form factor at $Q^2 = 0$, $G_A(0)$, is determined from neutron β decay. Assuming a dipole form, the Q^2 dependence of $G_A = G_A(0)(1 + Q^2/M_A^2)^{-2}$ can be characterized by the axial mass M_A. The value $M_A = 1.03 \pm 0.02$ is usually quoted as the world average [85,120], although a recent analysis claims an even smaller uncertainty ($M_A = 1.014 \pm 0.014$ [41]). It should be remarked that there are two independent experimental sources of information for this parameter, neutrino/antineutrino induced reactions and pion electroproduction. In the first case, bubble chamber data for ν-deuterium quasielastic (QE) scattering play a dominant role. The initial apparent disagreement between the values of M_A obtained with weak and electromagnetic probes was solved after correcting for hadronic effects [85] and now both sets of data are consistent. With these ingredients it looked straightforward to describe ν QE scattering in nuclei with the high precision required by the new and coming neutrino experiments, that aim to measure parameters such as the θ_{13} mixing angle or the leptonic CP-violating phase.

In this context, the charged current QE MiniBooNE data [40] have been quite surprising. First, the absolute values of the cross section are too large as compared to the consensus of prior theoretical models [116]. Actually, the cross section per nucleon on ^{12}C is clearly larger than for free nucleons. Second, their fit to the shape (excluding normalization) of the Q^2 distribution leads to an axial mass, $M_A = 1.35 \pm 0.17$ GeV, much larger than the previous world average. In fact, the large value of M_A also implies a substantial increase in the total cross section predicted by the Relativistic Fermi Gas (RFG) model used in the analysis, improving the agreement with the size of the cross section.

Similar results have been later obtained analyzing MiniBooNE data with more sophisticated treatments of the nuclear effects that work well in the study of electron scattering. For instance, Refs. [118,137] using the impulse approximation with state of the art spectral functions for the nucleons fail to reproduce data with standard values of M_A. Large axial mass values have also been obtained in Ref. [119] in a Fermi gas model and using spectral functions and in Ref. [117], where data have been analyzed in a relativis-

tic distorted-wave impulse approximation and with a relativistic Fermi gas model.

Certainly, there are some caveats that should be kept in mind like the flux uncertainty or inadequacies on the subtraction of background processes such as pion production. However, the associated uncertainties have been estimated and are properly included in the error bands provided in Ref. [40] and in the previously quoted analyses. Nonetheless, being the axial mass relatively well established by electron data, the failure to describe the MiniBooNE data with standard values of M_A could point out more to the incompleteness of the theoretical models than to the need of reconsidering the value of the parameter.

As a consequence, several new approaches incorporating new mechanisms that could contribute to the QE signal have been explored. An important step was undertaken in Refs. [44,45] with the inclusion of two nucleon mechanisms and other multinucleon excitations related to the Δ resonance. These works could reproduce the MiniBooNE total QE cross section without modifying the axial mass, suggesting that a good part of the experimental cross section was not properly QE scattering. The importance of meson exchange currents and multinucleon excitations has also been explored in Ref. [36].

The microscopic model for two nucleon excitation and pion production, discussed in the previous sections, was studied in Ref. [46], supporting the findings of Refs. [44, 45]. This latter model was a natural extension of the work in Refs. [38, 43, 112], where the purely quasielastic contribution to the inclusive electron and neutrino scattering on nuclei had been analyzed. We should remark that there are no free parameters in the description of nuclear effects, since they were fixed in previous studies of photon, electron, and pion interactions with nuclei [43, 123–127].

In Refs. [44–46] only the total cross section was evaluated and compared with the so called "unfolded" data of Ref. [40]. Certainly, the experimental data include energy and angle distributions and therefore provide a much richer information. Furthermore, the unfolded cross section is not a very clean observable after noticing the importance of multinucleon mechanisms, because the unfolding itself is model dependent and assumes that the events are purely QE. The same limitation occurs for the differential cross section $d\sigma/dQ^2$, given that Q^2 is also deduced assuming the events are QE. From that point of view, the best observable to compare with theoretical models,

and possibly constrain parameters, is the double differential cross section $d\sigma/dT_\mu dcos\theta_\mu$ because both the muon angle and energy are directly measured quantities.

For the QE part we will use here the full model of Ref. [38], as discussed in the previous sections, but without the inclusion of FSI interaction. The reason is that FSI was implemented in a nonrelativistic approach that makes it unsuitable for the large momenta transferred that are reached in the experiment under study. As it was discussed in [38], this FSI effects are always smaller than 7 percent for the total cross section[20] but could be more important in the angle and energy distributions. In Ref. [118], it was found that the main effect of FSI is a shift of ~ 10 MeV of the QE peak, although that could depend on details of the model [140].

To estimate the quality of the fit we use the following definition of χ^2 that properly takes into account the global normalization uncertainty ($\Delta\lambda = 0.107$) following the procedure of [141],

$$\chi^2 = \sum_{i=1}^{137} \left[\frac{\lambda \left(\frac{d^2\sigma^{exp}}{dT_\mu d\cos\theta}\right)_i - \left(\frac{d^2\sigma^{th}}{dT_\mu d\cos\theta}\right)_i}{\lambda\Delta\left(\frac{d^2\sigma}{dT_\mu d\cos\theta}\right)_i} \right]^2 + \left(\frac{\lambda-1}{\Delta\lambda}\right)^2, \qquad (2.114)$$

where λ is a global scale. $\frac{d^2\sigma^{exp}}{dT_\mu d\cos\theta}$ is the experimental cross section and $\Delta\left(\frac{d^2\sigma}{dT_\mu d\cos\theta}\right)$ its uncertainty, both taken from Ref. [40]. The sum runs over the 137 angle-energy bins with a cross section different from zero in Ref. [40]. As a first test, we have minimized χ^2 as a function of the axial mass in a simplified version of the model without multinucleon mechanisms and without RPA. This model should be quite similar to the one originally used in the MiniBooNE analysis. The main difference being that we use a local rather than global Fermi gas in the calculation. We obtain $M_A = 1.32 \pm 0.03$ with $\chi^2 = 35$. The fit is obviously very good and in agreement with Ref. [40]. The fitted scale is $\lambda = 0.97 + 0.03$ also supporting MiniBooNE findings, that a shape-only fit was also consistent with the total cross section.

As a second test, we consider the full model with the same axial mass used in our previous works ($M_A = 1.049$ GeV). The results corresponding to these two versions of the model are shown in Fig. 2.25. The full model also

[20] Thus, the results for the total cross section without FSI are still inside the uncertainty band of Ref. [46]

Table 2.1: Fit results for various models. See description in the text.

Model	Scale	Ma (GeV)	χ^2/# bins
LFG	0.96±0.03	1.321±0.030	33/137
Full	0.92±0.03	1.077±0.027	50/137
Full, $q_{cut} = 400$ MeV	0.83±0.04	1.007±0.034	30/123

agrees remarkably well with data. For this case we have $\chi^2 = 53$. This could look much worse, but it is still a very good agreement with χ^2 per degree of freedom much lower than one and it contains no fitted parameter. Furthermore, the shape is very good and χ^2 strongly depends on the normalization (scale and axial mass are strongly correlated). Therefore, from the quality of the fit only, one could not discriminate between the two versions of the model. However, we should recall that the RPA correlations and multinucleon mechanisms correspond to real nuclear effects that must be incorporated in the models.

Although, we think the consistency of MiniBooNE data with standard values of M_A has been established, one could still go further and try to use our full model to fit the data letting M_A to be a free parameter. We get $M_A = 1.077 \pm 0.027$ and $\lambda = 0.917 \pm 0.029$ with a strong correlation between both parameters. For this case, $\chi^2 = 50$. The 1 and 2 σ contours are plotted in Fig. 2.26. This is somewhat large a value for M_A but we think, the uncertainty size could be grossly underestimated. Notice first that, in the absence of a proper correlation matrix, the experimental uncertainties, except for the normalization, have been treated as fully uncorrelated. In addition, one should include in the minimization procedure not only the experimental but also the theoretical uncertainties related to other parameters of the model (e.g. πNN form factors, short range correlations, Δ in medium selfenergies, etc.).

The consideration of RPA and multinucleon mechanisms means that the present model is more appropriate than a pure impulse approximation for the low momentum transfer region. Nonetheless, at very low momenta a more detailed treatment of the nuclear degrees of freedom could be necessary. As done in Ref. [119], we could exclude from the analysis the bins with a large contribution of small momentum transfer. There is some arbitrariness in the actual choice of the cuts, but to allow for an easy comparison

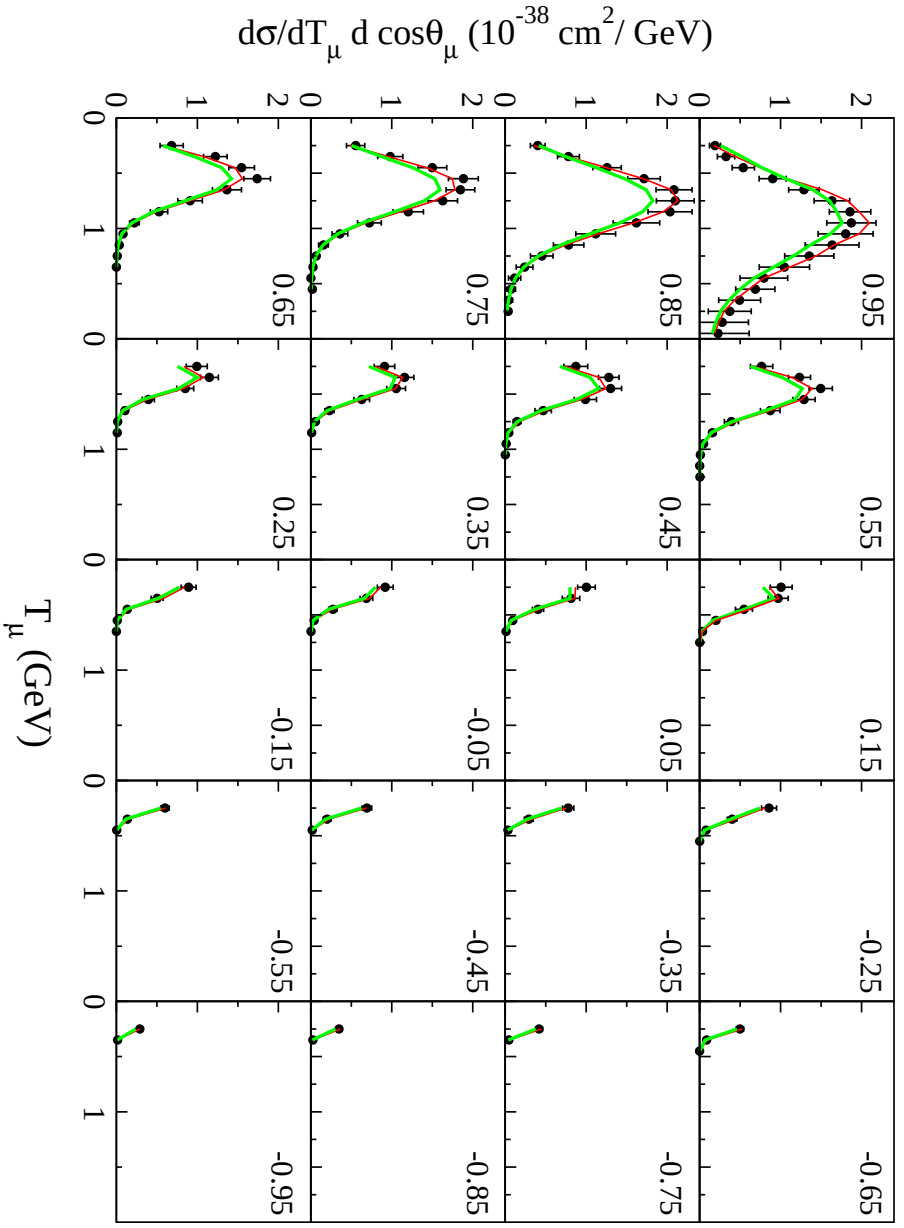

Figure 2.25: Muon angle and energy distribution $d\sigma/d\cos\theta_\mu dT_\mu$. Different panels correspond to the various angular bins labeled by their cosinus central value. Experimental points from Ref. [40]. Green line (no fit) is the full model (including multinucleon mechanisms and RPA) and calculated with $M_A = 1.049$ GeV. Red line is best fit ($M_A = 1.32$ GeV) for the model without RPA and without multinucleon mechanisms.

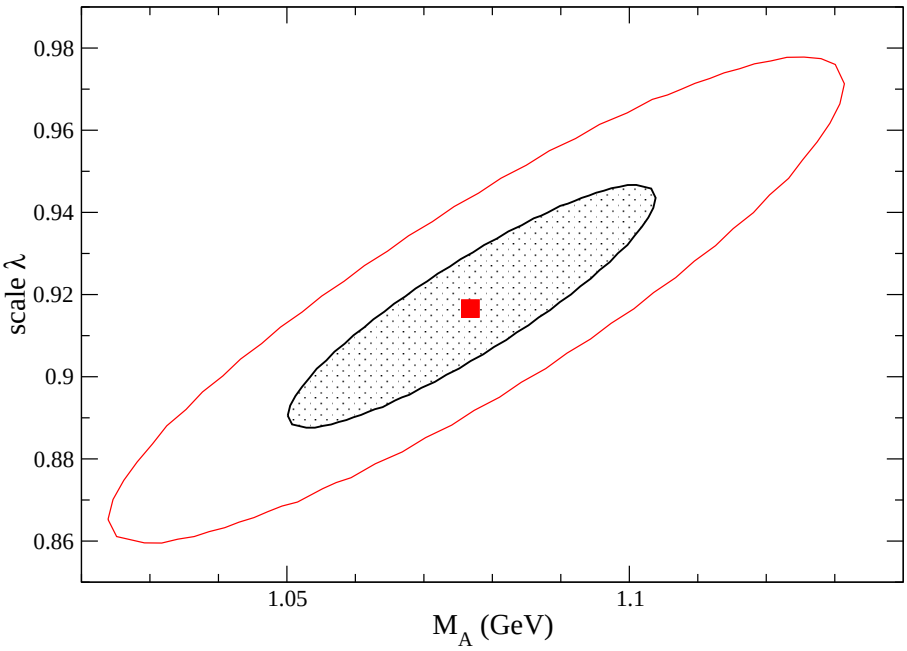

Figure 2.26: Best fit value of M_A and λ and 1 and 2 σ regions.

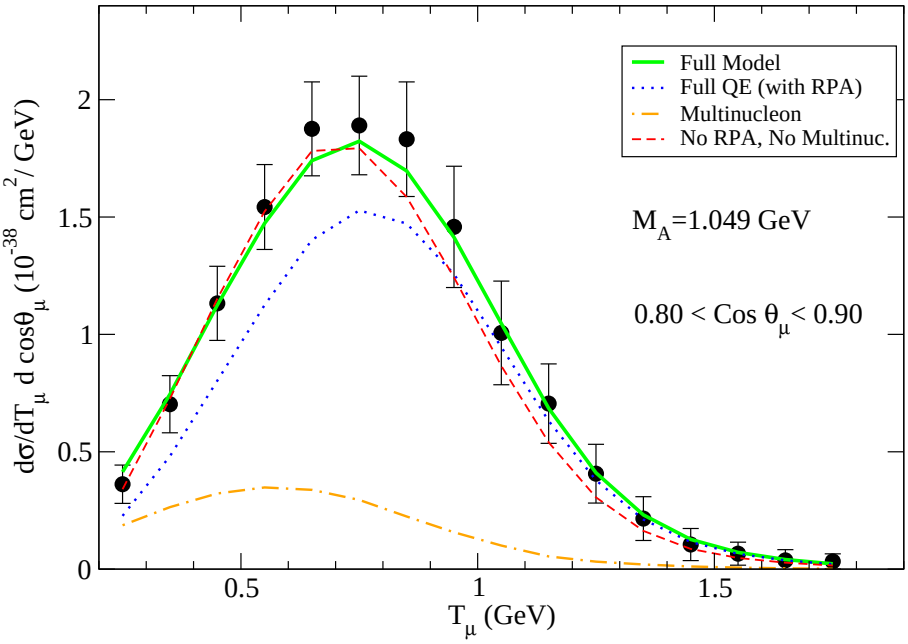

Figure 2.27: Muon angle and energy distribution $d\sigma/d\cos\theta_\mu dT_\mu$ for $0.80 < \cos\theta_\mu < 0.90$. Experimental data from Ref. [40] multiplied by 0.9. Axial mass is fixed to $M_A = 1.049$ GeV.

we have followed the procedure of Ref. [119] and implemented a transfer momentum threshold $q_{cut} = 400$ MeV. This eliminates 14 of the 137 measured bins (see Fig. 3 from [119]). The fitted axial mass is then reduced to $M_A = 1.007 \pm 0.034$ GeV and $\lambda = 0.83 \pm 0.04$. As it is the case for the full calculation, the inclusion of multinucleon mechanisms and RPA is essential to obtain axial masses consistent with the world average.

Finally, for illustration purposes, we show the contribution of the various mechanisms to the differential cross section at $0.80 < \cos\theta_\mu < 0.90$ in Fig. 2.27. We have taken $M_A = 1.049$ GeV as in our previous works [38, 46, 112] and scaled the experimental data to help in the discussion. The simple impulse approximation, without RPA or multinucleon effects is depicted by the dashed curve. Except for the scale correction it is an acceptable description of the data. One should remark that whereas the

model agrees well for low and medium muon energies, it is systematically below data at high energies. The inclusion of collective effects (RPA), dotted line, slightly improves the agreement at these high energies. However, RPA strongly decreases the cross section at low energies. Multinucleon mechanisms, which in average get a larger energy transferred and thus accumulate their contribution at low muon energy compensate that depletion. Therefore, the final picture for this observable is that of a delicate balance between a dominant single nucleon scattering, corrected by collective effects, and other mechanisms that involve directly two or more nucleons. It is also clear from this figure, that the proportion of multinucleon events contributing to the "QE" signal is quite large for low muon energies and thus, the algorithm commonly used to reconstruct the neutrino energy is badly suited for this region. This could have serious consequences in the determination of the oscillation parameters (see, e.g., discussion in Ref. [135] and Ref. [142]).

2.5 Summary

We have extended the QE contribution of the nuclear inclusive electron and neutrino scattering model developed in Refs. [38, 43] to the study of electroweak CC induced nuclear reactions, at intermediate energies of interest for future neutrino oscillation experiments. The model is based on a systematic many body expansion of the gauge boson absorption modes that includes one, two and even three body mechanisms, as well as the excitation of Δ isobars. The whole scheme has no free parameters, besides those adjusted to the weak pion production off the nucleon cross sections in the free space, since all nuclear effects were set up in previous studies of photon, electron and pion interactions with nuclei.

We have discussed at length, the recent CCQE MiniBooNE cross section data. To understand these measurements turns out to be essential mechanisms, where the $W-$boson is being absorbed by two or more nucleons without producing pions, as first suggested by M. Martini and collaborators [45]. Our evaluation of these pionless multinucleon emission contributions to the cross section is fully microscopical and it contains terms, which were either not considered or not properly taken into account in [45]. We end up with a reasonable description of the neutrino CC"QE" MiniBooNE and total inclu-

sive SciBooNE cross section data up to neutrino energies of around 1 GeV. On the other hand, we disagree on the apparent incompatibility among neutrino and electron-nucleus inclusive data, suggested by O. Benhar et al., since our neutrino model is just a natural extension of that developed in Refs. [43] and [123] to study electron– and photo-nuclear inclusive reactions. Indeed, we believe that the origin of the confusion can be traced back to the inability of the spectral function model advocated in [118] to properly describe the *dip* and $\Delta-$ regions, together with the mismatch existing in the definition of the quasielastic contribution between the theory and the experimental neutrino communities.

We have also analyzed the MiniBooNE CCQE double differential cross-section data using the theoretical model of Refs. [38, 46, 112]. The model, that starts from a local Fermi gas description of the nucleus, includes RPA correlations and multinucleon effects. The same model is quite successful in the analysis of nuclear reactions with electron, photon and pion probes and contains no additional free parameters. RPA and multinucleon knock-out have been found to be essential for the description of the data. Our main conclusion is that MiniBooNE data are fully compatible with former determinations of the nucleon axial mass, both using neutrino and electron beams in contrast with several previous analyses. The results also suggest that the neutrino flux could have been underestimated. Besides, we have found that the procedure commonly used to reconstruct the neutrino energy for quasielastic events from the muon angle and energy could be unreliable for a wide region of the phase space, due to the large importance of multinucleon events.

It is clear that experiments of neutrino reactions on complex nuclei have reached a precision level that requires for a quantitative description of sophisticated theoretical approaches. Apart from being important in the study of neutrino physics, these experiments are starting to provide very valuable information on the axial structure of hadrons.

Chapter 3

Nuclear structure functions in Deep Inelastic Scattering

3.1 Introduction

Until now we have been discussing microscopical models for neutrino interactions with hadrons at low and intermediate energies. But there are also processes carried out at higher energies where a description in terms of elastic neutrino-parton collisions is more adequate.
These experiments are usually carried out with heavy or medium-size nuclear targets. Thus, understanding the nuclear effects is very important to extract information about the underlying parton distribution functions (PDFs).
For the case of Deep Inelastic Scattering (DIS) with neutrinos, these nuclear effects have not been widely studied, and to characterize them, results of DIS with electrons are quite often used.
Although our aim is to face this problem for neutrino scattering, we have taken advantage from recent high precision measurements of electromagnetic DIS on light nuclei to test our model, with the final goal of extending it to neutrino/antineutrino scattering.
Recently Jefferson Lab(JLab) [68] using a high intensity electron beam of energy 5.767 GeV has measured the nuclear dependence of the structure function in some nuclei by studying the ratio $\mathrm{R}(x,Q^2)=\frac{2\sigma^A}{A\sigma^D}$, where σ^A is the inclusive cross section in nuclei and σ^D is the inclusive cross section

in deuterium. The experimental results for the ratio $\mathrm{R}(x, Q^2)$ have been presented by them [68] for $0.3 < x < 0.9$ and have re-confirmed the older EMC results [143–145] that the structure function of a nucleon is modified when it is placed inside a nucleus. This experiment shows that the slope of the EMC effect does not scale with the nuclear density and therefore the simple models to implement these nuclear effects, based on A or average density fits, for example as described by Gomez et al. [146], fail to describe the new and precise results for light nuclei.

The behavior of $R^A_{F2}(x, Q^2)$ can be broadly divided into four categories viz. $x \leq 0.1$ is the shadowing region, $0.1 \leq x \leq 0.3$ is the anti-shadowing region, $0.3 \leq x \leq 0.8$ is the EMC region and beyond $x \approx 0.8$, known as the Fermi motion region. Theoretically, many analysis have been done to study the EMC effect and various models have been proposed and discussed in the literature [147–150]. Several phenomenological parameterizations for the nuclear parton distribution functions(NPDFs) have been discussed in the literature like the works of Hirai et al. [151], Eskola et al. [152], Schienbein et al. [153, 154] which successfully reproduce the nuclear modifications in the deep inelastic lepton-nucleus and neutrino-nucleus scattering.

In this chapter, we study the nuclear medium effects on the structure function within a model based on the theoretical calculation of Ref. [67] with the aim of comparing it with the recent JLab data. The spectral function that describes the energy and momentum distribution of the nucleons in nuclei is obtained by using the Lehmann's representation for the relativistic nucleon propagator and nuclear many body theory is used to calculate it for an interacting Fermi sea in nuclear matter [138]. A local density approximation is then applied to translate these results into finite nuclei. The contributions of the pion and rho meson clouds are taken into account in a many body field theoretical approach which is based on Refs. [67, 155]. The model from Ref. [67] has been improved in several ways. The old model used the Bjorken limit and assumed the Callan-Gross relationship for nuclear structure functions $F_2^A(x)$ and $F_1^A(x)$. Due to the fact that JLab data have been taken in a region of relatively low Q^2 ($Q^2 \sim 3 - 6$ GeV^2) we have not assumed the Bjorken limit. Also, for low Q^2 and moderate x values Target Mass Corrections (TMC) might play an important role. We have incorporated them following Ref. [66]. Another difference with respect to Ref. [67] is the fact that for the ratios we divide by the deuteron struc-

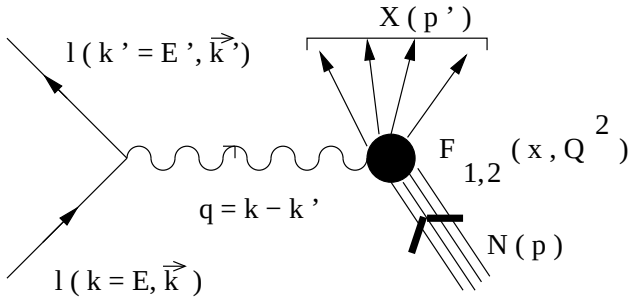

Figure 3.1: Feynman diagram for the deep inelastic lepton-nucleon scattering

ture function, rather than the nucleon one. This only implies substantial changes at moderate and high x values. We have also considered shadowing because it reduces the contribution coming from the pion and rho meson clouds [64,65]. For the numerical calculations, next to leading order (NLO) Parton Distribution Functions (PDF) for the nucleons have been taken from the parameterization of Martin et al. (MSTW) [156]. The NLO evolution of the deep inelastic structure functions has been taken from the works of Vermaseren et al. [157] and van Neerven and Vogt [158,159]. In the case of pions we have taken the pionic parton distribution functions given by Gluck et al. [160,161]. For the rho mesons, we have applied the same PDFs as for the pions as in Ref. [67].
The structure of the chapter is as follows: In Sect. 3.2 we introduce some basic formalism for lepton-nucleon scattering, in Sect. 3.3 we analyze the different nuclear effects, in Sect. 3.4 we consider the deuteron case and we end by comparing our results with data in Sect. 3.5.

3.2 Deep inelastic lepton-nucleon scattering

The double differential cross section for the reaction of scattering of a charged lepton from an unpolarized nucleon in the one photon exchange approximation,

$$l^-(k) + N(p) \rightarrow l^-(k') + X(p'),\ l = \ e,\ \mu \tag{3.1}$$

depicted in Fig. 3.1 is given, in terms of the Bjorken variables x and y, by

$$\frac{d^2\sigma}{dxdy} = \frac{8ME\pi\alpha^2}{Q^4}\left\{xy^2F_1(x,Q^2) + \left(1 - y - \frac{xyM}{2E}\right)F_2(x,Q^2)\right\} \quad (3.2)$$

where

$$x = \frac{Q^2}{2M\nu}, \quad y = \frac{\nu}{E_l} \quad (3.3)$$

and ν is the energy transferred to the hadronic system. $F_i(x,Q^2)$ are dimensionless structure functions. In the Bjorken limit, i.e. $Q^2 \to \infty$, $\nu \to \infty$, x finite, the structure functions $F_i(x,Q^2)$ depend only on the variable x and satisfy the Callan-Gross relation [162] given by $2xF_1(x) = F_2(x)$. Using this, the cross section of Eq.(3.2) can be expressed in terms of $F_2(x)$ and thus the ratio of cross sections is equal to the ratio of structure functions F_2. Even far from the Bjorken limit or when one goes beyond the lowest order (LO), where the Callan-Gross relation does not hold, the ratio of cross sections still equals the ratio of structure functions F_2 if the ratio of longitudinal to transverse cross sections $R = \sigma_L/\sigma_T$ does not depend on A. There is a considerable amount of experimental evidence supporting this fact (e.g. Fig. 6 of Ref. [148]). Therefore, in the following we only consider F_2 and compare directly F_2 ratios with cross section ones.

The nucleon structure functions are determined in terms of parton distribution functions for quarks and antiquarks. In this chapter, for the nucleons we work at NLO[1] and we have used the Parton Distribution Functions (PDF) of Martin et al. (MSTW) [156]. At this order, the expression for the F_2 and F_L structure functions can be expressed as functions of the PDFs by [157–159, 163]

$$x^{-1}F_{2,L} = \sum_{f=q,g} C_{2,L} \otimes f, \quad (3.4)$$

where $C_{2,L}$ are the coefficient functions for the quarks and gluons [157–159, 163] and f represents the quark and gluon distributions [156].

[1] On the other hand, the leading order (LO) pionic parton distribution functions of Gluck et al. [160, 161] have been used for pions as well as for rho mesons.

3.3 Nuclear effects

We have used the local density approximation (LDA) to incorporate nuclear medium effects[2]. Inside the nucleus, when the reaction given by Eq.(3.1) takes place, several nuclear effects like Fermi motion, binding, pion and rho meson cloud contributions must be taken into account. Fermi motion and nucleon binding are implemented through the use of a nucleon spectral function. The relativistic nucleon propagator in a nuclear medium can be cast as [67, 138]:

$$G(p) = \frac{M}{E(\mathbf{p})} \sum_r u_r(\mathbf{p}) \bar{u}_r(\mathbf{p}) \left[\int_{-\infty}^{\mu} d\,\omega \frac{S_h(\omega, \mathbf{p})}{p^0 - \omega - i\eta} + \int_{\mu}^{\infty} d\,\omega \frac{S_p(\omega, \mathbf{p})}{p^0 - \omega + i\eta} \right] \quad (3.5)$$

where $S_h(\omega, \mathbf{p})$ and $S_p(\omega, \mathbf{p})$ are the hole and particle spectral functions respectively. Full details can be found in Ref. [138]. We ensure that the spectral function is properly normalized and we get the correct Baryon number for the nucleus. Furthermore, we have also calculated the kinetic energy and the binding energy per nucleon and have found that the theoretical binding energy is very close to the experimentally observed ones for ^{9}Be, ^{12}C, ^{40}Ca and ^{56}Fe.

Our base equation for the nuclear structure function F_2^A in an isoscalar target is:

$$\begin{aligned} F_2^A(x, Q^2) &= 4 \int d^3r \int \frac{d^3p}{(2\pi)^3} \int_{-\infty}^{\mu} d\omega \; S_h(\omega, \mathbf{p}, \rho(\mathbf{r})) \frac{\left(1 - \gamma \frac{p_z}{M}\right)}{\gamma^2} \\ &\quad \times \left(\gamma'^2 + \frac{6x'^2(\mathbf{p}^2 - p_z^2)}{Q^2} \right) F_2^N(x', Q^2) \end{aligned} \quad (3.6)$$

with $p^0 = M + \omega$, $\gamma'^2 = 1 + 4x'^2 p^2/Q^2$ and x' is $Q^2/(2p \cdot q)$. This expression is equivalent to that of Ref. [64] after trivial algebraic transformations and taking into account the different normalization of the spectral function $\mathcal{P}_0(\epsilon, \mathbf{p})$ used in [64] such that

$$A \; \mathcal{P}_0(\epsilon, \mathbf{p}) \longrightarrow 4 \cdot 2\pi \int d^3r \; S_h(\omega, \mathbf{p}, \rho(\mathbf{r})) \, . \quad (3.7)$$

In an earlier study, the behaviour of different nucleon spectral functions has been analysed [165]. In particular, the spectral functions given by Fernández

[2]The nuclear densities have been taken from Ref. [164].

de Córdoba and Oset [138], Kulagin and Petti [64], and Ankowski et al. [108] were used and compared. It was found that the results do not change appreciably. Finally, we should comment that the present formalism has also been used to study the nuclear effects in the F_3 structure function [166].

3.3.1 π and ρ mesons contribution to the nuclear structure function

The pion and rho meson cloud contributions to the F_2 structure function have been implemented following the many body field theoretical approach of Refs. [67, 155]. The pion structure function $F_{2A,\pi}(x)$ is written as

$$F^A_{2,\pi}(x) = -6 \int d^3r \int \frac{d^4p}{(2\pi)^4}\, \theta(p^0)\, \delta ImD(p)\ \frac{x}{x_\pi}\, 2M\, F_{2\pi}(x_\pi)\, \theta(x_\pi - x)\, \theta(1 - x_\pi) \tag{3.8}$$

where $D(p)$ the pion propagator in the medium given in terms of the pion self energy Π_π:

$$D(p) = [p_0^2 - \vec{p}^{\,2} - m_\pi^2 - \Pi_\pi(p^0, p)]^{-1}\,, \tag{3.9}$$

where

$$\Pi_\pi = \frac{f^2/m_\pi^2 F^2(p) \vec{p}^{\,2} \Pi^*}{1 - f^2/m_\pi^2 V_L' \Pi^*}\,. \tag{3.10}$$

Here, $F(p) = (\Lambda^2 - m_\pi^2)/(\Lambda^2 + \vec{p}^{\,2})$ is the πNN form factor and Λ=1 GeV, $f = 1.01$, V_L' is the longitudinal part of the spin-isospin interaction and Π^* is the irreducible pion self energy that contains the contribution of particle - hole and delta - hole excitations. In Eq.(3.8), $\delta ImD(p)$ is given by

$$\delta ImD(p) \equiv ImD(p) - \rho\, \frac{\partial ImD(p)}{\partial \rho}\,|_{\rho=0} \tag{3.11}$$

and

$$\frac{x}{x_\pi} = \frac{-p^0 + p^z}{M} \tag{3.12}$$

Assuming SU(3) symmetry and following the same notation as in Ref. [160], the pion structure function at LO can be written in terms of pionic PDFs as

$$F_{2\pi}(x_\pi) = x_\pi \left(\frac{5}{9}\, v_\pi(x_\pi) + \frac{12}{9}\, \bar{q}_\pi(x_\pi) \right) \tag{3.13}$$

where $v_\pi(x_\pi)$ is the valence distribution and $\bar{q}_\pi(x_\pi)$ is the light SU(3)-symmetric sea distribution.
Similarly, the contribution of the ρ-meson cloud to the structure function is written as [67]

$$F^A_{2,\rho}(x) = -12 \int d^3r \int \frac{d^4p}{(2\pi)^4} \theta(p^0) \delta Im D_\rho(p) \frac{x}{x_\rho} 2M F_{2\rho}(x_\rho) \theta(x_\rho - x) \theta(1 - x_\rho) \tag{3.14}$$

where $D_\rho(p)$ is the ρ-meson propagator and $F_{2\rho}(x_\rho)$ is the ρ-meson structure function, which we have taken equal to the pion structure function $F_{2\pi}$ using the valence and sea pionic PDFs from reference [160]. Λ_ρ in ρNN form factor $F(p) = (\Lambda^2_\rho - m^2_\rho)/(\Lambda^2_\rho + \vec{p}^{\,2})$ has also been taken as 1 GeV.
Further details concerning the pion and ρ-meson propagator can be found in Ref. [67]. This model for the pion and ρ selfenergies has been abundantly used in the intermediate energy region and provides a quite solid description of a wide range of phenomenology in pion, electron and photon induced reactions in nuclei, see e.g. Refs. [43,123,124,126,127] and references in [67]. In particular, a careful study of the in medium pion propagator used here was carried out in Ref. [155]. There, several tests concerning the fulfillment of sum rules, and the preservation of the analytical properties of the meson propagator and the consistency of the results with similar calculations were considered.
In addition, the balance of light-cone momentum between bound nucleons and pions can be studied by means of a momentum sum rule as done in Ref. [64]. The pion $< y >_\pi$ and nucleon $< y >_N$ fractions of the light cone momentum are related by

$$< y >_\pi + < y >_N = \frac{M_A}{AM}, \tag{3.15}$$

where M_A is the nucleus mass. See section 5.3 of Ref. [64] for details. The sum rule should be valid for a nuclear model where the Hamiltonian would contain only pions and nucleons. In fact, our model for the nucleon spectral function is based on a phenomenological approach that also contains many other pieces in the nucleon-nucleon interaction and thus the sum rule is not directly applicable. Nonetheless, it can provide further constraints on the size of the mesonic contribution and it will be discussed in the results section.

The mesonic cloud contribution is expected to be negligible for deuteron as it depends, roughly speaking, quadratically on the baryon density which is quite small for this case[3]. Therefore, these contributions have not been included in the evaluation of the deuteron structure function.

3.3.2 Target mass corrections

Target mass corrections have been incorporated by means of the approximate formula [66]

$$F_2^{TMC}(x,Q^2) \simeq \frac{x^2}{\xi^2\,\gamma^3} F_2(\xi,Q^2)\left[1+\frac{6\,\mu\,x\,\xi}{\gamma}(1-\xi)^2\right], \tag{3.16}$$

where $\mu = \frac{M^2}{Q^2}$, $\gamma = \sqrt{1+\frac{4x^2M^2}{Q^2}}$ and ξ is the Natchmann variable defined as

$$\xi = \frac{2x}{1+\gamma}\,. \tag{3.17}$$

3.3.3 Coherent nuclear effects

Furthermore, we have taken into account the shadowing effect following the works of Kulagin and Petti [64]. We are interested in the relative effect in F_2^A that can be written as

$$\delta R_2 = \frac{\delta F_2^A}{F_2^N} = \frac{1+R^2}{1+R}\delta R_T \tag{3.18}$$

where $R(x,Q^2)$ is calculated for the free nucleon. For δR_T we use expression 63 in Ref. [64]. The most general expression for $R(x,Q^2)$, taking into account the target mass is:

$$R(x,Q^2) = \frac{F_L}{F_T} = \frac{\gamma^2F_2 - 2xF_1}{2xF_1} = \frac{\gamma^2F_2}{2xF_1} - 1. \tag{3.19}$$

[3] A direct application of our model to deuteron, produces a mesonic contribution that is always lower than a 0.6 percent of the nucleonic contribution for the analysed x range. Thus, its inclusion would have a very minor effect in the ratios. Nonetheless, we should mention that our formalism, which starts from selfenergies calculated in nuclear matter, is not expected to be very reliable for the calculation of the mesonic effects in deuteron.

3.4 Derivative expansion of F_2

The difference between dividing by the deuteron F_2^D or by the free isoscalar F_2^N structure function to calculate the ratios of structure functions is of only a few percent in the $x < 0.7$ region. However, the quality of data requires a proper description of F_2^D. On the other hand, our local density approach is not appropriate for such a light nucleus (or even for ^{4}He). Therefore, we need another method to calculate F_2 in these cases. In terms of the deuteron wave function, F_2^D can be written as

$$F_2^D(x,Q^2) = \int \frac{d^3p}{(2\pi)^3} |\Psi_D(\mathbf{p})|^2 \frac{\left(1-\gamma\frac{p_z}{M}\right)}{\gamma^2} \left(\gamma'^2 + \frac{6x'^2(\mathbf{p}^2 - p_z^2)}{Q^2}\right) F_2^N(x',Q^2). \tag{3.20}$$

Alternatively, a particularly appealing approach because of its simplicity, is the use of derivative expansions[4] that provide the structure function per nucleon of a nucleus in terms of the free nucleon one, its derivatives and a few expected values of nuclear observables [165, 167–170]. We can write

$$\begin{aligned} F_{2,DEx}^D(x,Q^2) &\simeq F_2^N(x,Q^2) + xF_2^{N\,\prime}(x,Q^2)\frac{< E > + < T_R >}{M} \\ &+ \frac{x^2}{2}F_2^{N\,\prime\prime}(x,Q^2)\frac{2 < T >}{3M}, \end{aligned} \tag{3.21}$$

The above equation is the derivative expansion for F_2 in the Bjorken limit. If one does not assume the Bjorken limit, the result is [165]

$$\begin{aligned} F_2^A\left(x,Q^2\right) &\simeq F_2^N\left(x,Q^2\right)\left[1 + \left(\gamma^2 - 1\right)\frac{< \mathbf{p}^2 >}{3M^2}\right] \\ &+ xF_2^{N'}(x,Q^2)\left(\frac{< E >}{M} + (2\gamma^2 - 2)\frac{< \mathbf{p}^2 >}{3M^2}\right) \\ &+ \frac{x^2}{2}F_2^{N''}(x,Q^2)\gamma^2\frac{< \mathbf{p}^2 >}{3M^2} \end{aligned} \tag{3.22}$$

where $< T >$ is the mean nucleon kinetic energy taken as 11.07 MeV, $< E >$ is the nucleon removal energy taken as 2.226 MeV, $< T_R > \simeq \left\langle \mathbf{p}^2 \right\rangle / 2M$ with $\left\langle \mathbf{p}^2 \right\rangle = 0.533\ fm^{-2}$ the average of the square of the nucleon momentum.

[4] In appendix E it will be shown how to obtain the derivative expansion for F_2^A and also for F_3^A.

One can see that, in the Bjorken limit ($\gamma^2 \to 1$), Eq. (3.22) reduces to Eq. (3.21) except for the recoil term $< T_R >$, which is negligible for medium and heavy nuclei (for which the work of Ref. [165] was done), but it is important for deuteron[5] and we have kept it in the calculations.
To include TMC, one must substitute in Eq. (3.21) the free nucleon structure function and its derivatives by the approximate one given in Eq. (3.16). The derivative expansions have some intrinsic limitations and it has been shown that they fail to converge to the results obtained by folding with the nuclear spectral functions for $x \gtrsim 0.5$, for the case of medium and heavy nuclei. A detailed study can be found in Ref. [165]. The convergence is expected to be much better for a loosely bound nucleus such as the deuteron. Indeed, F_2^D obtained using the Paris wave function [171] and the results of the derivative expansion differ by less than 0.6 percent up to $x = 0.6$ as shown in Fig. 3.2.
In Fig. 3.2, we also include for comparison the same ratio from Ref. [172], which uses a different set of PDFs. We have observed that the main difference with that calculation comes from the inclusion of a parametrization of the off-shell effects (see dashed-dotted line) absent in our model.

3.5 Results and discussion

Our aim in this section is to confront the model with the recent JLab results of Ref. [68] that correspond to ratios of cross sections in nuclei with cross sections in deuteron and more precisely with the slope of the x dependence that is more insensitive to the normalization uncertainties. Nonetheless, we will also show some results for the deuteron $F_2^D(x, Q^2)$ structure function as well as the ratio R(x,Q^2)=$\frac{2F_2^A}{AF_2^D}$ in intermediate mass nuclei like ^{40}Ca and ^{56}Fe.

In Fig. 3.3, we compare the theoretical calculation obtained using Eq. (3.20) with the experimental results of Benvenuti et al. [173]. Overall, we find a good agreement in the x region relevant for our study. Although the data correspond to large Q^2 values, this gives us confidence in the quality of this approach for the evaluation of the ratios with respect to other nuclei. In

[5]This is because $< T_R >= \frac{<T>}{(A-1)}$, so for light nuclei it cannot be ignored.

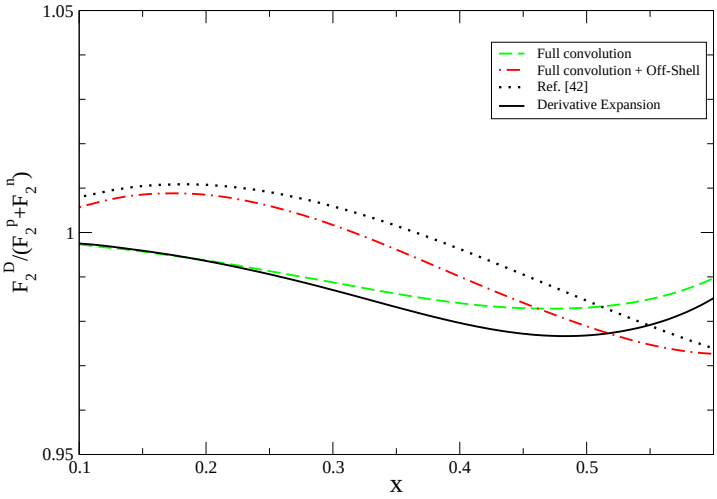

Figure 3.2: $F_2^D/(F_2^p + F_2^n)$ as a function of x at Q^2=10 GeV^2. Solid line: Derivative expansion. Dashed line: Eq. 3.20. Dashed dotted: Eq. 3.20 including off-shell effects following the prescription of Ref. [64]. Dotted line: Ref. [172].

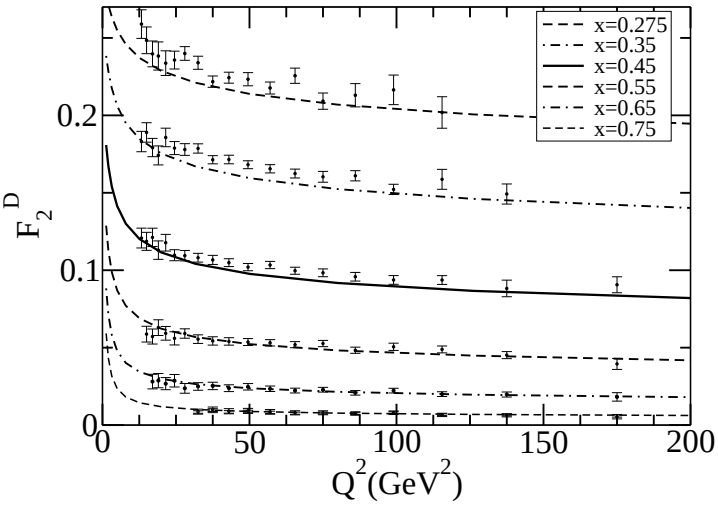

Figure 3.3: Electromagnetic structure function in deuteron F_2^D at different x values. The theoretical curves are obtained by using Eq. (3.20). Experimental data are taken from Ref. [173].

Fig. 3.4, we compare our results with data obtained with a muon beam on a deuterium target [174]. We also show the results for the free nucleon case. The nuclear corrections are very small for the range of x values analysed in the experiment.

One of the most interesting results of the recent JLab data is that for both Beryllium and Carbon the cross section ratios show a similar slope even when they have a quite different average nuclear density. This conflicts with some simple fits that describe well the slope for medium and heavy nuclei as a function of the average nuclear density or with simple A dependences [146]. On the other hand, the slope of the ratio in the region $0.3 < x < 0.6$ is particularly well suited to analysis because from the experimental point of view it is quite unaffected by normalization uncertainties. Also theoretically it is relatively simple because shadowing, or Fermi motion are of a little importance over this region of x.

In Fig. 3.5, we show the results for Beryllium. The dashed line has been calculated using Eq. (3.6) with TMC and the solid line corresponds to the full model, including the meson cloud contributions, shadowing and TMC.

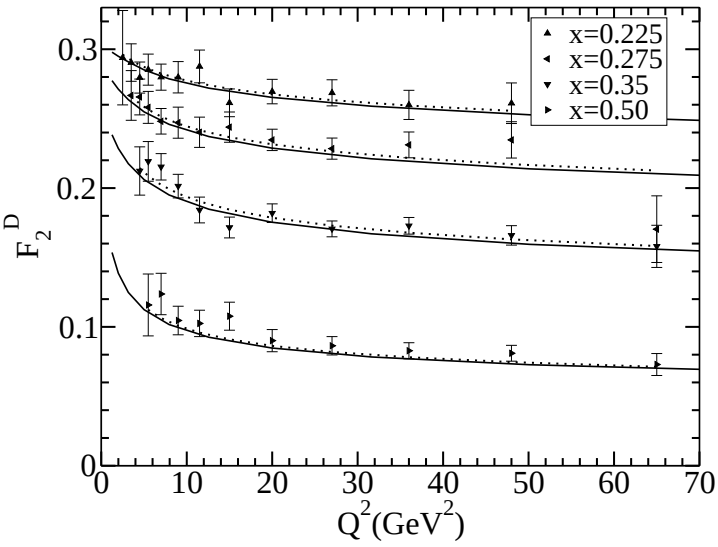

Figure 3.4: Electromagnetic structure function in deuteron F_2^D at different x values. Solid lines are obtained by using Eq. (3.20) and the dotted lines are the results for the free nucleon case. Experimental data are taken from Ref. [174].

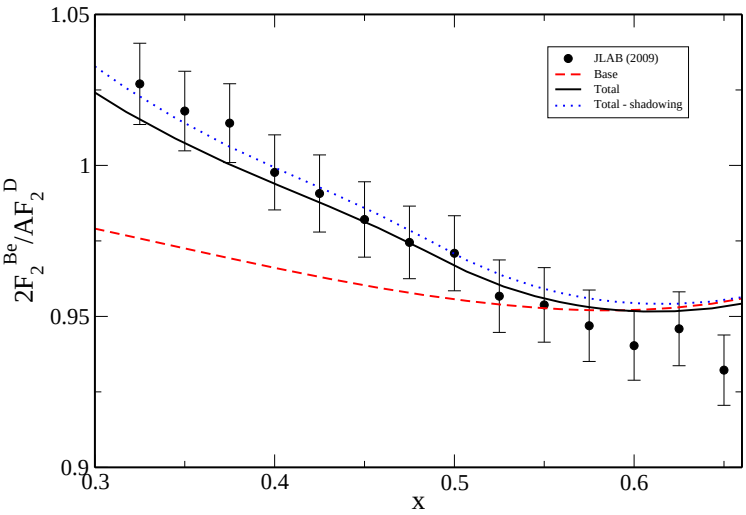

Figure 3.5: Ratio R(x,Q^2)=$\frac{2F_2^{Be}}{AF_2^D}$. Full model (solid line), without shadowing (dotted line) and without pion, rho and shadowing contributions (dashed line). For each value of x, Q^2 has been calculated using an electron beam of 5.767GeV and scattering angle of 40^0 corresponding to JLab kinematics. Data are cross section ratios from Ref. [68].

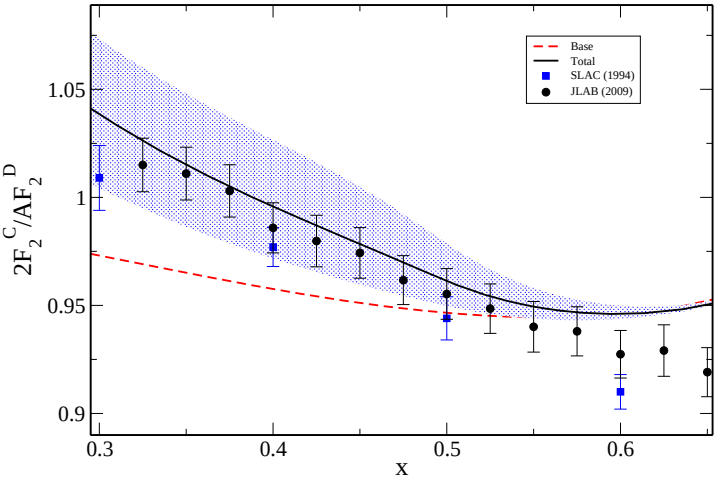

Figure 3.6: Ratio R(x,Q^2)=$\frac{2F_2^C}{AF_2^D}$. Full model: solid line with Λ, Λ_ρ = 1GeV; the band corresponds to $\pm$20% variation on Λ and Λ_ρ. Full model without pion, rho and shadowing: dashed line. Q^2 for calculation and JLab data [68] as described in previous figure. SLAC data [146] correspond to $Q^2 = 5$ GeV^2.

We show explicitly the effect of shadowing. It reduces the structure function ratio by around 1% at $x \sim 0.3$ and even less for higher x. We have found that TMC has a really minor effect in the ratio for these x values (less than 1% at $x \sim 0.6$ and even smaller for lower x values). Therefore, the difference between the base curve and the full one comes basically from the π and ρ contributions that play an important role. The size of the rho meson correction is about half that of the pion. We find that the full model agrees quite well with data both in slope and the size of the ratio.
A good agreement with data is also obtained for Carbon as shown in Fig. 3.6. The slope and size of the nuclear effects are similar to the Beryllium case. This could look surprising given the quite different average density as discussed in [68]. This points out to the fact that "average density" could not be the appropriate parameter for the description of the EMC effect in light nuclei. For example, this has been discussed in Sect. IV of Ref. [175]. Again, a determining factor in the agreement is the mesonic cloud contribution. Given this, some words of caution are needed here. Firstly, the

parton distribution functions are poorly known for the mesons and possible off-shell effects have not been included in the calculation. Secondly, the results depend on the meson selfenergies in the medium that also contain some uncertainties such as the specific form of the spin-isospin interaction, specially for the ρ meson. A full analysis of these uncertainties is beyond of the scope of this chapter. To give an idea of their size, we have shown in this figure the results for the ratio using the full model with Λ, Λ_ρ=1GeV and Λ, Λ_ρ=1.2GeV and 0.8GeV. We find that a 20% variation in the Λ's, results in a 2-3% change in the ratio.

We have also tested the momentum sum rule discussed in section 3.3.1. The mesons carry a light-cone momentum fraction of 3 percent for $\Lambda = 1$ GeV. The 2 percent prescribed by the sum rule can be obtained for a cut-off $\Lambda = 0.8$ GeV. This suggests that lower cut-off values should be preferred but one must be careful before reaching such conclusion. For instance, the nucleon momentum fraction is very sensitive to parameters like the expected value of the nucleon kinetic energy that are not very well known and has some uncertainty. We have used the values obtained with our nucleon spectral function. The same results are obtained for ^{9}Be. Heavier nuclei, such as iron and calcium, have a mesonic momentum fraction of 5 percent and fulfill the sum rule for $\Lambda = 0.75$ GeV.

In Fig. 3.6, the systematic difference in size between JLab and SLAC data is consistent with the normalization uncertainties quoted in Refs. [68, 146]. It may be noted, however, that the slope is very similar for both experiments and in good agreement with our results. These normalization differences have been recently discussed in Ref. [172].

For both nuclei, our results slightly overestimate data by around 2% at x around 0.6 and more above that. However, that region is much affected by possible off-shell effects [172], not included in our approach, and by high momentum components of the nucleons wave function. Therefore, we cannot make any strong statement about this discrepancy apart from the fact that we are reaching one of the limits of validity of our model.

We have also checked that the use of next to next to leading order PDFs, that considerably lengthens and complicates the calculation, does not appreciably change the results, at the level of precision of the current data and the size of other theoretical uncertainties.

There are JLab results even for lighter nuclei like ^{3}He and ^{4}He. Our local

density model is certainly not adequate for these cases that would require a more microscopical approach for the calculation of a proper nucleon spectral function and of the meson cloud contribution. Also, good data for larger x values are available. They are particularly sensitive to TMC and to high momentum components of the nucleon spectral functions. In order to analyse these data, further work would be required to extend the validity of the theoretical approach describing the nucleon spectral function.

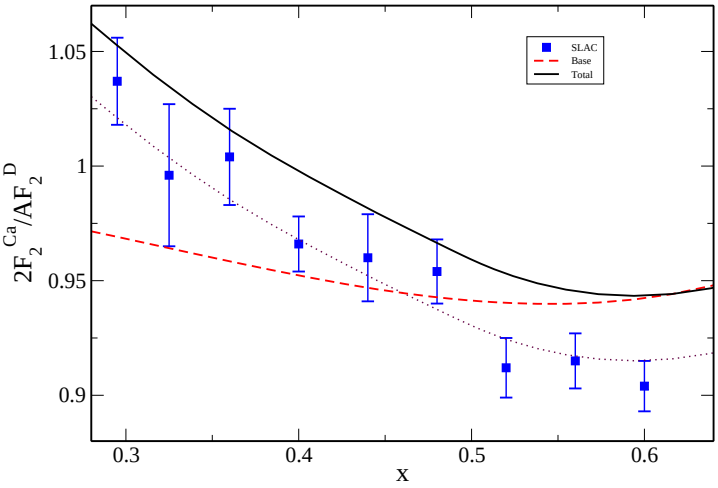

Figure 3.7: Ratio R(x,Q^2)=$\frac{2F_2^{Ca}}{AF_2^D}$. Full model: solid line. Full model without pion, rho and shadowing: dashed line. Dotted curve is the full result scaled by a factor 0.97. Calculations have been done for Q^2 = 5 GeV^2. The experimental points are taken from Ref. [146] (averaged Q^2).

As a further test, we have also studied the results for the ratio R(x,Q^2)=$\frac{2F_2^A}{AF_2^D}$ for intermediate mass nuclei like calcium and iron. The results are shown in Figs. 3.7 and 3.8. In both cases, we have compared with SLAC results from Ref. [146], with averaged Q^2. No significant Q^2 dependence was found in Ref. [146] for their kinematic range. The theoretical curves have been calculated for Q^2 = 5GeV^2 and we observe little sensitivity to that value. In the case of calcium, our results overestimate the data by around 3%. This is larger than the normalization uncertainties quoted in Ref. [146]. Nonethe-

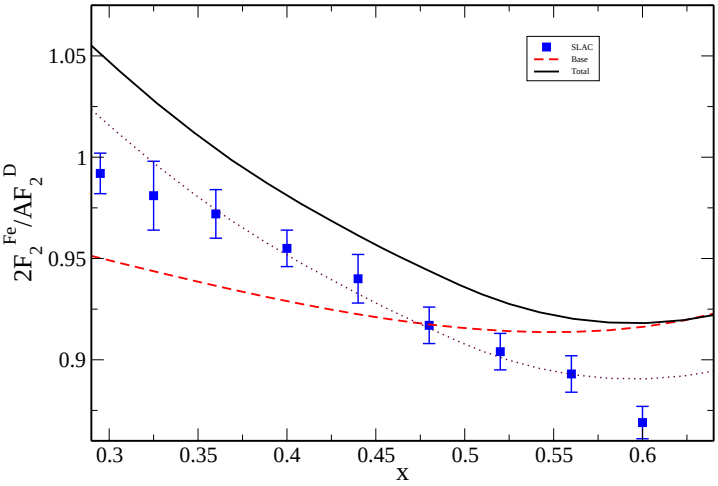

Figure 3.8: Ratio R(x,Q^2)=$\frac{2F_2^{Fe}}{AF_2^D}$. Lines have the same meaning as in Fig. 3.7. Calculations have been done for $Q^2 = 5$ GeV^2. Experimental points from Ref. [146] (averaged Q^2).

less, scaling our theoretical curve, we observe a good agreement with the slope of the structure function. The situation is much the same for heavier nuclei, such as iron. The slope is well reproduced and calculation overestimates again data by around a 3%. Similar results are obtained for silver and gold. This overestimation seems to be consistent with the results of recent global fits to the nuclear parton distribution functions (see e.g. Fig. 4 of Ref. [154]). Their results might point out to some normalization uncertainty in the SLAC results such that the medium and heavy nuclei ratios are too small. However, the recent more microscopical analysis of Ref. [172] that also finds normalization inconsistencies between light and heavy nuclei favours the interpretation that the recent JLab data should be rescaled by a global factor of around 0.98 and that the SLAC data are correct. We should also mention that the two discussed experiments had significantly different lepton energies and the simple A dependence assumed for the σ_L/σ_T ratio could have to be revised.
Certainly, these normalization issues should be settled with new and better

experiments. From the theoretical point of view, it seems that microscopical models are hardly able to reproduce at the same time the high statistic data from light nuclei at JLab and medium and heavy nuclei from other collaborations. In any case, this does not affect the main point discussed in this section, namely the slope produced by the nuclear effects that is well reproduced in our model.

3.6 Summary

In summary, the electromagnetic nuclear structure function F_2^A has been studied including nucleonic and mesonic degrees of freedom for a x region where shadowing, antishadowing and Fermi motion are not too important. We have started from up to date nucleonic PDFs. Nuclear effects like Fermi motion and binding have been incorporated by means of the use of a spectral function obtained for nuclear matter and implemented in nuclei using the local density approximation. A similar approach has been used for the inclusion of the contribution of mesonic clouds. Also shadowing and TMC have been considered. The deuteron structure function has been calculated using a derivative expansion and with the Paris wave function. The results successfully reproduce recent very precise JLab results for light nuclei at relatively low Q^2 values. Also the slope of previous experiments for heavier nuclei is well reproduced although we fail to agree with them on the absolute size by up to a 3%, larger than the quoted experimental uncertainty. We have found that the mesonic cloud (basically pion) gives an important contribution to the cross section ratios but it still has considerable uncertainties. Even small changes of the pion nuclear selfenergy can produce appreciable changes in the cross section ratios.
The success of this local density model for light nuclei is in contrast with the failure of simple models/parametrizations that fit well for the nuclear effects for medium and heavy nuclei as a function of average density or the mass number A [68]. The use of an approach that incorporates in an adequate manner the nucleon and meson properties in the nuclei is clearly mandatory for the analysis of the EMC effect in these cases.

Chapter 4

Conclusions

In this thesis we have explored the weak interaction on hadronic systems at intermediate energies. We have focused in processes not widely studied previously and whose knowledge can be relevant for the analysis of neutrino oscillations experiments as well as to widen our knowledge about the structure of the hadrons.
Beginning with neutrino reactions off free nucleons, we have extended previous models to account for strangeness production, in particular single kaon/antikaon production.
For single kaon production induced by neutrinos, we have developed the first model that properly incorporates all background terms required by chiral symmetry. The model has no free parameters and due to the absence of resonant mechanisms, it will describe the weak kaon production process for a wide range of energies, until associated kaon production becomes dominant. We have studied total cross sections (as a function of neutrino energy) as well as differential $\frac{d\sigma}{dQ^2}$ ones for several channels. We have also calculated flux-folded total cross sections for different experimental neutrino fluxes and have estimated the number of kaons that could have been produced in experiments like MiniBooNE. We have also estimated the number of kaons produced by the atmospheric neutrino flux in the Super-Kamiokande experiment because these kaons could be a source of background in experiments that search for proton decay. We think that these cross sections are large enough to be measured with the expected fluxes of Minerνa and T2K. The main improvement of the model with respect to previous ones is the inclu-

sion of contact term Feynman diagrams required by chiral symmetry. They are in fact the dominant term.

Next, we have studied single antikaon production off nucleons induced by antineutrinos. This is a more complicated process due to the presence of resonant mechanisms. For the pion case, the $\Delta(1232)$ plays a dominant role. We have developed a model that resembles those used for the pion production. We have included the background terms obtained from the chiral lagrangians and the resonant mechanisms with the corresponding member of the baryons decuplet, namely, the $\Sigma^*(1385)$. We have included these Σ^* resonant amplitudes and have found that, although their contribution alone is small, for some channels there is a sizable interference between this mechanism and the others we have considered. The fact that the contribution of the Σ^* alone is very small for total cross sections is a novel feature with respect to one pion production, where the resonance is in fact dominant.

We have also found that the number of antikaons produced in experiments like MiniBooNE is smaller than the number of kaons. This is due to the fact that the averaged energy of the antineutrino spectrum is below the threshold for antikaon production and also because the size of the flux for antineutrinos is considerably smaller than the corresponding one for neutrinos in this experiment. However, these predicted cross sections could be well measured in other experiments like MINERνA.

Once we have studied models for strangeness production, we have focused on neutrino and antineutrino inclusive reactions at low and intermediate energies. We have studied these processes in a many-body approach starting from QE region to the Δ-peak region, with especial emphasis to the dip region between them. The model is based on a systematic many body expansion of the gauge boson absorption modes that includes one, two and even three body mechanisms, as well as the excitation of Δ isobars.

We have given full details of the calculation of our 2p2h contribution to the inclusive cross section, and also to the "CCQE" cross section as measured by the MiniBooNE collaboration, where they define "QE" as the process in which only a muon is detected. We must mention that our model has no free parameters except those previously adjusted from photon, electron and pion interactions with nuclei and those adjusted from the weak pion production cross sections in the deuteron.

Furthermore, we have analyzed the CCQE double differential cross section

$\frac{d\bar{\sigma}}{dT_\mu\, d\cos\theta_\mu}$, published by the MiniBooNE collaboration. It was reported in their analysis a quite large effective axial mass from a fit to the shape of the Q^2-distribution. It was argued that such increase in the value of the axial mass is compatible also with the large flux-unfolded cross section that they also reported (larger than the prior theoretical consensus). However, this value for the axial mass enters into contradiction with the quoted world average value of $M_A = 1.03 \pm 0.02$ GeV. In our analysis, including 2p2h mechanisms, we do not need to increase that value to reproduce reasonably well the double differential cross section, although we systematically underestimate the data, but within the quoted normalization error. If we fit the axial mass to minimize the χ^2, we obtain $M_A = 1.077 \pm 0.027$ GeV.

Other important point to discuss is the reliability of the algorithm used to estimate the four-momentum transfer squared or the energy of the neutrino. The MiniBooNE collaboration assumes that all the events in which a muon is identified are purely QE. We have shown that the contribution of multi-nucleon mechanisms is sizable for wide regions of the phase space and therefore a measure of the kinetic energy of the muon and its scattering angle is not enough to characterize the energy of the incoming neutrino unless some assumptions are made for the interaction, like assuming purely QE scattering. But if one assumes purely QE scattering for events that come from multi-nucleon knockout, one is obtaining a wrong energy for the neutrino.

Let me mention some work which is currently in progress or is planned to do. In the field of neutrino/antineutrino interactions with free nucleons, we plan to review the models for associated production implemented in the Monte Carlo generators. There is also the possibility of extending the model of weak kaon/antikaon production off nucleons to complex nuclei and we want to calculate cross sections for coherent kaon/antikaon production off nuclei. In the topic of inclusive nuclear reactions at low and intermediate energies, we want to explore higher transferred energies. This means to include higher lying barionic resonances and processes of two pion production, where there are models in the literature for these mechanisms in free nucleons. Also, we plan to compute the Neutral Currents (NC) processes, where there are also valuable experimental data. And, of course, we will compare our Charged Current (CC) one pion production off carbon cross sections with the very valuable data reported very recently by the MiniBooNE Collaboration.

Finally, we have also studied the nuclear structure functions in the regime of DIS for electrons as a first test to develop the model for neutrino/antineutrino DIS. Much theoretical and experimental work has been made on the topic of DIS with electrons; but neutrino/antineutrino DIS has been less studied. We must also mention that neutrino/antineutrino DIS explores different flavour combinations in the structure functions than the ones explored with electron scattering. Furthermore, neutrino/antineutrino DIS is sensitive to other structure function F_3 which cannot be probed by electrons.
We have studied the nuclear medium effects on the electromagnetic structure function F_2. We have worked in the impulse approximation using a spectral function that describes the energy and momentum distribution of the nucleons in nuclei. This spectral function is obtained by using the Lehmann's representation for the relativistic nucleon propagator and nuclear many body theory is used to calculate it for an interacting Fermi sea in nuclear matter. The contributions of the pion and rho meson clouds are taken into account in a many body field theoretical approach. We have also incorporated Target Mass Corrections (TMC) that might play an important role. We have included shadowing, that reduces the contribution coming from the pion and rho meson clouds. Finally, we have explored the relevance of including higher order next to leading order (NLO) Parton Distribution Functions (PDFs) for the nucleons.
Our model successfully reproduces the recent and very precise data from JLab on light nuclei and shows a quite clear inconsistency between the normalization of JLab and some of the older experiments performed at SLAC.
In the field of Deep Inelastic Scattering, our primary goal was to develop a model to calculate lepton event rates and fully integrated cross sections. To accomplish this, we have firstly tested our model with the recent data on light nuclei reported by JLab for electromagnetic DIS. Now we are about to obtain predictions for neutrino/antineutrino DIS cross sections off ^{12}C to compare with NOMAD results, which are still in phase of data analysis.

Chapter 5

Resumen de la tesis

5.1 Introducción

Cuando, en 1930, Wolfgang Pauli propuso la existencia de una partícula neutra de espín $\frac{1}{2}$ que conservaría energía y momento con las partículas β emitidas por algunos núcleos en el proceso llamado desintegración beta, él mismo dudó de que tal partícula fuera a ser detectada algún día.
En 1956, muchos años después de esta propuesta, el neutrino fue detectado por primera vez por Reines y Cowan [1] en un experimento. Costó tantos años el descubrir el neutrino porque no lleva carga eléctrica y, por tanto, no ioniza la materia cuando pasa a través de ella.
La primera teoría de esta interacción fue propuesta por Enrico Fermi en 1933 [2, 3]. Enrico Fermi propuso una teoría efectiva para la desintegración beta con un vértice de cuatro fermiones. Muy pronto se descubrió que la forma de la interacción postulada por Fermi debía ser generalizada para incluir interacciones dependientes de espín, hecho que fue señalado por Gamow y Teller [4, 5].
Después de muchos intentos para averiguar la estructura tensorial de la interacción débil, Richard Feynman y Murray Gell-Mann [6], basándose en trabajos previos y conversaciones con Sudarshan y Marshak [7, 8], propusieron la forma $V - A$ para la corriente débil.
Esta clase de estructura para la corriente débil fue pensada después de la observación experimental de la violación de paridad en la desintegración beta del ^{60}Co [9].

Hasta ahora, tres diferentes sabores de neutrinos han sido descubiertos. Fue en 1962 cuando Lederman, Schwartz y Steinberger descubrieron el neutrino muónico [10] y demostraron que era diferente del descubierto por Reines y Cowan. El tercer tipo de neutrino, el neutrino tauónico fue detectado por primera vez por la colaboración DONUT en el año 2000 en el Fermilab [11].
Hoy en día sabemos que los neutrinos tienen masa porque oscilan de un sabor a otro. Cuando los neutrinos son producidos, tienen un sabor bien definido. Este estado de sabor bien definido puede ser expresado como una combinación lineal de estados propios del hamiltoniano, los cuales se propagan con una energía bien definida. Como tienen diferentes energías, las fases de las diferentes componentes no evolucionan igualmente con el tiempo. Por tanto, el estado inicial evoluciona a otro estado el cual no es simplemente el estado inicial multiplicado por una fase global. Por eso hay una probabilidad de transición de un estado de sabor a otro. Ha habido y hay enormes esfuerzos teóricos y experimentales para medir masas absolutas de los neutrinos [12–16], parámetros de la oscilación [17–21]... Para artículos de revisión sobre oscilaciones de neutrinos, véase [22–26].
Hoy en día, estamos entrando en una era de medidas de precisión de los parámetros de la matriz de Pontecorvo-Maki-Nakagawa-Sakata (PMNS): los ángulos de mezcla y la fase que viola CP en el sector leptónico.
Entender bien las interacciones de neutrinos a energías intermedias (alrededor de 1 GeV) es esencial para los experimentos pasados, actuales y futuros de oscilaciones de neutrinos. Entre éstos podemos citar Super-Kamiokande [27, 28], T2K [29], NOvA [30], OPERA [31], MiniBooNE [32], MicroBooNE [33]... Para este propósito experimentos dedicados específicamente a la dispersión de neutrinos han sido planeados: MINERνA [34] y otros...
Estos experimentos se llevan a cabo típicamente a energías intermedias, es decir, alrededor de 1 GeV. Esto es así porque estas energías maximizan la probabilidad de oscilación (una vez que se ha establecido la longitud de oscilación).
En esta región de energías, normalmente, el proceso seleccionado para medir los parámetros de oscilación es la dispersión cuasielástica por núcleos por corriente cargada $\nu_l + A \to l^- + A'$. Una de las razones es que la dispersión elástica por corrientes neutras es ciega al sabor del neutrino. En efecto, si uno tiene que detectar una oscilación de neutrino muónico a neutrino electrónico, uno debe ser capaz de detectar un muón o un electrón en el

estado final. Si uno se dedica a sucesos por corriente neutra, es imposible saber si ha habido oscilación porque la interacción en este canal es la misma para neutrino muónico que para neutrino electrónico y el neutrino en el estado final no es detectado. Otra razón para la elección de la dispersión cuasielástica es que tiene la sección eficaz más grande en este rango de energías, entre el umbral y unos pocos gigaelectronvoltios (véase por ejemplo la figura 1 en la referencia [35]).

Como hemos dicho antes, los neutrinos sólo interaccionan débilmente con la materia y, por tanto, sus secciones eficaces son pequeñas. Para medirlas, se usan detectores muy grandes donde los neutrinos colisionan con blancos nucleares como hierro, aceite mineral, agua o incluso agua pesada. Esto introduce una nueva dificultad relacionada con los efectos nucleares en dispersión de neutrinos. En efecto, partículas producidas en la interacción pueden ser dispersadas de nuevo o absorbidas antes de dejar el núcleo. Estas reinteracciones nucleares pueden conducir a una identificación errónea del canal de reacción y cambian la topología del estado hadrónico final medido. Los efectos nucleares están entre las mayores fuentes de incertidumbre sistemática en experimentos de oscilaciones de neutrinos.

Como mencionamos anteriormente, la probabilidad de oscilación depende de la energía del neutrino. Sin embargo, esta energía no puede ser medida directamente sino que tiene que ser reconstruida a partir de las energías de las partículas del estado final que son detectadas. Pero estas partículas son afectadas por efectos del medio nuclear, como he señalado anteriormente. Por tanto, el análisis experimental tiene que basarse en modelos para la interacción neutrino-núcleo. La comprensión teórica de los efectos nucleares es esencial para la interpretación de los datos.

Además del interés por las propiedades de los neutrinos, estos experimentos atraen la atención de la comunidad de física hadrónica y nuclear porque los neutrinos son una herramienta muy valiosa para obtener más información sobre la estructura del nucleón y resonancias bariónicas, ya que exploran tanto la estructura vectorial como la axial de los hadrones. Los factores de forma vectoriales son relativamente bien conocidos de experimentos de dispersión de electrones. Los experimentos actuales y futuros nos darán más información sobre los factores de forma axiales del nucleón y de las resonancias bariónicas.

Para que sirva como ejemplo, la sección eficaz de los procesos cuasielásticos

por corriente cargada depende de dos factores de forma vectoriales y uno axial. Se asume usualmente que la dependencia en Q^2 del factor de forma axial tiene una forma dipolar con un parámetro libre (la denominada masa axial) que ha de ser ajustado a partir de las distribuciones en Q^2.
El objetivo de esta tesis es participar en el desarrollo de un marco teórico fiable para analizar dispersión de neutrinos en blancos hadrónicos.
Empezando desde el umbral, tenemos la anteriormente mencionada dispersión cuasielástica y después los canales inelásticos: produccion de piones, producción de hiperones, resonancias bariónicas, kaones... En núcleos también tenemos mecanismos multinucleónicos. Y a energías más altas todavía, la dispersión profundamente inelástica es dominante. Empecemos discutiendo la dispersión cuasielástica.
El ingrediente básico para la dispersión cuasielástica en un modelo es la excitación de un nucleón por la sonda débil. Esto es conocido como la descripción de una partícula un agujero (1p1h) de la dispersión cuasielástica. Hay muchos modelos para dispersión cuasielástica en núcleos que contienen varios efectos nucleares: aproximación de SuperScaling y corrientes de intercambio de mesones [36]; interacciones de estado final (FSI) y SuperScaling [37]; FSI y correlaciones de largo alcance (RPA) [38]; dentro del marco del modelo de transporte GiBUU [39] y muchos otros. Hay casi un consenso teórico en el hecho de que todos los modelos de cuasielástico en núcleos están por debajo de los resultados publicados recientemente por la colaboración MiniBooNE [40], donde el análisis favorecía un incremento de la masa axial en el factor de forma axial para hacer coincidir los datos en un ajuste a la forma de la distribución en Q^2 con la sección eficaz total en función de la energía del neutrino. Este incremento de la masa axial efectiva entra en contradicción con el valor medio mundial $M_A = 1.016 \pm 0.026$ GeV [41], siendo este último valor extraído de medidas de dispersión cuasielástica por corriente cargada llevadas a cabo en blancos de deuterio. De amplitudes de electroproducción de piones, después de aplicar correcciones hadrónicas que pueden ser calculadas a bajo Q^2 utilizando teoría quiral de perturbaciones [42], el valor resultante obtenido es $M_A = 1.014 \pm 0.016$ GeV.
Se han hecho muchos esfuerzos teóricos para ir más allá de la descripción de una partícula un agujero de la dispersión cuasielástica. Esto significa considerar excitaciones de dos partículas dos agujeros (2p2h) que pueden contribuir a la sección eficaz de dispersión cuasielástica definida por Mini-

BooNE. Véase por ejemplo las referencias [43] (para dispersión de electrones) y [44–46] (para neutrino y antineutrino scattering).
En la referencia [38], la dispersión cuasielástica fue estudiada en el marco de un enfoque de Teoría de Muchos Cuerpos quedándose sólo con la contribución 1p1h pero incluyendo correcciones de RPA e interacciones de estado final con la inclusión de funciones espectrales nucleares realistas.
Uno de los objetivos de esta tesis es extender el trabajo de la referencia [38] a energías transferidas más grandes, donde grados de libertad de resonancias son importantes. Es también un objetivo de esta tesis extender a núcleos el trabajo previo de la referencia [47] sobre producción débil de piones en nucleones libres.
Además de la dispersión cuasielástica, otros procesos como producción de piones pueden ser usados para detectar neutrinos. La producción y posterior desintegración de resonancias del nucleón en interacciones de neutrinos es una parte significante de la sección eficaz total de neutrinos en la región de unos pocos GeV. Estas resonancias también han sido exploradas usando experimentos de dispersión de electrones, pero diferentes factores de forma contribuyen en el caso de neutrinos. La producción de resonancias es la parte menos determinada de la sección eficaz de neutrinos; y experimentos como NOνA y T2K esperan que estas interacciones sean una gran fracción de la sección eficaz en el rango de energías en el que están más interesados.
La producción de piones en núcleos puede ser coherente o incoherente. En el último caso, el núcleo final queda excitado. El modelo más conocido para este proceso en simulaciones de interacciones de neutrinos fue desarrollado por Rein y Sehgal [48]. Asume que la producción de piones en el nucleón está dominada por la excitación de resonancias bariónicas, descritas usando el modelo relativista de quarks de Feynman, Kislinger y Ravndal [49] para resonancias con masas invariantes de hasta 2 GeV. El modelo original despreciaba las masas de los leptones finales. Sin embargo, correcciones de masa finita en cinemática y corrientes han sido investigadas recientemente [50–52]. La riqueza de datos de fotoproducción y electroproducción de piones disponible gracias a varios experimentos en MIT/Bates, MAMI/Mainz y especialmente JLab ha sido usada para extraer las amplitudes de helicidad de transición electromagnética [53, 54]. Esta información empírica tan valiosa debería ser incorporada al análisis de experimentos de neutrinos.

Por contra, no hay casi información sobre la parte axial de la corriente de transición débil nucleón-resonancia. Conservación parcial de la corriente axial (PCAC) y dominancia del polo de pión del factor de forma pseudoescalar pueden ser aplicados para relacionar el acoplamiento axial para la contribución dominante a bajo Q^2 con el acoplamiento de la desintegración de la resonancia en πN.
Para pequeños valores de Q^2 sólo el factor de forma axial C_5^A es relevante y se le ha dedicado algún esfuerzo a su extracción a partir de datos de cámaras de burbujas en ANL y BNL.
La producción de piones en núcleos es coherente cuando el núcleo permanece en su estado fundamental. Tiene lugar predominantemente cuando el momento transferido al núcleo es pequeño, de modo que es menos probable que el núcleo se "rompa". La producción débil coherente de piones tiene una sección eficaz muy pequeña comparada con el caso incoherente, pero relativamente más grande que reacciones equivalentes inducidas por fotones o electrones. Esto se debe a la contribución no nula de la corriente axial en el régimen cinemático relevante [55].
Un buen conocimiento de producción de piones es muy importante para la interpretación de los experimentos de oscilaciones de neutrinos. Se sabe que la producción de π^+ por corriente cargada es el mayor fondo de contaminación para la señal cuasielástica. En efecto, si el pión, por ejemplo, es absorbido en el núcleo o no detectado, el evento parece cuasielástico.
Hay, por supuesto, modelos de producción débil de piones en nucleones libres [47, 48, 56–58] e incluso para doble producción de piones inducida por neutrinos [59]. Estos modelos contienen el principal mecanismo para la producción de piones, esto es, la excitación de la $\Delta(1232)$ pero también términos de background que son importantes en el umbral y que pueden ser obtenidos utilizando teoría quiral de perturbaciones. Usaremos el modelo de producción de piones de la referencia [47] como base para desarrollar un modelo de producción de piones en núcleos.
Podríamos mencionar algunos otros modelos para producción de hiperones, como los trabajos de las referencias [60–62]. El primero trata sobre producción cuasielástica débil de hiperones inducida por antineutrinos, mientras que el segundo y el tercero tratan sobre producción asociada de partículas extrañas.
Para más altas energías, otros canales que involucran producción de partículas

extrañas podrían ser relevantes, por ejemplo la producción de un único kaón en nucleones libres inducida por neutrinos o la de un antikaón inducida por antineutrinos (en este último caso incluyendo la excitación de resonancias con extrañeza $S = -1$, como la Σ^*). Se debe mencionar que, aunque están suprimidas por Cabibbo ($\Delta S = \pm 1$), estas secciones eficaces son más grandes (hasta 1.5 GeV de energía del neutrino) que las correspondientes para producción asociada ($\Delta S = 0$ y no suprimidas por Cabibbo) debido a los diferentes umbrales de producción.
Estudios de procesos exclusivos de producción de partículas extrañas inducidos por neutrinos serán llevados a cabo en MINERνA. Se esperan acumular miles de estos eventos, dependiendo por supuesto del canal. Estas medidas de secciones eficaces probablemente tendrán impacto también en otras áreas de la física de partículas. Por ejemplo, en la estimación, en experimentos de búsqueda de desintegración del protón, del background de procesos con $\Delta S = 1$ inducidos por neutrinos atmosféricos. La exposición a haces de antineutrinos ayudará en el estudio de $\Delta S = -1$ producción cuasielástica de hiperones y permitiría una nueva medida de los elementos de la matriz de Cabibbo-Kobayashi-Maskawa (CKM). En este experimento, otras secciones eficaces serán medidas, como las correspondientes a procesos de producción asociada $\Delta S = 0$, inducidos por corrientes neutras o cargadas.
Los datos existentes sobre producción de resonancias inducidas por neutrinos son insuficientes para el trabajo de especificar el complejo solapamiento entre amplitudes de resonancias de Δ y N^* y factores de forma relacionados que caracterizan el rango de energías entre $1 - 5$ GeV. Los programas de Monte Carlo simulan esta región cinemática utilizando predicciones teóricas antiguas desarrolladas por Rein y Sehgal [48] o resultados de experimentos de electroproducción. El esquema teórico y experimental de la región de resonancias es más complicado que las dispersiones cuasielástica y profundamente inelástica que bordean esta región. Y mucha parte de la muestra de eventos de MINOS [63] está dentro de esta región de resonancias.
A energías más altas, la sección eficaz está dominada por la dispersión profundamente inelástica (DIS) (véase fig 1 en la referencia [35]), donde las funciones de estructura del nucleón pueden ser escritas en términos de funciones de distribución de partones (PDFs) de quarks, antiquarks y gluones. La dispersión de neutrinos también juega un papel especial en la extracción de las distribuciones de partones. La habilidad de la corriente cargada para

"saborear" algunos sabores concretos de quarks potencia significativamente el estudio de las distribuciones de partones. Es también importante el hecho de que las interacciones débiles exploran otras funciones de estructura (F_3), en marcado contraste con sondas puramente electromagnéticas.
Los efectos nucleares en DIS han sido extensivamente estudiados usando haces de muones y electrones, pero sólo superficialmente con neutrinos. Experimentos de neutrinos con alta estadística sólo han sido posibles utilizando blancos nucleares pesados tales como blancos calorimétricos de hierro. Para el análisis de estos experimentos, parametrizaciones de los efectos nucleares obtenidos de experimentos con electrones/muones han sido aplicados a los resultados. Sin embargo, hay fuertes evidencias de que las correcciones nucleares para $e/\mu - A$ y $\nu - A$ son diferentes.
En la aproximación de impulso, las funciones de estructura nuclear pueden ser expresadas como una convolución de las funciones de estructura del nucleón con la función espectral nuclear. Esto tiene en cuenta efectos como movimiento de Fermi de los nucleones y energía de ligadura nuclear. Otros efectos como shadowing [64, 65] y correcciones por masa del blanco (TMC) [66], y la influencia de grados de libertad mesónicos son también relevantes. Desarrollaremos un modelo basado en el que desarrollaron Marco y Oset en la referencia [67], el cual está a su vez basado en un enfoque de Teoría Cuántica de Muchos Cuerpos. Compararemos este modelo con los recientes resultados de JLab sobre el efecto EMC en núcleos ligeros [68].
Por tanto, la estructura de esta tesis será la siguiente: en el primer capítulo discutiremos la extensión de modelos que explican producción de extrañeza en nucleones libres [69]; en el segundo capítulo discutiremos cómo implementar el modelo de la referencia [47] para la producción débil de piones en núcleos, con especial énfasis a las excitaciones de dos partículas dos agujeros (2p2h) [46]; y finalmente en el tercer capítulo trataremos con DIS de electrones con núcleos [70].

5.2 Conclusiones

En esta tesis hemos estudiado la interacción débil en sistemas hadrónicos a energías intermedias. Nos hemos concentrado en procesos no ampliamente estudiados en el pasado y cuyo conocimiento puede ser relevante para el

análisis de experimentos de oscilaciones de neutrinos, así como para ampliar nuestro conocimiento acerca de la estructura de los hadrones.
Empezando con reacciones de neutrinos en nucleones libres, hemos extendido modelos previos para explicar la producción de extrañeza, en particular la producción de un kaón/antikaón aislado (no acompañado por hiperones). Para la producción de kaones inducida por neutrinos, hemos desarrollado el primer modelo que incorpora adecuadamente todos los términos requeridos por la simetría quiral. El modelo no tiene parámetros libres y debido a la ausencia de resonancias con extrañeza $S = +1$, describe el proceso de producción débil de kaones para un amplio rango de energías, hasta que la producción asociada de kaones se hace dominante.
Hemos estudiado secciones eficaces totales (en función de la energía del neutrino) así como secciones eficaces diferenciales $\frac{d\sigma}{dQ^2}$ para varios canales. Hemos calculado secciones eficaces totales convolucionadas con el flujo de diferentes experimentos y hemos estimado el número de kaones que podrían haber sido producidos en experimentos como MiniBooNE. También hemos estimado el número de kaones producidos por el flujo de neutrinos atmosféricos en el experimento Super-Kamiokande, porque estos kaones podrían ser una fuente de contaminación en los experimentos que buscan la desintegración del protón. Creemos que estas secciones eficaces son lo suficientemente grandes para ser medidas con los flujos esperados de MINERνA y T2K. La principal novedad del modelo con respecto a los previos es la inclusión de diagramas de Feynman de términos de contacto, requeridos por los lagrangianos quirales. Estos mecanismos son, de hecho, el término dominante.
Después, hemos estudiado producción de antikaones en nucleones libres inducida por antineutrinos. Este proceso es más complicado de estudiar debido a la presencia de mecanismos resonantes. Para el caso de piones, la resonancia $\Delta(1232)$ tiene un papel dominante. Hemos desarrollado un modelo que se asemeja a aquellos usados para la producción de piones. Hemos incluido los términos de background obtenidos a partir de los lagrangianos quirales y los mecanismos resonantes con el correspondiente miembro del decuplete bariónico, la $\Sigma^*(1385)$. Hemos incluido estas amplitudes resonantes y hemos encontrado que para algunos canales hay una considerable interferencia entre este mecanismo y los otros que también hemos considerado. Hemos encontrado que el número de antikaones producidos en experimentos como MiniBooNE es menor que el número de kaones. Esto se debe al hecho

de que la energía media del espectro de antineutrinos está por debajo del umbral de producción de antikaones y también porque la magnitud del flujo para antineutrinos es considerablemente menor que para neutrinos en este experimento. Sin embargo, estas predicciones para las secciones eficaces podrían ser medidas en otros experimentos como MINERνA.

Después de estudiar modelos de producción de partículas con extrañeza, hemos estudiado dispersión de neutrinos y antineutrinos en núcleos a energías intermedias, con el objetivo primario de estudiar la reacción inclusiva. Hemos empleado un enfoque de teoría cuántica de Muchos Cuerpos comenzando desde la región del pico cuasielástico y terminando en la región del pico de la $\Delta(1232)$. Hemos puesto especial énfasis a la región intermedia entre ambos picos. Hemos detallado nuestro cálculo de la contribución de dos partículas dos agujeros (2p2h) a la sección eficaz inclusiva. Y también a la sección eficaz "CCQE" tal y como la define la colaboración MiniBooNE, donde ellos definen "QE" como el proceso donde sólo un muón es detectado. Debemos mencionar que nuestro modelo no tiene parámetros libres excepto aquellos previamente ajustados a reacciones de fotones, electrones y piones con núcleos y aquellos ajustados a reacciones de producción débil de piones en nucleones libres.

Además, hemos analizado la sección eficaz "CCQE" doblemente diferencial $\frac{d\bar{\sigma}}{dT_\mu\, d\cos\theta_\mu}$, recientemente publicada por la colaboración MiniBooNE. En su análisis de un ajuste a la forma de la distribución en Q^2 se obtenía una masa axial efectiva bastante elevada, en contradicción con el promedio mundial. Se argumentaba que tal incremento en el valor de la masa axial era compatible también con la sección eficaz desconvolucionada, que era anormalmente elevada (más grande que las predicciones teóricas previas). Sin embargo, en nuestro analisis, incluyendo mecanismos de excitación de dos partículas dos agujeros (2p2h), no necesitamos incrementar el valor de la masa axial para reproducir razonablemente bien la sección eficaz doblemente diferencial, aunque sistemáticamente infraestimamos los datos, pero dentro del error de normalización experimental. Si nosotros ajustamos la masa axial para minimizar el χ^2, obtenemos un valor de $M_A = 1.077 \pm 0.027$ GeV.

Otro importante punto a discutir es la fiabilidad del algoritmo usado para estimar el cuadrimomento transferido o la energía del neutrino. La colaboración MiniBooNE asume que todos los eventos en los que un muón es identificado son puramente cuasielásticos. Hemos mostrado que la contribución

de mecanismos de multinucleón es considerable para algunas regiones del espacio de fase y, por tanto, una medida de la energía cinética del muón y su ángulo de scattering no es suficiente para conocer la energía del neutrino incidente a menos que se asuman algunas hipótesis sobre la interacción, como asumir que los eventos son puramente cuasielásticos. Pero si uno asume dispersión puramente cuasielástica para eventos que proceden de choques con dos nucleones, se está obteniendo una energía errónea para el neutrino incidente. Por tanto, proponemos detectar el nucleón final o los nucleones finales para desenmarañar una contribución (eventos puramente QE) de la otra (emisión de dos nucleones).

Finalmente, también hemos estudiado las funciones de estructura nuclear en el régimen de dispersión profundamente inelástica (DIS) para electrones como un primer test para desarrollar un modelo para DIS de neutrinos. Muchos trabajos teóricos y experimentales se han hecho en el campo de DIS con electrones; pero DIS para neutrinos/antineutrinos ha sido menos estudiado. Debemos también mencionar que la dispersión profundamente inelástica de neutrinos/antineutrinos explora diferentes combinaciones de sabor en las funciones de estructura que las exploradas con dispersión de electrones. Además, la dispersión inelástica de neutrinos es sensible a otra función de estructura F_3 que no es accesible con electrones.

Hemos estudiado los efectos del medio nuclear en la función de estructura electromagnética F_2. Hemos trabajado en la aproximación de impulso usando una función espectral que describe la distribución de energía y momento de los nucleones en núcleos. Esta función espectral es obtenida utilizando la representación de Lehmann para el propagador de nucleón relativista y la Teoría Nuclear de Muchos Cuerpos es usada para calcularlo para un mar de Fermi con interacción en materia nuclear. Las contribuciones de las nubes mesónicas son tenidas en cuenta en un enfoque de Teoría Cuántica de Muchos Cuerpos. Hemos incorporado correcciones de masa del blanco (TMC) que podrían jugar un papel importante. Hemos incluido shadowing porque reduce la contribución proveniente de las nubes mesónicas. Finalmente, hemos explorado la relevancia de incluir funciones de distribución de partones a Next to Leading Order (NLO).

Nuestro modelo reproduce con éxito los recientes y muy precisos datos de JLab en núcleos ligeros y muestra una inconsistencia bastante clara entre la normalización de JLab y algunos de los viejos experimentos llevados a cabo

en SLAC.
Finalmente, me gustaría mencionar algunos trabajos planeados para el futuro o que actualmente están en proceso de elaboración.
En el campo de interacciones de neutrinos/antineutrinos con nucleones libres, nos gustaría revisar los modelos para producción asociada implementados en los generadores Monte Carlo. Existe también la posibilidad de extender el modelo de producción débil de kaones/antikaones a núcleos complejos y el estudio de las secciones eficaces de producción coherente de kaones/antikaones en núcleos.
En el campo de reacciones nucleares inclusivas a energías intermedias, queremos explorar energías transferidas más altas. Esto implica incluir resonancias de nucleón más pesadas y procesos de producción de dos piones, donde hay modelos en la literatura para estos mecanismos en nucleones libres. También existe la posibilidad de calcular los mismos procesos que hemos calculado con corriente cargada, pero ahora con corriente neutra débil, donde también hay datos experimentales. Y, por supuesto, existe nuestro objetivo de comparar nuestras predicciones de secciones eficaces de producción de un pión por corriente cargada en carbono con los muy valiosos datos publicados muy recientemente por la colaboración MiniBooNE.
Y finalmente, en el campo de dispersión profundamente inelástica, nuestro primer objetivo es desarrollar un modelo para calcular el número de eventos producidos en algunos experimentos y secciones eficaces completamente integradas con las funciones de estructura nucleares. Para conseguir esto, primero hemos hecho un test de nuestro modelo con los datos recientes publicados por JLab en núcleos ligeros para DIS con electrones. Y estamos a punto de obtener predicciones para secciones eficaces de neutrinos/antineutrinos en el régimen de DIS en ^{12}C para comparar con resultados de la colaboración NOMAD, los cuales están todavía en fase de análisis.

Appendix A

A.1 Nucleon propagator in nuclear matter

In this section we are going to derive Eq. (2.22), which is the nucleon propagator in a non-interacting Fermi sea. Let me start with the wave plane expansion of the Dirac field

$$\Psi(x) = \sum_k \sum_{r=1}^{2} \left\{ a_r(\vec{k}) u_r(\vec{k}) e^{-ikx} + c_r^\dagger(\vec{k}) v_r(\vec{k}) e^{ikx} \right\} \tag{A.1}$$

$$\bar{\Psi}(x) = \sum_k \sum_{r=1}^{2} \left\{ a_r^\dagger(\vec{k}) \bar{u}_r(\vec{k}) e^{ikx} + c_r(\vec{k}) \bar{v}_r(\vec{k}) e^{-ikx} \right\} \tag{A.2}$$

where the symbol $\sum_k$ actually stands for an integral over the momentum $\vec{k}$

$$\sum_k = \frac{1}{(2\pi)^3} \int \frac{d^3k}{2E(\vec{k})} = \frac{1}{(2\pi)^3} \int d^4k\, \delta(k^2 - m^2) \theta(k^0) \tag{A.3}$$

Furthermore, we have the following anticommutation relations between the creation and annihilation operators

$$\left\{ a_r(\vec{k}), a_s^\dagger(\vec{k}\,') \right\} = \left\{ c_r(\vec{k}), c_s^\dagger(\vec{k}\,') \right\} = \delta_{rs}\, \Delta_{\vec{k}\vec{k}\,'} \tag{A.4}$$

being the rest of anticommutation relations equal to zero. Also, $\Delta_{\vec{k}\vec{k}\,'} = (2\pi)^3\, 2E(\vec{k})\, \delta^3(\vec{k} - \vec{k}\,')$.
Now, we perform a separation between states with momentum above or below the Fermi momentum k_F and we make a redefinition of the creation and

annihilation operators for those states that are below the Fermi momentum.

If $|\vec{k}| > k_F$ then $\begin{cases} a_r(\vec{k}) = a_r(\vec{k}) \\ a_r^\dagger(\vec{k}) = a_r^\dagger(\vec{k}) \end{cases}$

If $|\vec{k}| < k_F$ then $\begin{cases} a_r(\vec{k}) = b_r^\dagger(\vec{k}) \\ a_r^\dagger(\vec{k}) = b_r(\vec{k}) \end{cases}$

The meaning of the above two equations is the following one: to annihilate a particle below the Fermi momentum is the same than creating a hole in the Fermi sea; and to create a particle below the Fermi momentum is the same than annihilating a hole in the Fermi sea.

With the anticommutation relations given in Eq. (A.4), we can easily find the following ones

$$\left\{a_r(\vec{k}), b_s(\vec{k}\,')\right\} = 0 \tag{A.5}$$

$$\left\{a_r^\dagger(\vec{k}), b_s^\dagger(\vec{k}\,')\right\} = 0 \tag{A.6}$$

$$\left\{b_r(\vec{k}), b_s^\dagger(\vec{k}\,')\right\} = \delta_{sr}\Delta_{\vec{k}\,'\vec{k}} \tag{A.7}$$

The left-hand sides of eqs. (A.5) and (A.6) are equal to zero because $|\vec{k}| > k_F$ and $|\vec{k}\,'| < k_F$.

Now, we can decompose the "sum" over $\vec{k}$ of Eqs. (A.1) and (A.2) in two "sums": one sum for momenta below the Fermi momentum; and other sum for momenta above the Fermi momentum, for instance:

$$\begin{aligned} \Psi(x) &= \sum_{k<k_F}\sum_{r=1}^{2}\left[b_r^\dagger(\vec{k})u_r(\vec{k})e^{-ikx}\right] + \sum_{k>k_F}\sum_{r=1}^{2}\left[a_r(\vec{k})u_r(\vec{k})e^{-ikx}\right] \\ &+ \sum_{k}\sum_{r=1}^{2}\left[c_r^\dagger(\vec{k})v_r(\vec{k})e^{ikx}\right] \end{aligned} \tag{A.8}$$

$$\begin{aligned} \bar{\Psi}(x) &= \sum_{k<k_F}\sum_{r=1}^{2}\left[b_r(\vec{k})\bar{u}_r(\vec{k})e^{ikx}\right] + \sum_{k>k_F}\sum_{r=1}^{2}\left[a_r^\dagger(\vec{k})\bar{u}_r(\vec{k})e^{ikx}\right] \\ &+ \sum_{k}\sum_{r=1}^{2}\left[c_r(\vec{k})\bar{v}_r(\vec{k})e^{-ikx}\right] \end{aligned} \tag{A.9}$$

Let me calculate the T-ordered product of the Dirac fields

$$\begin{aligned} iG_{\alpha\beta}(x,y) &= \left\langle \phi_0 \left| \mathcal{T}(\Psi_\alpha(x)\bar{\Psi}_\beta(y)) \right| \phi_0 \right\rangle \\ &= \theta(x^0-y^0)\left\langle \phi_0 \left| \Psi_\alpha(x)\bar{\Psi}_\beta(y) \right| \phi_0 \right\rangle - \theta(y^0-x^0)\left\langle \phi_0 \left| \bar{\Psi}_\beta(y)\Psi_\alpha(x) \right| \phi_0 \right\rangle \end{aligned} \tag{A.10}$$

where we have only used the definition of a time-ordered product for two Dirac fields. The indices α and β stand for the spinor components of the fields. And finally, the symbol $|\phi_0\rangle$ stands for the ground state of a non-interacting Fermi gas.
We must specify how the creation and annihilation operators act on this ground state. Indeed, we have the following relations

$$\left.\begin{array}{lll} a_r(\vec{k})\,|\phi_0\rangle = 0 & \Longleftrightarrow & 0 = \langle\phi_0|\, a_r^\dagger(\vec{k}) \\ b_r(\vec{k})\,|\phi_0\rangle = 0 & \Longleftrightarrow & 0 = \langle\phi_0|\, b_r^\dagger(\vec{k}) \\ c_r(\vec{k})\,|\phi_0\rangle = 0 & \Longleftrightarrow & 0 = \langle\phi_0|\, c_r^\dagger(\vec{k}) \end{array}\right\}$$

The above equations mean that one cannot annihilate a particle above the Fermi momentum because those states are empty. Also, one cannot annihilate a hole below the Fermi momentum because there are no holes, every state below the Fermi momentum is occupied.
With these expressions, we can compute the first term in Eq. (A.10)

$$\begin{aligned} \left\langle \phi_0 \left| \Psi_\alpha(x)\bar{\Psi}_\beta(y) \right| \phi_0 \right\rangle &= \sum_{k,k'>k_F}\sum_{r,s} \left\langle \phi_0 \left| a_r(\vec{k})a_s^\dagger(\vec{k}\,') \right| \phi_0 \right\rangle u_{r,\alpha}(\vec{k})\bar{u}_{s,\beta}(\vec{k}\,') \\ &\times\ e^{-i(kx-k'y)} = \sum_{k>k_F}\sum_{r} u_{r,\alpha}(\vec{k})\bar{u}_{r,\beta}(\vec{k})e^{-ik(x-y)} \\ &= \sum_{k>k_F} e^{-ik(x-y)}(\not{k}+m)_{\alpha\beta} \end{aligned} \tag{A.11}$$

And we can also compute the second term in Eq. (A.10)

$$\begin{aligned}
\left\langle \phi_0 \left| \bar{\Psi}_\beta(y)\Psi_\alpha(x) \right| \phi_0 \right\rangle &= \sum_{k,k'<k_F} \sum_{r,s} \left\langle \phi_0 \left| b_s(\vec{k}\,')b_r^\dagger(\vec{k}) \right| \phi_0 \right\rangle \bar{u}_{s,\beta}(\vec{k}\,')u_{r,\alpha}(\vec{k}) \\
&\times \quad e^{-i(kx-k'y)} \\
&+ \quad \sum_{k,k'} \sum_{r,s} \left\langle \phi_0 \left| c_s(\vec{k}\,')c_r^\dagger(\vec{k}) \right| \phi_0 \right\rangle \bar{v}_{s,\beta}(\vec{k}\,')v_{r,\alpha}(\vec{k})e^{i(kx-k'y)} \\
&= \quad \sum_{k<k_F} \sum_{r} u_{r,\alpha}(\vec{k})\bar{u}_{r,\beta}(\vec{k})e^{-ik(x-y)} \\
&+ \quad \sum_{k} \sum_{r} v_{r,\alpha}(\vec{k})\bar{v}_{r,\beta}(\vec{k})e^{ik(x-y)} \\
&= \quad \sum_{k<k_F} e^{-ik(x-y)}(\not{k}+m)_{\alpha\beta} + \sum_{k} e^{ik(x-y)}(\not{k}-m)_{\alpha\beta}
\end{aligned} \tag{A.12}$$

With this, the expected value of the time ordered product of two Dirac fields is

$$\begin{aligned}
iG_{\alpha\beta}(x,y) &= \theta(x^0-y^0) \sum_{k>k_F} e^{-ik(x-y)}(\not{k}+m)_{\alpha\beta} \\
&- \theta(y^0-x^0) \sum_{k} e^{ik(x-y)}(\not{k}-m)_{\alpha\beta} \\
&- \big(1-\theta(x^0-y^0)\big) \sum_{k<k_F} e^{-ik(x-y)}(\not{k}+m)_{\alpha\beta} \\
&= \theta(x^0-y^0) \sum_{k} e^{-ik(x-y)}(\not{k}+m)_{\alpha\beta} \\
&- \theta(y^0-x^0) \sum_{k} e^{ik(x-y)}(\not{k}-m)_{\alpha\beta} - \sum_{k<k_F} e^{-ik(x-y)}(\not{k}+m)_{\alpha\beta} \\
&= iS_{\alpha\beta}(x-y) - \sum_{k<k_F} e^{-ik(x-y)}(\not{k}+m)_{\alpha\beta}
\end{aligned} \tag{A.13}$$

where the last term in the above equation can be written as

$$\begin{aligned}
\textstyle\sum_{k<k_F} \quad & e^{-ik(x-y)}(\not{k}+m)_{\alpha\beta} = \frac{1}{(2\pi)^3}\int d^4k\,\delta(k^2-m^2)\theta(k^0)\theta(k_F-|\vec{k}|) \\
\times \quad & e^{-ik(x-y)}(\not{k}+m)_{\alpha\beta} \\
= \quad & (2\pi)\int \frac{d^4k}{(2\pi)^4}\frac{\theta(k_F-|\vec{k}|)}{2E(\vec{k})}\delta(k^0-E(\vec{k}))\,\theta(k^0)e^{-ik(x-y)}(\not{k}+m)_{\alpha\beta}
\end{aligned} \tag{A.14}$$

And finally, writing the Feynman propagator, $S_{\alpha\beta}$, in integral form, we have

$$\begin{aligned}
iG_{\alpha\beta}(x,y) &= i\int \frac{d^4k}{(2\pi)^4}\frac{(\not{k}+m)_{\alpha\beta}}{k^2-m^2+i\epsilon}e^{-ik(x-y)} \\
&- \int \frac{d^4k}{(2\pi)^4}\frac{2\pi\,\theta(k_F-|\vec{k}|)}{2E(\vec{k})}(\not{k}+m)_{\alpha\beta}\,\delta(k^0-E(\vec{k}))\theta(k^0)e^{-ik(x-y)} \\
&= i\int \frac{d^4k}{(2\pi)^4}e^{-ik(x-y)}(\not{k}+m)_{\alpha\beta} \\
&\times \left(\frac{1}{k^2-m^2+i\epsilon}+\frac{2\pi i\,\theta(k_F-|\vec{k}|)}{2E(\vec{k})}\delta(k^0-E(\vec{k}))\theta(k^0)\right)
\end{aligned} \tag{A.15}$$

Thus, in configuration space, $G_{\alpha\beta}(x,y)$ is the Fourier transform of $G_{\alpha\beta}(k)$, which is

$$G_{\alpha\beta}(k) = (\not{k}+m)_{\alpha\beta}\left\{\frac{1}{k^2-m^2+i\epsilon}+\frac{2\pi i}{2E(\vec{k})}\delta(k^0-E(\vec{k}))\theta(k^0)\theta(k_F-|\vec{k}|)\right\} \tag{A.16}$$

The expression between braces in the above equation can be written in several ways. One of them is

$$
\begin{aligned}
G(k) &= \frac{1}{k^2 - m^2 + i\epsilon} + \frac{\pi i}{E(\vec{k})}\delta(k^0 - E(\vec{k}))\theta(k^0)n(\vec{k}) \\
&= \frac{1}{k^0 + E(\vec{k}) + i\epsilon}\left(\frac{1}{k^0 - E(\vec{k}) + i\epsilon} + 2\pi\, i\, n(\vec{k})\,\delta(k^0 - E(\vec{k}))\right) \\
&= \frac{1}{k^0 + E(\vec{k}) + i\epsilon}\left(\mathcal{P}\left(\frac{1}{k^0 - E(\vec{k})}\right) - i\pi\delta(k^0 - E(\vec{k}))\left(1 - 2n(\vec{k})\right)\right) \\
&= \frac{1}{k^0 + E(\vec{k}) + i\epsilon}\left\{n(\vec{k})\left(\mathcal{P}\left(\frac{1}{k^0 - E(\vec{k})}\right) + i\pi\delta(k^0 - E(\vec{k}))\right)\right. \\
&+ \left.(1 - n(\vec{k}))\left(\mathcal{P}\left(\frac{1}{k^0 - E(\vec{k})}\right) - i\pi\delta(k^0 - E(\vec{k}))\right)\right\} \\
&= \frac{1}{k^0 + E(\vec{k}) + i\epsilon}\left(\frac{n(\vec{k})}{k^0 - E(\vec{k}) - i\epsilon} + \frac{(1 - n(\vec{k}))}{k^0 - E(\vec{k}) + i\epsilon}\right) \qquad \text{(A.17)}
\end{aligned}
$$

where $E(\vec{k}) = \sqrt{\vec{k}^{\,2} + m^2}$ and the symbol $\mathcal{P}$ stands for the Cauchy principal value.

Appendix B

B.1 Low density limit

In this chapter we are going to demonstrate that the hadronic tensor for π production, in Eq. (2.45), fulfills the impulse approximation in the low density limit. In this limit we have the following approximation for the relativistic Lindhard function

$$\mathrm{Im}\bar{U}_R(q-k_\pi;k_F^h,k_F^p) \approx -\pi\rho_{\mathrm{hole}}(r)\frac{M}{E(\vec{q}-\vec{k}_\pi)}\delta(q^0-k_\pi^0+M-E(\vec{q}-\vec{k}_\pi)) \tag{B.1}$$

With this approximation, we obtain the following expression for the hadronic tensor of Eq. (2.45)

$$\begin{aligned} W^{\mu\nu} &= \frac{\pi}{8M}\theta(q^0)\int\frac{d^3r}{2\pi}\int\frac{d^3k_\pi}{(2\pi)^3}\frac{\theta(q^0-E_\pi(\vec{k}_\pi))}{E_\pi(\vec{k}_\pi)E'_N(\vec{q}-\vec{k}_\pi)} \\ &\times \delta(q^0+M-E_\pi(\vec{k}_\pi)-E'_N(\vec{q}-\vec{k}_\pi)) \\ &\times \left\{\rho_p(r)\left(A^{\mu\nu}_{p\to p\pi^+}\right)_{<\vec{p}>\to 0}+\rho_n(r)\left(A^{\mu\nu}_{n\to n\pi^+}+A^{\mu\nu}_{n\to p\pi^0}\right)_{<\vec{p}>\to 0}\right\} \end{aligned} \tag{B.2}$$

The differential cross section (with respect to the kinematic variables of the outgoing lepton) can be cast as [47]

$$\frac{d\sigma}{d\Omega(\hat{k}')dE'_l}=\frac{|\vec{k}\,'|}{|\vec{k}|}\frac{G_F^2}{4\pi^2}L_{\mu\nu}\int\frac{d^3k_\pi}{E_\pi(\vec{k}_\pi)}W^{\mu\nu}_{cc\,\pi} \tag{B.3}$$

where

$$W^{\mu\nu}_{cc\,\pi} = \frac{1}{4M}\overline{\sum_{\rm spin}}\int \frac{d^3p'}{(2\pi)^3}\frac{1}{2E'_N}\delta^4(p'+k_\pi-q-p)\left\langle N'\pi\left|j^\mu_{cc+}(0)\right|N\right\rangle\left\langle N'\pi\left|j^\nu_{cc+}(0)\right|N\right\rangle^* \tag{B.4}$$

We can identify the phase space integral in Eq. (B.3) with the hadronic tensor

$$\begin{aligned} W^{\mu\nu}_{N\to N'\pi} &= \int \frac{d^3k_\pi}{E_\pi(\vec{k}_\pi)}\frac{1}{8M}\frac{1}{(2\pi)^3}\frac{1}{E'_N(\vec{q}-\vec{k}_\pi)}\delta(q^0+M-E_\pi(\vec{k}_\pi)-E'_N(\vec{q}-\vec{k}_\pi)) \\ &\times \frac{1}{2}\underbrace{\mathrm{Tr}\left(J^\mu_{N\to N'\pi}(\not{p}+M)\gamma^0 J^{\nu\dagger}_{N\to N'\pi}\gamma^0(\not{p}'+M)\right)} \end{aligned} \tag{B.5}$$

where the quantity between $\underbrace{\quad}$ is $A^{\mu\nu}_{N\to N'\pi}$.
If we return to expression (B.2), one can easily see that it can be written as

$$\begin{aligned} W^{\mu\nu} &= \overbrace{\int d^3r\,\rho_p(r)}\left[\frac{1}{8M}\int\frac{d^3k_\pi}{(2\pi)^3E_\pi\,E'_N(\vec{q}-\vec{k}_\pi)}\delta(q^0+M-E_\pi-E'_N(\vec{q}-\vec{k}_\pi))\right. \\ &\times \left.\frac{1}{2}\left(A^{\mu\nu}_{p\to p\pi^+}\right)_{<\vec{p}>\to 0}\right] + \underbrace{\int d^3r\,\rho_n(r)}\left[\frac{1}{8M}\int\frac{d^3k_\pi}{(2\pi)^3E_\pi\,E'_N(\vec{q}-\vec{k}_\pi)}\right. \\ &\times \left.\delta(q^0+M-E_\pi-E'_N(\vec{q}-\vec{k}_\pi))\left(\frac{1}{2}A^{\mu\nu}_{n\to n\pi^+}+\frac{1}{2}A^{\mu\nu}_{n\to p\pi^0}\right)_{<\vec{p}>\to 0}\right] \\ &= Z\,W^{\mu\nu}_{p\to p\pi^+}+N\left(W^{\mu\nu}_{n\to n\pi^+}+W^{\mu\nu}_{n\to p\pi^0}\right) \end{aligned} \tag{B.6}$$

And we recover in this way the impulse approximation.

Appendix C

C.1 Tensor $A_\Delta^{\mu\nu}$

In this appendix we are going to show that the following tensors fulfill the property $A^{\mu\nu} = A^{\nu\mu *}$. This property allows me to decompose those tensors in a symmetric part which is real and in an antisymmetric part which is purely imaginary.
In section 2.2.3, the tensor $A_\Delta^{\mu\nu}$ was defined as

$$A_\Delta^{\mu\nu}(p,q) = \mathrm{Tr}\left[(\not{p}+M)\gamma^0\Gamma^{\alpha\nu\dagger}\gamma^0 P_{\alpha\beta}(p_\Delta)\Gamma^{\beta\mu}\right] \tag{C.1}$$

Let me calculate the complex conjugate of this tensor

$$\begin{aligned} A_\Delta^{\mu\nu *} &= \mathrm{Tr}\left[\left((\not{p}+M)\gamma^0\Gamma^{\alpha\nu\dagger}\gamma^0 P_{\alpha\beta}(p_\Delta)\Gamma^{\beta\mu}\right)^\dagger\right] \\ &= \mathrm{Tr}\left[\Gamma^{\beta\mu\dagger}P^\dagger_{\alpha\beta}\gamma^0\Gamma^{\alpha\nu}\gamma^0(\not{p}+M)^\dagger\right] \end{aligned} \tag{C.2}$$

With the help of the following relations,

$$(\not{p}+M)^\dagger = \gamma^0(\not{p}+M)\gamma^0 \tag{C.3}$$

$$\gamma^0\gamma^0 = \mathbf{1} \tag{C.4}$$

We easily find

$$A_\Delta^{\mu\nu *} = \mathrm{Tr}\left[\Gamma^{\beta\mu\dagger}\gamma^0\gamma^0 P^\dagger_{\alpha\beta}\gamma^0\Gamma^{\alpha\nu}(\not{p}+M)\gamma^0\right] \tag{C.5}$$

And finally, using these two last properties,

$$\mathrm{Tr}(AB) = \mathrm{Tr}(BA) \tag{C.6}$$

$$\gamma^0 P^\dagger_{\alpha\beta}\gamma^0 = P_{\beta\alpha} \tag{C.7}$$

we find

$$\begin{aligned} A_{\Delta}^{\mu\nu *} &= \mathrm{Tr}\left[(\not{p}+M)\gamma^0\Gamma^{\beta\mu\dagger}\gamma^0 P_{\beta\alpha}\Gamma^{\alpha\nu}\right] \\ &= \mathrm{Tr}\left[(\not{p}+M)\gamma^0\Gamma^{\alpha\mu\dagger}\gamma^0 P_{\alpha\beta}\Gamma^{\beta\nu}\right] = A_{\Delta}^{\nu\mu} \end{aligned} \tag{C.8}$$

where in the last step of Eq. (C.8) we have performed the reshuffling of dummy indices $\beta \leftrightarrow \alpha$.

C.2 Tensor $A_1^{\mu\nu}$

In Eq. (2.74), it is defined the following tensor

$$\begin{aligned} A_1^{\mu\nu}(p,l,q,k_\pi) &= \mathrm{Tr}\left[J^{\mu}_{n\to p\pi^0}(p,q,k_\pi)(\not{p}+M)(\not{q}-\not{k}_\pi)\gamma_5(\not{p}+\not{q}-\not{k}_\pi+M)\right] \\ &\times \mathrm{Tr}\left[\not{k}_\pi\gamma_5(\not{l}+M)\gamma^0 J^{\nu\dagger}_{p\to p\pi^+}(l,q,q-k_\pi)\gamma^0(\not{l}+\not{k}_\pi+M)\right] \\ &+ \mathrm{Tr}\left[J^{\mu}_{p\to p\pi^+}(l,q,q-k_\pi)(\not{l}+M)\not{k}_\pi\gamma_5(\not{l}+\not{k}_\pi+M)\right] \\ &\times \mathrm{Tr}\left[(\not{q}-\not{k}_\pi)\gamma_5(\not{p}+M)\gamma^0 J^{\nu\dagger}_{n\to p\pi^0}(p,q,k_\pi)\gamma^0(\not{p}+\not{q}-\not{k}_\pi+M)\right] \end{aligned} \tag{C.9}$$

Let me calculate the complex conjugate of this tensor

$$\begin{aligned} A_1^{\mu\nu *} &= \mathrm{Tr}\left[\left(J^{\mu}_{n\to p\pi^0}(\not{p}+M)(\not{q}-\not{k}_\pi)\gamma_5(\not{p}+\not{q}-\not{k}_\pi+M)\right)^\dagger\right] \\ &\times \mathrm{Tr}\left[\left(\not{k}_\pi\gamma_5(\not{l}+M)\gamma^0 J^{\nu\dagger}_{p\to p\pi^+}\gamma^0(\not{l}+\not{k}_\pi+M)\right)^\dagger\right] \\ &+ \mathrm{Tr}\left[\left(J^{\mu}_{p\to p\pi^+}(\not{l}+M)\not{k}_\pi\gamma_5(\not{l}+\not{k}_\pi+M)\right)^\dagger\right] \\ &\times \mathrm{Tr}\left[\left((\not{q}-\not{k}_\pi)\gamma_5(\not{p}+M)\gamma^0 J^{\nu\dagger}_{n\to p\pi^0}\gamma^0(\not{p}+\not{q}-\not{k}_\pi+M)\right)^\dagger\right] \\ &= \mathrm{Tr}\left[\gamma^0(\not{p}+\not{q}-\not{k}_\pi+M)\gamma^0\gamma_5\gamma^0(\not{q}-\not{k}_\pi)\gamma^0\gamma^0(\not{p}+M)\gamma^0 J^{\mu\dagger}_{n\to p\pi^0}\right] \\ &\times \mathrm{Tr}\left[\gamma^0(\not{l}+\not{k}_\pi+M)\gamma^0\gamma^0 J^{\nu}_{p\to p\pi^+}\gamma^0\gamma^0(\not{l}+M)\gamma^0\gamma_5\gamma^0\not{k}_\pi\gamma^0\right] \\ &+ \mathrm{Tr}\left[\gamma^0(\not{l}+\not{k}_\pi+M)\gamma^0\gamma_5\gamma^0\not{k}_\pi\gamma^0\gamma^0(\not{l}+M)\gamma^0 J^{\mu\dagger}_{p\to p\pi^+}\right] \\ &\times \mathrm{Tr}\left[\gamma^0(\not{p}+\not{q}-\not{k}_\pi+M)\gamma^0\gamma^0 J^{\nu}_{n\to p\pi^0}\gamma^0\gamma^0(\not{p}+M)\gamma^0\gamma_5\gamma^0(\not{q}-\not{k}_\pi)\gamma^0\right] \end{aligned}$$

where we have used Eq. (C.3) and the fact that γ^0 and γ_5 are hermitian matrices. Using now Eq. (C.4), the cyclic propertie of the trace and

$$\{\gamma^\mu, \gamma_5\} = 0 \tag{C.10}$$

we easily find that

$$\begin{aligned} A_1^{\mu\nu *} &= \mathrm{Tr}\left[(\not{q} - \not{k}_\pi)\gamma_5(\not{p} + M)\gamma^0 J^{\mu\dagger}_{n\to p\pi^0}\gamma^0(\not{p} + \not{q} - \not{k}_\pi + M)\right] \\ &\times \mathrm{Tr}\left[J^\nu_{p\to p\pi^+}(\not{l} + M)\not{k}_\pi\gamma_5(\not{l} + \not{k}_\pi + M)\right] \\ &+ \mathrm{Tr}\left[\not{k}_\pi\gamma_5(\not{l} + M)\gamma^0 J^{\mu\dagger}_{p\to p\pi^+}\gamma^0(\not{l} + \not{k}_\pi + M)\right] \\ &\times \mathrm{Tr}\left[J^\nu_{n\to p\pi^0}(\not{p} + M)(\not{q} - \not{k}_\pi)\gamma_5(\not{p} + \not{q} - \not{k}_\pi + M)\right] = A_1^{\nu\mu} \end{aligned} \tag{C.11}$$

Appendix D

D.1 Selfenergy of the pion

In this appendix, we are going to calculate the pion selfenergy in a non-relativistic approximation. Let me write the Yukawa lagrangian for the vertices. From this lagrangian, we will obtain the non-relativistic reduction of the vertices.

$$\mathcal{L}_{\pi NN} = ig\bar{\Psi}_\alpha(x)\,\gamma_5\,\tau^i_{\alpha\beta}\,\phi_i(x)\,\Psi_\beta(x) \tag{D.1}$$

where g is the coupling constant, $\alpha, \beta = 1, 2$ are indices for the strong isospin, $\vec{\tau}$ are the three Pauli matrices, $\vec{\phi}(x)$ are the three fields for the pions and $\Psi(x) = \begin{pmatrix} p(x) \\ n(x) \end{pmatrix}$ is the isospin doublet for the nucleon fields.
Just applying the Feynman rules for the diagram of Fig. D.1, we obtain

$$\begin{aligned} -i\Pi^{ij}(q) &= g^2\tau^i_{\beta'\alpha'}\,\tau^j_{\alpha\beta}\,\delta_{\alpha'\alpha}\,\delta_{\beta\beta'}\int\frac{d^4p}{(2\pi)^4}G(p)G(p+q) \\ &\times \ \mathrm{Tr}\left[\gamma_5(\not{p}+M)\gamma_5(\not{p}+\not{q}+M)\right] \\ &= g^2\mathrm{Tr}(\tau^i\tau^j)\int\frac{d^4p}{(2\pi)^4}G(p)G(p+q) \\ &\times \ \sum_{r,r'}\mathrm{Tr}\left[\gamma_5 u_r(\vec{p})\bar{u}_r(\vec{p})\gamma_5 u_{r'}(\vec{p}\,')\bar{u}_{r'}(\vec{p}\,')\right] \end{aligned} \tag{D.2}$$

where $\vec{p}\,' = \vec{p} + \vec{q}$. The traces are

$$\mathrm{Tr}(\tau^i\tau^j) = 2\delta^{ij} \tag{D.3}$$

$$\mathrm{Tr}\left[\gamma_5 u_r(\vec{p})\bar{u}_r(\vec{p})\gamma_5 u_{r'}(\vec{p}\,')\bar{u}_{r'}(\vec{p}\,')\right] = \left(\bar{u}_{r'}(\vec{p}\,')\gamma_5 u_r(\vec{p})\right)\left(\bar{u}_r(\vec{p})\gamma_5 u_{r'}(\vec{p}\,')\right) \tag{D.4}$$

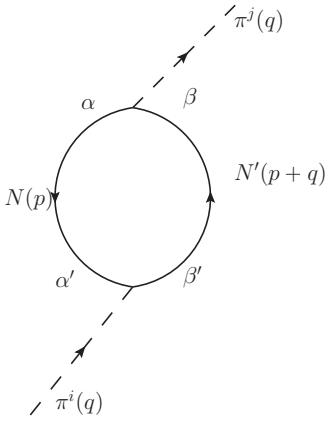

Figure D.1: Selfenergy diagram of a pion. The indices $\alpha, \beta, \alpha', \beta'$ are strong isospin indices, which are summed. The indices i, j for the pion indicate the charge of the pion.

If now we consider Dirac spinors normalized in such a way that these can be written as $u_r(\vec{p}) = \sqrt{E+M}\begin{pmatrix} \varphi_r \\ \frac{\vec{\sigma}\cdot\vec{p}}{E+M}\varphi_r \end{pmatrix}$ with φ_r a canonical basis of Pauli spinors, then we have (up to corrections of order $\frac{\vec{p}^2}{M^2}$)

$$\bar{u}_{r'}(\vec{p}\,')\gamma_5 u_r(\vec{p}) = \varphi^\dagger_{r'}\,\sigma_i(p^i - p'^i)\,\varphi_r \tag{D.5}$$

Therefore, Eq. (D.4) can be written in a non-relativistic reduction as

$$\mathrm{Tr}\left[\gamma_5 u_r(\vec{p})\bar{u}_r(\vec{p})\gamma_5 u_{r'}(\vec{p}\,')\bar{u}_{r'}(\vec{p}\,')\right] = \left(\varphi^\dagger_{r'}\,\vec{\sigma}\cdot\vec{q}\,\varphi_r\right)\left(\varphi^\dagger_r\,\vec{\sigma}\cdot(-\vec{q})\,\varphi_{r'}\right) \tag{D.6}$$

Finally, with the aid of

$$\sum_{r=1}^{2}\varphi_r\varphi^\dagger_r = \mathbf{1} \tag{D.7}$$

we can write the selfenergy of the pion as

$$\begin{aligned} -i\Pi^{ij}(q) &= 2g^2\delta^{ij}\int\frac{d^4p}{(2\pi)^4}G(p)G(p+q)\mathrm{Tr}\left[\sigma_k q^k\ \mathbf{1}\ \sigma_l(-q^l)\ \mathbf{1}\right] \\ &= -2g^2\delta^{ij}q^kq^l\int\frac{d^4p}{(2\pi)^4}G(p)G(p+q)\,\mathrm{Tr}\left[\sigma_k\sigma_l\right] \\ &= -4g^2\delta^{ij}\vec{q}^{\,2}\int\frac{d^4p}{(2\pi)^4}G(p)G(p+q) \end{aligned} \tag{D.8}$$

with $G(p)$ given (in the non-relativistic approximation) by

$$G(p)=\frac{1}{2M}\left\{\frac{n(\vec{p})}{p^0-E(\vec{p})-i\eta}+\frac{1-n(\vec{p})}{p^0-E(\vec{p})+i\eta}\right\} \tag{D.9}$$

and the following relation between couplings holds

$$\frac{g}{2M}=\frac{f_{\pi NN}}{m_\pi}=\frac{g_A}{2f_\pi} \tag{D.10}$$

with these replacements, Eq. (D.8) reads

$$\begin{aligned} -i\Pi^{ij}(q) &= -4g^2\delta^{ij}\vec{q}^{\,2}\int\frac{d^4p}{(2\pi)^4}\frac{1}{2M}\left\{\frac{n(\vec{p})}{p^0-E(\vec{p})-i\eta}+\frac{1-n(\vec{p})}{p^0-E(\vec{p})+i\eta}\right\} \\ &\times\ \frac{1}{2M}\left\{\frac{n(\vec{p}+\vec{q})}{p^0+q^0-E(\vec{p}+\vec{q})-i\eta}+\frac{1-n(\vec{p}+\vec{q})}{p^0+q^0-E(\vec{p}+\vec{q})+i\eta}\right\} \\ &= -4\delta^{ij}\vec{q}^{\,2}\left(\frac{g_A}{2f_\pi}\right)^2 i\int\frac{d^3p}{(2\pi)^3}\left\{\frac{n(\vec{p})(1-n(\vec{p}+\vec{q}))}{q^0+E(\vec{p})-E(\vec{p}+\vec{q})+i\eta}\right. \\ &+\ \left.\frac{n(\vec{p}+\vec{q})(1-n(\vec{p}))}{-q^0-E(\vec{p})+E(\vec{p}+\vec{q})+i\eta}\right\} \\ &= -i\,\delta^{ij}\vec{q}^{\,2}\left(\frac{g_A}{2f_\pi}\right)^2 U_N(q) \end{aligned} \tag{D.11}$$

where $U_N(q)$ is the Lindhard function for the particle-hole (ph) excitation and is defined as

$$U_N(q)\equiv 4\int\frac{d^3p}{(2\pi)^3}\left\{\frac{n(\vec{p})(1-n(\vec{p}+\vec{q}))}{q^0+E(\vec{p})-E(\vec{p}+\vec{q})+i\eta}+\frac{n(\vec{p}+\vec{q})(1-n(\vec{p}))}{-q^0-E(\vec{p})+E(\vec{p}+\vec{q})+i\eta}\right\} \tag{D.12}$$

In Eq. (D.11) one can see that the charge of the pion is not changed when it excites a particle-hole (because of the factor δ^{ij}).

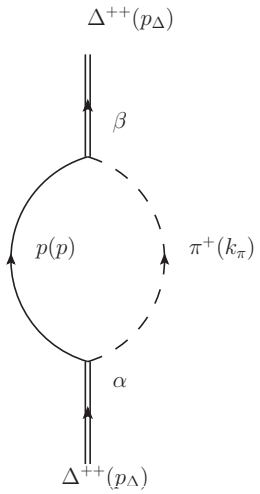

Figure D.2: Δ-selfenergy Feynman diagram.

D.2 Selfenergy of the Δ

To calculate the Δ-selfenergy we need the $N\Delta\pi$ lagrangian, which is given by

$$\mathcal{L}_{\pi N\Delta} = \frac{f^*_{\pi N\Delta}}{m_\pi}\bar{\Psi}_\mu \vec{T}^\dagger \cdot (\partial^\mu \vec{\phi})\psi + \text{h.c.} \tag{D.13}$$

where $f^*_{\pi N\Delta} = 2.14$ is the coupling constant, $\bar{\Psi}_\mu$ is the 4-plet that contains the Rarita-Schwinger fields for the Δ-isobar, $\vec{T}^\dagger$ is the isospin transition operator, $\vec{\phi}$ are the pion fields and, finally, $\psi = \begin{pmatrix} p \\ n \end{pmatrix}$ is the isospin doublet for the nucleon fields.
If we perform the scalar product in the spherical basis and we also perform the matricial product with the matrix $\vec{T}^{\dagger}1$, then we are left with the following lagrangian (if we only select the piece that goes with $\partial^\mu\phi_{-1}$, which is the field that creates a π^- or annihilates a π^+)

$$\mathcal{L} = -\frac{f^*_{\pi N\Delta}}{m_\pi}\partial^\mu\phi_{-1}\left(\overline{\Delta^{++}_\mu}p + \frac{1}{\sqrt{3}}\overline{\Delta^{+}_\mu}n\right) + \text{h.c.} \tag{D.14}$$

[1] It is actually a 4×2 matrix of Clebsch-Gordan coefficients.

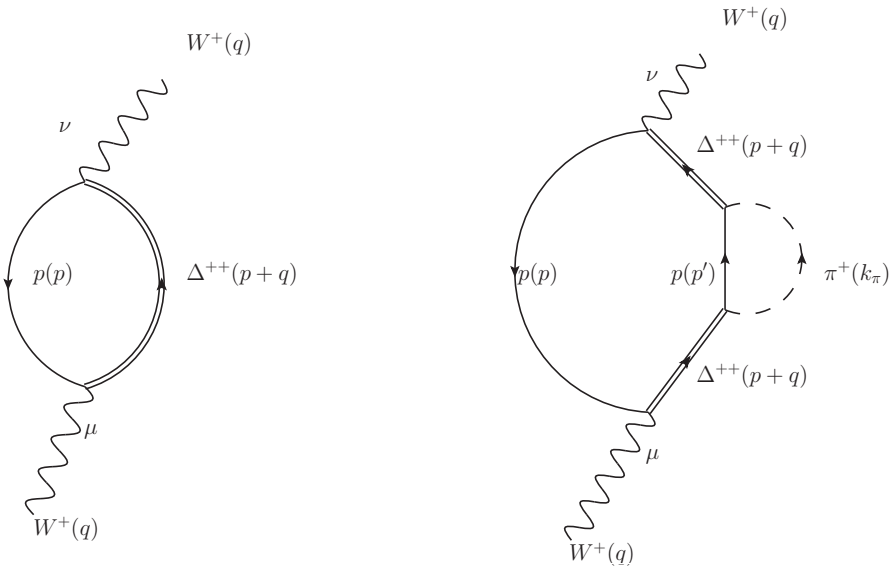

Figure D.3: Equivalent Feynman diagrams

Then, applying the Feynman rules, we obtain the following Δ-selfenergy

$$-i\Sigma^{\alpha\beta}(p_\Delta) = \left(\frac{f^*_{\pi N\Delta}}{m_\pi}\right)^2 \int \frac{d^4k_\pi}{(2\pi)^4} k_\pi^\alpha k_\pi^\beta \,(\not{p}_\Delta - \not{k}_\pi + M)\, G(p_\Delta - k_\pi; \rho_p) D_0(k_\pi) \tag{D.15}$$

The above equation is a matrix in Dirac space and a symmetric Lorentz tensor and it will be a very helpful expression to show the equivalence between the diagrams shown in fig. D.3.

Let me write again Eq. (2.32) when in both currents (implicit in the definition of the tensor $A^{\mu\nu}$ of Eq. 2.34) we only select the ΔP amputated amplitude. This contribution to the W-selfenergy would come from the diagram in the right-hand side of Fig. D.3, and it would read

$$\begin{aligned} -i\Pi^{\mu\nu}_{\Delta P}(q) &= -i\left(\frac{g}{2\sqrt{2}}\right)^2 \int \frac{d^4k_\pi}{(2\pi)^4} D_0(k_\pi) \int \frac{d^4p}{(2\pi)^4} G(p;\rho_p) G(p+q-k_\pi;\rho_p) \\ &\times \mathrm{Tr}\left[J^\mu_{\Delta P}(\not{p}+M)\gamma^0 J^{\nu\dagger}_{\Delta P}\gamma^0(\not{p}+\not{q}-\not{k}_\pi+M)\right] \end{aligned} \tag{D.16}$$

And now, in Ref. [47], one can find the amputated amplitude for the ΔP mechanism

$$J^{\mu}_{\Delta P} = i\frac{f^{*}_{\pi N\Delta}}{m_{\pi}}\sqrt{3}\cos\theta_{c}\frac{k^{\alpha}_{\pi}}{(p+q)^{2}-M^{2}_{\Delta}+iM_{\Delta}\Gamma_{\Delta}}P_{\alpha\beta}(p+q)\Gamma^{\beta\mu}(p,q) \tag{D.17}$$

If we compute the adjoint hermitic of the above equation, we get

$$\begin{aligned}
\gamma^{0}J^{\nu\dagger}_{\Delta P}\gamma^{0} &= -i\frac{f^{*}_{\pi N\Delta}}{m_{\pi}}\frac{\sqrt{3}\cos\theta_{c}\,k^{\delta}_{\pi}}{(p+q)^{2}-M^{2}_{\Delta}-iM_{\Delta}\Gamma_{\Delta}}\gamma^{0}\Gamma^{\sigma\nu\dagger}(p,q)P^{\dagger}_{\delta\sigma}(p+q)\gamma^{0} \\
&= -i\frac{f^{*}_{\pi N\Delta}}{m_{\pi}}\frac{\sqrt{3}\cos\theta_{c}\,k^{\delta}_{\pi}}{(p+q)^{2}-M^{2}_{\Delta}-iM_{\Delta}\Gamma_{\Delta}}\gamma^{0}\Gamma^{\sigma\nu\dagger}(p,q)\gamma^{0}\gamma^{0}P^{\dagger}_{\delta\sigma}(p+q)\gamma^{0} \\
&= -i\frac{f^{*}_{\pi N\Delta}}{m_{\pi}}\frac{\sqrt{3}\cos\theta_{c}\,k^{\delta}_{\pi}}{(p+q)^{2}-M^{2}_{\Delta}-iM_{\Delta}\Gamma_{\Delta}}\gamma^{0}\Gamma^{\sigma\nu\dagger}(p,q)\gamma^{0}P_{\sigma\delta}(p+q)
\end{aligned} \tag{D.18}$$

where in the second step we have inserted an identity matrix between $\Gamma^{\sigma\nu\dagger}$ and $P^{\dagger}_{\delta\sigma}$; and in the last step we have used Eq. (C.7).
Inserting these two currents in Eq. (D.16), we obtain

$$\begin{aligned}
-i\Pi^{\mu\nu}_{\Delta P}(q) &= -i\left(\frac{g}{2\sqrt{2}}\right)^{2}\int\frac{d^{4}p}{(2\pi)^{4}}\int\frac{d^{4}k_{\pi}}{(2\pi)^{4}}D_{0}(k_{\pi})G(p;\rho_{p})G(p+q-k_{\pi};\rho_{p}) \\
&\times \left(\frac{f^{*}_{\pi N\Delta}}{m_{\pi}}\right)^{2}\left(\sqrt{3}\right)^{2}\cos^{2}\theta_{c}\frac{k^{\alpha}_{\pi}k^{\delta}_{\pi}}{\left|(p+q)^{2}-M^{2}_{\Delta}+iM_{\Delta}\Gamma_{\Delta}\right|^{2}} \\
&\times \mathrm{Tr}\left[P_{\alpha\beta}\Gamma^{\beta\mu}(\not{p}+M)\gamma^{0}\Gamma^{\sigma\nu\dagger}\gamma^{0}P_{\sigma\delta}(\not{p}+\not{q}-\not{k}_{\pi}+M)\right]
\end{aligned} \tag{D.19}$$

Using the cyclic property of the trace, and taking out from the integral in $d^{4}k_{\pi}$ all the possible terms that do not involve the four-momentum k_{π}, we

get

$$-i\Pi^{\mu\nu}_{\Delta P}(q) = -i\left(\frac{g}{2\sqrt{2}}\right)^2\left(\sqrt{3}\right)^2\cos^2\theta_c\int\frac{d^4p}{(2\pi)^4}\frac{G(p;\rho_p)}{\left|(p+q)^2-M_\Delta^2+iM_\Delta\Gamma_\Delta\right|^2}$$

$$\times\ \mathrm{Tr}\Bigg[\Gamma^{\beta\mu}(p,q)(\not{p}+M)\gamma^0\Gamma^{\sigma\nu\dagger}(p,q)\gamma^0P_{\sigma\delta}(p+q)$$

$$\cdot\ \underbrace{\left(\int\frac{d^4k_\pi}{(2\pi)^4}\left(\frac{f^*_{\pi N\Delta}}{m_\pi}\right)^2k_\pi^\delta k_\pi^\alpha D_0(k_\pi)G(p+q-k_\pi;\rho_p)(\not{p}+\not{q}-\not{k}_\pi+M)\right)}P_{\alpha\beta}\Bigg] \tag{D.20}$$

where the underbraced expression in the above equation is precisely $-i\Sigma^{\delta\alpha}(p_\Delta)$, with $p_\Delta = p+q$.

Therefore, the contribution of the $\Delta P\otimes\Delta P$ diagram to the W-selfenergy can be written as

$$\begin{aligned}-i\Pi^{\mu\nu}_{\Delta P}(q) &= -\left(\frac{g}{2\sqrt{2}}\right)^2\left(\sqrt{3}\right)^2\cos^2\theta_c\int\frac{d^4p}{(2\pi)^4}\frac{G(p;\rho_p)}{\left|(p+q)^2-M_\Delta^2+iM_\Delta\Gamma_\Delta\right|^2}\\ &\times\ \mathrm{Tr}\left[\Gamma^{\beta\mu}_{(p,q)}(\not{p}+M)\gamma^0\Gamma^{\sigma\nu\dagger}_{(p,q)}\gamma^0P_{\sigma\delta}(p+q)\Sigma^{\delta\alpha}_{(p+q)}P_{\alpha\beta}(p+q)\right]\end{aligned} \tag{D.21}$$

In principle, the Δ-selfenergy can be expressed in terms of a linear combination of the five orthogonal spin projection operators introduced in Eq. (10) of Ref. [176]. The coefficients, A_i, of such linear combination will be matrices in the Dirac space and Lorentz scalars. We will enormously simplify the discussion here neglecting Δ-offshell effects. Within this approximation, the spin-3/2 projector of Ref. [176] reduces to that used here ($-P^{\mu\nu}/2M_\Delta$) to construct the Δ-propagator. This on-shell spin-3/2 projection operator satisfies the following relations

$$\not{p}_\Delta P_{\alpha\beta}(p_\Delta) = P_{\alpha\beta}(p_\Delta)\not{p}_\Delta = M_\Delta P_{\alpha\beta}(p_\Delta) \tag{D.22}$$

$$P^{\mu\nu}(p_\Delta)P_{\nu\alpha}(p_\Delta) = -2M_\Delta P^\mu{}_\alpha(p_\Delta) \tag{D.23}$$

Since in Eq. (D.21) the Δ-selfenergy always appears contracted between two on-shell spin-3/2 projection operators, we can assume the following expansion for the Δ-selfenergy

$$\Sigma^{\delta\alpha}(p+q) = -\Sigma_\Delta P^{\delta\alpha}(p+q) + \underbrace{\cdots}_{\perp\,P_{\alpha\beta}(p+q)} \tag{D.24}$$

where Σ_Δ is a scalar quantity. Within this assumption, we easily find

$$P_{\sigma\delta}(p_\Delta)\Sigma^{\delta\alpha}(p_\Delta)P_{\alpha\beta}(p_\Delta) = -4M_\Delta^2\Sigma_\Delta P_{\sigma\beta}(p_\Delta) \tag{D.25}$$

with $p_\Delta = p + q$. Therefore, Eq. (D.21) can be simplified to

$$\begin{aligned} -i\Pi^{\mu\nu}_{\Delta P}(q) &= \left(\frac{g}{2\sqrt{2}}\right)^2 \left(\sqrt{3}\right)^2 \cos^2\theta_c \int \frac{d^4p}{(2\pi)^4} \frac{G(p;\rho_p)\, 4M_\Delta^2\Sigma_\Delta}{\left|(p+q)^2 - M_\Delta^2 + iM_\Delta\Gamma_\Delta\right|^2} \\ &\times \underbrace{\mathrm{Tr}\left[\Gamma^{\beta\mu}(p,q)(\not{p}+M)\gamma^0\Gamma^{\sigma\nu\dagger}(p,q)\gamma^0 P_{\sigma\beta}(p+q)\right]}_{} \end{aligned} \tag{D.26}$$

where the underbraced quantity is precisely the tensor $A_\Delta^{\mu\nu}$ defined in Eq. (2.23).

We can, again, decompose the polarization tensor in its symmetric (anti-symmetric) part, with the aid of the symmetry properties of the tensor $A_\Delta^{\mu\nu}$. But, when applying the Cutkosky's rules to obtain the imaginary part of $\Pi^{\mu\nu}_{\Delta P}$, there always appears the imaginary part of the Δ-selfenergy. If we carry out all these calculations, we get the following result

$$\begin{aligned} W^{\mu\nu} &= \theta(q^0)\left(\sqrt{3}\right)^2 \cos^2\theta_c \int \frac{d^3r}{2\pi} \int \frac{d^3p}{(2\pi)^3} \frac{n(\vec{p})}{E(\vec{p})} \frac{4M_\Delta^2\,\mathrm{Im}\Sigma_\Delta(p+q)}{\left|(p+q)^2 - M_\Delta^2 + iM_\Delta\Gamma_\Delta\right|^2} \\ &\times A_\Delta^{\mu\nu}|_{p^0=E(\vec{p})} \end{aligned} \tag{D.27}$$

If the above equation (which is the contribution to the hadronic tensor for a proton hole) is compared with Eq. (2.28), and taking into account that

$$\mathrm{Im}G_\Delta(p+q) = \frac{-M_\Delta\Gamma_\Delta(p+q)}{\left|(p+q)^2 - M_\Delta^2 + iM_\Delta\Gamma_\Delta\right|^2} \tag{D.28}$$

we get the following relation

$$\mathrm{Im}\Sigma_\Delta = \frac{\Gamma_\Delta}{4M_\Delta} \tag{D.29}$$

And with this, the equivalence between the Feynman diagrams of Fig. D.3 is shown in a quantitative way.

Appendix E

E.1 Derivative expansions for the DIS structure functions

The advent of new and high statistics deeply inelastic neutrino scattering experiments apart from providing valuable data on F_2 and $x\,F_3$ [177, 178] has shown again the importance of nuclear effects that render difficult the extraction of the nucleon structure functions. Furthermore, the use of nuclear targets is necessary due to the smallness of the cross sections. Qualitatively, the nuclear effects are well known. Shadowing, antishadowing, Fermi motion, binding,... have all been widely studied for charged leptons in the context of the European Muon Collaboration (EMC) effect. For a review, see [148, 149]. Moreover, it is well known that nuclear effects are substantially different for neutrino reactions due to the presence of the axial current and the different valence and sea quark contributions for each observable [153]. This situation asks for a detailed and quantitative microscopical understanding of the nuclear effects, rather than the parametrizations that have been used sometimes, like recently by the NuTeV Collaboration [178]. One of the basic ingredients in all calculations is the nuclear spectral function. This presents some serious difficulties, as these functions are not so well known to the precision level reached by current experiments. Therefore, the analysis might introduce unwanted model dependences. However, it was soon noticed that under some approximations the nuclear structure functions could be written as simple expansions on the nucleon structure functions and their derivatives. All the nuclear information would then be encoded in the expected values of some nuclear magnitudes, like the average

kinetic energy of the nucleons or the mean nucleon removal energy. These kind of approximations, both for charged lepton and for neutrino induced reactions, have been widely used in the literature [168, 170, 175, 179–183]. The aim of this appendix is to investigate the quality of these expansions and to what extent they could be used in the analysis of lepton deep inelastic scattering experiments. In order to do that, once the formalism is established, we will make a comparative study for $F_{2,3}$ and for a few typical nuclear spectral functions used in the literature.
The nuclear structure functions can be written as a convolution of the nuclear spectral functions and nucleon structure functions. See for instance [65] and references therein. In the rest frame of the nucleus, the F_2 and F_3 structure functions are

$$\begin{aligned} F_2^A(x,Q^2) &= \sum_{\tau=p,n}\int \frac{d\epsilon\, d^3p}{(2\pi)^4}\mathcal{P}^\tau(\epsilon,\mathbf{p})\frac{(1+\gamma\frac{p_z}{M})}{\gamma^2}\left(1+4\frac{p^2x'^2}{Q^2}+6\frac{x'^2\mathbf{p}_\perp^2}{Q^2}\right) \\ &\times \quad F_2^\tau(x',Q^2), \qquad \text{(E.1)} \\ F_3^A(x,Q^2) &= \sum_{\tau=p,n}\int \frac{d\epsilon\, d^3p}{(2\pi)^4}\mathcal{P}^\tau(\epsilon,\mathbf{p})\left(1+\frac{p_z}{\gamma M}\right)\frac{x'}{x}F_3^\tau(x',Q^2), \qquad \text{(E.2)} \end{aligned}$$

where $\mathcal{P}^{p(n)}(\epsilon,\mathbf{p})$ is the nuclear spectral function, normalized to the number of protons (neutrons) in the nucleus, and describes the probability of finding a proton (neutron) with momentum $\mathbf{p}$ and removal energy ϵ. The four-momentum of the nucleon can be written as $p=(M+\epsilon,\mathbf{p})$, with $\epsilon\leq 0$. The z axis is oriented in such a way that $\mathbf{q}$ lies on it, $\mathbf{p}_\perp$ is the transverse momentum of the nucleon and $\gamma=|\mathbf{q}|/q^0$. Here, x' is the natural Bjorken variable for the nucleon in the nucleus, i.e. $x'=Q^2/(2p\cdot q)$; while x is the Bjorken variable in the nucleon rest frame, $x=Q^2/(2Mq^0)$. They are related by

$$x'=\frac{x}{z} \quad \text{where} \quad z=1+\frac{\epsilon}{M}+\gamma\frac{p_z}{M}. \qquad \text{(E.3)}$$

For isoscalar nuclei such as ^{40}Ca, only the isoscalar component of the spectral function and the structure function have to be accounted for.

When this is done in (E.1) and (E.2), these read as

$$F_2^A(x,Q^2) = A\int \frac{d\epsilon d^3p}{(2\pi)^4}\mathcal{P}_0(\epsilon,\mathbf{p})\frac{(1+\gamma\frac{p_z}{M})}{\gamma^2}\left(1+4\frac{p^2x'^2}{Q^2}+6\frac{x'^2\mathbf{p}_\perp^2}{Q^2}\right) \times F_2^N\left(\frac{x}{z},Q^2\right), \tag{E.4}$$

$$F_3^A(x,Q^2) = A\int \frac{d\epsilon d^3p}{(2\pi)^4}\mathcal{P}_0(\epsilon,\mathbf{p})\left(1+\frac{p_z}{\gamma M}\right)\frac{x'}{x}F_3^N\left(\frac{x}{z},Q^2\right), \tag{E.5}$$

where $\mathcal{P}_0(\epsilon,\mathbf{p})$, which is the isoscalar part of the nuclear spectral function, is now normalized to unity and we perform the calculations for the nuclear structure functions averaged over neutrinos and antineutrinos, i.e., we only consider the symmetric $\nu+\bar{\nu}$ combination [64, 65].

In a nucleus, the expected values of $\frac{\langle\epsilon\rangle}{M}$ and $\frac{\langle\mathbf{p}^2\rangle}{M^2}$ averaged with the nuclear spectral function are much smaller than unity. Thus, $z\approx 1$ and $x'\approx x$. Under these assumptions, we can perform a Taylor expansion of the integrands in expressions (E.4) and (E.5) around $z=1$, keeping terms up to order ϵ/M and $\mathbf{p}^2/M^2$. In this way we will be able to take out of the integral the structure functions and their derivatives and we will be left with expected values of the removal energy ϵ and momentum squared $\mathbf{p}^2$. This statement is true if the nuclear spectral functions only depend on the modulus of the momentum $|\mathbf{p}|$ (as it is in the case of the nuclear spectral functions we will consider) and not upon its direction.

Under this assumption we can drop the expected values of p_z (or any other component of the momentum) and $\epsilon\, p_z$ because they are identically zero due to symmetry considerations.

We will begin with the structure function $F_2^A\left(x,Q^2\right)$. After performing the Taylor expansion, keeping terms up to order ϵ/M and $\mathbf{p}^2/M^2$, and dropping those terms which go with $\langle p_z\rangle/M$ or $\langle\epsilon\, p_z\rangle/M^2$ (because they

are identically zero as stated above), we obtain

$$\begin{aligned}\frac{F_2^A\left(x,Q^2\right)}{A} &\simeq F_2^N\left(x,Q^2\right)\left[1+\left(\gamma^2-1\right)\frac{\left\langle \mathbf{p}^2\right\rangle}{3M^2}\right] \\ &- x\frac{\partial F_2^N\left(x,Q^2\right)}{\partial x}\left[\frac{\langle\epsilon\rangle}{M}+\left(2-\gamma^2\right)\frac{\left\langle \mathbf{p}^2\right\rangle}{3M^2}\right] \\ &+ \left(x\frac{\partial F_2^N\left(x,Q^2\right)}{\partial x}+\frac{x^2}{2}\frac{\partial^2 F_2^N\left(x,Q^2\right)}{\partial x^2}\right)\gamma^2\frac{\left\langle \mathbf{p}^2\right\rangle}{3M^2}, \quad \text{(E.6)}\end{aligned}$$

where $\langle\mathcal{O}\rangle$ is the expected value of the operator $\mathcal{O}(\epsilon,\mathbf{p})$ averaged with the isoscalar spectral function $\mathcal{P}_0(\epsilon,\mathbf{p})$:

$$\langle\mathcal{O}\rangle=\int\frac{d\epsilon\, d^3p}{(2\pi)^4}\,\mathcal{P}_0(\epsilon,\mathbf{p})\,\mathcal{O}(\epsilon,\mathbf{p}). \quad \text{(E.7)}$$

We have also used the fact that, with a nuclear spectral function which depends only on the modulus of the momentum, the expected value of momentum squared is shared equally among every squared component, i.e: $\left\langle p_i^2\right\rangle=\frac{\left\langle \mathbf{p}^2\right\rangle}{3}$. In the Bjorken limit, $(\gamma\to 1)$, (E.6) coincides with the expansions used by Frankfurt *et al.* [168] and Ciofi degli Atti *et al.* [170].
If we do the same for the nuclear structure function $F_3^A\left(x,Q^2\right)$, we obtain

$$\begin{aligned}\frac{F_3^A\left(x,Q^2\right)}{A} &\simeq F_3^N\left(x,Q^2\right)-\frac{\langle\epsilon\rangle}{M}\left\{F_3^N\left(x,Q^2\right)+x\,\frac{\partial F_3^N\left(x,Q^2\right)}{\partial x}\right\} \\ &+ \frac{\left\langle \mathbf{p}^2\right\rangle}{3M^2}\left\{\left(\gamma^2-1\right)\left[F_3^N+x\,\frac{\partial F_3^N}{\partial x}\right]+\gamma^2\left[x\,\frac{\partial F_3^N}{\partial x}+\frac{x^2}{2}\,\frac{\partial^2 F_3^N}{\partial x^2}\right]\right\} \\ &, \quad \text{(E.8)}\end{aligned}$$

a similar result to that of Kulagin [181]. To allow for an easier comparison, in the above expressions, γ^2 can be rewritten as

$$\gamma^2=1+\frac{4M^2x^2}{Q^2}. \quad \text{(E.9)}$$

Then, the only difference between (E.8) and that of [181] is that, for simplicity, we do not consider the off-shell dependence in the nucleon structure

function F_3^N. In our calculation, the only source of off-shell dependence is through the nuclear spectral function $\mathcal{P}_0$. Thus, we do not have the term $\partial_{p^2} F_3^N$ that appears in [181].

For our study we have selected the ^{40}Ca nucleus, which is isoscalar and already will show important medium effects. The free nucleon structure functions have been taken from [184] and we have chosen several different nuclear spectral functions. The first one (labelled I) is a phenomenological model of the spectral function which has a mean field part and high-momentum components coming from NN-correlations and it is described in Kulagin *et al.* [64] where it was used in a global study of nuclear structure functions. The second one (labelled II), that also contains correlations is taken from [108] where it has been tested in the calculation of several electron scattering observables. The third spectral function is taken from the semiphenomenological model based on a many body calculation and the local density approximation that is described in [138] (labelled III). Finally, we also consider the simple mean field spectral function of [183](labelled IV), which was used in the study of the EMC effect.

In figure E.1, we show the results of the ratio $R_2 = \frac{F_{2A}}{F2}$ for the nuclear spectral functions (I), (II) and (III). This gives us some idea of the uncertainties related to these functions. The differences are small, even when the spectral funtions have been obtained with diverse methods and are in fact quite different if one studies in detail their energy and momentum dependence. However, the expected values of the mean removal energy $\langle \epsilon \rangle$ and the mean kinetic energy per nucleon $\langle T \rangle = \left\langle \frac{\mathbf{p}^2}{2M} \right\rangle$ are quite similar, as can be seen in Table E.1. In particular, spectral functions (I) and (III) that

Table E.1: Expected values of the nucleon removal and kinetic energies for the nuclear spectral functions of Kulagin *et al.* [64] (I), Ankowski *et al.* [108] (II) and Fernandez de Cordoba *et al.* [138] (III).

Spectral Function	(I)	(II)	(III)
$\langle \epsilon \rangle$ (MeV)	-49	-40	-47
$\langle T \rangle$ (MeV)	30.1	26.2	28.8

have quite close expected values also produce very similar ratios, whereas (II) which has an appreciably smaller binding energy gives slightly larger values for the ratio. In figure E.2, we compare the full results for the same

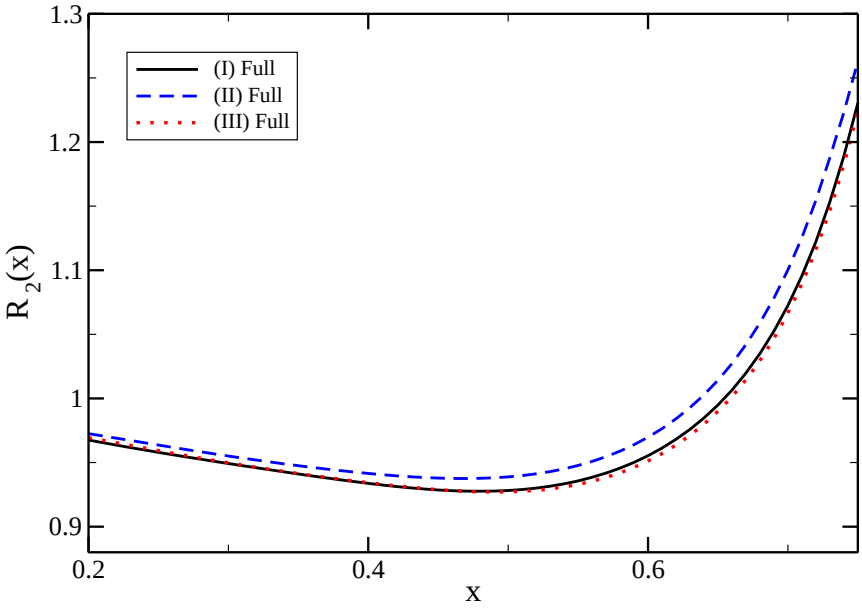

Figure E.1: $R_2 = \frac{F_{2A}}{F_2}$ ratio for ^{40}Ca at $Q^2 = 20$ GeV^2 with the nuclear spectral functions (I), (II) and (III) described in the text.

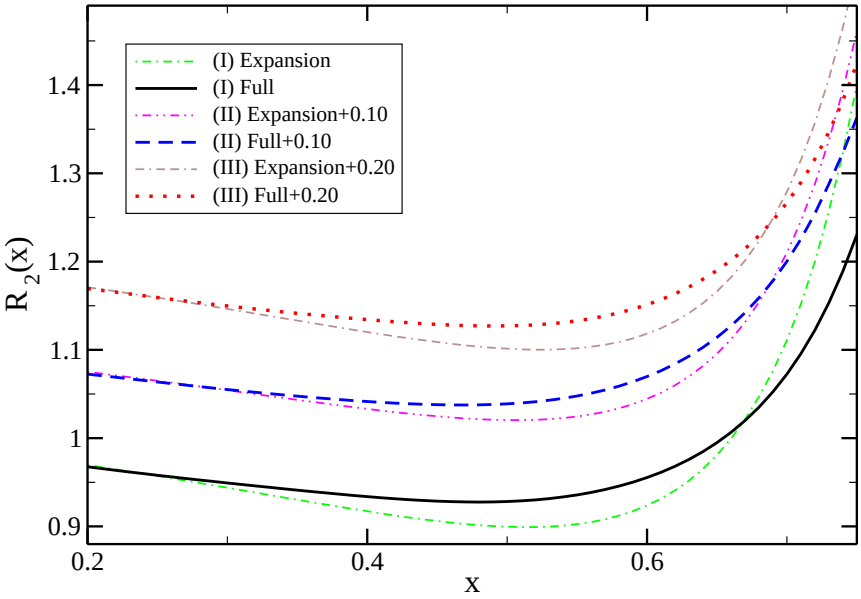

Figure E.2: $R_2 = \frac{F_{2A}}{F2}$ ratio for ^{40}Ca at $Q^2 = 20$ GeV^2. Comparison of the full results with the approximation of (E.6) for the nuclear spectral functions (I), (II) and (III).

ratio (E.4) whith those obtained making use of the approximation of (E.6). The use of this expansion has been assumed to be a good approximation for $x \leq 0.5$ [170, 179, 180]. Obviously, the series expansion agrees well at low values of x with the full results. However, in the three cases produces lower values for the ratio at intermediate x showing a maximum deviation of a 3-4% around $x = 0.5 - 0.6$. This region, with a dip in the ratio, is dominated by the mean removal energy (or equivalently the binding energy) per nucleon. Although this could look a small error, we should remark that it means increasing the deviation due to nuclear effects from the value 1 by around a 30% . At higher x's, where Fermi motion of the nucleons provides the dominant effect, the series expansions grow faster than the full results and become larger for $x \gtrsim 0.65$. Thus, we find that for typical nuclear spectral functions the convergence of the series expansion is not so good except at very low x, where in any case other effects not considered here, like shadowing play a major role. The results for the $R_3 = \frac{F_{3A}}{F_3}$ ratio are shown in

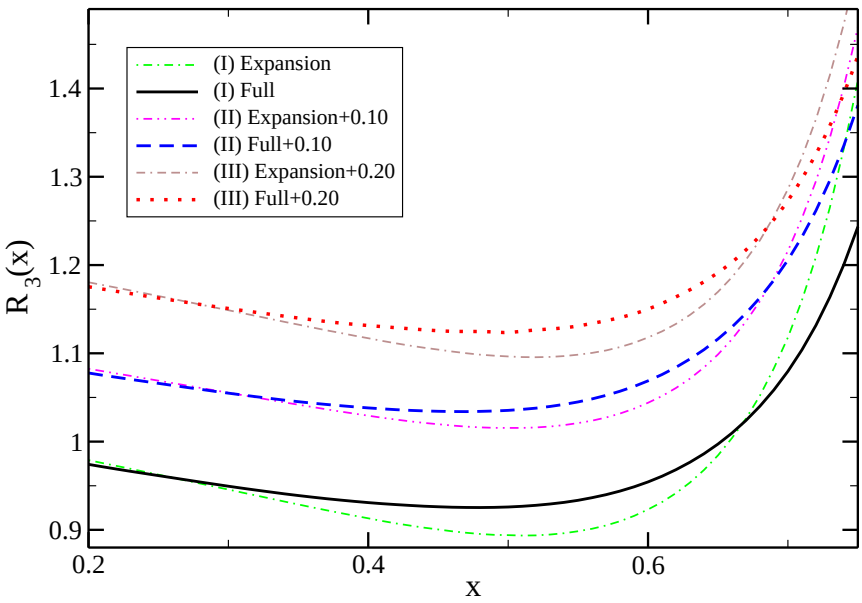

Figure E.3: $R_3 = \frac{F_{3A}}{F_3}$ ratio for ^{40}Ca at $Q^2 = 20$ GeV^2. Comparison of the full results with the approximation of (E.8) for the nuclear spectral functions (I), (II) and (III).

figure E.3. The full model for R_3 is given by (E.5) and the series expansion by (E.8). As it was the case for R_2, there is a dip region dominated by the binding energy and the Fermi motion of the nucleons produces the large rising at high values of x. The comparison of the full results and the series expansions shows the same features as for R_2. The expansions systematically underestimate the ratios at intermediate values of x and overestimate them for $x > 0.7$. This overestimation of the effect of the Fermi motion was already discussed in [181]. There, it was also claimed that in the limit of high Q^2 and for heavy nuclei the expansion should be a good approxiamtion up to $x \lesssim 0.75$. However, after studying R_2 and R_3 at different Q^2 values, apart from the one shown in this appendix, we have found that for medium nuclei the convergence of the series is only good at very low x where other nuclear effects are very relevant.

In order to obtain a better convergence one would need to reach a higher order in the expansions. This implies also the sensitivity to nuclear expected values of higher powers of the nucleons momenta as $< (p/M)^4 >$. One should notice that due to correlations these expected values are not negligible [185, 186]. The three spectral functions considered above contain high momentum components and one may expect any expansion up to order p^2 to fail to have a good convergence. To test this point, we have also calculated R_2 for the case of a simpler mean field spectral function which does not incorporate nucleon correlations and does not have those high momentum components [183]. This function was used to analyse the A dependence of the position and magnitude of the dip. Here, we have used the same parton distribution functions as in the original reference [183]. The results are shown in figure E.4. In this case, there is an almost perfect agreement between the full results and the expansion.

In summary, we have studied the quality of some series expansions commonly used to incorporate approximately the nuclear effects in the analysis of DIS processes. We have found that for realistic enough nuclear spectral functions, that include nucleon correlations and have high momentum components, the convergence of the series to the full result is poor except at very low values of x, where in fact, other nuclear effects, like shadowing or antishadowing, are more relevant. At high x values, in the Fermi motion region, the expansions clearly overestimate the full result. This was known and expected. However, even at relatively low x values, where the

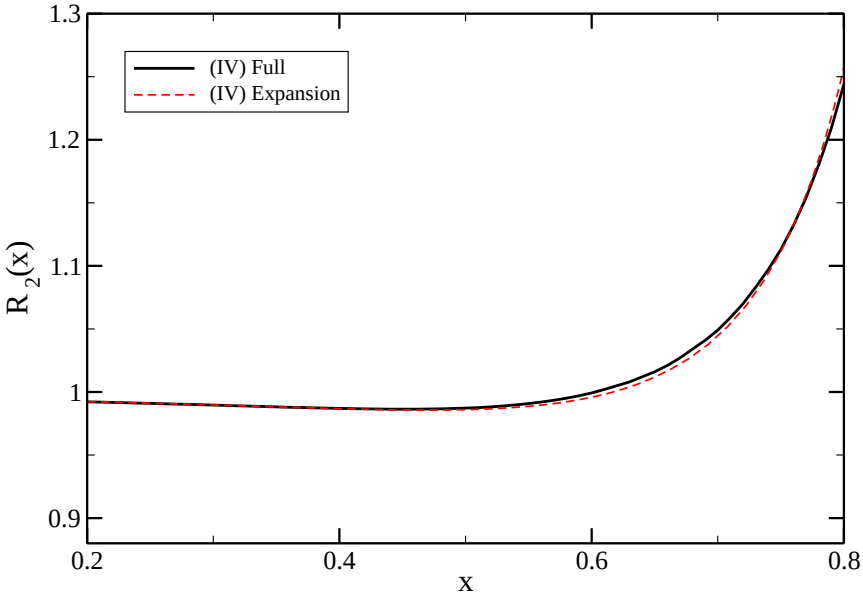

Figure E.4: $R_2 = \frac{F_{2A}}{F2}$ ratio for ^{40}Ca. Comparison of the full results with the approximation of (E.6) for the nuclear spectral functions (IV).

expansions were suppossed to provide a good approximation, we have found that they systematically underestimate the value of F_2 and F_3, artificially increasing the size of the nuclear corrections.

Bibliography

[1] C. L. Cowan, F. Reines, F. B. Harrison, H. W. Kruse and A. D. McGuire, "Detection of the free neutrino: A Confirmation," Science **124** (1956) 103.

[2] E. Fermi, "An attempt of a theory of beta radiation. 1," Z. Phys. **88**, 161 (1934).

[3] E. Fermi, "Trends to a Theory of beta Radiation. (In Italian)," Nuovo Cim. **11**, 1 (1934).

[4] G. Gamow and E. Teller, "Selection rules for the beta-disintegration," Phys. Rev. **49**, 895 (1936).

[5] G. Gamow and E. Teller, "Some Generalizations of the beta Transformation Theory," Phys. Rev. **51**, 289 (1937).

[6] R. P. Feynman and M. Gell-Mann, "Theory of Fermi interaction," Phys. Rev. **109**, 193 (1958).

[7] E. C. G. Sudarshan and R. e. Marshak, "Chirality invariance and the universal Fermi interaction," Phys. Rev. **109**, 1860 (1958).

[8] R. E. Marshak, S. Okubo and G. Sudarshan, "V-A theory and the decay of the hyperon," Phys. Rev. **113**, 944 (1959).

[9] C. S. Wu, E. Ambler, R. W. Hayward, D. D. Hoppes and R. P. Hudson, "Experimental test of parity conservation in beta decay," Phys. Rev. **105**, 1413 (1957).

[10] G. Danby, J. M. Gaillard, K. A. Goulianos, L. M. Lederman, N. B. Mistry, M. Schwartz and J. Steinberger, "Observation of High-Energy Neutrino Reactions and the Existence of Two Kinds of Neutrinos," Phys. Rev. Lett. **9**, 36 (1962).

[11] K. Kodama *et al.* [DONUT Collaboration], "Observation of tau neutrino interactions," Phys. Lett. B **504**, 218 (2001) [arXiv:hep-ex/0012035].

[12] A. Osipowicz *et al.* [KATRIN Collaboration], "KATRIN: A Next generation tritium beta decay experiment with sub-eV sensitivity for the electron neutrino mass. Letter of intent," arXiv:hep-ex/0109033.

[13] R. N. Mohapatra, "New Contributions to Neutrinoless Double beta Decay in Supersymmetric Theories," Phys. Rev. D **34** (1986) 3457.

[14] H. V. Klapdor-Kleingrothaus, I. V. Krivosheina, A. Dietz and O. Chkvorets, "Search for neutrinoless double beta decay with enriched Ge-76 in Gran Sasso 1990-2003," Phys. Lett. B **586** (2004) 198 [arXiv:hep-ph/0404088].

[15] C. E. Aalseth *et al.* [IGEX Collaboration], "The IGEX Ge-76 neutrinoless double beta decay experiment: Prospects for next generation experiments," Phys. Rev. D **65** (2002) 092007 [arXiv:hep-ex/0202026].

[16] R. Arnold *et al.* [NEMO Collaboration], "First results of the search of neutrinoless double beta decay with the NEMO 3 detector," Phys. Rev. Lett. **95** (2005) 182302 [arXiv:hep-ex/0507083].

[17] T. Schwetz, M. Tortola and J. W. F. Valle, "Global neutrino data and recent reactor fluxes: status of three-flavour oscillation parameters," New J. Phys. **13** (2011) 063004 [arXiv:1103.0734 [hep-ph]].

[18] Y. Fukuda *et al.* [Super-Kamiokande Collaboration], "Evidence for oscillation of atmospheric neutrinos," Phys. Rev. Lett. **81** (1998) 1562-1567. [hep-ex/9807003].

[19] M. Apollonio *et al.* [CHOOZ Collaboration], "Limits on neutrino oscillations from the CHOOZ experiment," Phys. Lett. **B466** (1999) 415-430. [hep-ex/9907037].

[20] M. H. Ahn *et al.* [K2K Collaboration], "Indications of neutrino oscillation in a 250 km long baseline experiment," Phys. Rev. Lett. **90**, 041801 (2003). [hep-ex/0212007].

[21] S. Fukuda *et al.* [Super-Kamiokande Collaboration], "Determination of solar neutrino oscillation parameters using 1496 days of Super-Kamiokande I data," Phys. Lett. **B539** (2002) 179-187. [hep-ex/0205075].

[22] M. C. Gonzalez-Garcia and M. Maltoni, "Phenomenology with Massive Neutrinos," Phys. Rept. **460** (2008) 1 [arXiv:0704.1800 [hep-ph]].

[23] M. Maltoni, T. Schwetz, M. A. Tortola, J. W. F. Valle, "Status of global fits to neutrino oscillations," New J. Phys. **6** (2004) 122. [hep-ph/0405172].

[24] S. M. Bilenky, S. T. Petcov, "Massive Neutrinos and Neutrino Oscillations," Rev. Mod. Phys. **59** (1987) 671.

[25] T. -K. Kuo, J. T. Pantaleone, "Neutrino Oscillations in Matter," Rev. Mod. Phys. **61** (1989) 937.

[26] S. M. Bilenky, C. Giunti, W. Grimus, "Phenomenology of neutrino oscillations," Prog. Part. Nucl. Phys. **43** (1999) 1-86. [hep-ph/9812360].

[27] Y. Ashie *et al.* [Super-Kamiokande Collaboration], "A Measurement of Atmospheric Neutrino Oscillation Parameters by Super-Kamiokande I," Phys. Rev. D **71** (2005) 112005 [arXiv:hep-ex/0501064].

[28] J. Hosaka *et al.* [Super-Kamiokande Collaboration], "Three flavor neutrino oscillation analysis of atmospheric neutrinos in Super-Kamiokande," Phys. Rev. D **74** (2006) 032002 [arXiv:hep-ex/0604011].

[29] Y. Itow *et al.* [The T2K Collaboration], "The JHF-Kamioka neutrino project," arXiv:hep-ex/0106019.

[30] D. S. Ayres *et al.* [NOvA Collaboration], "NOvA proposal to build a 30-kiloton off-axis detector to study neutrino oscillations in the Fermilab NuMI beamline," arXiv:hep-ex/0503053.

[31] M. Guler *et al.* [OPERA Collaboration], "OPERA: An appearance experiment to search for nu/mu ¡–¿ nu/tau oscillations in the CNGS beam. Experimental proposal,"

[32] A. A. Aguilar-Arevalo *et al.* [The MiniBooNE Collaboration], "A Search for electron neutrino appearance at the $\Delta m^2 \sim 1\mathrm{eV}^2$ scale," Phys. Rev. Lett. **98** (2007) 231801 [arXiv:0704.1500 [hep-ex]].

[33] M. Soderberg [MicroBooNE Collaboration], "MicroBooNE: A New Liquid Argon Time Projection Chamber Experiment," AIP Conf. Proc. **1189** (2009) 83 [arXiv:0910.3497 [physics.ins-det]].

[34] D. Drakoulakos *et al.* [Minerva Collaboration], "Proposal to perform a high-statistics neutrino scattering experiment using a fine-grained detector in the NuMI beam," arXiv:hep-ex/0405002.

[35] G. P. Zeller, "Low Energy Neutrino Cross Sections From K2k, Miniboone, Sciboone, And Minerva," J. Phys. Conf. Ser. **136** (2008) 022028.

[36] J. E. Amaro, M. B. Barbaro, J. A. Caballero, T. W. Donnelly and C. F. Williamson, "Meson-exchange currents and quasielastic neutrino cross sections in the SuperScaling Approximation model," Phys. Lett. B **696** (2011) 151 [arXiv:1010.1708 [nucl-th]].

[37] J. E. Amaro, M. B. Barbaro, J. A. Caballero, T. W. Donnelly and J. M. Udias, "Final-state interactions and superscaling in the semi-relativistic approach to quasielastic electron and neutrino scattering," Phys. Rev. C **75** (2007) 034613 [arXiv:nucl-th/0612056].

[38] J. Nieves, J. E. Amaro and M. Valverde, "Inclusive quasi-elastic neutrino reactions: Combined study of the inclusive muon capture in C-12 and the LSND measurement of the reaction C-12(nu/mu,mu-)X near threshold," Phys. Rev. C **70** (2004) 055503 [Erratum-ibid. C **72** (2005) 019902] [arXiv:nucl-th/0408005].

[39] T. Leitner, O. Buss, L. Alvarez-Ruso and U. Mosel, "Electron- and neutrino-nucleus scattering from the quasielastic to the resonance region," Phys. Rev. C **79** (2009) 034601 [arXiv:0812.0587 [nucl-th]].

[40] A. A. Aguilar-Arevalo *et al.* [MiniBooNE Collaboration], "First Measurement of the Muon Neutrino Charged Current Quasielastic Double Differential Cross Section," Phys. Rev. D **81** (2010) 092005 [arXiv:1002.2680 [hep-ex]].

[41] A. Bodek, S. Avvakumov, R. Bradford and H. S. Budd, "Vector and Axial Nucleon Form Factors:A Duality Constrained Parameterization," Eur. Phys. J. C **53** (2008) 349 [arXiv:0708.1946 [hep-ex]].

[42] V. Bernard, N. Kaiser and U. G. Meissner, "Measuring the axial radius of the nucleon in pion electroproduction," Phys. Rev. Lett. **69** (1992) 1877.

[43] A. Gil, J. Nieves and E. Oset, "Many body approach to the inclusive (e,e') reaction from the quasielastic to the Delta excitation region," Nucl. Phys. A **627**, 543 (1997) [arXiv:nucl-th/9711009].

[44] M. Martini, M. Ericson, G. Chanfray and J. Marteau, "Neutrino and antineutrino quasielastic interactions with nuclei," Phys. Rev. C **81** (2010) 045502 [arXiv:1002.4538 [hep-ph]].

[45] M. Martini, M. Ericson, G. Chanfray and J. Marteau, "A unified approach for nucleon knock-out, coherent and incoherent pion production in neutrino interactions with nuclei," Phys. Rev. C **80** (2009) 065501 [arXiv:0910.2622 [nucl-th]].

[46] J. Nieves, I. Ruiz Simo and M. J. Vicente Vacas, "Inclusive Charged–Current Neutrino–Nucleus Reactions," Phys. Rev. C **83** (2011) 045501 [arXiv:1102.2777 [hep-ph]].

[47] E. Hernandez, J. Nieves and M. Valverde, "Weak pion production off the nucleon," Phys. Rev. D **76** (2007) 033005 [arXiv:hep-ph/0701149].

[48] D. Rein and L. M. Sehgal, "Neutrino Excitation Of Baryon Resonances And Single Pion Production," Annals Phys. **133** (1981) 79.

[49] R. P. Feynman, M. Kislinger and F. Ravndal, "Current matrix elements from a relativistic quark model," Phys. Rev. D **3** (1971) 2706.

[50] K. S. Kuzmin, V. V. Lyubushkin and V. A. Naumov, "Polarization of tau leptons produced in quasielastic neutrino nucleon scattering," Mod. Phys. Lett. A **19** (2004) 2919 [arXiv:hep-ph/0403110].

[51] C. Berger and L. M. Sehgal, "Lepton mass effects in single pion production by neutrinos," Phys. Rev. D **76** (2007) 113004 [arXiv:0709.4378 [hep-ph]].

[52] K. M. Graczyk and J. T. Sobczyk, "Lepton mass effects in weak charged current single pion production," Phys. Rev. D **77** (2008) 053003 [arXiv:0709.4634 [hep-ph]].

[53] D. Drechsel, S. S. Kamalov and L. Tiator, "Unitary Isobar Model - MAID2007," Eur. Phys. J. A **34** (2007) 69 [arXiv:0710.0306 [nucl-th]].

[54] I. G. Aznauryan, "Multipole amplitudes of pion photoproduction on nucleons up to 2-Gev within dispersion relations and unitary isobar model," Phys. Rev. C **67** (2003) 015209 [arXiv:nucl-th/0206033].

[55] J. E. Amaro, E. Hernandez, J. Nieves and M. Valverde, "Theoretical study of neutrino-induced coherent pion production off nuclei at T2K and MiniBooNE energies," Phys. Rev. D **79** (2009) 013002 [arXiv:0811.1421 [hep-ph]].

[56] O. Lalakulich, T. Leitner, O. Buss and U. Mosel, "One pion production in neutrino reactions: including non-resonant background," Phys. Rev. D **82** (2010) 093001 [arXiv:1007.0925 [hep-ph]].

[57] E. A. Paschos, L. Pasquali and J. Y. Yu, "Single pion production in neutrino reactions and estimates for charge-exchange effects," Nucl. Phys. B **588** (2000) 263 [arXiv:hep-ph/0005255].

[58] I. Budagov *et al.*, "Single pion production by neutrinos on free protons," Phys. Lett. B **29** (1969) 524.

[59] M. Valverde, J. Nieves, E. Hernandez, S. K. Singh and M. J. Vicente Vacas, "Production of Two Pions Induced by Neutrinos," Mod. Phys. Lett. A **23** (2008) 2309 [arXiv:0802.1269 [hep-ph]].

[60] S. K. Singh and M. J. Vicente Vacas, "Weak quasi-elastic production of hyperons," Phys. Rev. D **74** (2006) 053009 [arXiv:hep-ph/0606235].

[61] R. E. Shrock, "Associated Production By Weak Charged And Neutral Currents," Phys. Rev. D **12** (1975) 2049.

[62] G. B. Adera, B. I. S. Van Der Ventel, D. D. van Niekerk and T. Mart, "Strange-particle production via the weak interaction," Phys. Rev. C **82** (2010) 025501.

[63] K. Lang, "MINOS: The physics program and the construction status," Int. J. Mod. Phys. A **18** (2003) 3857.

[64] S. A. Kulagin and R. Petti, "Global study of nuclear structure functions," Nucl. Phys. A **765** (2006) 126 [arXiv:hep-ph/0412425].

[65] S. A. Kulagin and R. Petti, "Neutrino inelastic scattering off nuclei," Phys. Rev. D **76** (2007) 094023 [arXiv:hep-ph/0703033].

[66] I. Schienbein *et al.*, "A Review of Target Mass Corrections," J. Phys. G **35** (2008) 053101 [arXiv:0709.1775 [hep-ph]].

[67] E. Marco, E. Oset and P. Fernandez de Cordoba, "Mesonic and binding contributions to the EMC effect in a relativistic many body approach," Nucl. Phys. A **611** (1996) 484 [arXiv:nucl-th/9510060].

[68] J. Seely *et al.*, "New measurements of the EMC effect in very light nuclei," Phys. Rev. Lett. **103** (2009) 202301 [arXiv:0904.4448 [nucl-ex]].

[69] M. Rafi Alam, I. Ruiz Simo, M. Sajjad Athar and M. J. Vicente Vacas, "Weak Kaon Production off the Nucleon," Phys. Rev. D **82** (2010) 033001 [arXiv:1004.5484 [hep-ph]].

[70] M. Sajjad Athar, I. Ruiz Simo and M. J. Vicente Vacas, "Nuclear medium modification of the F(2)(x,Q**2) structure function," Nucl. Phys. A **857** (2011) 29 [arXiv:0910.4879 [nucl-th]].

[71] T. Marrodan Undagoitia *et al.*, "Proton decay in the large liquid scintillator detector LENA: Study of the background," J. Phys. Conf. Ser. **39** (2006) 269.

[72] K. Kobayashi *et al.* [Super-Kamiokande Collaboration], "Search for nucleon decay via modes favored by supersymmetric grand unification models in Super-Kamiokande-I," Phys. Rev. D **72** (2005) 052007 [arXiv:hep-ex/0502026].

[73] W. A. Mann, T. Kafka, M. Derrick, B. Musgrave, R. Ammar, D. Day and J. Gress, "K meson production by muon-neutrino - deuterium reactions near threshold: implications for nucleon decay searches," Phys. Rev. D **34** (1986) 2545.

[74] S. L. Mintz and L. Wen, "New results for the production of Lambda and Sigma0 hyperons in antineutrino scattering from protons," Eur. Phys. J. A **33** (2007) 299.

[75] H. K. Dewan, "Strange Particle Production In Neutrino Scattering," Phys. Rev. D **24** (1981) 2369.

[76] Y. Hayato, "A neutrino interaction simulation program library NEUT," Acta Phys. Polon. B **40** (2009) 2477.

[77] G. P. Zeller, "Low energy neutrino cross sections: Comparison of various Monte Carlo predictions to experimental data," arXiv:hep-ex/0312061.

[78] S. Scherer, "Introduction to chiral perturbation theory," Adv. Nucl. Phys. **27** (2003) 277 [arXiv:hep-ph/0210398].

[79] N. Cabibbo, E. C. Swallow and R. Winston, "Semileptonic hyperon decays," Ann. Rev. Nucl. Part. Sci. **53** (2003) 39 [arXiv:hep-ph/0307298].

[80] J. A. Oller, M. Verbeni and J. Prades, "Meson-baryon effective chiral lagrangians to O(q**3)," JHEP **0609** (2006) 079 [arXiv:hep-ph/0608204].

[81] R. Flores-Mendieta, "V(us) from hyperon semileptonic decays," Phys. Rev. D **70** (2004) 114036 [arXiv:hep-ph/0410171].

[82] L. S. Geng, J. Martin Camalich and M. J. Vicente Vacas, "SU(3)-breaking corrections to the hyperon vector coupling $f_1(0)$ in covariant baryon chiral perturbation theory," Phys. Rev. D **79** (2009) 094022 [arXiv:0903.4869 [hep-ph]].

[83] O. Benhar, N. Farina, H. Nakamura, M. Sakuda and R. Seki, "Electron and neutrino nucleus scattering in the impulse approximation regime," Phys. Rev. D **72** (2005) 053005 [arXiv:hep-ph/0506116].

[84] T. Leitner, O. Buss, U. Mosel and L. Alvarez-Ruso, "Neutrino induced pion production at MiniBooNE and K2K," Phys. Rev. C **79** (2009) 038501 [arXiv:0812.1787 [nucl-th]].

[85] V. Bernard, L. Elouadrhiri and U. G. Meissner, "Axial structure of the nucleon," J. Phys. G **28** (2002) R1.

[86] K. S. Kuzmin, V. V. Lyubushkin and V. A. Naumov, "Quasielastic axial-vector mass from experiments on neutrino-nucleus scattering," Eur. Phys. J. C **54** (2008) 517.

[87] A. A. Aguilar-Arevalo *et al.* [MiniBooNE Collaboration], "Measurement of muon neutrino quasi-elastic scattering on carbon," Phys. Rev. Lett. **100** (2008) 032301 [arXiv:0706.0926 [hep-ex]].

[88] R. Gran *et al.* [K2K Collaboration], "Measurement of the quasi-elastic axial vector mass in neutrino oxygen interactions," Phys. Rev. D **74** (2006) 052002.

[89] A. A. Amer, "Production Of Strange Particles By Neutrinos And Anti-Neutrinos," Phys. Rev. D **18** (1978) 2290.

[90] C. Andreopoulos *et al.*, "The GENIE Neutrino Monte Carlo Generator," Nucl. Instrum. Meth. A **614** (2010) 87.

[91] S. J. Barish *et al.*, "Study Of Neutrino Interactions In Hydrogen And Deuterium. 1. Description Of The Experiment And Study Of The Reaction Neutrino D $\rightarrow$ Mu- P P(S)," Phys. Rev. D **16** (1977) 3103.

[92] A. K. Ichikawa, "The T2K long-baseline neutrino experiment," Lect. Notes Phys. **781** (2009) 17.

[93] A. A. Aguilar-Arevalo *et al.* [MiniBooNE Collaboration], "Measurement of ν_μ and $\bar{\nu}_\mu$ induced neutral current single π^0 production cross sections on mineral oil at $E_\nu \sim O(1GeV)$," Phys. Rev. D **81** (2010) 013005.

[94] M. Honda, T. Kajita, K. Kasahara, S. Midorikawa and T. Sanuki, "Calculation of atmospheric neutrino flux using the interaction model calibrated with atmospheric muon data," Phys. Rev. D **75** (2007) 043006.

[95] M. Doring, E. Oset, S. Sarkar, "Radiative decay of the Lambda(1520)," Phys. Rev. **C74** (2006) 065204. [nucl-th/0601027].

[96] S. Taylor *et al.* [CLAS Collaboration], "Radiative decays of the Sigma(1385)0 and Lambda(1520) hyperons," Phys. Rev. C **71** (2005) 054609 [Erratum-ibid. C **72** (2005 PHRVA,C72,039902.2005) 039902] [arXiv:hep-ex/0503014].

[97] O. Lalakulich and E. A. Paschos, "Resonance production by neutrinos. I. J = 3/2 resonances," Phys. Rev. D **71** (2005) 074003 [arXiv:hep-ph/0501109].

[98] L. Alvarez-Ruso, S. K. Singh and M. J. Vicente Vacas, "nu d –¿ mu-Delta++ n reaction and axial vector N Delta coupling," Phys. Rev. C **59** (1999) 3386 [arXiv:nucl-th/9804007].

[99] E. Hernandez, J. Nieves, M. Valverde and M. J. Vicente Vacas, "N-Delta(1232) axial form factors from weak pion production," Phys. Rev. D **81** (2010) 085046 [arXiv:1001.4416 [hep-ph]].

[100] K. Nakamura *et al.* [Particle Data Group], "Review of particle physics," J. Phys. G **37** (2010) 075021.

[101] A. A. Aguilar-Arevalo, C. E. Anderson, S. J. Brice, B. C. Brown, L. Bugel, J. M. Conrad, R. Dharmapalan, Z. Djurcic *et al.*, "Measurement of the neutrino component of an anti-neutrino beam observed by a non-magnetized detector," [arXiv:1102.1964 [hep-ex]].

[102] S. A. Adjei, D. A. Dicus, V. L. Teplitz, "Charged Current Two Pion Production From Nucleons," Phys. Rev. **D24** (1981) 623.

[103] T. Kitagaki, H. Yuta, S. Tanaka, A. Yamaguchi, K. Abe, K. Hasegawa, K. Tamai, S. Kunori *et al.*, "Charged Current Exclusive Pion Production In Neutrino Deuterium Interactions," Phys. Rev. **D34** (1986) 2554-2565.

[104] A. A. Aguilar-Arevalo *et al.* [MiniBooNE Collaboration], "Measurement of the Neutrino Neutral-Current Elastic Differential Cross Section on Mineral Oil at $E_\nu \sim 1$ GeV," Phys. Rev. D **82** (2010) 092005 [arXiv:1007.4730 [hep-ex]].

[105] A. A. Aguilar-Arevalo *et al.* [MiniBooNE Collaboration], "Measurement of Neutrino-Induced Charged-Current Charged Pion Production Cross Sections on Mineral Oil at $\mathrm{E}_\nu \sim 1$ GeV," arXiv:1011.3572 [hep-ex].

[106] Y. Nakajima *et al.* [SciBooNE Collaboration], "Measurement of inclusive charged current interactions on carbon in a few-GeV neutrino beam," Phys. Rev. D **83** (2011) 012005 [arXiv:1011.2131 [hep-ex]].

[107] L. Alvarez-Ruso, "Neutrino interactions: challenges in the current theoretical picture," arXiv:1012.3871 [nucl-th].

[108] A. M. Ankowski and J. T. Sobczyk, "Construction of spectral functions for medium nuclei," Phys. Rev. C **77** (2008) 044311 [arXiv:0711.2031 [nucl-th]].

[109] A. M. Ankowski, O. Benhar and N. Farina, "Analysis of the Q^2-dependence of charged-current quasielastic processes in neutrino-nucleus interactions," Phys. Rev. D **82** (2010) 013002 [arXiv:1001.0481 [nucl-th]].

[110] C. Maieron, M. C. Martinez, J. A. Caballero and J. M. Udias, "Nuclear model effects in charged current neutrino nucleus quasielastic scattering," Phys. Rev. C **68** (2003) 048501 [arXiv:nucl-th/0303075].

[111] M. C. Martinez, P. Lava, N. Jachowicz, J. Ryckebusch, K. Vantournhout and J. M. Udias, "Relativistic models for quasi-elastic neutrino scattering," Phys. Rev. C **73** (2006) 024607 [arXiv:nucl-th/0505008].

[112] J. Nieves, M. Valverde and M. J. Vicente Vacas, "Inclusive nucleon emission induced by quasi-elastic neutrino nucleus interactions," Phys. Rev. C **73** (2006) 025504 [arXiv:hep-ph/0511204].

[113] S. K. Singh and E. Oset, "Quasielastic neutrino (anti-neutrino) reactions in nuclei and the axial vector form-factor of the nucleon," Nucl. Phys. A **542** (1992) 587.

[114] M. Sajjad Athar, S. Chauhan and S. K. Singh, "Theoretical study of lepton events in the atmospheric neutrino experiments at SuperK," Eur. Phys. J. A **43** (2010) 209 [arXiv:0908.1443 [nucl-th]].

[115] A. Liesenfeld *et al.* [A1 Collaboration], "A measurement of the axial form-factor of the nucleon by the p(e,e' pi+)n reaction at W = 1125-MeV," Phys. Lett. B **468** (1999) 20 [arXiv:nucl-ex/9911003].

[116] S. Boyd, S. Dytman, E. Hernandez, J. Sobczyk and R. Tacik, "Comparison of models of neutrino-nucleus interactions," AIP Conf. Proc. **1189** (2009) 60.

[117] A. V. Butkevich, "Analysis of flux-integrated cross sections for quasi-elastic neutrino charged-current scattering off ^{12}C at MiniBooNE energies," Phys. Rev. C **82** (2010) 055501 [arXiv:1006.1595 [nucl-th]].

[118] O. Benhar, P. Coletti and D. Meloni, "Electroweak nuclear response in quasi-elastic regime," Phys. Rev. Lett. **105** (2010) 132301 [arXiv:1006.4783 [nucl-th]].

[119] C. Juszczak, J. T. Sobczyk and J. Zmuda, "On extraction of value of axial mass from MiniBooNE neutrino quasi-elastic double differential cross section data," Phys. Rev. C **82** (2010) 045502 [arXiv:1007.2195 [nucl-th]].

[120] V. Lyubushkin *et al.* [NOMAD Collaboration], "A study of quasi-elastic muon neutrino and antineutrino scattering in the NOMAD experiment," Eur. Phys. J. C **63** (2009) 355 [arXiv:0812.4543 [hep-ex]].

[121] T. Sato, D. Uno and T. S. H. Lee, "Dynamical model of weak pion production reactions," Phys. Rev. C **67** (2003) 065201 [arXiv:nucl-th/0303050].

[122] K. M. Graczyk, D. Kielczewska, P. Przewlocki and J. T. Sobczyk, "C_5^A axial form factor from bubble chamber experiments," Phys. Rev. D **80** (2009) 093001 [arXiv:0908.2175 [hep-ph]].

[123] R. C. Carrasco and E. Oset, "Interaction of real photons with nuclei from 100-MeV to 500-MeV," Nucl. Phys. A **536** (1992) 445.

[124] E. Oset, H. Toki and W. Weise, "Pionic modes of excitation in nuclei," Phys. Rept. **83**, 281 (1982).

[125] L. L. Salcedo, E. Oset, M. J. Vicente-Vacas and C. Garcia-Recio, "Computer simulation of inclusive pion nuclear reactions," Nucl. Phys. A **484** (1988) 557.

[126] J. Nieves, E. Oset and C. Garcia-Recio, "A Theoretical approach to pionic atoms and the problem of anomalies," Nucl. Phys. A **554**, 509 (1993).

[127] J. Nieves, E. Oset and C. Garcia-Recio, "Many body approach to low-energy pion nucleus scattering," Nucl. Phys. A **554**, 554 (1993).

[128] C. Albertus, J. E. Amaro and J. Nieves, "What does free space Lambda-Lambda interaction predict for Lambda-Lambda hypernuclei?," Phys. Rev. Lett. **89**, 032501 (2002) [arXiv:nucl-th/0110046].

[129] M. Valverde, J. E. Amaro and J. Nieves, "Theoretical uncertainties on quasielastic charged-current neutrino-nucleus cross sections," Phys. Lett. B **638**, 325 (2006) [arXiv:hep-ph/0604042].

[130] C. Garcia-Recio, E. Oset and L. L. Salcedo, "S wave optical potential in pionic atoms," Phys. Rev. C **37** (1988) 194.

[131] E. Oset and L. L. Salcedo, "Delta selfenergy in nuclear matter," Nucl. Phys. A **468** (1987) 631.

[132] L. Alvarez-Ruso, L. S. Geng, S. Hirenzaki and M. J. Vicente Vacas, "Charged current neutrino induced coherent pion production," Phys. Rev. C **75** (2007) 055501 [Erratum-ibid. C **80** (2009) 019906] [arXiv:nucl-th/0701098].

[133] E. Hernandez, J. Nieves and M. Valverde, "Coherent pion production off nuclei at T2K and MiniBooNE energies revisited," Phys. Rev. D **82** (2010) 077303 [arXiv:1007.3685 [hep-ph]].

[134] M. Hirata, J. H. Koch, E. J. Moniz and F. Lenz, "Isobar Hole Doorway States and pi O-16 Scattering," Annals Phys. **120** (1979) 205.

[135] T. Leitner and U. Mosel, "Neutrino-nucleus scattering reexamined: Quasielastic scattering and pion production entanglement and implications for neutrino energy reconstruction," Phys. Rev. C **81** (2010) 064614 [arXiv:1004.4433 [nucl-th]].

[136] L. B. Auerbach *et al.* [LSND Collaboration], "Measurements of charged current reactions of muon neutrinos on C-12," Phys. Rev. C **66** (2002) 015501 [arXiv:nucl-ex/0203011].

[137] O. Benhar and D. Meloni, "Impact of nuclear effects on the determination of the nucleon axial mass," Phys. Rev. D **80** (2009) 073003 [arXiv:0903.2329 [hep-ph]].

[138] P. Fernandez de Cordoba and E. Oset, "Semiphenomenological approach to nucleon properties in nuclear matter," Phys. Rev. C **46** (1992) 1697.

[139] C. F. Perdrisat, V. Punjabi and M. Vanderhaeghen, "Nucleon Electromagnetic Form Factors," Prog. Part. Nucl. Phys. **59**, 694 (2007).

[140] J. E. Amaro, M. B. Barbaro, J. A. Caballero, T. W. Donnelly and J. M. Udias, "Relativistic analyses of quasielastic neutrino cross sections at MiniBooNE kinematics," arXiv:1104.5446 [nucl-th].

[141] G. D'Agostini, "On the use of the covariance matrix to fit correlated data," Nucl. Instrum. Meth. A **346**, 306 (1994).

[142] E. Fernandez-Martinez and D. Meloni, "Importance of nuclear effects in the measurement of neutrino oscillation parameters," Phys. Lett. B **697** (2011) 477.

[143] J. J. Aubert *et al.* [European Muon Collaboration], "The Ratio of the Nucleon Structure Functions f2 (n) for Iron and Deuterium," Phys. Lett. B **123** (1983) 275.

[144] R. G. Arnold *et al.*, "Measurements of the a-Dependence of Deep Inelastic electron Scattering from Nuclei," Phys. Rev. Lett. **52** (1984) 727.

[145] A. Bodek *et al.*, "A Comparison of the Deep Inelastic Structure Functions of Deuterium and Aluminum Nuclei," Phys. Rev. Lett. **51** (1983) 534.

[146] J. Gomez *et al.*, "Measurement of the A-dependence of deep inelastic electron scattering," Phys. Rev. D **49** (1994) 4348.

[147] M. Arneodo, "Nuclear effects in structure functions," Phys. Rept. **240** (1994) 301.

[148] D. F. Geesaman, K. Saito and A. W. Thomas, "The nuclear EMC effect," Ann. Rev. Nucl. Part. Sci. **45** (1995) 337.

[149] N. Armesto, "Nuclear shadowing," J. Phys. G **32** (2006) R367 [arXiv:hep-ph/0604108].

[150] G. A. Miller, "Implications of the nuclear EMC effect," Eur. Phys. J. A **31** (2007) 578.

[151] M. Hirai, S. Kumano and T. H. Nagai, "Determination of nuclear parton distribution functions and their uncertainties in next-to-leading order," Phys. Rev. C **76** (2007) 065207 [arXiv:0709.3038 [hep-ph]].

[152] K. J. Eskola, H. Paukkunen and C. A. Salgado, "EPS09: A New Generation of NLO and LO Nuclear Parton Distribution Functions," JHEP **0904** (2009) 065 [arXiv:0902.4154 [hep-ph]].

[153] I. Schienbein, J. Y. Yu, C. Keppel, J. G. Morfin, F. Olness and J. F. Owens, "Nuclear parton distribution functions from neutrino deep inelastic scattering," Phys. Rev. D **77** (2008) 054013 [arXiv:0710.4897 [hep-ph]].

[154] I. Schienbein, J. Y. Yu, K. Kovarik, C. Keppel, J. G. Morfin, F. Olness and J. F. Owens, "PDF Nuclear Corrections for Charged and Neutral Current Processes," Phys. Rev. D **80** (2009) 094004 [arXiv:0907.2357 [hep-ph]].

[155] C. Garcia-Recio, J. Nieves and E. Oset, "Pion cloud contribution to K+ nucleus scattering," Phys. Rev. C **51** (1995) 237 [arXiv:nucl-th/9407041].

[156] A. D. Martin, W. J. Stirling, R. S. Thorne and G. Watt, "Parton distributions for the LHC," Eur. Phys. J. C **63** (2009) 189 [arXiv:0901.0002 [hep-ph]].

[157] J. A. M. Vermaseren, A. Vogt and S. Moch, "The Third-order QCD corrections to deep-inelastic scattering by photon exchange," Nucl. Phys. B **724** (2005) 3 [arXiv:hep-ph/0504242].

[158] W. L. van Neerven and A. Vogt, "NNLO evolution of deep inelastic structure functions: The Singlet case," Nucl. Phys. B **588** (2000) 345 [arXiv:hep-ph/0006154].

[159] W. L. van Neerven and A. Vogt, "NNLO evolution of deep inelastic structure functions: The Nonsinglet case," Nucl. Phys. B **568** (2000) 263 [arXiv:hep-ph/9907472].

[160] M. Gluck, E. Reya and A. Vogt, "Pionic parton distributions," Z. Phys. C **53** (1992) 651.

[161] M. Gluck, E. Reya and I. Schienbein, "Pionic parton distributions revisited," Eur. Phys. J. C **10** (1999) 313 [arXiv:hep-ph/9903288].

[162] C. G. . Callan and D. J. Gross, "High-energy electroproduction and the constitution of the electric current," Phys. Rev. Lett. **22** (1969) 156.

[163] S. Moch, J. A. M. Vermaseren and A. Vogt, "The longitudinal structure function at the third order," Phys. Lett. B 606 (2005) 123.

[164] H. De Vries, C. W. De Jager and C. De Vries, "Nuclear charge and magnetization density distribution parameters from elastic electron scattering," Atom. Data Nucl. Data Tabl. 36 (1987) 495.

[165] I. Ruiz Simo and M. J. Vicente Vacas, "Study of the derivative expansions for the nuclear structure functions," J. Phys. G **36** (2009) 015104 [arXiv:0807.5055 [nucl-th]].

[166] M. Sajjad Athar, S. K. Singh and M. J. Vicente Vacas, "Nuclear effects in F(3) structure function of nucleon," Phys. Lett. B **668** (2008) 133 [arXiv:0711.4443 [nucl-th]].

[167] S. V. Akulinichev, S. A. Kulagin and G. M. Vagradov, "The Role Of Nuclear Binding In Deep Inelastic Lepton Nucleon Scattering," Phys. Lett. B 158 (1985) 485.

[168] L. L. Frankfurt and M. I. Strikman, "On The Normalization Of Nucleus Spectral Function And The EMC Effect," Phys. Lett. B 183, 254 (1987).

[169] S. A. Kulagin, "Deep inelastic scattering on nuclei: impulse approximation and mesonic corrections," Nucl. Phys. A **500** (1989) 653.

[170] C. Ciofi Degli Atti and S. Liuti, "On the effects of nucleon binding and correlations in deep inelastic electron scattering by nuclei," Phys. Lett. B 225 (1989) 215.

[171] M. Lacombe, B. Loiseau, R. Vinh Mau, J. Cote, P. Pires and R. de Tourreil, "Parametrization of the deuteron wave function of the Paris n-n potential," Phys. Lett. B **101** (1981) 139.

[172] S. A. Kulagin and R. Petti, "Structure functions for light nuclei," Phys. Rev. C **82** (2010) 054614 [arXiv:1004.3062 [hep-ph]].

[173] A. C. Benvenuti *et al.* [BCDMS Collaboration], "A high statistics measurement of the deuteron structure functions F2 (x, Q**2) and R from deep inelastic muon scattering at high Q**2," Phys. Lett. B **237** (1990) 592.

[174] M. Arneodo *et al.* [New Muon Collaboration], "Measurement of the proton and deuteron structure functions, F2(p) and F2(d), and of the ratio sigma-L / sigma-T," Nucl. Phys. B **483** (1997) 3 [arXiv:hep-ph/9610231].

[175] C. Ciofi degli Atti, L. L. Frankfurt, L. P. Kaptari and M. I. Strikman, "On the dependence of the wave function of a bound nucleon on its momentum and the EMC effect," Phys. Rev. C **76** (2007) 055206 [arXiv:0706.2937 [nucl-th]].

[176] M. Benmerrouche, R. M. Davidson and N. C. Mukhopadhyay, "Problems of describing spin 3/2 baryon resonances in the effective lagrangian theory," Phys. Rev. C **39** (1989) 2339.

[177] J. M. Conrad, M. H. Shaevitz and T. Bolton, "Precision measurements with high energy neutrino beams," Rev. Mod. Phys. **70** (1998) 1341 [arXiv:hep-ex/9707015].

[178] M. Tzanov *et al.* [NuTeV Collaboration], "Precise measurement of neutrino and anti-neutrino differential cross sections," Phys. Rev. D **74** (2006) 012008 [arXiv:hep-ex/0509010].

[179] C. Ciofi degli Atti and S. Liuti, "Realistic Microscopic Approach To Deep Inelastic Scattering Of Electrons Off Few Nucleon Systems," Phys. Rev. C **41** (1990) 1100.

[180] C. Ciofi degli Atti and S. Liuti, "Classical European Muon Collaboration effect from few body systems to nuclear matter: Can binding effects explain it?," Phys. Rev. C **44** (1991) 1269.

[181] S. A. Kulagin, "Nuclear effects in F3 structure function for finite and asymptotic Q**2," Nucl. Phys. A **640** (1998) 435 [arXiv:nucl-th/9801039].

[182] G. A. Miller and J. R. Smith, "Return of the EMC effect," Phys. Rev. C **65** (2002) 015211 [Erratum-ibid. C **66** (2002) 049903] [arXiv:nucl-th/0107026].

[183] J. R. Smith and G. A. Miller, "Return of the EMC effect: Finite nuclei," Phys. Rev. C **65** (2002) 055206 [arXiv:nucl-th/0202016].

[184] M. Gluck, E. Reya and A. Vogt, "Dynamical parton distributions revisited," Eur. Phys. J. C **5** (1998) 461 [arXiv:hep-ph/9806404].

[185] C. Ciofi degli Atti, S. Simula, L. L. Frankfurt and M. I. Strikman, "Two nucleon correlations and the structure of the nucleon spectral function at high values of momentum and removal energy," Phys. Rev. C **44** (1991) 7.

[186] C. Ciofi degli Atti and S. Simula, "Realistic model of the nucleon spectral function in few and many nucleon systems," Phys. Rev. C **53** (1996) 1689 [arXiv:nucl-th/9507024].